Alma Mater Studiorum – Università di Bologna

DOTTORATO DI RICERCA IN

Scienze Chimiche

Ciclo XXV

Settore Concorsuale di afferenza: 03/C1

Settore Scientifico disciplinare: CHIM/06

De Novo Design of Foldamers for Preparation of Nanostructured Materials

Presentata da: **Nicola Castellucci**

Coordinatore Dottorato	**Relatore**
Prof.ssa Adriana Bigi	**Prof.ssa Claudia Tomasini**

Esame finale anno 2013

Table of contents

List of abbreviations

Ala	Alanine
Asn	Asparagine
Asp(O*c*Hex)	*Cyclo*hexyl-aspartic acid
Boc	Benzyloxycarbonyl-
DBU	1,8-diazabicyclo[5.4.0]undec-7-ene
DCM	Dichloromethane
Gly	Glycine
HATU	*O*-(7-azabenzotriazol-1-yl)-*N*,*N*,*N*′,*N*′-tetramethyl-uronium hexafluorophosphate
HBTU	*O*-(benzotriazol-1-yl)-*N*,*N*,*N*′,*N*′-tetramethyl-uronium hexafluorophosphate
HPLC	High-performance liquid chromatography
Imz	Imidazolidin-2-one-4-carboxylate
MD	Molecular Dynamic
NMR	Nuclear magnetic resonance
Oxd	4-carboxy-5-methyl-oxazolidin-2-one
Phe	Phenylalanine
POPC	1-palmitoyl-2-oleoyl-sn-glycero-3-phosphocholine
TEA	Triethylamine
TFA	Trifluoroacetic acid
Val	Valine
Xaa	α-amino acid

1 Introduction

1.1 Build up the molecules of life: from amino acids to proteins

The complex and interrelated reactions which make up living processes are dependent upon the presence of proteins, not only as catalyst, but in their role as structural molecules, as storage and carrier molecules, and as molecular motors. Nature uses a very limited set of building blocks—e.g. twenty amino acids in proteins and four nucleobases in DNA —with specific abilities to impart well-defined folds. However, these building blocks emerged not only because they are well suited, but also because they complied with evolutionary constraints, in particular the initial obligation to be within a few steps of prebiotic chemicals.

The presence of chiral molecules is widespread in biological systems, which are primarily homochiral systems. For example, almost exclusively L-amino acids form proteins, while DNA is made up primarily of D-deoxyribose. The naturally occurring L-amino acids predominantly form right-handed helices, while their stereoisomers D-amino acids favor left-handed helices.

1.1.1 Folding in protein structure

Two amino acids can undergo a condensation reaction, where the free amine group reacts with the carbonyl unit of a carboxyl group of another amino acid. The formation of this peptide bond produces a dipeptide and a H_2O molecule. Adding additional amino acids to the growing peptide chain (always form N-term to C-term direction in living cells) it is produced a polypeptide chain or protein.

All of these functions require that the nascent amino-acid chain correctly folds into the biologically active, three-dimensional structure of the native state. In pioneering studies, Christian Boehmer Anfisen (Nobel Prize in Chemistry in 1972) showed that all the necessary information for the nascent chain to fold into the native structure is contained in the sequence of amino acids.[1] In his Thermodynamic Hypothesis he assumed that a native protein adopts the thermodynamically most stable conformation in a *given solvent* at a particular temperature. In order for proteins to fold

[1] Anfisen, C. B. *"Principles that govern the folding of protein chains"* Science, **1973**, *181*, 223-230.

spontaneously into their native state, the native state must be lower in Gibbs energy than the unfolded state.

The nature of contribution of various interactions to protein folding and stability has been of interest for some time. In 1990, Ken Dill confirmed the theory proposed by Walter Kauzmann in 1959.

Summarizing their papers, it is possible to conclude that the interactions which are consider to dominate protein stability are the hydrophobic effect (i), hydrogen bonding (ii) and configurational entropy (iii).[2]

i. Hydrophobic effect: As proteins are the subject of this section, it is possible to define the hydrophobic effect as the energetic process associated with the transfer of hydrophobic surface from the protein interior to water, the medium of the cell. This includes the energetic associated with changes in Van der Waals interactions experienced by the hydrophobic groups, as well as the energetic associated with the restructuring of water which takes place upon hydrating hydrophobic groups.

ii. Hydrogen bonding: Hydrogen bonding refers to the partial sharing of a hydrogen atom between a donor atom to which it is covalently bound, and an acceptor atom which has a lone pair of electrons. In proteins, the intramolecular hydrogen bond competes with hydrogen bond to water molecules. It is this completion that determines the contribution of hydrogen bonding to protein stability. Hydrogen-bond strength, which depends on the electronegativity and orientation of the bonding atoms, is in the range of 2-10 kcal/mol.

iii. Configurational entropy: In an unfolded protein, the polypeptide chain can adopt different rotomeric position around ϕ and ψ torsional angles, and side chains can adopt different rotamers around χ angles. Upon adopting the native state, nearly all ϕ and ψ torsional angles are restricted to a single position, as the majority of χ angles. This loss of degrees of freedom translates into a loss of configurational entropy. It is the loss of configurational entropy which must be overcome by favorable interactions in order to fold a stable protein.

[2] Dill, K. A. *"Dominant forces in protein folding"* Biochemistry, **1990**, *29*, 7133-7155.

Proteins are complex biomacromolecules that can be constituted until thousands of amino acid residues. To describe and understand this kind of biopolymer, the structures are approached at several levels of complexity, arranged in a kind of conceptual hierarchy. Four levels of protein structure are commonly defined.

Primary structure: in biochemistry the primary structure of a biomolecule is the description of its atom and bond composition. Dealing with a linear biomolecule (proteins or nucleotidic acids), the primary structure is the sequence of amino acids along their backbone. However, proteins can become cross-linked, most commonly by disulfide bonds, and the primary structure also requires specifying the cross-linking atoms. Secondary structure refers to particularly stable arrangements of amino acid residues giving rise to recurring structural patterns. The tertiary structure of a protein describes the folding of its secondary structural elements and specifies the positions of each atom in the protein, including those of its side chains. The known protein structures have come to light through X-ray crystallographic or nuclear magnetic resonance (NMR) studies.

When a protein has two or more polypeptide subunits, their arrangement in space is referred to as quaternary structure (Figure 1).

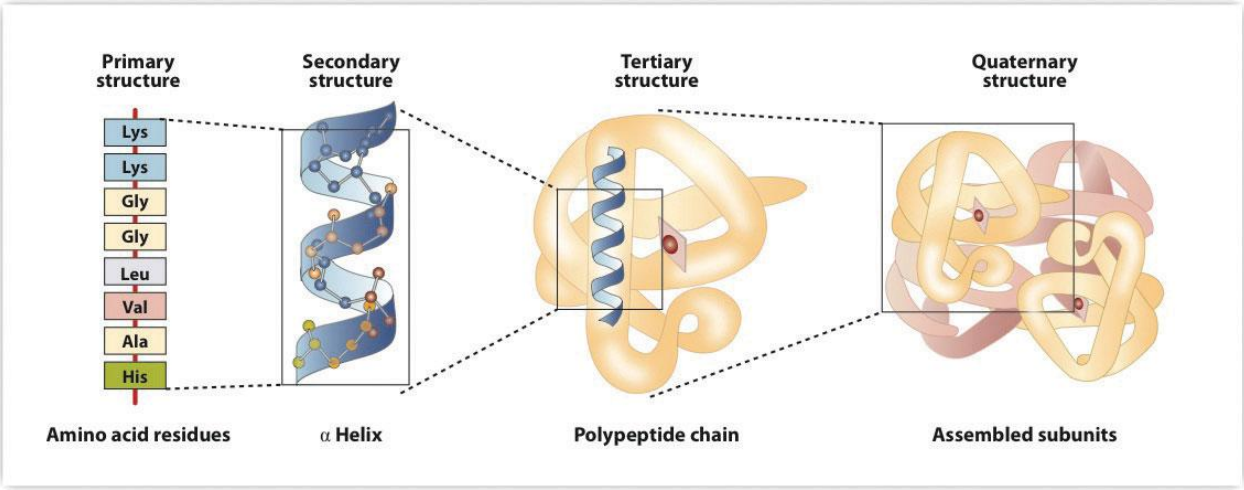

Figure 1. Peptide structures.

Immersed in water, a polypeptide chain will not stay in an elongated form, but fold up according to the polarity of the side chains which it contains and the rotation of peptide backbone bond angles largely determined by Van der Waals radii of side chains.

The geometrical character of the peptide bond is that of a rigid plane between the two flanking α-carbon atoms. The reason for this structural stability (there is no rotation around the C-N bond)

can be explained by the electronic resonance character of the O=C-N structure. The double bond character changes between the O-C and C-N bonds (Figure 2).

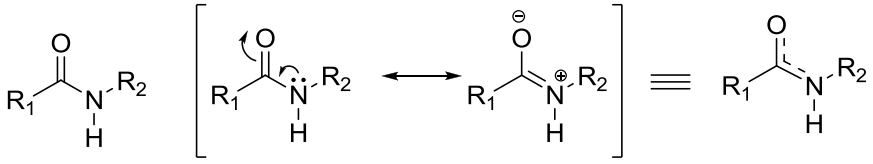

Figure 2. Electronic resonance character of peptide bond due to the π -like molecular orbital that extends over all 3 atoms (O-C-N).

Evidence for this structure comes from X-ray crystallographic studies of simple peptides showing that the N-Cα bond length is 1.46 Å as expected for a single bond. The C-N peptide bond is 1.33 Å long, only a little longer than the value of 1.27 Å for the average C=N bond length in model compounds (Figure 3). Similar X-ray studies show that the six atoms CαNHCOCα are very close to be co-planar.

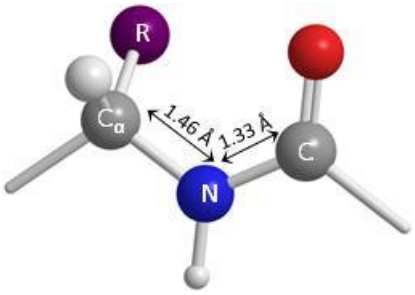

Figure 3. Bond length in peptide backbone.

To understand protein structures it is necessary to consider two torsion angles (also called dihedral angles) in the backbone which define the tilt between two neighboring amide planes (the plane of the peptide bond) with the Cα at the center of rotation:

Figure 4. The two torsion (dihedral) angles in the peptide backbone.

With those dihedral angles it is possible to predict the allowed backbone conformations of a peptide through interplay of rotation around the bonds defined by the torsion angles Phi (ϕ) and

Psi (ψ) and the steric hindrance of side groups determined by their Van der Waals radii (Figure 5). The resulting conformational map is called Ramachandran plot.

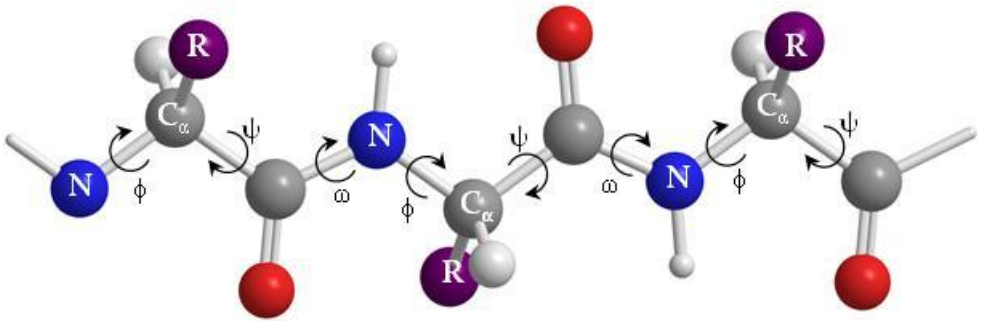

Figure 5. Peptide backbone and torsion angles.

Most areas of the Ramachandran diagram represent forbidden conformations of a polypeptide chain. Sterically forbidden conformations have ϕ and ψ values that would bring atoms closer than the corresponding Van der Waals distance (the distance of closest contact between nonbonded atoms).

Only three small regions of the diagram are physically accessible to most residues. The observed ϕ and ψ values of accurately determined structures nearly always fall within these allowed regions of the Ramachandran plot (Figure 6). There are, however, some notable exceptions:

1. The cyclic side chain of Pro limits its range of f values to angles of around 260°, making it, not surprisingly, the most conformationally restricted amino acid residue;

2. Gly, the only residue without a side chain, is much less sterically hindered than the other amino acid residues. Hence, its permissible range of f and c covers a larger area of the Ramachandran diagram. At Gly residues, polypeptide chains often assume conformations that are forbidden to other residues.

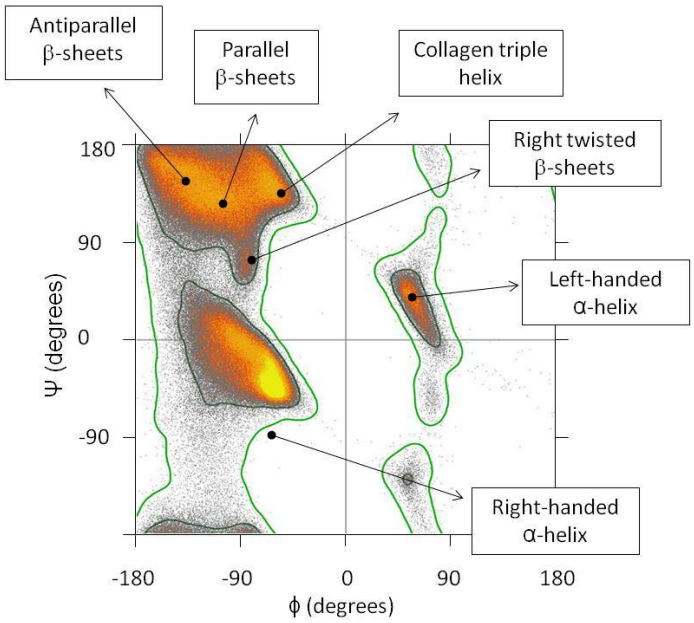

Figure 6. Ramachandran plot for all residues except Gly and Pro.

Three important regions of the Ramachandran plot describe the most commonly found secondary structures in proteins:

α -helix: a right handed helical structure with average torsion angles

β -sheet: parallel or anti-parallel pleated sheet structures

β -turn: minimal loop structures of 3 to 4 amino acids with defined torsion angles

The α -helix

The α-helix is one of two secondary structures (the other being the β-sheet) predicted and discovered by Linus Pauling and Robert B. Corey in 1951.[3] It is a right-handed helix with the following spatial parameters:

ϕ = -57°

ψ = -47°

n = 3.6 (number of residues per turn)

pitch = 0.54 nm (or 5.4 Å)

[3] Pauling, L.; Corey, R. B. "*Configurations of polypeptide chains with favored orientations around single bonds*" Proc Nat. Acad. Sci. **1951**, *37*, 729-740.

The helix has a specific hydrogen bonding pattern, where the backbone C=O group of residue n binds with the N-H of residue n+4. The atomic distance between the N and O measures 0.28 nm. The H-bonds are almost parallel to the helix axis and the total dipole moment gives the helix a dipole moment that points from the N-term (+) to the C-term (-). This helix dipole is important in the interaction of neighboring helices in the packing of secondary structural motifs into the 3-D structure. The core of the helix is packed. The backbone atoms are in Van der Waals contact with each other across the helix axis.

As a real example, in Figure 7 there's the 35-residue peptide corresponding to the very hydrophobic transmembrane region of the tyrosine kinase receptor neu, NeuTM35.[4]

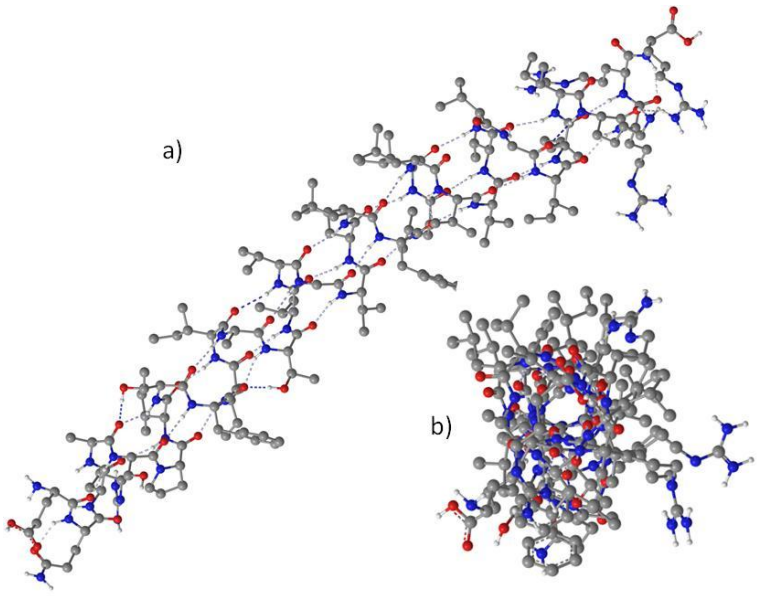

Figure 7. Balls and sticks model showing the helical arrangement of one of the chains of NeuTM35: (a) top view, (b) view along the *c* axis.

The β -strand and β-pleated sheet

In 1952, Pauling and Corey predicted the β-pleated sheet structure as an alternative secondary structure to the α -helix in proteins. β-strands are elongated peptide segments with atomic distances from side chain n to side chain n+2 of 0.7 nm. In the β conformation the backbone of the

[4] DOI:10.2210/pdb1iij/pdb

polypeptide chain is extended into a zigzag rather than helical structure. The zigzag polypeptide chains can be arranged side by side to form a structure resembling a series of pleats. In this arrangement, hydrogen bonds form between adjacent segments of polypeptide chain.

The individual segments that form a β sheet are usually nearby on the polypeptide chain, but can also be quite distant from each other in the linear sequence of the polypeptide; they may even be in different polypeptide chains. The R groups of adjacent amino acids protrude from the zigzag structure in opposite directions. The adjacent polypeptide chains in a β-sheet can be either parallel or antiparallel (having the same or opposite amino-to-carboxyl orientations, respectively) (Figure 8).

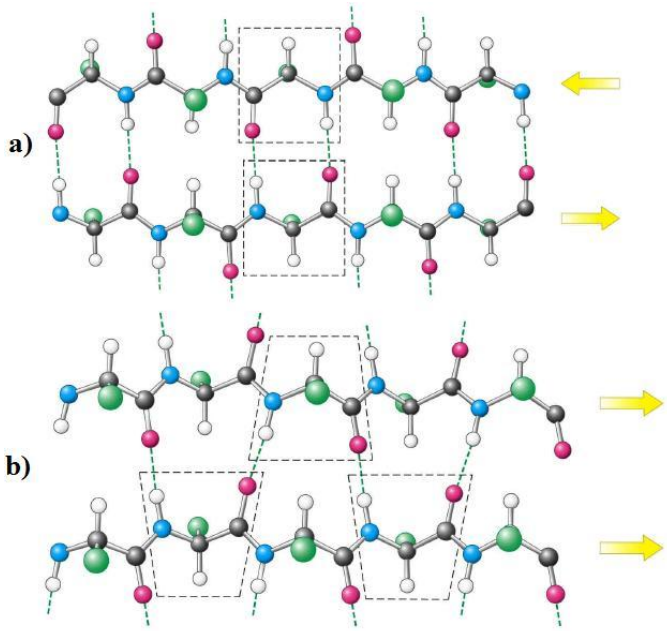

Figure 8. Backbone of parallel (a) and antiparallel (b) β-sheet.

More than two strands can form into sheets which form extended right-handed twists. Such extended β -pleated sheets (called super secondary structures) can often be found in the cores of proteins. Alternatively, bundles of 4 closely packed α -helices (so called α -helical bundles) are also found at the center of globular proteins.

The β-turns

To combine helices and sheets in their various combinations, protein structures must contain turns that allow the peptide backbone to fold back. In Figure 9 two types of β-turns are reported.

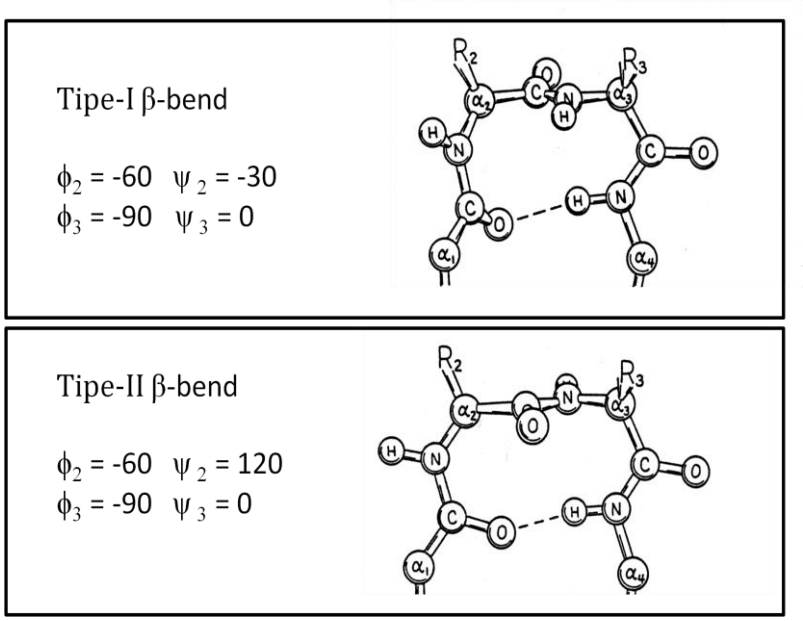

Figure 9. Backbone of Type-I β-bend and Type-II β-bend.

These turns can be found almost always on the surface of proteins and often contain Pro and/or Gly. Proline gives the backbone a special rigidity (fixed ϕ torsion angle at -60°, Ca -N) and glycine has a high flexibility because of its hydrogen substituent. Turn structures are also stabilized through H-bond formation.

Figure 10 elucidates the role of β-turns, where, two different tryptophan zippers (trpzip) are presented. On the left, the first peptide is represented in both cartoon model type (Figure 10a) and balls and sticks type (Figure 10b) where, to permit a better view, all residues are hidden.[5] In this first peptide, a type-I β-turn links two antiparallel β-bend (Figure 10a). In a similar fashion, in the second peptide (Figure 10b) a type-II β-turn links two antiparallel β-bends.[6]

[5] DOI:10.2210/pdb1le0/pdb
[6] DOI:10.2210/pdb1le1/pdb

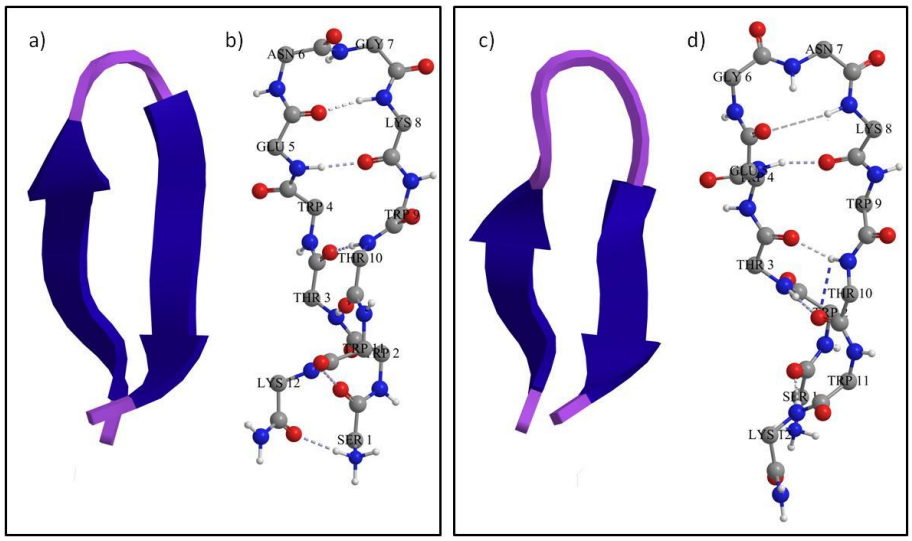

Figure 10. It is shown how two different secondary structures can coexist: in (a) type-I β-turn links two antiparallel β-bend, while in (b) a type-II β-turn links two antiparallel β-bend.

1.1.2 The role of proline in protein folding

Proline is unique among the natural amino acids in that its side chain is cyclized to the backbone, restricting its backbone dihedral angle to ϕ = -75°, giving proline an exceptional rigidity and a considerably restricted conformational space.

The structural role of proline depends on the position it occupies in a protein. When in the middle of α helices and β sheets, proline acts as a structural disruptor, but it is generally found at the beginning of α helices and edge of β sheets, as well as in turns. It has been noted that *cis-trans* isomerization of X-Pro peptide groups is one of the rate-determining steps for folding and unfolding of various proteins and several studies have investigated the *cis-trans* isomerization of proline-containing peptides.

Polyproline is known to form helical structures with two well-characterized conformations: a left-handed polyproline helix (PPII) is formed when the sequential residues all adopt backbone dihedral angles (ϕ, ψ) of (-75°, 146°), with all prolyl bonds in the *trans*-isomer conformation (i.e. backbone dihedral angle ω = 180) with 3 residues per turn; and a more compact right-handed polyproline helix (PPI) is formed with all sequential residues adopting dihedral angles of roughly (-75, 160) and all prolyl bonds assume a *cis*-isomer conformation (i.e. backbone dihedral angle ω = 0) with 3.3 residues per turn (Figure 11). Of the 20 natural amino acids, only proline is "comfortable" in the *cis*-isomer conformation, and proline seems to be quite effective in stabilizing

left-handed helices. The probability distribution for *cis-trans* prolyl bonds is affected by neighboring amino acids, pH and ionic strength, solvent and chain length.

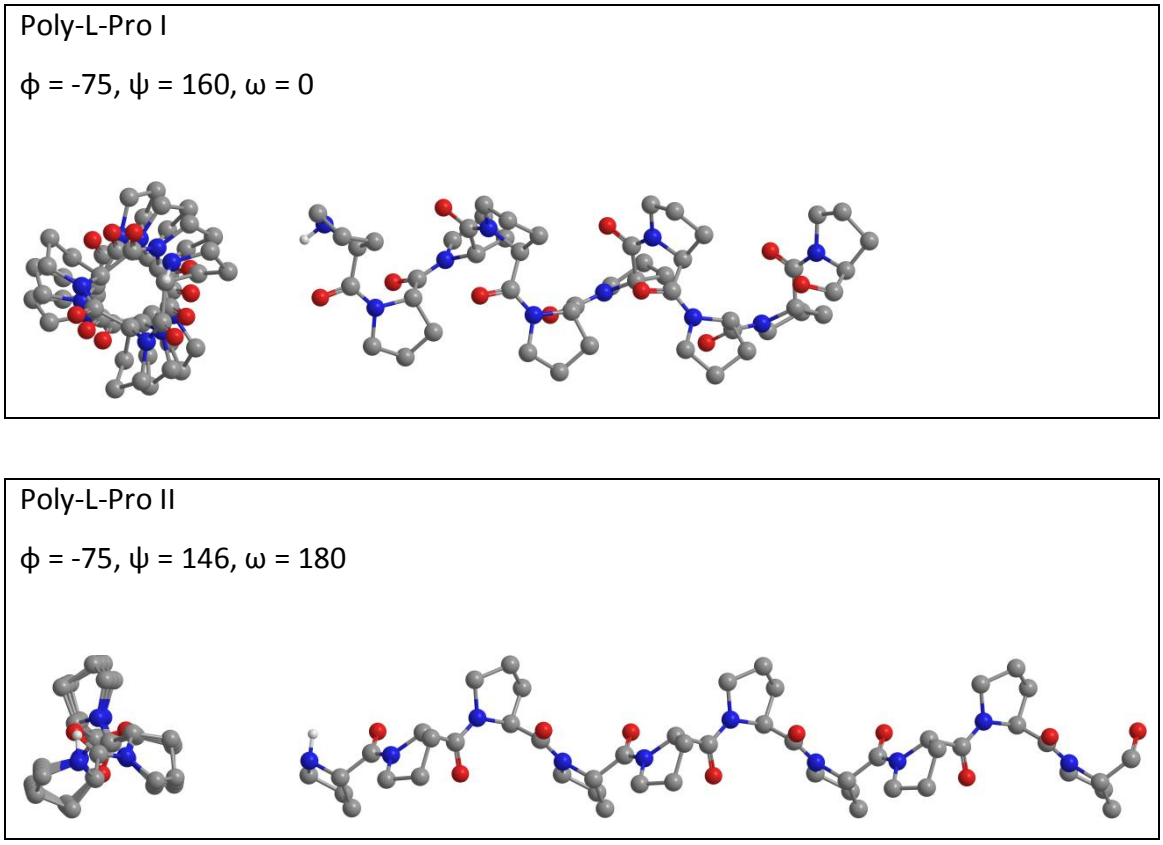

Figure 11. Balls and sticks model showing the helical arrangement of one of Poly-L-Pro I and Poly-L-Pro II.

It has been noted experimentally that the PPII structure is favored in water, benzyl alcohol, and most of the other solvents, while the PPI structure is favored in the presence of aliphatic alcohols like propanol. It is now known that the prolyl ring can flip between its two states irrespective of the *cis-trans* nature of the peptide bond.

1.2 Foldamers: the scientific answer to natural folding

As it was stated in the previous chapter, folding is the process nature has selected to control the conformation of its biomacromolecules allowing fundamental chemical functions such as enzyme catalysis, information storage and duplication in nucleic acids, as well as energy capture and conversion. In contrast, chemists can make molecules that escape evolutionary pressure. Over the years, they have worked to expand the registry of structures and functions of folded biopolymers through the use of non-natural building blocks, or through the arrangement of natural building blocks into non-natural sequences. This broad ensemble of "artificial folded molecular architectures" has been defined as "foldamers".[7]

The word "foldamers" was coined by Samuel H. Gellman in 1996[8] to describe discrete artificial oligomers that adopt specific and stable conformations similar to those seen among proteins and nucleic acids.

This neologism means "folding molecules" and refers mainly to medium size molecules (about 500-5000 amu) that fold into definite secondary structures (i.e. helices, turns and sheets), thus being able to mimic biomacromolecules despite their smaller size. The remarkable range of chemical capabilities of biomacromolecules suggests that it might be possible to design analogous capabilities into unnatural polymers that fold into compact and specific conformations. Therefore, realization of the potential of folding polymers may be limited more by the human imagination than by physical barriers. The essential requirement of a foldamer is to possess a well defined, repetitive secondary structure, imparted by conformational restrictions of the monomeric unit.

Before the term ''foldamer'' was coined, many nucleic acid analogues and peptide analogues had already been successfully designed to mimic the structures and, potentially, the biological properties of their natural counterparts. Typical examples are peptide nucleic acids (PNAs)[9] and N-substituted oligoglycines (peptoids).[10] The motivations behind such efforts are varied, but these studies suggest a collective, emerging realization that control over oligomer and polymer folding could lead to new types of molecules with useful properties.

---

[7] Hecht, S.; Huc, I. "*Foldamers: structure, properties and applications"* Wiley-VCH, Weinheim, **2007**.

[8] Gellman, S. H. *"Foldamers: a manifesto"* Acc. Chem. Res. **1998**, *31*, 173-180.

[9] Nielsen, P. E.; Egholm, M.; Berg, R. H.; Buchardt, O. *"Sequence-selective recognition of DNA by strand displacement with a thymine-substituted polyamide"* Science, **1991**, *254*, 1497-1500.

[10] Simon, R. J.; Kania, R. S.; Zuckermann, R. N.; Huebner, V. D.; Jewell, D. A.; Banville, S.; Ng, S.; Wang, L.; Rosenberg, S.; Marlowe, C. K.; Spellmeyer, D. C.; Tan, R.; Frankel, A. D.; Santi, D. V.; Cohen, F. E.; Bartlett, P. A. *"Peptoids: a modular approach to drug discovery"* Proc. Natl. Acad. Sci. U. S. A. **1992**, *89*, 9367-9371.

Over the last seventeen years, the field has rapidly expanded away from early efforts in peptidomimetics and nucleic acid analogues towards a systematic exploration of folding in a diverse range of structures.

This research sector is nowadays particularly developed because of a number of factors. The first is the desire to achieve chemical functions matching those of nature. Then, thanks' to technical improvements, biopolymers are a level of complexity that chemists can now routinely address.

To have an idea of the steady increase of this research topic, Figure 12 shows the number of papers published in the period 1996 to 2012.

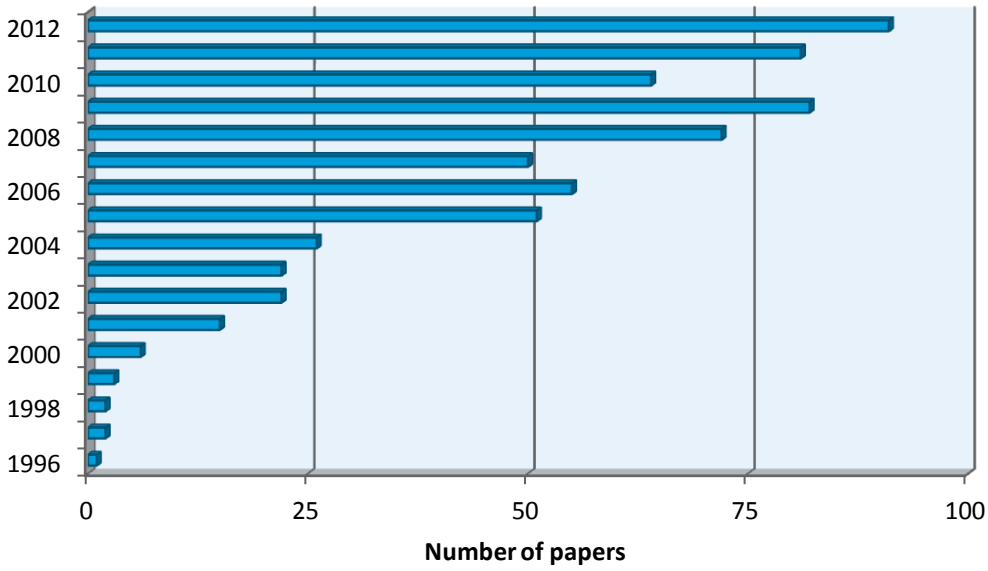

Figure 12. Number of papers which deal with foldamers published in the period 1996 to 2012.

The path to creating useful foldamers involves several steps:

i. One must identify new polymeric backbones with suitable folding propensities. This goal includes developing a predictively useful understanding of the relationship between the repetitive features of monomer structure and conformational properties at the polymer level.

ii. One must endow the resulting foldamers with interesting chemical functions, by design, by randomization and screening ("evolution"), or by some combination of these two approaches.

iii. For technological utility, one must be able to produce a foldamer efficiently, which will generally include preparation of the constituent monomers in stereochemically pure form and optimization of heteropolymer synthesis.

The propensity to fold of these new synthetic molecules is due to many internal or external parameters. Internal factors consist of the overall shape and rigidity of the molecule and its ability to establish attractive or repulsive intramolecular non-covalent interactions. These factors depend on monomer size and shape, linkage orientation, rotational restrictions, local intramolecular interactions, and interactions between monomers remote from each other in a sequence. Generally, a molecule that behaves as a foldamer has a certain degree of backbone rigidity that limits the entropic cost of adopting an organized conformation. External factors include solvent effects such as hydrophobic effects, aggregation (dimerization-induced folding), host-guest complexation (guest-induced folding), and contacts with interfaces (folding on surfaces).

The folded secondary structures of foldamers are similar to those found in biopolymers (helices, linear strands, turns and sheets). The helix in particular is by far the most frequently characterized object.

Nevertheless, foldamers that display folding motifs unknown or uncommon in biopolymers do exist. These include, for example, pillar-like architectures (stacks of aromatic rings, Figure 13),[11] knots (Figure 14)[12] and spiral-like objects ('tail-biters', Figure 15).[13]

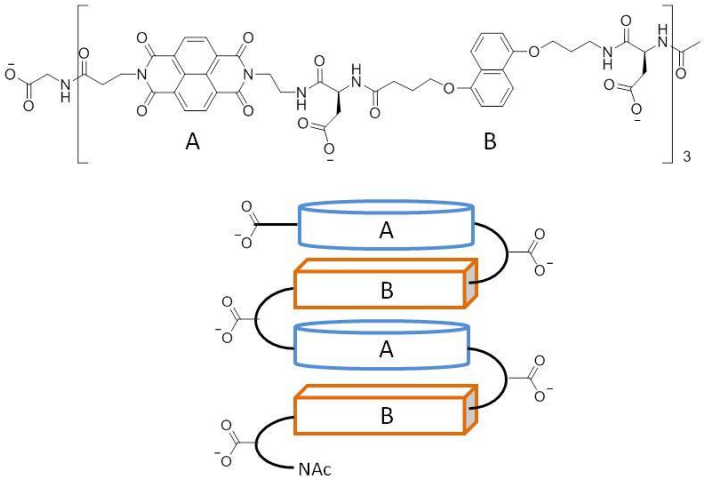

[11] Lokey, R. S.; Iverson, B. L. "*Synthetic molecules that fold into a pleated secondary structure in solution*" Nature, **1995**, *375*, 303-305.

[12] Brüggemann, J.; Bitter, S.; Müller, S.; Müller, W. M.; Müller, U.; Maier, N. M.; Lindner, W.; Vögtle, F. "*Spontaneous knotting-from oOligoamide threads to trefoil knots*" Angew. Chem., Int. Ed. **2007**, *46*, 254-259.

[13] Hunter, C. A.; Spitaleri, A.; Tomas, S. "*Tailbiter: a new amide foldamer*" Chem. Commun. **2005**, *29*, 3691-3693.

Figure 13. Pillar-like architectures due to stacks of aromatic rings A and B of the molecule.

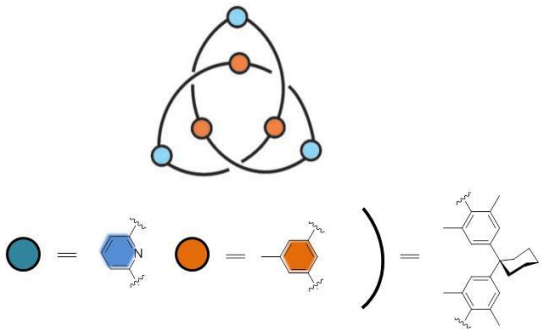

Figure 14. Example of amide knot.

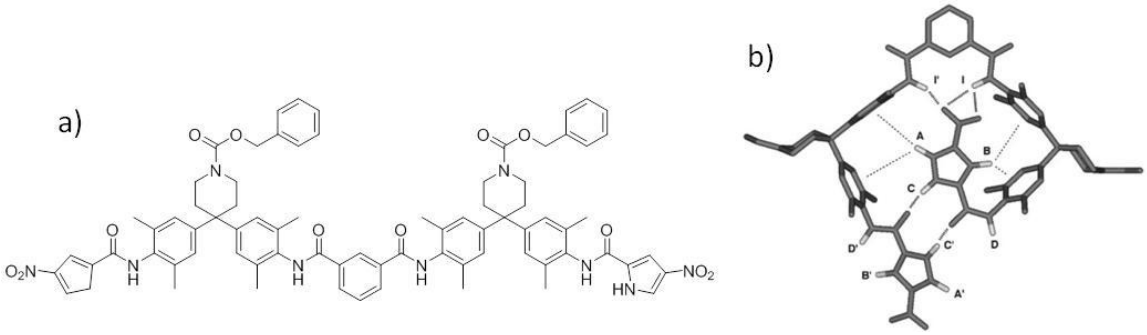

Figure 15. Structure of tailbiter foldamer (a) and its three-dimensional structure, calculated using the folding-induced changes in chemical shift.

In his work, William F. DeGrado divided foldamers into two general molecular classes, determined by the presence or absence of aromatic units within the monomer unit (Figure 16).[14]

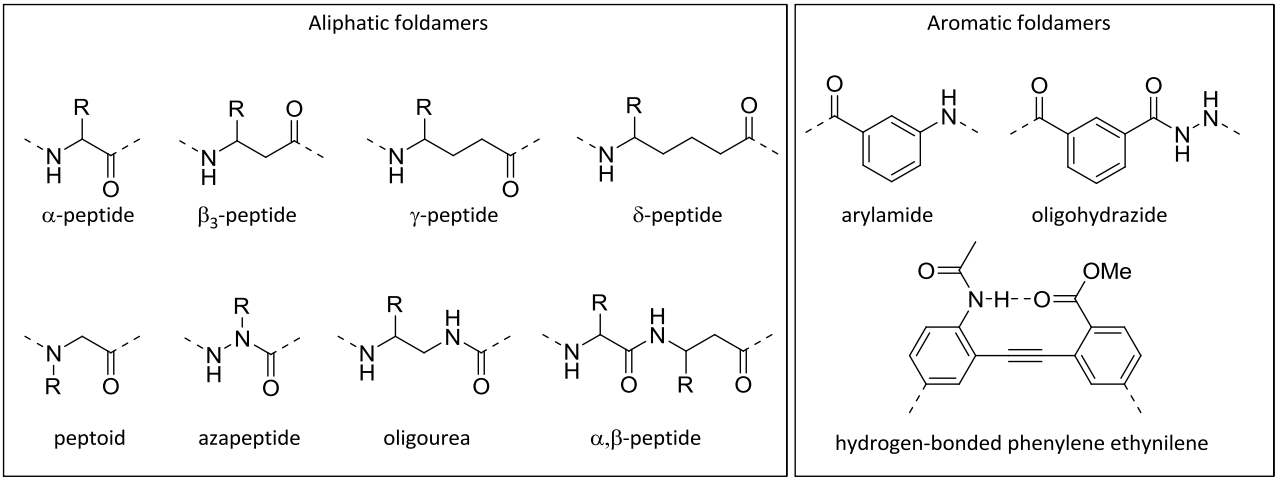

Figure 16. Examples of foldamer frameworks.

[14] Goodman, C. M.; Choi, S.; Shandler, S.; DeGrado, W. F. "*Foldamers as versatile frameworks for the design and evolution of function*" Nature Chemical Biology, **2007**, *3*, 252-262.

“Aliphatic” foldamers or, in general, foldamers synthesized using a biomimetic approach, have saturated carbon chains separating amide or urea groups. Example of this group include the β-, γ- and δ-, oligoureas, azapeptides, pyrrolinones, α-aminoxy-peptides and sugar-based peptides.

The helices formed by foldamers are characterized by their handedness and the number of atoms within repeating hydrogen bonding rings of their structures. A second feature of the helix is the orientation of the amide groups; hydrogen bonding generally causes the carbonyl of successive amides to either point toward the N terminus or the C terminus, thereby giving rise to exposed amides at the ends of the helices. While in conventional peptides, the main conformations are 3_{10}- and α-helices, very different conformations are observed when additional methylene groups are inserted between the amides of the monomers. The second molecular class of foldamers makes use of aromatic spacers within the backbone. Examples of this group include oligo-phenylene-ethynylenes, sequences of alternating aromatic electron donors and acceptors, aryl-oligomers in particular those based on aza-heterocycles (pyridines, pyrimidines, pyridazines, etc.), aromatic tertiary amide, imide or urea oligomers and aromatic oligoamides (Figure 17).

The latter ones have been rapidly growing as an important class of foldamers due to a number of remarkable properties, including the high stability of their folded structures, the predictability of their folding modes, their propensity to crystallize (giving access to structural data at atomic resolution), and their relative ease of synthesis. There is no doubt that foldamer diversity will further increase even though designing, synthesizing, and structurally characterizing a new foldamer can all prove very challenging.

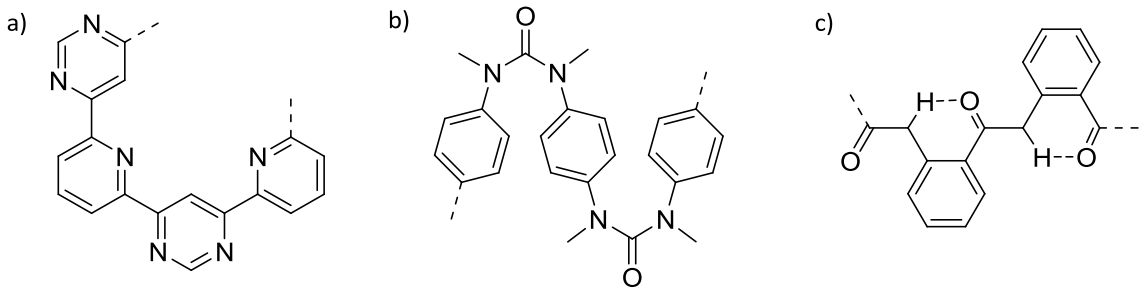

Figure 17. a) Aza-aromatic oligomers. b) Tertiary aromatic ureas. c) Aromatic oligoamides.

Recently, several examples of hybrid foldamers have been reported, containing mixtures of α- and β-, α- and γ- or β- and γ-amino acids in alternating order.[15] These foldamers allow the formation of new kind of helices, besides those that may be obtained only from α-, β- or γ-peptides, as shown in Figure 18.

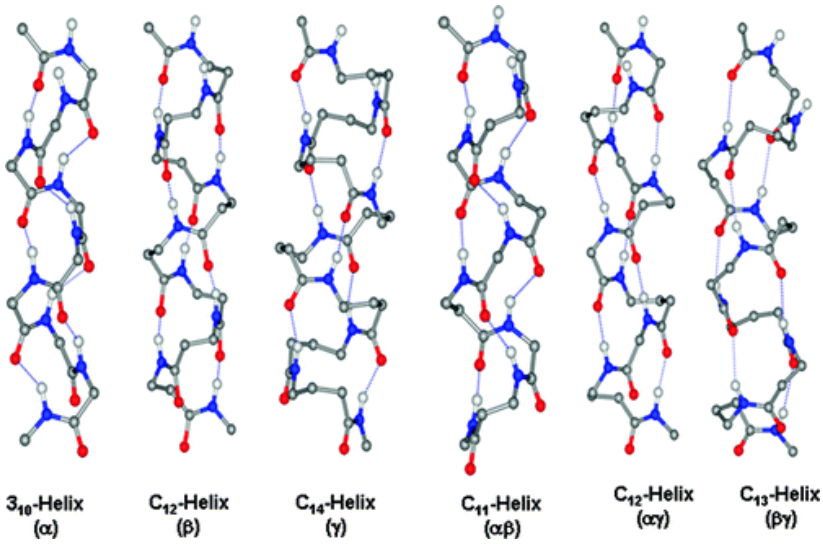

Figure 18. Helices with 4→1 hydrogen-bond patterns in α, β, γ and hybrid peptides.

The virtues of alternating longer sequences of α- and β-amino acids, so called α/β-peptide foldamers, have been recognized only a few years ago. During this course, several new helix types have also been discovered. In the year 2004, two groups independently investigated the solution properties of α/β-peptides with a 1:1 backbone alternation.[16]

Beside helical structures with hydrogen bonds pointing only into one direction, either backward or forward along the sequence, also mixed helices (β-helices) with hydrogen bonds alternately changing in forward and backward direction were found in these regular hybrid peptides.[17]

[15] Prema Vasudev, G.; Chatterjee, S.; Shamala N.; Balaram, P. "*Structural chemistry of peptides containing backbone expanded amino acid residues: conformational features of β, γ, and hybrid peptides*" Chem. Rev. **2001**, *111*, 657-687.
[16] Hayen, A.; Schmitt, M. A.; Ngassa, F. N.; Thomasson K. A.; Gellman, S. H. "*Two helical conformations from a single foldamer backbone: "Split Personality" in Short α/β-Peptides*" Angew. Chem. Int. Ed. **2004**, 43, 505-510.
[17] Baruah, P. K.; Sreedevi, N. K.; Gonnade, R.; Ravindranathan, S.; Damodaran, K.; Hofmann, H.-J.; Sanjayan, G. J. "*Enforcing periodic secondary structures in hybrid peptides: a novel hybrid foldamer containing periodic γ-turn motifs*" J. Org. Chem. **2007**, 72, 636-639.

1.3 New pseudopeptide foldamers based on oxazolidinone ring

Peptidomimetic modifications are frequently used as attractive methods to provide more conformationally constrained and thus more stable and bioactive peptides. Among peptidomimetic approaches, particularly attractive are pseudopeptides, or peptide bond surrogates in which peptide bonds have been replaced with other chemical groups.

In the previous chapter, it was stressed the central role of proline in the conformational behaviour of peptides which contain it. From a synthetic point of you, the direct use of proline is not recommended because of its *cis-trans* isomerization problems. The possibility of controlling this isomerisation is very important in the design of peptidomimetics. As a consequence, many proline surrogates have been designed for the study and control of conformational transitions in peptides and proteins. For instance, many pseudoprolines (ψ-Pro) have been obtained by cyclocondensation of the amino acids cysteine, threonine or serine with aldehydes or ketones.

In the last few years the design and synthesis of oligomers based on proline units, both in the presence and absence of stabilizing hydrogen bonds, have been extensively pursued.

1.3.1 Conformational studies of oxazolidin-2-one derivatives

Five-membered cycles that contain a nitrogen and a carboxy unit adjacent to one another in the ring may be assigned to the family of pseudoprolines. The research group of professor Claudia Tomasini demonstrated that the presence of pseudoproline units like L-pyroglutamic acid and *trans*-(4*S*,5*R*)-4-carboxy-5-methyl oxazolidin-2-one (L-Oxd) in more complex molecular architectures can lead to the formation of stable conformations, both in solution and in solid state (Figure 19).

The acylation product of those pseudoprolines leads to a particular backbone, in which the nitrogen atom of the ring is adjacent to both an exocyclic and an endocyclic carbonyl group, forcing them to a strict *trans* conformation. This effect is due to the tendency of the two carbonyl groups to orient themselves apart from one another.

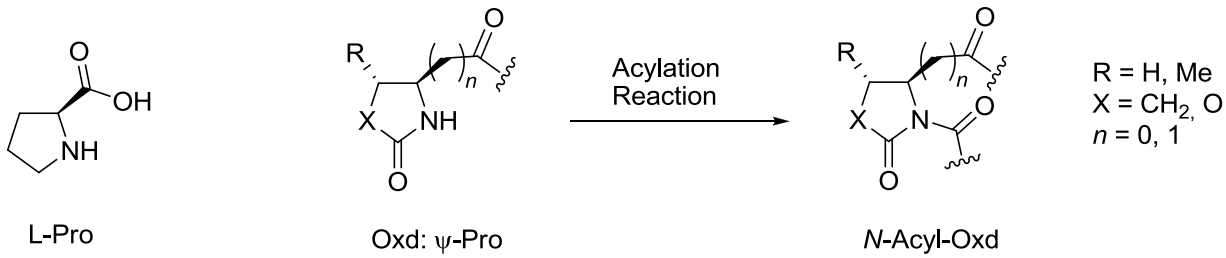

Figure 19. The L-Oxd is a pseudoproline. In the figure is also shown the preferential conformation of the *N*-acylated form.

The particular behaviour of this kind of derivatives was confirmed with several techniques.

An interesting outcome was obtained from the analysis of the ^{1}H NMR spectrum of oligopseudopeptide Boc-L-Ala-L-Ala-*p*Glu-OBn. This compounds shows a signal centered at 5.6 ppm (Figure 20), which corresponds to the α-hydrogen of protected alanine and is very deshielded compared with Boc-L-Ala-L-Pro-OBn (δ=4.46 ppm).

This outcome should be ascribed to the presence of the carbonyl of the γ-lactam which strongly deshields H_a that is nearby the carbonyl, so that the peptide bond is in the *trans* conformation.[18]

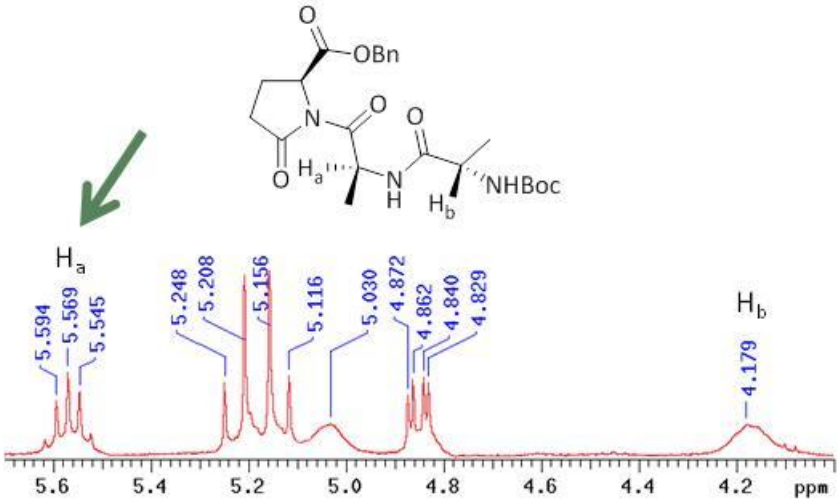

Figure 20. The chemical shifts of H_a proton clusters in a region significantly downfield from that common to peptide H_b protons.

The ^{1}H NMR spectrum of the dimer Boc-L-Oxd-L-Oxd-OBn shows the same deshielding effect, as the chemical shift of the heterocycle A hydrogen H_a resonates at 5.49 ppm, while H_b resonates at 4.59 ppm (Figure 21).[19]

[18] Villa, M.; Tomasini, C. "*Pyroglutamic acid as a pseudoproline moiety: a facile method for its introduction into polypeptide chains*" Tetr. Lett. **2001**, *42*, 5211-5214.

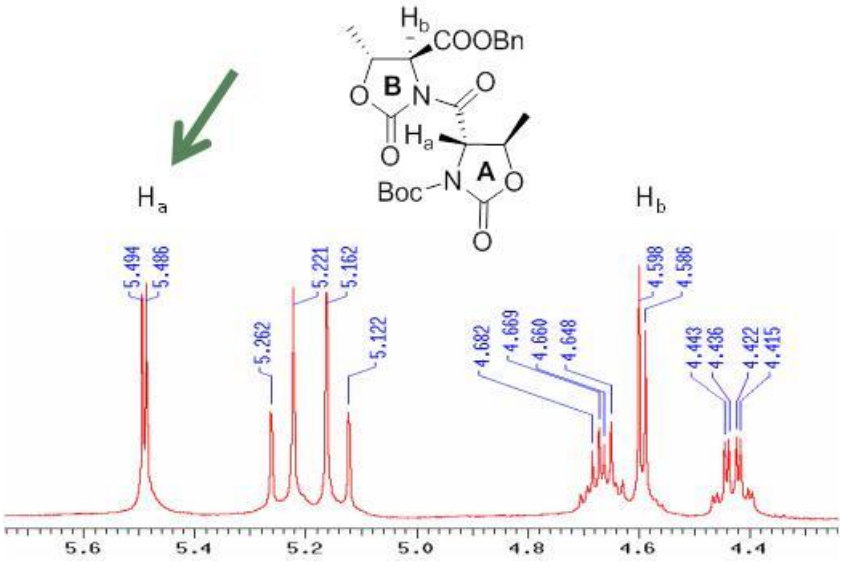

Figure 21. The doublet due to H_a proton is particularly deshielded if compared to the signal of H_b proton.

Finally, the occurrence of a nonconventional, weak C-H···O=C hydrogen bond interaction was confirmed by X-ray diffraction for the Boc-(L-*p*Glu)$_2$-OH dipeptide (Figure 22).[20]

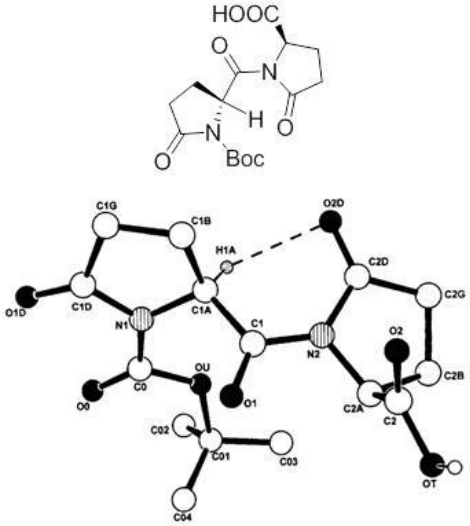

Figure 22. X-ray diffraction structure of Boc-(L-*p*Glu)$_2$-OH.

A further confirmation of a preferred and ordered geometry was obtained by Circular Dichroism measurements (CD).

[19] Lucarini, S.; Tomasini, C. "*Synthesis of oligomers of* trans*-(4S,5R)-4-carboxybenzyl 5-methyl oxazolidin-2-one: an approach to new foldamers*" J. Org. Chem. **2001**, *66*, 727-732.

[20] Bernardi, F.; Garavelli, M.; Scatizzi, M.; Tomasini, C.; Trigari, V.; Crisma, M.; Formaggio, F.; Peggion, C. and Toniolo, C. "*Pseudopeptide foldamers: the homo-oligomers of pyroglutamic acid*" Chem. Eur. J. **2002**, *8*, 2516-2525.

CD is a valuable tool that can reveal important characteristics of the secondary structure of biological molecules like sugars, proteins, nucleic acids, peptides.

CD spectroscopy measures differences in the absorption of left-handed polarized light versus right-handed polarized light which arise due to structural asymmetry. The absence of regular structure results in zero CD intensity, while an ordered structure results in a spectrum which can contain both positive and negative signals.

Indeed, analyzing the ellipticity as a function of the wavelength, it is possible to build a mathematical model of the tridimensional geometry of the molecule, like helix or β-sheet.

To understand the role of oxazolidinones moieties in the formation of stable structures, a lot of different oligomers where synthesized. The simplest ones are L-Oxd homo-oligomers (Figure 23). Solution conformation analysis were done using FTIR absorption, ^{1}H NMR and CD techniques.[21]

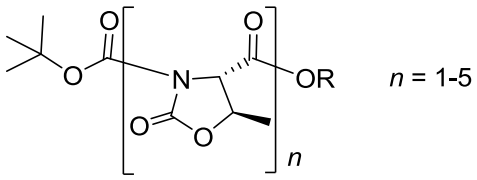

Figure 23. Chemical structure of the Boc-(L-Oxd)$_n$-OBn species investigated.

The CD spectra series (Figure 24) suggests conclusions similar to those observed for the L-*p*Glu series in a previews work, where Tomasini discovered the formation of a new type of helical structure, similar to that adopted by poly-(L-Pro)$_n$ with *trans* tertiary peptide bonds (type II).

[21] Tomasini, C.; Trigari, V.; Lucarini, S.; Bernardi, F.; Garavelli, M.; Peggion, C.; Formaggio, F.; Toniolo, C. "*Pseudopeptide Foldamers − The Homo-oligomers of benzyl (4S,5R)-5-Methyl-2-oxo-1,3-oxazolidine-4-carboxylate*" Eur. J. Org. Chem. **2003**, 259-267.

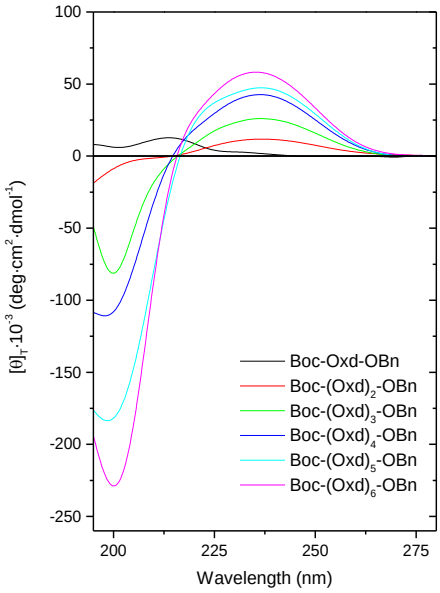

Figure 24. Normalized per-residue CD spectra (1 mm in MeOH) of Boc-(L-Oxd)$_n$-OBn (n = 1-6).

The simplest hybrid oligomers that can be prepared have the general formula Boc-(Gly-L-Oxd)$_n$-OBn (Gly = glycine) (Figure 25).[22]

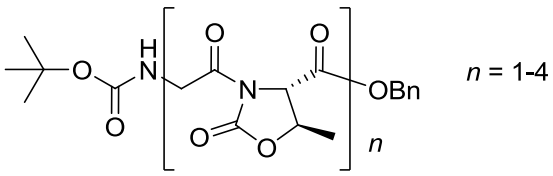

Figure 25. Chemical structure of the Boc-(Gly-L-Oxd)$_n$-OBn species investigated.

The regular increase in C=O···H-N hydrogen bonds from n = 1 to n = 4 suggested by the IR analysis was also detected on investigation of the DMSO-d_6 dependence of the NH proton chemical shift. The per-residue CD signals change on going from n = 1 to n = 4 with a dramatic increase in absorbance, thus showing that an extra effect besides the chromophore absorption is present. This can be attributed to the formation of hydrogen bonds and, as a result, of a secondary structure.

[22] Luppi, G.; Soffrè, C.; Tomasini, C. "*Stabilizing effects in oxazolidin-2-ones-containing pseudopeptides*" Tetrahedron: Asymmetry, **2004**, *15*, 1645-1650.

To investigate the preferred conformations of oligomers of the Boc-(AA-Oxd)$_n$-OBn series further, Gly was replaced with Ala, thus introducing a methyl group as a side chain.[23] The relative stoichiometry of residues is crucial for the formation of well-ordered secondary structures.

Oligomers of both the Boc-(L-Ala-L-Oxd)$_n$-OBn (Ala = alanine) (Figure 26) and the Boc-(L-Ala-D-Oxd)$_n$-OBn (Figure 27) series were therefore synthesized, in order to check whether the Gly pro-*S* hydrogen or the pro-*R* hydrogen should be replaced. FT-IR and NMR techniques revealed that only the monomeric unit L-Ala-D-Oxd permits the formation of internal hydrogen bonds, confirming that only one side of the previous glycine face was actually involved in the helix formation.

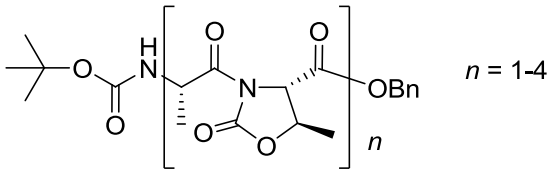

Figure 26. Chemical structure of the Boc-L-Ala-L-Oxd-OBn series.

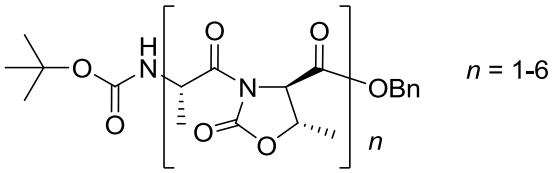

Figure 27. Chemical structure of the Boc-L-Ala-D-Oxd-OBn series.

Further confirmation of helix formation in the longer oligomers of the Boc-(L-Ala-D-Oxd)$_n$-OBn set was obtained by recording the CD spectra of all the free acid derivatives of two series in MeOH solution. The per-residue CD spectra of the Boc-(L-Ala-L-Oxd)$_n$-OH set (not shown) do not exhibit any significant change from the monomers to the higher oligomers, thus showing that no configuration-based effects take place.

The per-residue CD spectra of the Boc-(L-Ala-D-Oxd)$_n$-OH set are shown in Figure 28. Ellipticity increases, associated with reversal of the Cotton effect, were observed for Boc-(L-Ala-D-Oxd)$_5$-OH and, more dramatically, for Boc-(L-Ala-D-Oxd)$_6$-OH, thus suggesting the formation of ordered secondary structures. To define their natures, the CD spectrum of Boc-(L-Ala-D-Oxd)$_6$-OH,

[23] Tomasini, C.; Luppi, G.; Monari, M. "*Oxazolidin-2-one-Containing Pseudopeptides That Fold into β-Bend Ribbon Spirals*" J. Am. Chem. Soc. **2006**, *128*, 2410-2420.

recorded at different concentrations (not shown), does not show any change as the concentration decreases: this finding excludes formation of self-associated secondary structures.

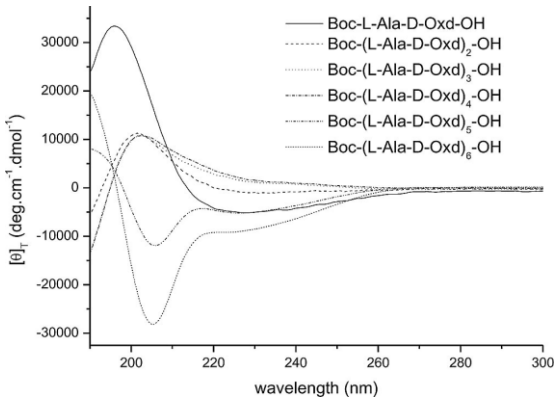

Figure 28. Normalized per-residue CD spectra of Boc-(L-Ala-D-Oxd)$_n$-OH (n = 1-6, 1 mm in MeOH)

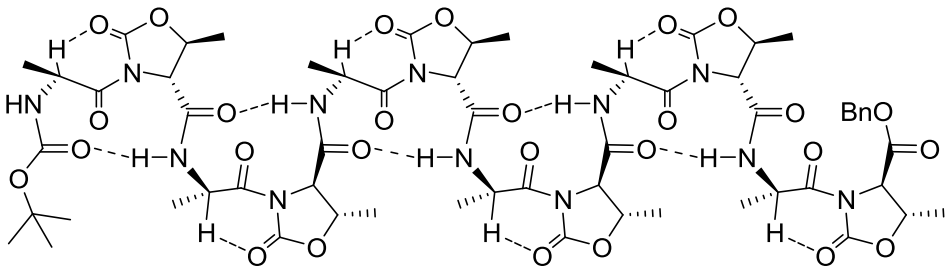

Figure 29. Conformation of Boc-(L-Ala-D-Oxd)$_6$-OBn, with the three stabilizing effects shown: (a) the rigid -CO-N(CH)-CO- moiety, (b) the C=O···H-C H-bonds and (c) the C=O···H-N H-bonds.

Of the ordered peptide secondary structures that could be formed, the CD spectra of the α and 3_{10} helixes and the β pleated sheet conformations were considered. From a general inspection of the spectra shown in Figure 28, Boc-(L-Ala-D-Oxd)$_5$-OH and Boc-(L-Ala-D-Oxd)$_6$-OH clearly fold in the 3_{10} helix configuration. More precisely, a β bend ribbon spiral structure can be attributed to Boc-(L-Ala-D-Oxd)$_5$-OH and Boc-(L-Ala-D-Oxd)$_6$-OH. It may be considered a subtype of the polypeptide 3_{10} helix, being stabilized by alternate intramolecular C=O···H-N H-bonds and having approximately the same folding of the peptide chain (Figure 29).

The last example of hybrid oligomers reported here is the Boc-(L-Phe-D-Oxd)$_n$-OBn series. The structures of Boc-(L-Phe-D-Oxd)$_n$-OBn (n = 2-5) (Figure 30) were investigated both in solution and in the solid state.[24]

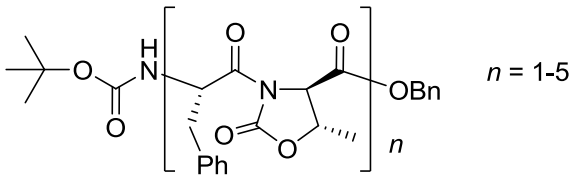

Figure 30. Chemical structure of the Boc-L-Phe-D-Oxd-OBn series.

Again, information on the preferred conformations of the oligomers in solution was obtained by analysis of FTIR, ^{1}H NMR and CD absorption spectra. All data suggest that at least four L-Phe-D-Oxd units are required to obtain a folded structure, as was also observed for the oligomers of the L-Ala-D-Oxd series; in the higher oligomers, the tendency to form ordered secondary structures increases and seems to be fully manifested at the pentamer level. Unfortunately, CD spectroscopy did not provide conclusive results, due to the strong absorptions of the phenyl groups around 200 nm.

[24] Angelici, G.; Falini, G.; Hofmann, H.-J.; Huster, D.; Monari, M.; Tomasini, C. "*Nanofibers from oxazolidi-2-one containing hybrid foldamers: What is the Right Molecular Size?*" Chem. Eur. J. **2009**, *15*, 8037-8048.

2 In-solution conformational studies

2.1 Conformational studies of Phe-rich foldamers by VCD spectroscopy and *ab-initio* calculations

In the previous chapters, the conformational analysis in the liquid phase of hybrid foldamers that contain the pseudoprolines group Oxd, was described. The carbonyl present into the cycle introduces a constrain into the chain that forces the pseudo-peptide bond always into the *trans* conformation, favoring the secondary structures formation, even in the presence of a relatively small number of residues.

As mentioned in the previous chapter, the relative configuration of the Oxd and the alternated amino acid is very important, since the L-Ala-D-Oxd series tends to form β-bend ribbon spirals, while the L-Ala-L-Oxd series does not. In the present chapter, longer oligomers of the same series with general formula Boc-(L-Phe-L-Oxd)$_n$-OR (where n = 2-5 and R = H or OBn), are described.

The conformational analysis has been carried out by ^{1}H NMR, IR, ECD (electronic circular dichroism), and VCD (vibrational circular dichroism) spectroscopy, accompanied by *ab-initio* calculations. In particular, the latter two techniques can be very useful in the determination of the preferred secondary structure of this class of foldamers.

2.1.1 VCD Technique

Spectroscopic techniques have been potential tools in the secondary structure analysis of proteins and peptides, both qualitatively and quantitatively. Electronic circular dichroism (ECD) and Fourier transform infrared (FTIR) spectroscopy were widely used in protein structural analysis under various conditions. Vibrational circular dichroism (VCD) spectroscopy is a relatively new technique for the study of conformational preference of proteins and peptides. It measures the differential absorbance of left and right circularly polarized light in the infrared region originating from molecular vibrations. VCD can provide important conformational information in cases where ECD is complicated by the overlap of backbone amide and side-chain aromatic chromophores. This feature is particularly relevant for the studies of peptides containing aromatic amino acid residues that contribute significantly to electronic absorption in the near-UV region (190-230 nm), which is generally considered to arise exclusively from the backbone amide contribution. The conformational preferences of proteins in aqueous solutions have been studied using VCD. These

previous studies have shown that the amide I vibrational bands give characteristic VCD spectra for α helix, β-sheet, combination of α and β, random coil, and β-turn structures in solutions.

The VCD method of analysis involves comparison of the experimentally measured VCD spectrum to the one calculated from *ab-initio* quantum chemistry.

The block diagram for the optical layout of a FT-VCD spectrometer is given in Figure 1.

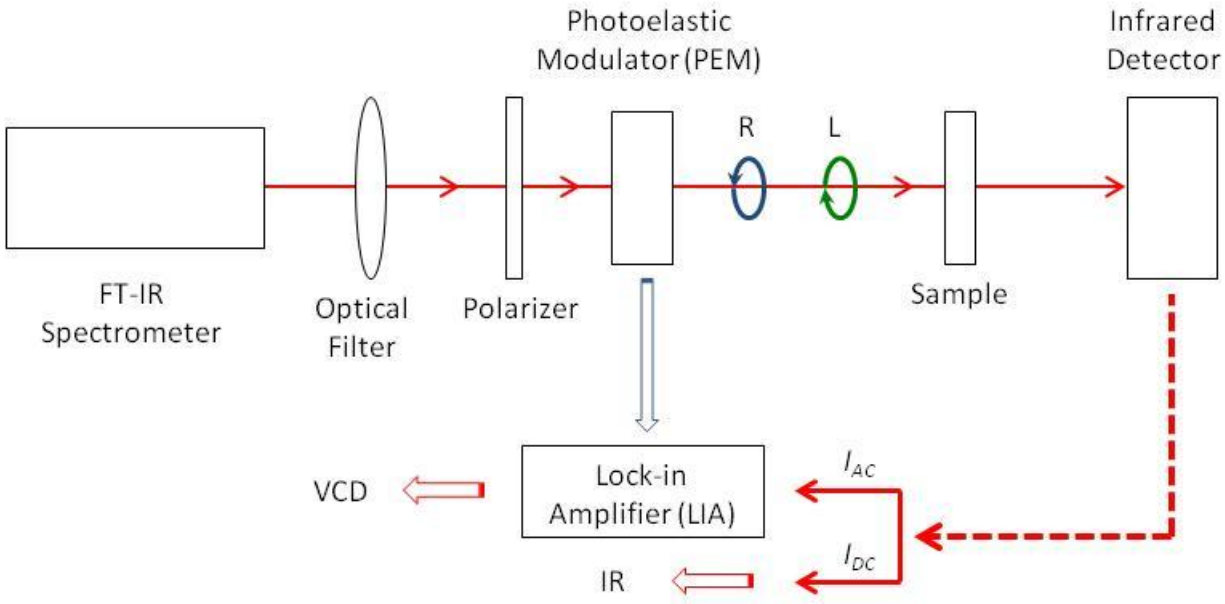

Figure 31. Block diagram for the optical layout of a FT-VCD spectrometer.

IR radiation from a glower source is directed through an interferometer that encodes each spectral point with a Fourier frequency. The radiation from the interferometer passes through an optical filter so that it is linearly polarized to define a single state of polarization. Then the IR beam passes through a photoelastic modulator (PEM) (that sine-wave modulates the polarization between LCP and RCP states in the frequency range of tens of kilohertz) and finally propagates through the sample, which imposes an intensity modulation on the beam at the PEM frequency of Fourier frequencies in the spectrum where there is VCD. A cooled infrared detector then converts the IR beam intensity to an electrical signal that is processed by the subsequent electronics. There are two electronic pathways. One is the usual pathway for the measurement of the IR spectrum, and the other pathway includes a lock-in amplifier tuned to the PEM frequency, which demodulates the spectral information at the frequency and leads to the VCD spectrum.

In VCD analysis is important to assess the conformational flexibility and to determine which conformers are significantly populated under the experimental measurements conditions. To

identify low energy conformation, a conformational search can be carried out at the molecular mechanics level, with software such as HyperChem (Hypercube, Gainesville, FL), Spartan (Wavefunction, Irvine, CA), Macro-Model (Schrodinger, Portland, OR), Irsight II (Accelrys, San Diego CA) or Confort (Tripos, St. Louis, MO).

For molecules with few conformers, it is often beneficial to calculate the optimized conformers and energies at a semiempirical level (PM3 or AM1) in order to identify the starting conformations for DFT calculations.

For identification of dominant solution conformations, the observed IR and VCD spectra are compared with overlays of the calculated spectra for a group of low-energy conformers. Based on the calculated relative energies for conformers (usually within 1 kcal/mol above the lowest energy conformers), the fractional Boltzmann populations at the measurement temperature is calculated:

$$\frac{N_i}{N_0} = \exp(-\Delta E_i / RT)$$

$$\sum_i N_i = 1$$

N_0 = population of the lowest energy conformer

N_i = population of conformer *i*

Composite IR and VCD spectra are generated by weighting with Boltzmann populations and are afterwards compared with their experimental counterparts. Such comparison allows identification of the dominant conformations in solution, besides the absolute configuration. This is one of the major advantages of the VCD technique over X-ray analysis, the latter providing only the lattice conformation.

When large deviations are found in comparing composite calculated spectra with experimental spectra, the presence of additional conformations and/or unanticipated solvent effects should be explored. Such events are usually met when molecules prone to hydrogen bonding or other strong intermolecular associations are investigated.

2.1.2 Synthesis

Boc-L-Phe-L-Oxd-OBn **1** can be prepared in high yield by addition of Boc-L-Phe-OH to L-Oxd-OBn in the presence of HBTU and TEA in dry acetonitrile (Scheme 1). The L-Oxd-OBn moiety can easily be synthesized in multigram scale starting from L-Thr.[25]

The oligomer series Boc-(L-Phe-L-Oxd)$_n$-OBn (*n* = 2, 3, 4, 6) **4**-**10** have been synthesized in solution. Boc-(L-Phe-L-Oxd)-OH **2** has been obtained by selective deprotection of the C-terminal benzyl ester with H_2 in methanol in the presence of Pd/C (5%), and H-L-Phe-L-Oxd-OBn·CF_3CO_2H **3** was prepared by cleavage of the N-terminal Boc moiety with anhydrous TFA in dichloromethane (Scheme 1).

Then, **2** and **3** were coupled using HBTU and TEA in dry acetonitrile in an inert atmosphere providing **4** in satisfactory yield. By deprotection of the carbobenzoxy group with H_2 in methanol in the presence of Pd/C (5%), the corresponding acid **5** was prepared. Repetition of these two steps produces Boc-(L-Phe-L-Oxd)$_3$-OBn **6** in good yield. The longer oligomers Boc-(L-Phe-L-Oxd)$_4$-OBn **8** and Boc-(L-Phe-L-Oxd)$_6$-OBn **10** have been obtained by coupling Boc-(L-Phe-L-Oxd)$_2$-OH **5** and Boc-(L-Phe-L-Oxd)$_4$-OH **9**, respectively, with H-(L-Phe-L-Oxd)$_2$-OBn·CF_3CO_2H **7** using HBTU and TEA in dry acetonitrile.

All the deprotection steps were performed with excellent yields, while the coupling step yields ranged between 68 and 84%. The purification by flash chromatography of the longer oligomers proved to be difficult due to the low solubility of Boc-(L-Phe-L-Oxd)$_3$-OBn **6**, Boc-(L-Phe-L-Oxd)$_4$-OBn **8**, and Boc-(L-Phe-L-Oxd)$_6$-OBn **10** in any solvent, as all the products were blocked in the silica gel and the yields dramatically decreased. This obstacle was overcome by performing the purification with the help of an ultrasound bath. The reaction crude was dissolved in ethyl acetate and washed with water to eliminate the water-soluble byproduct (HOBt in part, unreacted amines and acids, etc.), and then it was concentrated and the solvent replaced with cyclohexane. This mixture was sonicated so that the byproduct, tetramethylurea, and the remaining part of HOBt dissolved in the apolar solvent, and the desired product could be recovered pure after filtration. Following this procedure, the oligomers **6**, **8**, and **10** were obtained pure in satisfactory yields.

[25] Tomasini, C.; Trigari, V.; Lucarini, S.; Bernardi, F.; Garavelli, M.; Peggion, C.; Formaggio, F.; Toniolo, C. "*Pseudopeptide Foldamers. The Homo-oligomers of the Benzyl (4S,5R)-5-Methyl-2-oxo-1,3-oxazolidine-4-carboxylate*" *Eur. J. Org. Chem*. **2003**, 259-267.

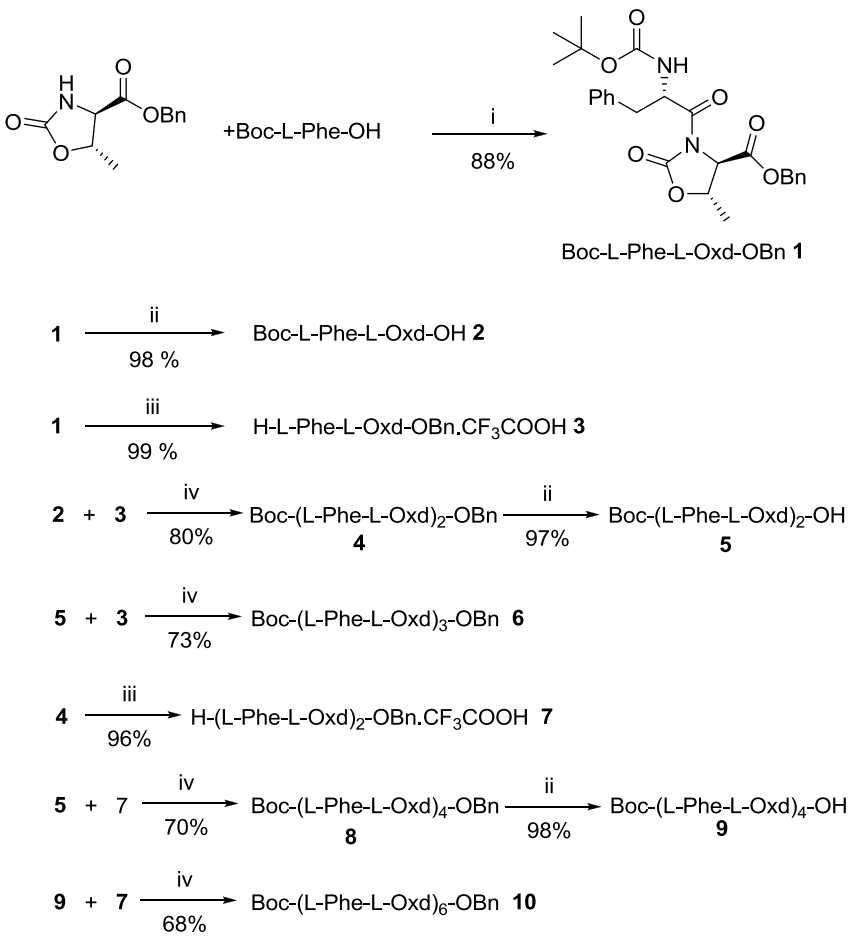

Scheme 1. (i) HBTU (1.1 equiv), TEA (2 equiv), dry CH3CN, r. t. = 1 h; (ii) H2, Pd/C (10%), MeOH, r. t. = 16 h; (iii) TFA (18 equiv), dry CH_2Cl_2, r. t. = 4 h; (iv) HBTU (1.1 equiv), TEA (3 equiv), dry CH_3CN, r. t. = 1 h.

2.1.3 Conformational Analysis in solution

Information on the preferred conformation of the oligomers in solution was obtained by the analysis of FT-IR, ^{1}H NMR, ECD, and VCD absorption spectra and by DFT (density functional theory) quantum chemical calculations on Boc-L-Phe-L-Oxd-OBn.

For a conformational analysis in solution, IR-spectroscopy is very useful because the analysis of the N-H stretching regions helps one to detect if intramolecular N-H···O=C hydrogen bonds are formed, since nonhydrogen-bonded amide NH bonds exhibit a stretching signal above 3400 cm^{-1}, while hydrogen-bonded amide NH bonds[26] produce a stretching band below 3400 cm^{-1}.

The FT-IR spectra were recorded for 3 mM solutions in both methylene chloride (aprotic polar solvent) and carbon tetrachloride (apolar solvent). This low concentration was chosen in order to avoid possible self-aggregation and due to the low solubility of the longer oligomers **6**, **8**, and **10**.

[26] Yang, J.; Gellman, S. H. *"Energetic superiority of two-center hydrogen bonding in a model system"* J. Am. Chem. Soc. **1998**, *120*, 9090-9091.

Figure 32 shows the FT-IR absorption spectra of the oligomers **1**, **4**, **6**, **8**, and **10** in methylene chloride and carbon tetrachloride.

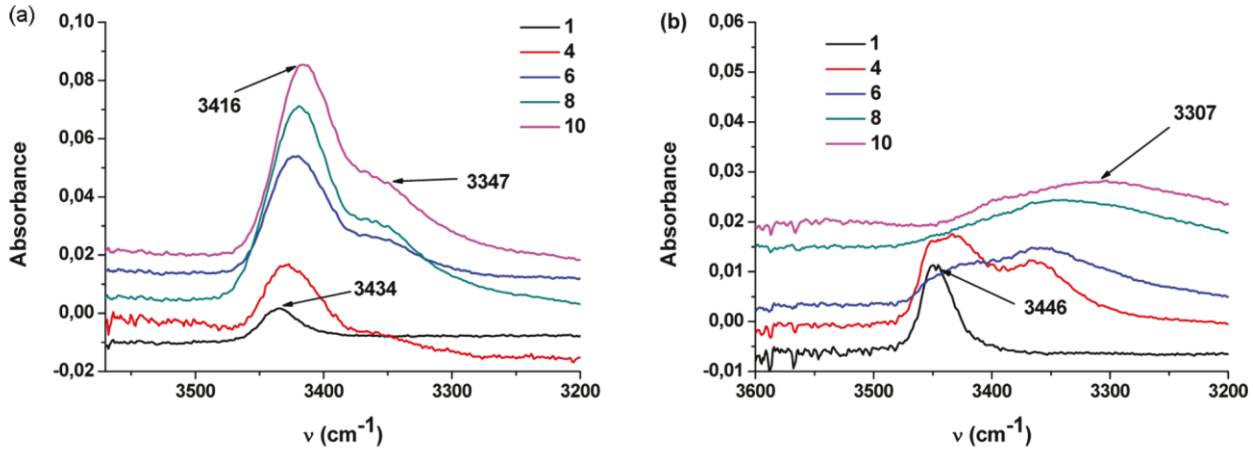

Figure 32. (a) N-H stretching regions of the IR absorption spectra for 3 mM samples of oligomers **1**, **4**, **6**, **8**, and **10** in CH_2Cl_2 at room temperature. (b) N-H stretching regions of the IR absorption spectra for 3 mM samples of oligomers **1**, **4**, **6**, **8**, and **10** in CCl_4 at room temperature.

For all compounds in methylene chloride, a strong band above 3400 cm^{-1} was recorded and indicates that no hydrogen bond is formed (Figure 32a). A shoulder centered below 3400 cm^{-1} (about 3340 cm^{-1}) appears for **4**, **6**, **8**, and **10**: it becomes stronger with increasing foldamer chain length but never becomes the main stretching band. The formation of this shoulder suggests that an equilibrium takes place among different conformations. In an apolar solvent, like carbon tetrachloride, the results are quite different: while for compound **1**, only one band centered at 3446 cm^{-1} is observed, for longer oligomers, a broad band centered at about 3300 cm^{-1} appears (Figure 32b). This effect may be due to equilibrium between structures, or it simply could be ascribed to the formation of intermolecular hydrogen bonds due to the self-aggregation of these compounds in an apolar solvents.

Additional information on the folding propensity of these compounds in solution were obtained my means of ^{1}H NMR experiments in solution. The occurrence of intramolecular C=O···H-N hydrogen bonds was checked also by investigating the dependence of the NH proton chemical shifts on an increasing percentage (up to 10%) of DMSO-d_6 in a 3 mM $CDCl_3$ solution. DMSO is a strong hydrogen-bond acceptor, and if DMSO is bound to a free NH proton, a considerable downfield shift of the proton signal can be expected.[27]

[27] Kopple, K. D.; Ohnishi, M.; Go, A. *"Conformations of cyclic peptides. IV. Nuclear magnetic resonance studies of cyclo-pentaglycyl-L-leucyl and cyclo-diglycyl-L-histidyldiglycyl-L-tyrosyl"* Biochemistry, **1969**, *8*, 4087-4095.

The Δδ values (difference of NH proton chemical shifts for the spectra recorded in pure $CDCl_3$ and in 9:1 $CDCl_3$/DMSO-d_6) for NH hydrogens of oligomers Boc-(L-Phe-L-Oxd)$_n$-OBn **6**, **8**, and **10** are summarized in Table 1. All the hydrogen amides have Δδ values above 1.8 ppm: these values are very high and account for non-hydrogen-bonded NH amide protons. In any case, it is worth mentioning that the NH-Boc hydrogens have small Δδ values that become smaller as the foldamer becomes longer.[28]

Table 1. Δδ (ppm) for NH Titration for Oligomers Boc-(L-Phe-L-Oxd)$_n$-OBn with n = 3, 4, and 6.

Compound	NH-Boc	NH_1	NH_2	NH_3	NH_4	NH_5
6	0.19	1.98	2.08			
8	0.10	1.98	2.05	2.07		
10	0.08	1.85	1.99	1.96	1.97	2.16

2.1.4 Circular dichroism techniques

To get more information about the preferred conformations adopted by those molecules, circular dichroism techniques have been used.

ECD measurements were recorded for 1 mM methanol solutions at room temperature for all compounds. The overlap of the spectra of **1**, **4**, **6**, **8**, and **10**, normalized per residue, is reported in Figure 33 and exhibits, for all foldamers, a positive band centered at 195 nm, due to either the peptide transition or the strong B transitions of Phe that are usually located around 188 nm.

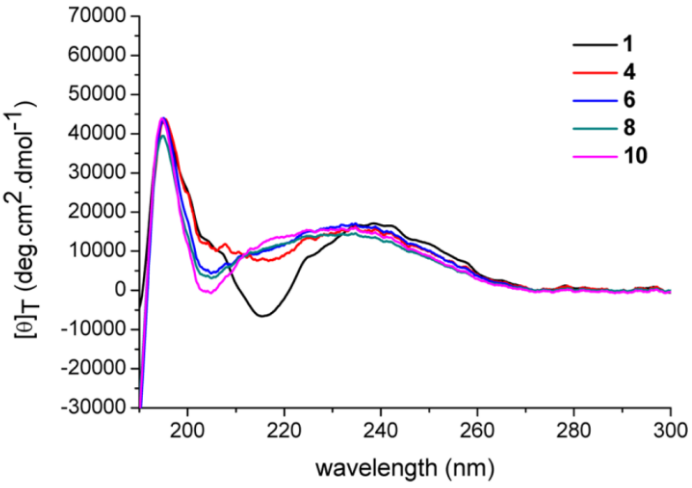

[28] Stevens, E. S.; Sugawara, N.; Bonora, G. M.; Toniolo, C. *"Conformational analysis of linear peptides. 3. Temperature dependence of NH chemical shifts in chloroform"* J. Am. Chem. Soc. **1980**, *102*, 7048-7050.

Figure 33. Normalized per-residue ECD spectra of the Boc-(L-Phe-L-Oxd)$_n$-OBn (n = 1-6) series in MeOH solution (1 mM).

The ECD spectra of compound **1** display a negative signal at ca. 215 nm and a strong positive band at 195 nm, while at 190 nm, a negative ellipticity value is shown. In addition, a broad positive unfeatured band between 270 and 220 nm (crossover points) is displayed and may be attributed to the aromatic contribution of the Phe residue, a strongly absorbing chromophore. Some spectral features of longer oligomers are probably due to a mixture of conformers present in solution. It is clear from Figure 33 that the negative feature at 215 nm in **1** becomes weaker and blue shifted with increasing chain length (in **10** it falls at 205 nm). A similar blue shift is shown by the positive broad band from 238.5 nm in **1** to 234.0 nm in **10**. These spectral features seem to rule out the possibility of a self-assembly of the oligomer, driven by the stacking interaction of aromatic units, while a PPII conformation could be taken into account supported by the fact that the broad band due to the aromatic chromophore contributions (with its maximum at 234 nm) could hide the characteristic positive peak around 220 nm.

In order to gain further information regarding the preferred conformations of these systems, we also recorded VCD spectra in the mid-IR region.

As explained above, aromatic ECD chromophores interfere with the signals characteristic of the amino groups, which are usually associated with backbone conformations of peptides and proteins.

VCD measurements were recorded at room temperature for 20 mM solutions in carbon tetrachloride for **1**; for longer oligomers the solubility in this solvent is too low to obtain VCD spectra. For this reason all Boc-(L-Phe-L-Oxd)$_n$-OBn compounds (n = 1, 2, 3, 4, 6) were considered in 20 mM CD_3OD solutions. The concentrations needed in VCD spectroscopy are actually quite large, and this should be kept in mind when comparing with the previous analysis based on the ECD and IR of dilute solutions.

A qualitative comparison of the VCD spectra recorded in methanol, with help from the literature data on peptides, can be carried out. In Figure 34 we report the IR and VCD spectra for all oligomers in the L form. To provide evidence for the differences in the behavior of different-sized foldamers, we normalized IR and VCD spectra, dividing ε and Δε by n, for each Boc-(L-Phe-L-Oxd)$_n$-OBn considered. We distinguish the two regions: 900-1600 cm^{-1} on the right side and 1600-1800 cm^{-1} on the left side (the latter contains the carbonyl stretching modes coupled with the NH in-plane bending modes, defining the amide I modes, which are so often used in the study of

peptides and proteins).[29] Regarding the amide I bands, the negative feature at 1675 cm^{-1}, dominating over the positive component at higher frequency, may be suggestive of β structures for compounds **4**, **6**, **8**, and **10**. However, in usual amino-acidic peptides, this band appears at wavenumbers lower than 1650 cm^{-1}; the copresence of a positive component at higher energy is compatible with PPII-type conformations, which in the case of peptides present precisely a couplet. The fact that observed wavenumbers do not correspond to the values usually observed for peptides can be attributed to the Oxd unit.

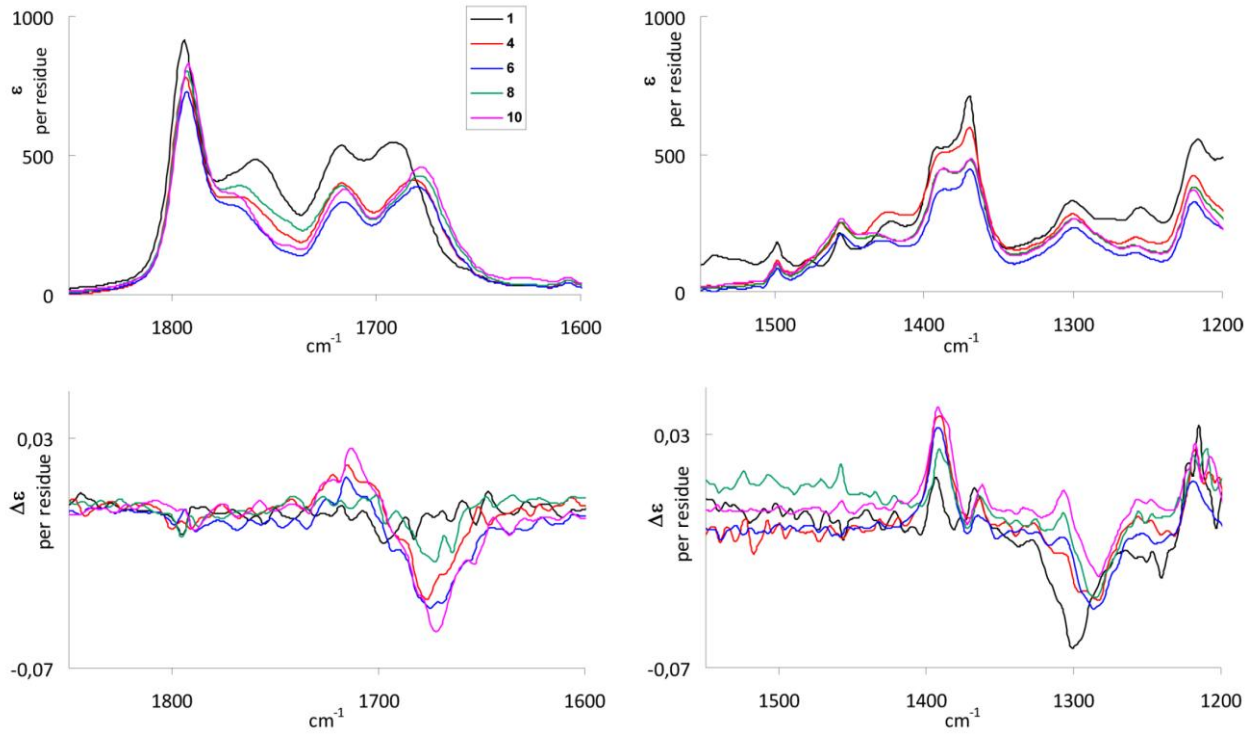

Figure 34. IR and VCD spectra of the Boc-(L-Phe-L-Oxd)$_n$-OBn (n = 1, 2, 3, 4, 6) series in methanol-d_4. The ε and Δε are presented in residue units (see text).

Both IR and VCD spectra of compound **1** are somewhat different from those of the longer foldamers, in agreement with ECD findings.

To gain further information on these systems and to verify the latter observation, we recorded VCD spectra also in CCl_4 for compound **1**, which can be dissolved in sufficient amount.

The VCD spectra of the two enantiomers are reported in the bottom part of Figure 35, while in the top part we provide the corresponding IR spectra; still we distinguish the two regions 1600-900 and 1600-1800 cm^{-1}.

[29] Cantor, C. R.; Schimmel, P. R. *"Biophysical Chemistry"* W. H. Freeman and Co.: San Francisco, **1980**.

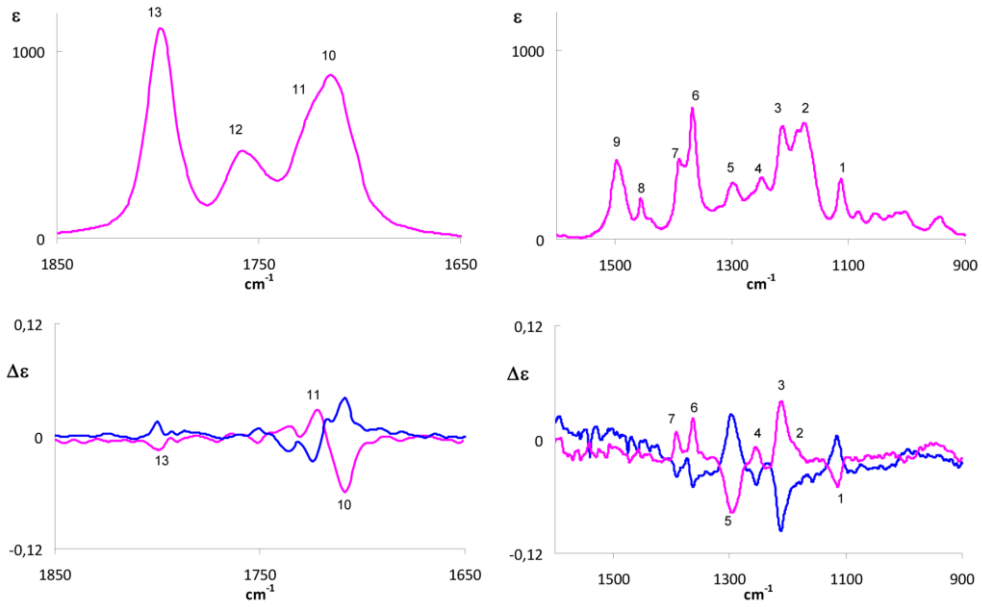

Figure 35. IR (top) and VCD (bottom) spectra of Boc-L-Phe-L-Oxd-OBn **1** (pink trace) and of the enantiomer Boc-D-Phe-D-Oxd-OBn (blue trace) in CCl_4 (20 mM solution). Numbers are introduced to facilitate correspondence between IR and VCD.

The shape of the IR spectrum presents differences with respect to the one in methanol; in particular the band at 1690 cm^{-1} is not present. This suggests that, as expected, the preferential conformations are strongly dependent on the solvent nature.

2.1.5 DFT Calculations

In order to understand the preferred conformation adopted by monomer **1** in an apolar solvent, DFT calculations have been performed to simulate its VCD spectrum. The data from CCl_4 can be considered representative of the isolated molecule, i.e., interactions with solvent molecules are expected to be small. For this reason, such data are the easiest ones to simulate and calculations in vacuo can be considered a good approximation.[30] We performed DFT calculations on compound **1** by first optimizing geometries and then by calculating vibrational frequencies, normal modes, and infrared and VCD intensities (dipole and rotational strengths), allowing us to finally simulate spectra for due comparison with experimental data (based on the assumption of Lorentzian bandshapes with a 12 cm^{-1} width). The relevant conformational degrees of freedom for compound **1** are shown in Figure 32. The conformational search has been conducted at the PM3 level and at the B3LYP/6-31+G** level.

[30] Stephens, P. J.; Devlin, F. J. *"Determination of the structure of chiral molecules using ab initio vibrational circular dichroism spectroscopy"* Chirality, **2000**, *12*, 172-179.

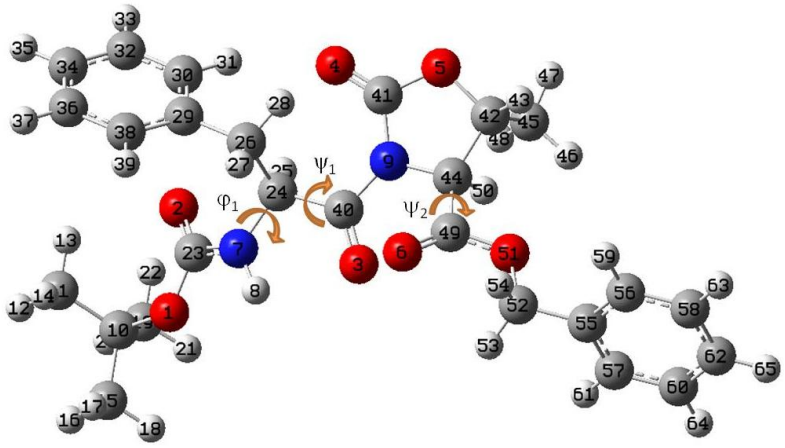

Figure 36. Atom numbers and definition of dihedral angles for compound **1**.

In Figure 37 we show only the comparison between the Boltzmann weighted averages of the calculated spectra and the experimental data. The most populated conformers exhibit VCD and IR spectra resembling the experimental ones; this is important since it means that the calculated geometries and populations adequately represent the situation in CCl_4 solution.

With those data we may conclude that the most-populated conformer exhibits values for the φ_1 and ψ_1 angles typical of a PPII helix[31] (the PPII and β structures have similar ψ but different φ values).

The former band at 1710 cm^{-1} can be attributed to the amide I mode, which is normally taken as a marker of peptide secondary structure; it has the aspect of a strong negative band at lower frequencies followed by a positive feature at higher frequencies which can be ascribed to a PPII structure. We notice, however, that the frequency is much higher than the standard amide I frequency (ca. 1650 cm^{-1}); this may be due to both the short foldamer length and the presence of the non-amino-acidic group, Oxd. In conclusion, considering the overall spectrum, we maintain that the observed VCD signals are compatible with the lower-energy conformers whose backbone angles are consistent with a PPII or a β geometry, but different from higher-energy conformers with φ_1 and ψ_1 angles appropriate for α or 3_{10} helices. We reiterate, though, that the description given is just indicative of the backbone dihedral angles assumed by Boc-l-Phe-l-Oxd-OBn **1**, which is too short to show a real peptide secondary structure.

[31] Eker, F.; Gribenow, K.; Cao, X.; Schweitzer-Stenner, R. *"Preferred peptide backbone conformations in the unfolded state revealed by the structure analysis of alanine-based (AXA) tripeptides in aqueous solution"* Proc. Natl. Acad. Sci. U.S.A. **2004**, *101*, 10054-10059.

Figure 37. Comparison of experimental IR (top) and VCD (bottom) spectra of **1** with the corresponding Boltzmann average calculated spectra.

2.2 Cyclopeptides

Cyclopeptides can act as antibiotics, regulators of membrane ion transport, and templates for protein design.[32] In recent years, new reports of nanotube formation from cyclopeptides have added another dimension to their utility as new biomaterials. The incorporation of chosen, non-amino acids into cyclopeptides is a promising approach to designs capable of performing specific tasks.[33]

Although such hybrid cyclopeptides are common in the microbial world, some groups of synthetic organic chemists have only recently began to explore such designs for creating architecturally beautiful and functionally useful macrocyclic hybrid peptides.[34]

Conformational studies on cyclopeptides as *cyclo*-(L-Pro-Gly)$_3$ and *cyclo*-(L-Pro-Gly)$_4$[35] shows that they are very flexible molecules: in polar solvents *cyclo*-(L-Pro-Gly)$_3$, adopts an asymmetric conformation which contains one *cis* Gly-Pro peptide bond, while in the nonpolar solvents, the conformer is C_3 symmetric and has all peptide bonds *trans*.

This effect should be avoided using oxazolidin-2-one rings, because the presence of the endocyclic carbonyls force it exclusively in the *trans* conformation (see the previous chapter).

The group of Tomasini has recently reported the synthesis of six cyclopseudopeptides all having general formula *cyclo*-(L-Xaa-D-Oxd)$_n$ (with n = 3 or 4).[36] In these compounds, the CHα proton chemical shift of the nearby amino acid is less deshielded with a chemical shift below 5 ppm, probably because of the cycle constraint, also confirmed by the low cyclization yields.[37]

In the present chapter, a medium-sized ring containing four units, all formed by an α-amino acid and a Oxd group in the same configuration (L or D) is described. In the final sequence, the four LL

---

[32] Darshan, R. *"Designer hybrid cyclopeptides for membrane ion transport and tubular structures"* Acc. Chem. Res. **2001**, *34*, 919-930.

[33] Brea, R. J. Reiriz, C. Granja, J. R. *"Towards functional bionanomaterials based on self-assembling cyclic peptide nanotubes"* Chem. Soc. Rev. **2010**, *39*, 1448-1456.

[34] Yoo, B.; Shin, S. B.; Y. Huang, M. L.; Kirshenbaum, K. *"Peptoid Macrocycles: Making the Rounds with Peptidomimetic Oligomers"* Chem. Eur. J. **2010**, *16*, 5528-5537.

[35] a) Deber, C. M.; Blout E. R. *"Cyclic peptides. Amino acid-cyclic peptides complexes"* J. Am. Chem. Soc. **1974**, *96*, 7566-7568; b) Madison, V.; Deber, C.M.; Blout, E. R. *"Cyclic peptides. 17. Metal and amino acid complexes of* cyclo*(pro-gly)4 and analogues studied by nuclear magnetic resonance and circular dichroism"* J. Am. Chem. Soc. **1977**, *99*, 4788-4798; c) Madison, V.; Atreyi, M.; Deber, C. M.; Blout, E. R. *"Cyclic peptides. IX. Conformations of a synthetic ion-binding cyclic peptide, cyclo-(pro-gly)3, from circular dichroism and 1H and 13C nuclear magnetic resonance"* J. Am. Chem. Soc. **1974**, *96*, 6725-6734.

[36] Angelici, G.; Tresanchez Carrera, R.; Luppi, G.; Tomasini, C. *"The Design and Synthesis of Dansyl-Containing Cyclic Pseudopeptides"* Eur. J. Org. Chem. **2008**, 3552-3558.

[37] a) Tomasini, C.; Luppi, G.; Monari, M. "*Oxazolidin-2-ones-containing pseudopeptides that fold into β-bend ribbon spirals"* J. Am. Chem. Soc., **2006**, *128*, 2410-2420; b) Bernardi, F.; Garavelli, M.; Statizzi, M.; Tomasini, C.; Trigari, V.; Crisma, M.; Formaggio, F.; Peggion, C.; Toniolo, C. "*Pseudopeptide foldamers. The homo-oligomers of pyroglutamic acid"* Chem. Eur. J., **2002**, *8*, 2516-2525.

or DD units are alternated so that, after cyclization, *cyclo*-(L-Xaa-L-Oxd-D-Xaa-D-Oxd-L-Xaa-L-Oxd-D-Xaa-D-Oxd) is formed (Figure 38).

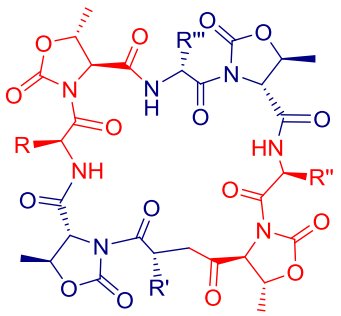

11

Figure 38. General structure of the compound **11**, a 24-membered ring containing the alternated L-Xaa-L-Oxd and D-Xaa-D-Oxd units.

2.2.1 Synthesis

Compound **11** (Figure 38) has been synthesized in the liquid phase and in a few steps, all obtained with satisfactory yields (Scheme 2). First of all, the four units shown in Figure 39 have been synthesized in solution by reaction of a Boc-Xaa-OH with H-Oxd-OBn, in the presence of HBTU and an excess of DBU. They all have the general formula Boc-Xaa-Oxd-OBn, and contain four different amino acids [Val, Ala, Asp(O*c*Hex), Gly] to have information on the cycle preferred conformation. The four compounds Boc-L-Val-L-Oxd-OBn **12**, Boc-D-Ala-D-Oxd-OBn **13**, Boc-L-Asp(O*c*Hex)-L-Oxd-OBn **14** and Boc-Gly-D-Oxd-OBn **15** (Figure 39) have all been obtained in high yield, after purification by silica gel chromatography.

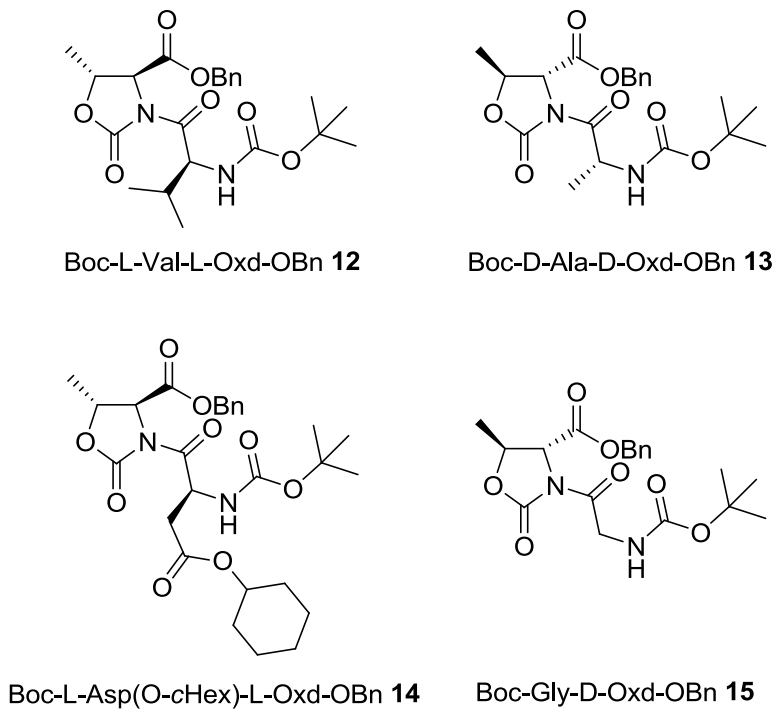

Figure 39. Building blocks utilized in this work.

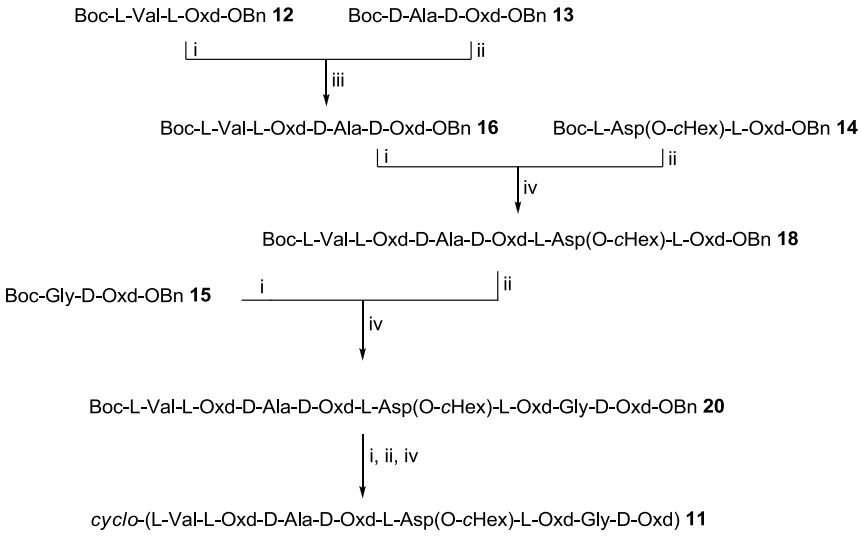

Scheme 2. Reagents and conditions: (i) H_2, Pd/C (10%), MeOH, r.t., 2 h; (ii) TFA (18 equiv.), dry CH_2Cl_2, r.t., 3 h; (iii) HBTU (1 equiv.), DBU (2 equiv.), dry CH_3CN, r.t., 3 h; (iv) HATU (1 equiv.), TEA (3 equiv.), dry CH_3CN, r.t., 45 min.

The synthesis of the open chain Boc-L-Val-L-Oxd-D-Ala-D-Oxd-L-Asp(O*c*Hex)-L-Oxd-Gly-D-Oxd-OBn **20** was obtained in three steps, by coupling the Boc-Xaa-Oxd-OBn units and alternating the L and the D moieties (Scheme 2). In any case one moiety was treated with trifluoroacetic acid in dichloromethane to remove the Boc moiety and the other one with H_2 and Pd/C to obtain the free carboxy unit, then the two compounds were used without any purification and coupled in the presence of HBTU and triethylamine (TEA). Following this protocol, we prepared the tetramer **16**, then the hexamer **18** and finally the octamer **20**. In any case a flash chromatography purification was required after each coupling step. The yields were generally good, ranging between 75% and 80%.

The cyclization step proved to be more difficult, because a large ring with 24 atoms was prepared. Therefore, first of all we removed the protective benzyl group by reaction with H_2 in the presence of Pd/C to obtain the free acid **21** in quantitative yield and then the Boc moiety by reaction with trifluoroacetic acid to prepare the corresponding amine as its triflouroacetic salt. This compound was directly cyclised in acetonitrile in low concentration (1 mM) to promote the ring formation. By reaction with HATU and an excess of TEA, the desired cycle **11** was prepared. Because it is very polar and water soluble, it could not be purified by silica gel chromatography, so it was first washed with little amounts of acetonitrile, then purified with HPLC (H_2O/acetonitrile 80: 20 → 70:30 as eluant) and obtained pure in 62% yield from **20**.

2.2.2 Conformational Analysis in solution

Information on the preferred conformation of the oligomers in solution was obtained by the analysis of FT-IR and ^{1}H NMR.

The infrared (IR) spectrum of cycle **11** suggests that no hydrogen bond is formed. The preferential conformation of this very flexible ring was studied by ^{1}H NMR analysis, with the main target of checking if the NH hydrogens are close to one another or if a large hollow is retained after cyclization. All the NMR spectra were recorded in DMSO-d_6, because of its low solubility in $CDCl_3$. First, ^{1}H NMR and *g*COSY spectra have been recorded to assign all the chemical shifts, mainly to the CHα and to the NH hydrogens, to check if the rigid *trans* conformation of the imido group is retained (Figure 40 and Table 2), is in contrast with the results obtained for the *cyclo*-(L-Xaa- D-Oxd)$_n$ previously reported.[36]

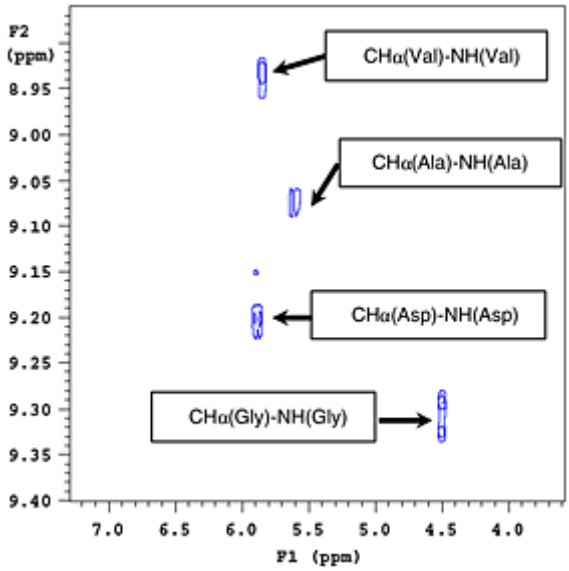

Figure 40. Enlargement of a *g*COSY ^{1}H NMR spectrum of **11**, showing the coupling between NH and the vicinal CHα of the four amino acids.

Table 2. Chemical shift of the NH and CHα hydrogens of 11, compared with the CHα hydrogen of **12**,**12**,**14**,**1**5

Amino Acid	**δ (NH)**	**δ (CHα)**	**δ (CHα)-12-15**
L-Val	8.95	5.84	5.46
D-Ala	9.09	5.59	5.35
L-Asp(OcHex)	9.21	5.85	5.76
Gly	9.30	4.50	4.74

[a]The spectrum is recorded in DMSO-d_6.

[b]These chemical shifts are referred to the spectra of the precursors **12**, **13**, **14**, **15** and are recorded in $CDCl_3$.

The chemical shifts of the four CHα hydrogens are very deshielded compared with the normal chemical shifts of an α-amino acid, and retain nearly the same position that they have in the four building blocks **12**, **13**, **14**, **15**, that are totally free of any constraint. This outcome is a confirmation that the local constraint typical of the 4-carboxy-oxazolidin-2-ones is a strong effect, present also in medium-sized rings.

To have information on the preferential conformation of the cycle **11**, we recorded a NOESY 2D spectrum on a 10 mM of it in DMSO-d_6.

In Figure 41 it is summarized the significative NOE enhancements of **11** in DMSO-d_6. To have a confirmation that these enhancements are due to the formation of the cycle, it was also recorded the same experiment on the open chain **20** to make a comparison between the two results.

The signals that the two compounds share are presented in blue, while the interactions that exist only in the cycle and not in the open chain are reported in red.

From these experiments, it's possible to gather that the open chain presumably lies in an open form, while the cycle **11** does not.

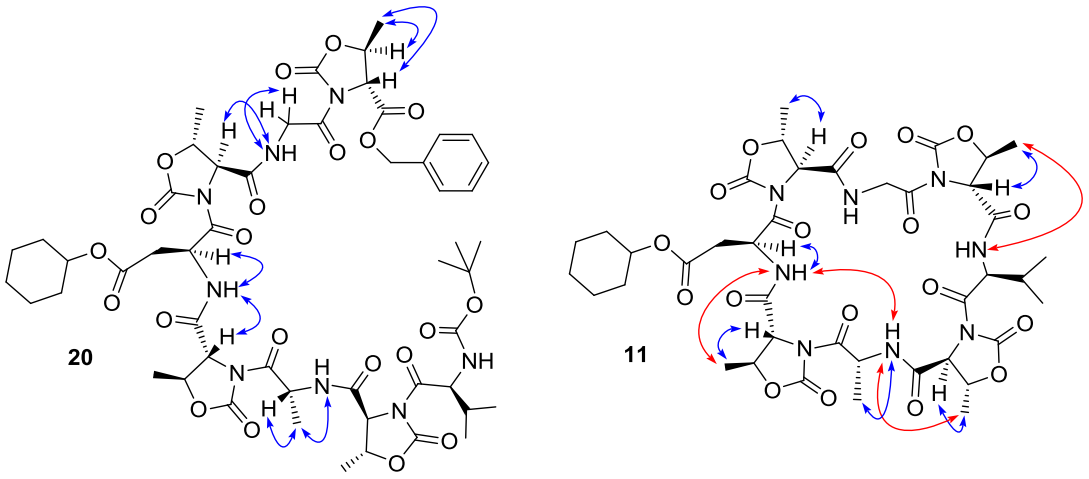

Figure 41. NOE enhancements as gathered from the NOESY 2D spectrum of **20** (left) (10 mM solution in DMSO-d_6, mixing time 900 ms) and **11** (right) (10 mM solution in DMSO-d_6, mixing time 700 ms).

3 Supramolecolar materials

3.1 Introduction

Traditionally objects and devices have been made through a "top-down" approach where an item is carved, or moulded out of a larger bulk material. Nanomaterials require specialized techniques such as electron-beam and atomic force microscopy based lithography. A "bottom-up" approach provides an alternative route to the development of nanoscale objects and devices. An obvious source of inspiration for the design of nanoscale materials from the bottom up is provided by Nature. Evolution has produced a range of self-assembling nanoscale systems based on lipids, nucleic acids and amino acids (see the first chapter). In these systems, disordered mixtures of molecular building blocks spontaneously arrange themselves to form highly organized structures with well defined properties.[38]

We know that there is a relationship between amino acid sequence and structure. In peptide based nanomaterials, the structure formed by a single peptide can interact with another complementary peptide via non-covalent interactions: ionic, hydrophobic, hydrogen bonding and π-stacking. When a large number of these building blocks are held together, supramolecular structures can be formed.

Of the enormous number of possible peptide sequences, only comparatively few are encountered in biological systems. The challenge is to find the rules that link peptide sequences to structures. Researchers have made significant progress in this area and it now becomes possible to design structures that have specific properties to fulfill a specific purpose.

There are many potential applications of self-assembled peptide systems, since they represent attractive natural building blocks for the design of new nanostructures and nanomaterials, such as, wires, layers, gels, scaffolds, templates and liquid crystal.

Moreover, there is an interest in growing cells in a more ''natural'' environment. To do this, an artificial extracellular matrix (ECM) is needed. In their natural environment (i.e. within tissues), cells grow through a matrix of proteins and glycoproteins, the most common being collagen. A number of peptide based fibrous networks have been developed to allow cell growth in a 3D environment similar to an ECM.

[38] Ulijn, R. V.; Smith, A. M. *"Designing peptide based nanomaterials"* Chem. Soc. Rev., **2008**, *37*, 664-67.

Aggeli et al.[39] presented a generic statistical mechanical model for the self assembly of chiral rod-like units, such as β-sheet-forming peptides, into helical tapes, which with increasing concentration associate into twisted ribbons (double tapes), fibrils (twisted stacks of ribbons), and fibers (entwined fibrils).

Besides the use of β-sheets as a basis for fibrous structures, also α-helices may be used as components of coiled-coils for the purposes of self-assembly, as described first by Pauling, Corey and Crick.[40]

In this context, the self-assembly of small peptides made of only 2-3 amino acids has been recently studied by Banerjee and co-workers, who demonstrated that one can obtain stable β-sheet or helix-like structures by interaction of small peptides that are held together by 2-3 hydrogen bonds.[41]

In a remarkable work, Tomasini and coworkers reported the formation of a fibrous supramolecular material based on the molecule Boc-L-Phe-D-Oxd-OBn **22**.[42]

This material was obtained as a fiber-like white solid after slow solvent evaporation of a solution of Boc-L-Phe-D-Oxd-OBn (20-25 mM) in a mixture (1:1) of cyclohexane/ethyl acetate (Figure 42b). The molecule also shows good solubility in polar solvents such as acetonitrile, methanol, diethyl ether and ethyl acetate, but is not soluble in water. It assembles to form a fiber-like material under a wide variety of solution conditions. This material shows strong birefringence and has defined edges. It is made of bundles of crystalline-shaped filaments clustered and aligned along the main bundle direction (Figure 42c).

[39] Aggeli, A.; Nyrkova, I. A.; Bell, M.; Harding, R.; Carrick, L.; McLeish, T. C. B.; Semenov, A. N.; Boden, N. "*Hierarchical self-assembly of chiral rod-like molecules as a model for peptide b-sheet tapes, ribbons, fibrils, and fibers"* PNAS, **2001**, *98*, 11857-11862.

[40] Pauling, L.; Corey, R. B. *"Structure of the nucleic acids"* Nature, **1953**, *171*, 59-61.

[41] a) Samit, G.; Drew, M. G. B.; Banerjee, A. *"Dipeptide nanotubes, with* N-*terminally located ω-amino acid residues, that are stable proteolytically, thermally, and over a wide range of pH"* Chem. Mater. **2008**, *20*, 2282-2290; b) Bose, P. P.; Das, A. K.; Hedge, R. P.; Shamala, N.; Banerjee, A. *"pH-sensitive nanostructural transformation of a synthetic self-assembling water-soluble tripeptide: nanotube to nanovesicle"* Chem. Mater. **2007**, *19*, 6150-6157.

[42] Angelici, G.; Falini, G.; Hofmann, H.-J.; Huster, D.; Monari, M.; Tomasini, C. "*A fiberlike peptide material stabilized by single intermolecular hydrogen bonds*" Angew. Chem. Int. Ed., **2008**, *47*, 8075-8078.

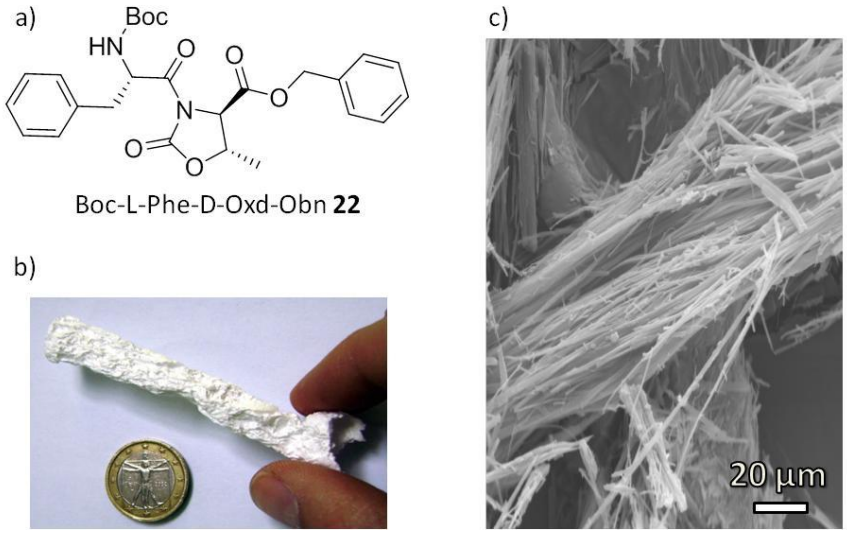

Figure 42. (a) Chemical structure of compound **22**. (b) Boc-L-Phe-D-Oxd-OBn after slow evaporation of a mixture cyclohexane/ethyl acetate (1:1). (b) SEM image of filament bundles of Boc-L-Phe-D-Oxd-OBn. Scale bar: 20 µm.

Interestingly, the thicknesses and the widths of the mature filaments are almost constant, regardless of the solvent conditions for assembly, whereas their lengths vary widely even under a single set of experimental conditions. The material is stable. Its overall shape was conserved in the precipitation media for several months and even after it had been air-dried. Only strong thermal treatment, such as by an electron beam, provoked the disintegration of the material.

The solid-state structure of Boc-L-Phe-D-Oxd-OBn can be considered a borderline case of a parallel β sheet structure; indeed, all the examples reported in the literature show fiber-forming peptides that are stabilized in the solid state by at least two N-H···O=C hydrogen bonds. In contrast, this fiber-like material is stabilized only by single hydrogen bonds between dipeptide units.

3.2 Imidazolidinones Vs Oxazolidinones

As it was demonstrated that compound **21** forms fibers with the monomers arranged in infinite chains connected only by a single hydrogen bond, we were tempted to look for other molecules with such unusual properties.

For this purpose, it was synthesized the pseudodipeptide Boc-L-Phe-D-Imz-OBn **23** (Imz = imidazolidin-2-one-4-carboxylate) and investigated its structure in the solid state. This compound is similar to Boc-L-Phe-D-Oxd-OBn but contains an additional NH group in the heterocyclic ring oriented nearly orthogonal to the pre-existing one (Figure 43). The presence of two NH hydrogen bonds that are not oriented along the same axis should favor the formation of a two-dimensional

arrangement. This effect should drive the formation of layers instead of fibers, that were obtained with Boc-L-Phe-D-Oxd-OBn, which can form only one hydrogen bond.

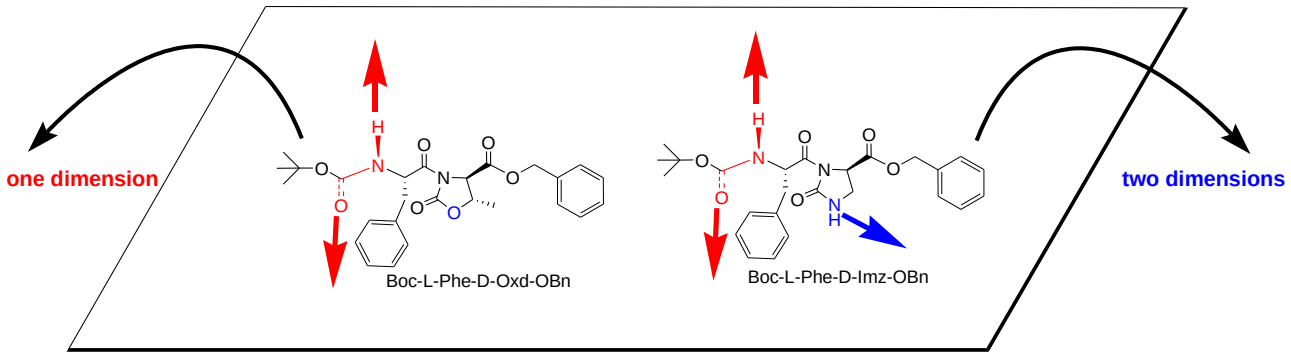

Figure 43. Schematic structural comparison of Boc-L-Phe-D-Oxd-OBn and Boc-L-Phe-D-Imz-OBn (red and blue arrows show the hydrogen bond directions).

The dipeptide Boc-L-Phe-D-Imz-OBn **23** was prepared in a single step starting from the readily available Boc-L-Phe-D-Asn-OBn and utilizing a modified methodology for the Hofmann rearrangement that was recently described by Tomasini.[43] This method was necessary because the preparation of an imidazolidin-2-one-4-carboxylate could not be performed by reaction of 1,2-diaminopropanoic acid (DAP) with triphosgene, due to the low availability of DAP and the poor reaction yield (Scheme 3).

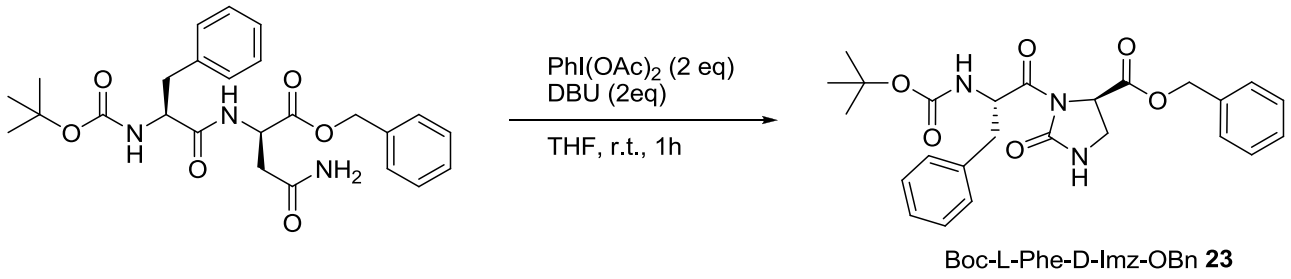

Scheme 3. Synthesis of Boc-L-Phe-D-Imz-OBn **23**

[43] Angelici, G.; Contaldi, S.; Green, S. L.; Tomasini, C *"Synthesis of imidazolidin-2-one-4-carboxylate and of (tetrahydro) pyrimidin-2-one-5-carboxylate via an efficient modification of the Hofmann rearrangement"* Org. Biomol. Chem. **2008**, *6*, 1849-1852.

The rearrangement is a very general reaction and can be applied both to protected asparagine and to asparagine-containing protected polypeptides. It is promoted by the readily available $PhI(OAc)_2$ in the presence of DBU and provides the desired heterocycle in high yield (Figure 44).

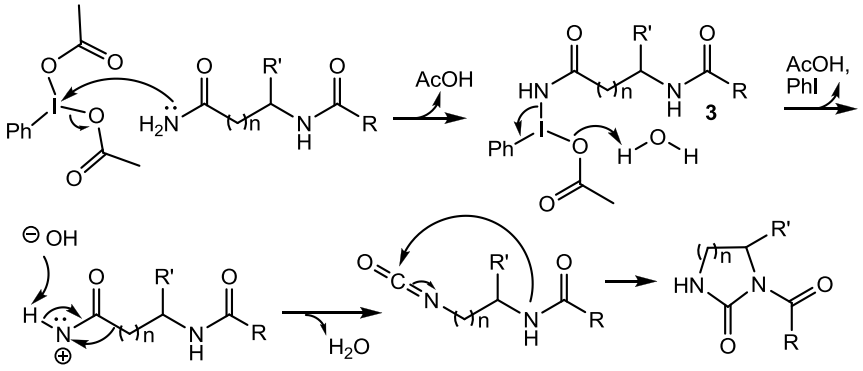

Figure 44. Suggested mechanism of the modified Hofmann rearrangement for the synthesis of 4-substituted imidazolidin-2-one.

After preparation and purification with conventional methods, Boc-L-Phe-D-Asn-OBn was treated with $PhI(OAc)_2$ and DBU in tetrahydrofuran for 1 h to furnish the desired compound **23** in 65% yield after flash chromatography.

The conformation of compound **23** was analyzed in solution and in the solid state. A first analysis was performed, comparing the IR spectrum of a 3 mM solution of **23** in dichloromethane with the spectrum of a 1% mixture of 1 in KBr. The spectral regions concerning the NH and CO stretching bands are reported in Figure 45.

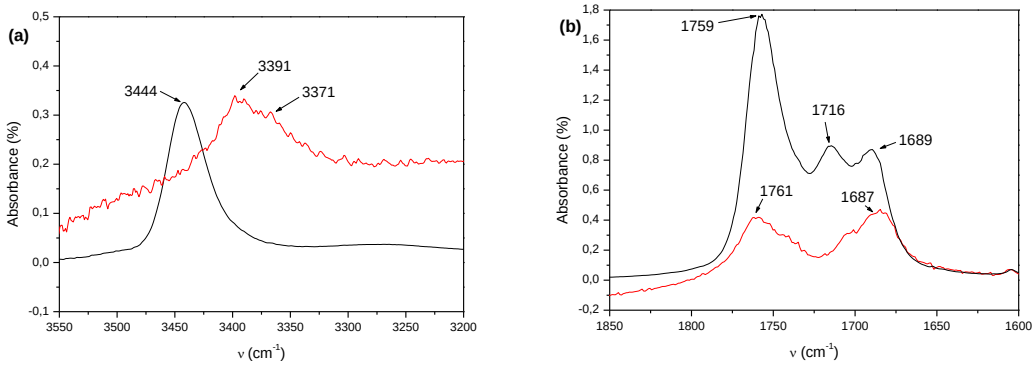

Figure 45. FT-IR absorption spectra (a) in the N-H stretching region (3600-3200 cm^{-1}) and (b) in the C=O stretching region (1850-1600 cm^{-1}) for 3 mM samples of **23** in pure CH_2Cl_2 (black line) and as a 1% solid mixture with KBr (red line) at room temperature.

While hydrogen bonding is clearly present in the solid state as shown by two peaks (3391 and 3371 cm^{-1}) belonging to a broadband, no hydrogen bonding is present in the diluted solution (3444 cm^{-1}), and thus intramolecular NH hydrogen bonds are absent. A strong variation of the spectrum in the CO region confirms this result.

Several attempts were made to obtain macroscopic ordered structures in the solid state by slow evaporation of solutions of **23** in different solvents. The formation of crystal aggregates of **23** was observed by slow evaporation of a 1:1 mixture of cyclohexane/ethyl acetate, which was used for the evaporation of Boc-L-Phe-D-Oxd-OBn.

In contrast, slow evaporation from protonated solvents such as methanol, ethanol, and isopropanol provided crystals, which were useful for single crystal X-ray diffraction studies. Interestingly, the nature of the alcohol has an influence on the preferential elongation and macroscopic side-aggregation of the crystals (Figure 46), which show a common tendency to aggregate laterally along their main axis (Figure 46a,c,e). In the aggregates of **23a**, the lateral association extends over several hundred micrometers. Their image under the optical microscope with cross polars shows them preferentially iso-oriented (insets in Figure 46a). The degree of order in crystal association continuously decreased when ethanol and isopropanol were used as solvents, as shown by the reduced birefringence of crystals **23b** and **23c** (insets in Figure 46c,e). Crystals suitable for single crystal X-ray diffraction were obtained from isopropanol solutions in a crystallization trial using seed crystals from the homogeneous precipitation in the same solvent (Figure 46f). The observation of crystals by SEM (Figure 46b,d,f) shows that each crystal is made of several layers which are cast on the top of each other. This superstructure organization is also present in the single crystals obtained from isopropanol by seeding (inset of Figure 46f). Thus, in all these crystals a plywood structure is present, with a varying degree of order as a function of the precipitation conditions.

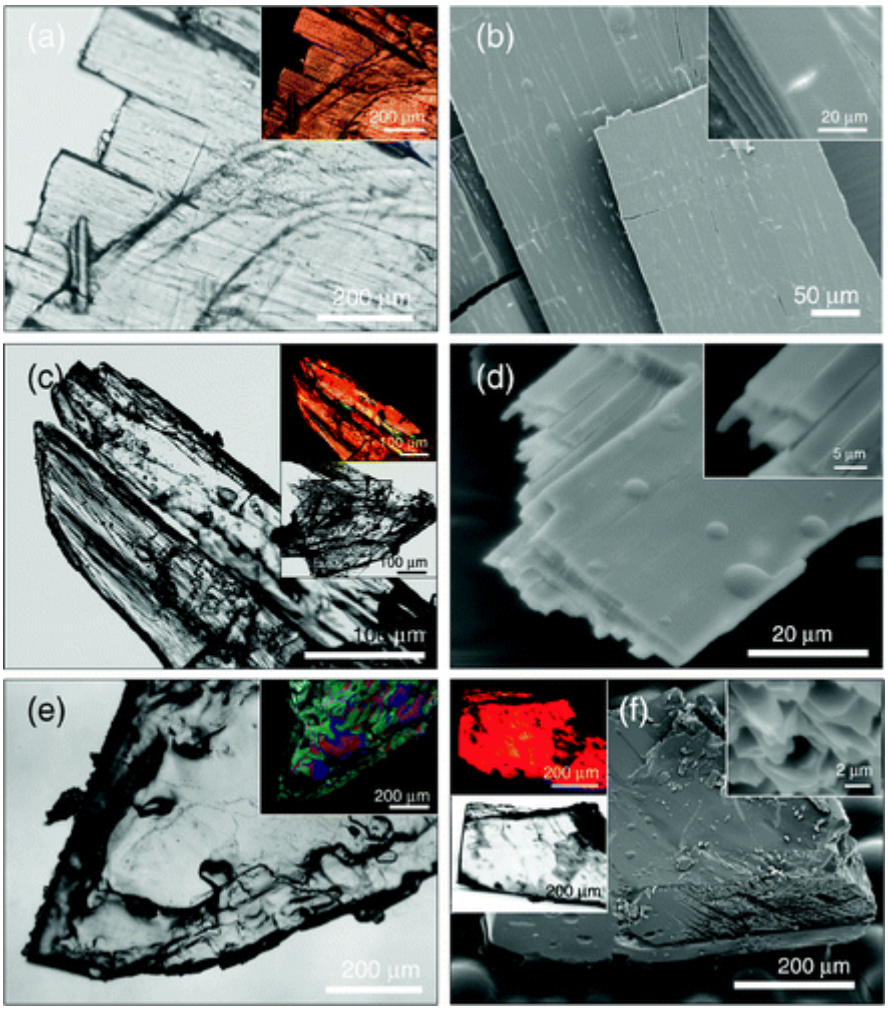

Figure 46. Optical micrographs of crystals of **23** precipitated by slow evaporation from solutions of **23** in (a) **23g** from methanol, (c) **23b** from ethanol, and (e) **23c** from isopropanol. The top insets in (a, c, e) show the same images under cross polars. The bottom inset (c) shows an aggregate of plate-like crystals precipitated from an ethanol solution. In the left insets in (f) optical micrographs of a crystal of **23c** are shown obtained in a seeding crystallization trial from an isopropanol solution. Scanning electron microscopy images of crystals of **23a**, **23b**, and **23c** are shown in (b), (d), and (f), respectively. The plywood structure is evident for **23a** (b) and **23b** (d). The insets in (b) and (d), and that on the right in (f), show that all crystals are made of several layers.

The formation of these plate-like crystals only by slow evaporation of the protonated solvents suggests the idea that the solvents may play an active role in crystal formation.[44] The obtained single crystals were analyzed by X-ray diffraction (XRD) and thermal analysis. Crystals of **23** grown from methanol and ethanol, respectively, show the formation of methanol (**23a**) and ethanol solvates (**23b**). In addition to the solvent, two independent molecules of **23** are present in the unit cell (Figure 47).

[44] Guha, S.; Drew, M. G. B.; Banerjee, A. *"Solvent-induced dynamic single-crystal-to-single-crystal transformation of a synthetic peptide-based cyclic compound"* Cryst.Eng.Comm. **2009**, *11*, 756-762.

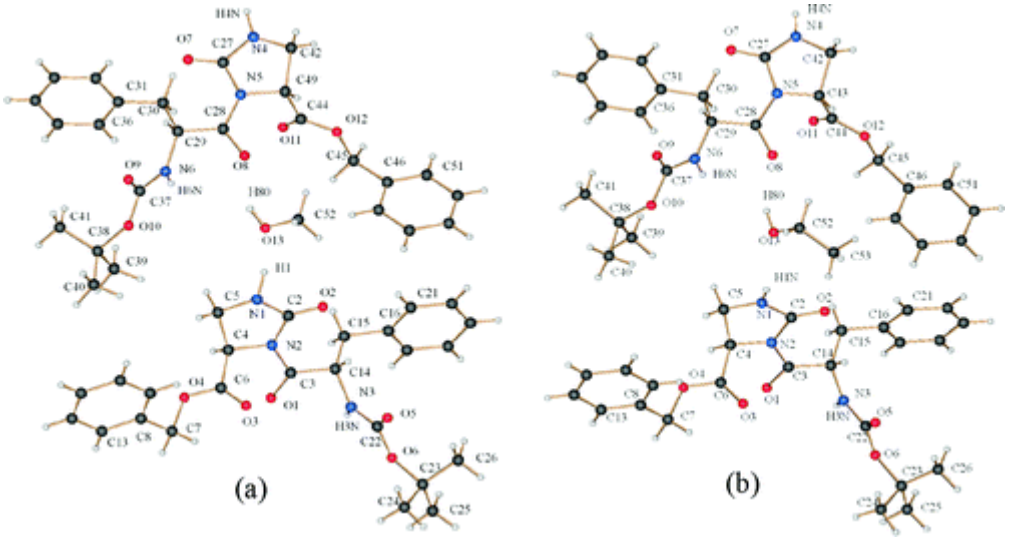

Figure 47. View of the content of the unit cell of **23** crystallized with (a) methanol (structure **23a**) and (b) ethanol (structure **23b**).

The two peptide molecules in structure **23a** have approximately the same backbone conformation (Figure 47). The two conformers differ only in the orientation of the benzyl ring of the OBn moiety. In the unit cell, each conformer belongs to a separate infinite chain of peptide molecules, which are arranged in parallel orientation. Two consecutive residues in the chains are connected by only one NH···O=C hydrogen bond between the amidic NH proton of the L-Phe residue of the one peptide molecule and the carbonyl function of the Boc group of the other one.

The infinite chains are arranged in an antiparallel orientation along the *a* axis (Figure 48a). The phenyl rings are in a displaced stacked arrangement, but the offset of the phenyls prevents π-π stacking. The conformation of the monomers and the arrangement of the chains is in close correspondence to that found in Boc-L-Phe-D-Oxd-OBn (**22**). The presence of the NH unit in D-Imz, replacing the oxygen atom in the D-Oxd ring, allows the formation of further hydrogen bonds. This possibility leads to an interconnection of two peptide chains via the bifurcated NH bond involving the Imz NH group of a peptide molecule of one chain and two carbonyls of the other chain. One carbonyl group comes from an L-Phe residue, and the other from the D-Imz constituent of the other chain. Although the NH···OC distances are larger (2.35 and 2.52 Å) than those found in typical hydrogen bonds, the general electrostatic effect in this arrangement favors the interconnection. In comparison to the D-Oxd crystals, the packing is more complex because of the presence of one methanol molecule that acts as a linker between the two chains establishing two

H-bonds using both the oxygen and hydrogen atoms (O13-H80···O8, O13···H1-N1) of the solvent molecule (Figure 48b).

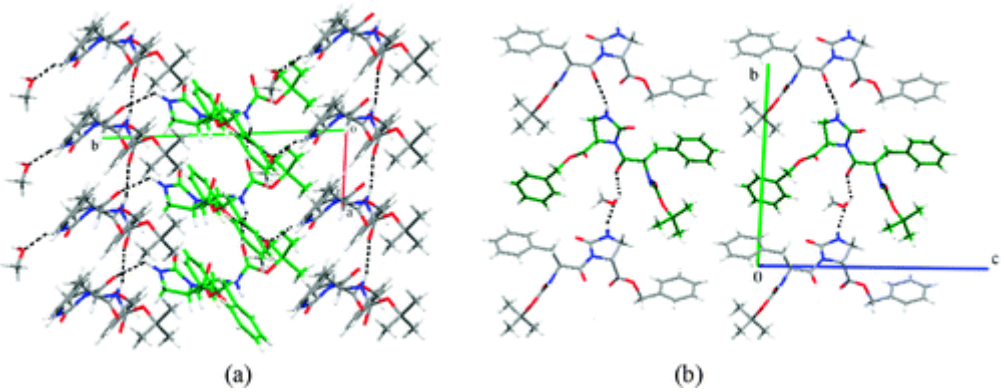

Figure 48. (a) View down the c axis showing the chains of the two different conformers running along the a axis; (b) view down the *a* axis showing the H-bond interactions among chains of the two different conformers of **23**. Dark dotted lines indicate hydrogen bonds; color code: C gray (in one conformer) and green (in the second conformer), O red, N blue.

The single crystal X-ray diffraction study carried out on crystals of **23** grown from ethanol shows the formation of an ethanol solvate **23b** isostructural with the methanol solvate **23a**. And, therefore, the crystal packing is almost identical to that described for **23a** and needs no further comments.

A crystal suitable for single crystal X-ray diffraction studies could also be obtained from isopropanol. In this case, no solvent molecules are involved in the crystal structure of **23c**, probably due to the larger size of the isopropanol molecule, that can no longer be accommodated in the cavity between two molecules of **23**. In the crystal packing of **23c**, two different types of intermolecular hydrogen bonds are present (Figure 49). One hydrogen bond connects the amidic NH hydrogen of the L-Phe unit with the carbonyl oxygen of the CO group of the D-Imz moiety belonging to another peptide molecule. The other involves the NH proton of the D-Imz ring and the carbonyl oxygen of a Boc group of another peptide molecule. These weak interactions generate also a 2D-network parallel to the ab plane, which is different from that observed in the packing of **23**g and **23b**, respectively. Quantum chemical calculations on the two different crystal packings with six peptide molecules but without solvent molecules show a slight preference for the packing of **23c** by 8.3 kJ/mol at the HF/6-31G* level of *ab*-initio MO theory. By interaction with an additional solvent molecule, the methanol/ethanol solvate packings can obviously compensate for this disadvantage.

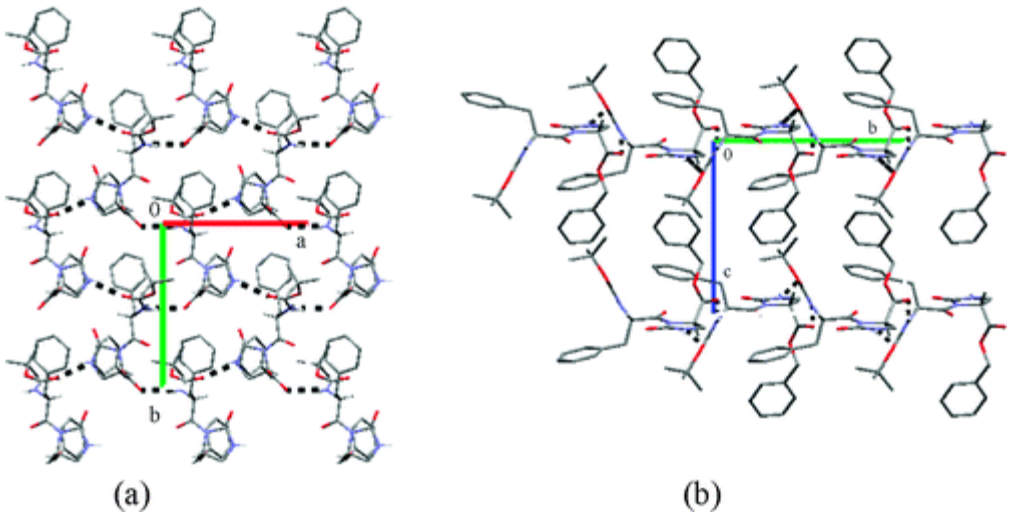

Figure 49. (a) View down the *c* axis and (b) view down the *a* axis of the crystal packing of **23**c (hydrogen atoms omitted for clarity).

In order to investigate the effect of temperature on the structure of the plate-like crystals of **23a**, **23b**, and **23c**, calorimetric and X-ray powder diffraction analyses were carried out (Figure 50). The heating profile of single crystals of **23a** (Figure 50a) shows a broad endothermic peak at 46 °C followed by two sharp endothermic peaks, a strong one at 89 °C and a weak one at 141 °C. For a better understanding, the structural reorganization of **23a** associated with the thermal treatment was followed by X-ray powder diffraction (Figure 50b). The experimental X-ray diffraction pattern of **23a** collected at room temperature (Figure 50b, polymorph **23a**-I) shows all the peaks present in the diffraction pattern calculated from the single crystal structure of **23a** (Figure 50b, polymorph **23a**-C) and some additional peaks belonging to the diffraction pattern of **23a** after the thermal treatment just above the temperature first endothermic peak (Figure 50b, polymorph **23a**-II). The **23a** material TGA profile analysis indicates a weight loss of 3.8 % in the temperature range between 23 and 68 °C. Thus, the first endothermic peak could be associated with the loss of methanol molecules from the crystal lattice (stoichiometric content of 3.3% w/w). These observations suggest that the material precipitating at room temperature is a mixture of crystals containing solvent and solvent-free crystals. No differences in the morphology of these two species of crystals have been observed. Above a temperature of 100 °C after the strong endothermic peak at 89 °C, the polymorph of **23a**-III is formed, which melts at a temperature of 141 °C giving an amorphous material (Figure 50b, polymorph **23a**-IV). The heating profile of single

crystals of **23b** (Figure 50c) shows two overlapping endothermic peaks at 95 and 109 °C followed by a very weak one at 144 °C.

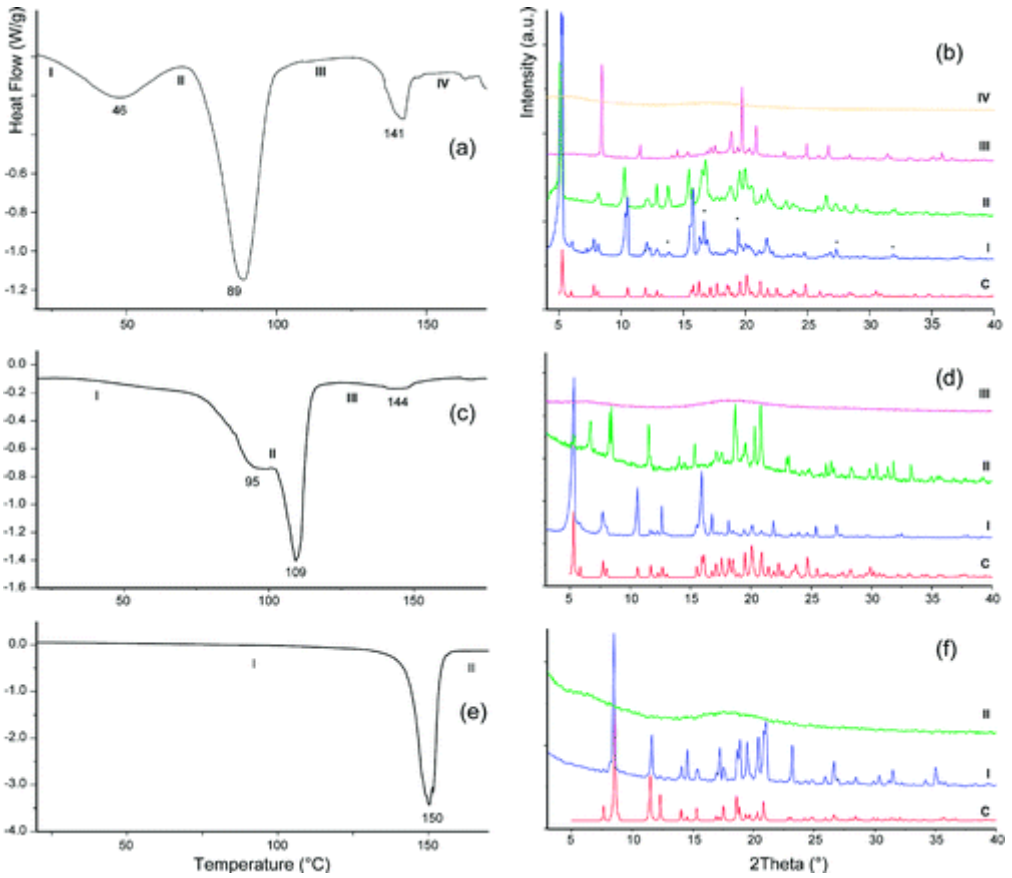

Figure 50. Differential scanning calorimetry profiles of crystals of **23** precipitated from a solution of (a) methanol (**23a**), (c) ethanol (**23b**), and (e) isopropanol (**23c**). (b) X-ray powder diffraction patterns of single crystals of **23a** after thermal treatment up to the temperature I-IV. (d) X-ray powder diffraction patterns of single crystals of **23b** after thermal treatment up to the temperature I-III. (f) X-ray powder diffraction patterns of single crystals of **23c** after thermal treatment up to the temperature I and II. In panels b, d, and f, the calculated powder diffraction pattern from the single crystal structure (c) is reported for comparison with I. In panel b, the asterisks in I indicate the diffraction peaks, which belong to the desolvated form II.

Also in this case the structural reorganization of **23b** associated with the thermal treatment was followed by X-ray powder diffraction (Figure 50d). The experimental X-ray diffraction pattern of **23b**-I collected at room temperature shows all the peaks present in the diffraction pattern calculated from the single crystal structure of **23b**-**c**. This indicates that the material precipitating at room temperature is a pure phase. At a temperature of 97 °C after the endothermic peak at 95 °C, a second polymorph of **23b**-II is formed. This polymorph melts at a temperature of 109 °C giving the amorphous material **23b**-III. The material **23b** TGA profile indicates a weight loss of 5.8% in the range of temperature between 65 and 120 °C. This value is close to the stoichiometric content of solvent in **23b** (5.8% w/w).

Finally, single crystals of **23c** (Figure 50e) show a heating profile, in which only one strong endothermic peak at 150 °C is present. The material **23c** is a pure phase, as shown by the correspondence among all the peaks present in the experimental X-ray powder diffraction pattern (Figure 50f, **23c**-I) and the one calculated from the single crystal structure (**23c**-C). Moreover, this compound melts at 150 °C, giving the amorphous material **23c**-II. This material does not host solvent in its crystal lattice, as confirmed by the absence of peaks in the first derivative of the TGA profile below the decomposition temperature. All these materials start to decompose at temperatures above 180 °C.

3.3 L-Phe-D-Oxd: a "privileged scaffold"

To understand the importance of the L-Phe-D-Oxd scaffold to build new architectures and, in particular, the role of the D-Oxd group, we decided to explore how it behaved when it was included in more complex structures and if the term "privileged scaffold" could be used to define it. This term was first proposed by Evans et al. to describe selected structural types that bind to multiple, unrelated classes of protein receptors as high-affinity ligands.[45] These privileged structures are typically rigid, polycyclic heteroatomic systems capable of orienting a variety of substituent patterns in a well-defined three-dimensional space.[46]

3.3.1 Different behaviour of two epimers

In this paragraph, the self-assembly of two epimers, Boc-L-Phe-D-Oxd-(*S*)-β^3-hPhg-OBn (**24**) and Boc-L-Phe-D-Oxd-(*R*)-β^3-hPhg-OBn (**25**), is described. Both of these molecules contain the scaffold L-Phe-D-Oxd, but differ for the introduction of the two enantiomers of β^3-homophenylglycine. The reversal of the stereogenic center contained in this moiety is crucial on the preferred molecular conformation and, as a result, on the crystal morphology.

Compounds **24** and **25** are easily prepared by coupling of the already described Boc-L-Phe-D-Oxd-OH moieties with (*R*)-β^3-hPhg-OBn or (*S*)-β^3-hPhg-OBn, respectively, in high yield by standard

[45] Evans, B. E.; Rittle, K. E.; Bock, M. G.; DiPardo, R. M.; Freidinger, R. M.; Whitter, W. L.; Lundell, G. F.; Veber, D. F.; Anderson, P. S.; Chang, R. S. L.; Lotti, V. J.; Cerino, D. J.; Chen, T. B.; Kling, P. J.; Kunkel, K. A.; Springer, J. P.; Hirshfield, J. *"Methods for drug discovery: development of potent, selective, orally effective cholecystokinin antagonists"* J. Med. Chem. **1988**, *31*, 2235-2246.

[46] Nicolaou, K. C.; Pfefferkorn, J. A.; Roecker, A. J.; Cao, G.-Q.; Barluenga, S.; Mitchell, H. J. *"Natural product-like combinatorial libraries based on privileged structures. 1. General principles and solid-phase synthesis of benzopyrans"* J. Am. Chem. Soc. **2000**, *122*, 9939-9953.

methods in solution. The coupling steps are reported in Scheme 4. The compounds were obtained pure as white solids after purification by flash chromatography (cyclohexane/ethyl acetate 8/2 as eluants).

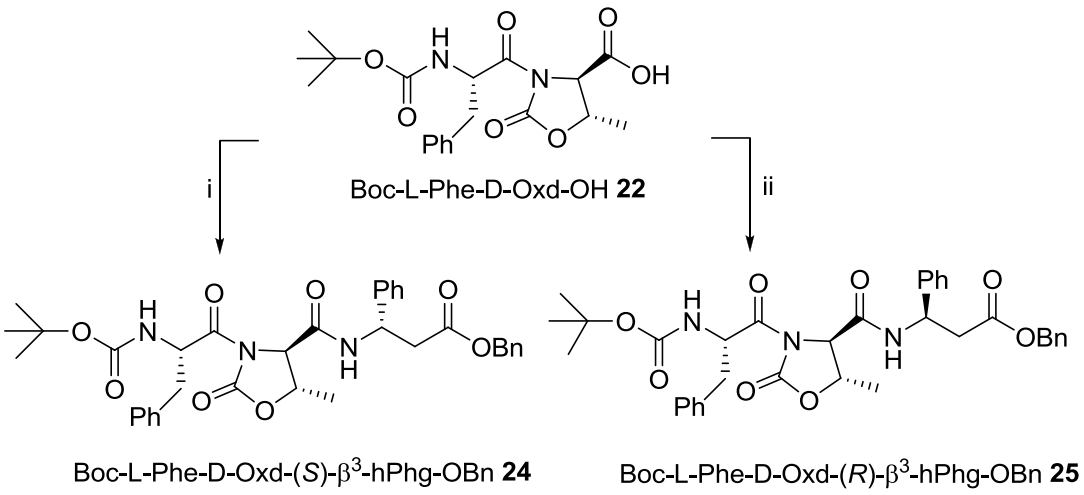

Scheme 4. (i) $CF_3COO^-\ ^+H_3N$-(*S*)-β^3-hPhg-OBn (1 equiv), HBTU (1.1 equiv), TEA (3 equiv), dry CH_3CN, 40 min, r.t.; (ii) $CF_3COO^-\ ^+H_3N$-(*R*)-β^3-hPhg-OBn (1 equiv), HBTU (1.1 equiv), TEA (3 equiv), dry CH_3CN, 40 min, r.t.

The preferential conformation assumed by the two compounds was analyzed by FT-IR spectroscopy in diluted solution (3 mM) Figure 51. It is possible to recognize the presence of a chelate NH hydrogen bond for the compound **25**, as demonstrated by the peaks centered at 3350 and 1670 cm^{-1}, while **24** does not. This outcome suggests that only **25** forms a γ-turn structure.

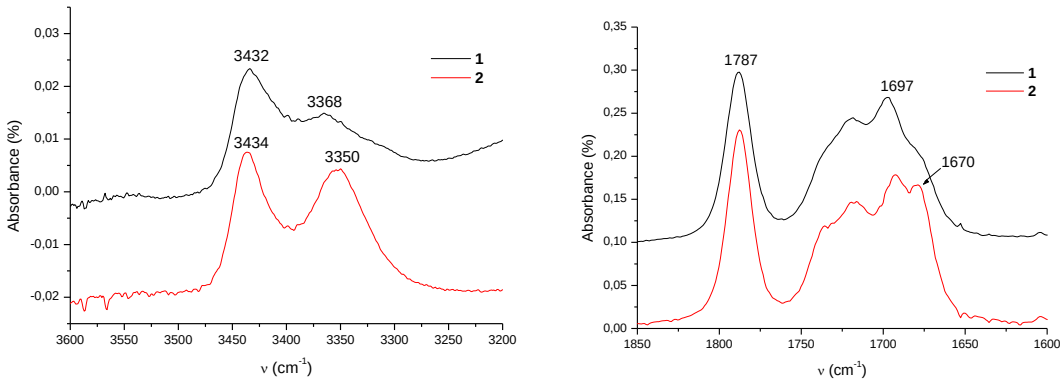

Figure 51. FT-IR absorption spectra in the N-H (left) and C=O (right) stretching regions for 3 mM concentration samples of oligomers **24** and **25** in pure CH_2Cl_2 at room temperature.

This outcome is confirmed by solution NMR spectroscopy, where we investigated the DMSO-d_6 dependence of the NH proton chemical shifts. DMSO is a strong hydrogen bond acceptor and, if bound to a free NH proton, a considerable downfield shift of the proton signal can be expected. Both compounds have two NH groups, belonging to a carbamate group and an amide group, respectively. While the chelation of the carbamate NH is uncertain for both compounds, it is possible to notice that the Phe-NH group is poorly chelated for **24** and much more chelated for **25**, thus confirming the outcome of the FT-IR spectra.

The FT-IR spectra of **24** and **25** in the solid state are very similar and show that all the NH hydrogens are hydrogen bonded, as all the stretching signals are below 3400 cm^{-1} (Figure 52).

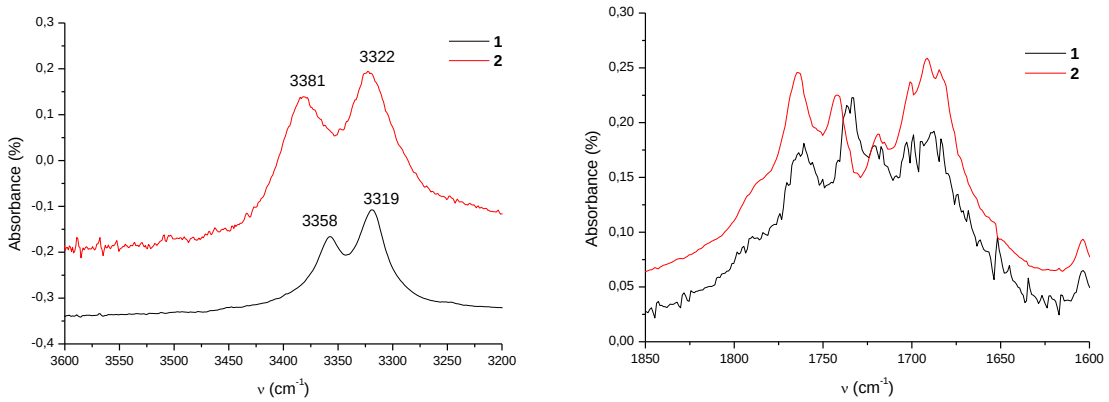

Figure 52. FT-IR absorption spectra in the N-H (left) and C=O (right) stretching regions for a 1% solid mixture with KBr of oligomers **24** and **25** at room temperature.

From the analysis of the two compounds in solution and in the solid state, it is only possible to say that both compounds tend to aggregate in the solid state, without any information about how they do it. For this purpose, an analysis of the two compounds was carried out by means of microscopy and X-ray diffraction.

A wide morphological variety of samples based on compounds **24** and **25** obtained by evaporation from different solvents were analyzed by optical and electronic microscopy.

The samples were precipitated by overnight evaporation of aliquots (20.0 mg each) from several solvents (methanol, ethanol, acetonitrile, cyclohexane/ethyl acetate, 1:1 mixture, or diethyl ether, 1.0 mL each). A fast precipitation was also achieved by rotary evaporation. The obtained solids showed different morphologies depending on the kind of solvent and the solvent evaporation rate. In any case, the precipitation of **24** provoked the formation of a solid material made of

filamentous aggregates, in which the crystals showed a preferential direction of growth and had a strong tendency to aggregate laterally. This material always showed birefringence suggesting a high crystallinity (Figure 53a,c). Only when **24** was exsiccated by means of a rotary evaporator a powder-like material was obtained. Crystals of **24** suitable for a single crystal X-ray diffraction investigation were obtained only from methanol evaporation. An image of these crystals by scanning electron microscopy is reported in Figure 53c. They appear elongated in one direction with a hexagonal cross-section. Their length varied from one crystal to another in the range of several hundred of micrometers, while their thickness was almost constant around 20 μm. On the contrary, compound **25** did not always precipitate forming a filamentous structure (data not shown). It precipitated as a mixture of powder and small (around 1 μm) elongated crystal aggregates from acetonitrile, cyclohexane/ethyl acetate, or diethyl ether, while by evaporation from protonated solvents, methanol or ethanol, elongated single crystals were obtained (Figure 53b,d). Of these, only the ones precipitated from ethanol were suitable for single crystal X-ray diffraction studies (see later). These crystals were also observed by scanning electron microscopy that showed an irregular morphology in which plate-like shapes are visible.

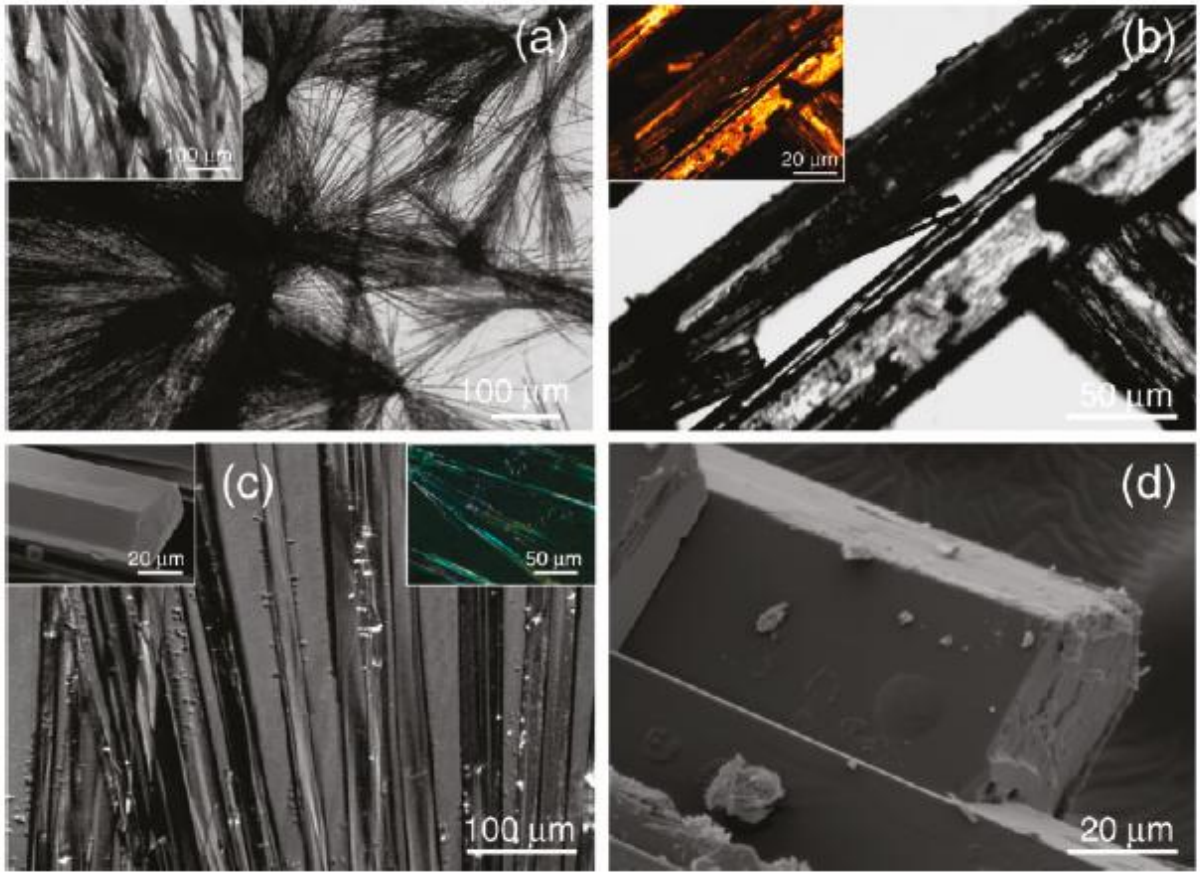

Figure 53. (a) Optical micrographs of **24** precipitated from cyclohexane/ethyl acetate. The elongated growth of the crystal is observable together with their high lateral aggregation. (c) Single crystals of **24** precipitated from ethanol, they are birefringent and have a hexagonal cross-section. (b, d) Crystals of **25** precipitated from ethanol observed by means of an optical and an electron microscope, respectively.

The crystals of **24** and **25** that precipitated from different solvents were analyzed by X-ray powder diffraction. Compound **24** gave only one kind of crystals, irrespective of the solvent used (methanol, ethanol, acetonitrile, cyclohexane/ethyl acetate, or diethyl ether) in the crystallization trials. Interestingly, the same kind of crystals precipitated even when the process was carried out in very harsh conditions, such as rotary evaporator (Figure 54a). This tendency to precipitate in a unique conformation may indicate a high stability of this form, which may be already present in solution, before the precipitation process starts. Compound **25** showed a different behavior with respect to compound **24**. It precipitated as a crystalline polymorph from methanol or acetonitrile, as a different polymorph from ethanol, and as a third polymorph from cyclohexane/ethyl acetate or diethyl ether (Figure 54b). The exsiccation of **25** using a rotary evaporator provoked the formation of a low crystallinity material, which could be a new polymorph or a mixture of polymorphs already precipitated from other solvents. It is conceivable to consider that the precipitation of this latter polymorph is strongly affected by the polarity and protonation of the solvent, as well as by the rate of crystallization. It is also interesting to note that the material precipitated from ethanol contained traces of the polymorphs obtained after precipitation from methanol or acetonitrile (Figure 55b).

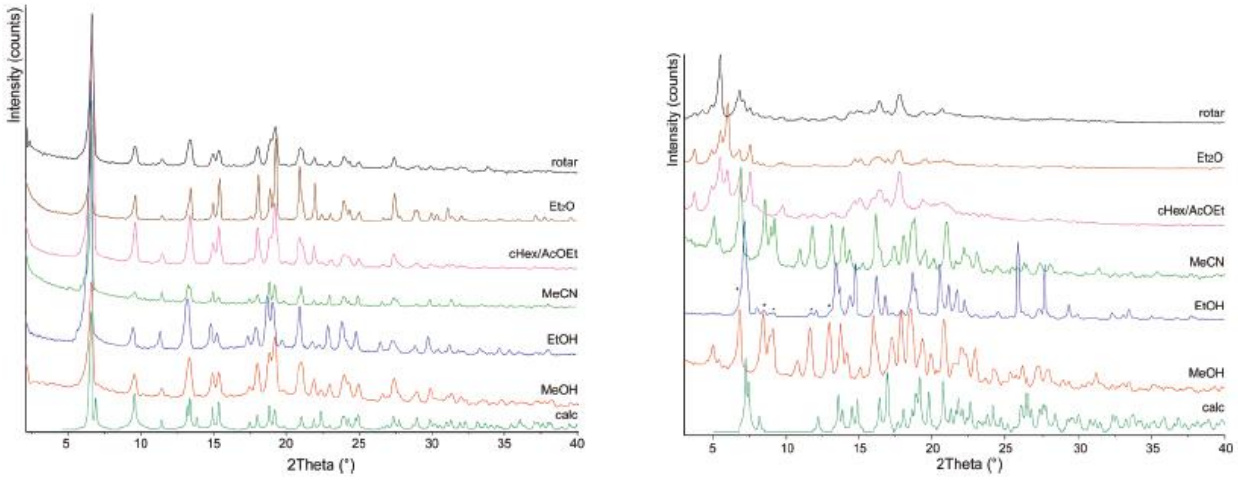

Figure 54. (Left) X-ray powder diffraction patterns of **24** precipitated from different solvents and exsiccated using a rotary evaporator. The calculated diffraction pattern from the structure of **24** obtained from crystals precipitated from methanol is shown as well. (Right) X-ray powder diffraction patterns of **25** precipitated from different solvents and exsiccated using a rotary evaporator. The calculated diffraction pattern from the structure of **25** obtained from crystals precipitated from ethanol is shown as well. Rotar indicate a material exsiccated by means of a rotary evaporator; MeOH, EtOH, MeCN, *c*Hex/AcOEt, and Et_2O indicate a material precipitated from methanol, ethanol,

acetonitrile, cyclohexane/ethyl acetate, and diethyl ether respectively; calc indicates the calculated diffraction pattern.

Crystals suitable for an X-ray diffraction study were grown only by slow evaporation of a solution of **24** in methanol and of **25** in ethanol, both at room temperature. Any effort to grow from methanol crystals of **25**, suitable for X-ray studies, was unsuccessful.

The X-ray molecular structures of **24** and **25** are reported together in Figure 55, panels a and b, respectively, and relevant torsion angles for both are listed in Table 2. The two molecules are epimers and differ only for the configuration of the stereogenic center C6 which is *S* in **24** and *R* in **25**. As a consequence of this different stereogenic center, **25** has a higher degree of folding than **24** (closer contact O8···H15A 3.05 Å), but no classical intramolecular hydrogen bond is observed in both epimers, in contrast with the behavior of **25** in solution.

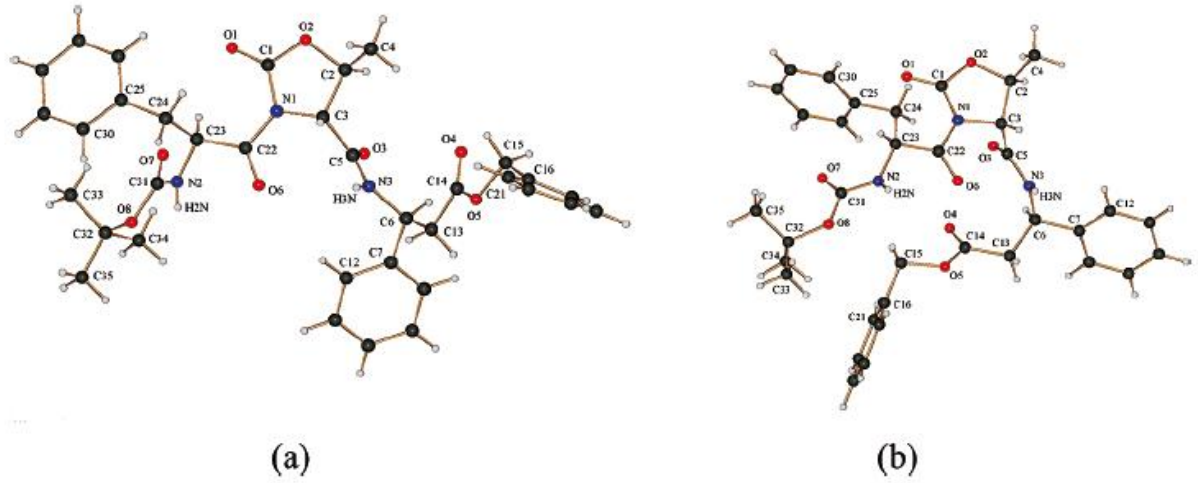

Figure 55. X-ray molecular structures of the two epimers **24** (a) and **25** (b).

Each molecule of **24** is engaged in four intermolecular N-H···O=C hydrogen bonds of two types with the adjacent neighbors. Two interactions connect the amidic hydrogens of the side chain bearing the Boc group and the carbonylic oxygens of the amidic unit of the other side arm [N2-H2N···O3′, symm. op.: (I) -x + y, -x, z + 1/3; O3···H2N″-N2″, symm. op.: (II) -y, x - y, -1/3 + z], while the ones of the second type involve the amidic hydrogen H_3N and the carbonylic oxygen of the D-Oxd ring [N3-H3N···O1′, O1···H3N″-N3″]. The crystal packing of **24** (Figure 56) therefore consists of parallel chains with a helical arrangement (Figure 57) running along the c axis. The formation of a

ternary helix in the solid state is in agreement with the SEM analysis as the crystals of **24** from methanol appear elongated in one direction with a hexagonal cross-section (Figure 53c).

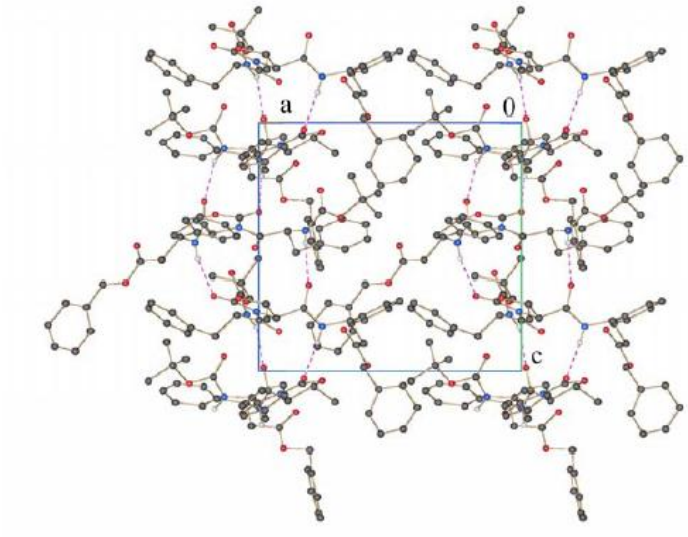

Figure 56. View down the b axis of the crystal packing of **24** showing the N-H···O=C H bonds. Only the hydrogen atoms involved in H bonding are shown.

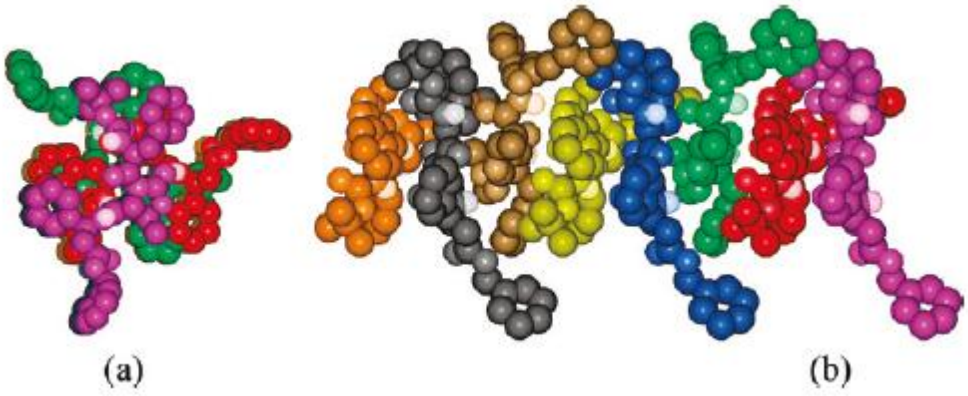

Figure 57. Space filling model showing the helical arrangement of one of the chains of **24**: (a) top view, (b) view along the *c* axis. The molecules are represented in different colors for clarity. The hydrogen atoms involved in N-H···CO hydrogen bonds are represented as white cups.

A closer inspection of the crystal packing of **24** reveals the presence of weaker intermolecular non classical H bonds beside the already mentioned N-H···CO hydrogen bonds generating the 1-D network. In particular, two of these H bonds are established between the carbonylic oxygen O1 and the acidic proton of the D-Oxd ring of an adjacent molecule. Other two weak H bonds are observed between the endocyclic oxygen of the D-Oxd ring and one proton of a phenyl ring. All

these intermolecular interactions further stabilize the 1-D network, being oriented almost parallel to the stronger N-H···OC hydrogen bonds.

A completely different packing is observed for epimer **25** (Figure 58) which maintains one intermolecular NH···OC hydrogen bond between equivalent amidic groups as observed in Boc-L-Phe-D-Oxd-OBn (**22**). In addition, a second weaker hydrogen bond is observed between the amidic hydrogen of the other amide group and the uncoordinated carboxylic oxygen bearing the Bn group. As a result, epimer **25** is engaged in four interactions that are weak in comparison with those found in Boc-L-Phe-D-Oxd-OBn (**22**), but the hydrogen bonding pattern in the crystal lattice shows the formation of infinite 1-D H-bonded polymer of tape running along the a axis.

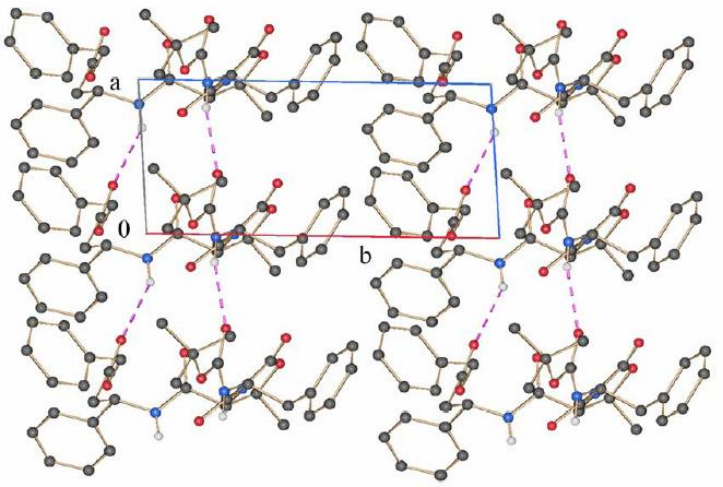

Figure 58. View down the c axis of the crystal packing of **25** showing the N-H···CO hydrogen bonds. Only the hydrogen atoms involved in N-H···CO hydrogen bonding are shown.

The supramolecular assembly of **25** is completed by other hydrogen bonding interactions. In detail the 1-D supramolecular polymer of **25** is further stabilized by CH/π bonding between the acidic hydrogen (H6) of one molecule and one phenyl ring of the neighbors. As a difference with the crystal packing of **24**, there are also weak interchain H bonds involving the endocyclic oxygen O2 of the D-Oxd ring and an aromatic hydrogen H19.

To further investigate the effect of the absolute configuration variation of the β_3-hPhg moiety on the properties of **24** and **25** in the solid state, single crystals of **24** and **25**, obtained respectively, from methanol and ethanol, were also analyzed in their thermal properties by differential scanning calorimetry and thermogravimetry. Compound **24** undergoes an endothermic transition at a temperature of 170 °C, where it fuses converting to an amorphous material. After this first

thermal event, **24** shows a successive broad endothermic peak having a temperature of onset at about 206 °C and maximum at about 222 °C (Figure 59). At 206 °C **24** starts to decompose, as shown by thermogravimetric analysis (TGA). Compound **25** shows a differential scanning calorimetry (DSC) profile similar to that of **24**. First an endothermic peak appears at 167 °C, which is associated with a transition from the crystalline to an amorphous state (Figure 9), and then a broad endothermic peak follows with an onset and maximum temperature of about 218 and 240 °C, respectively.

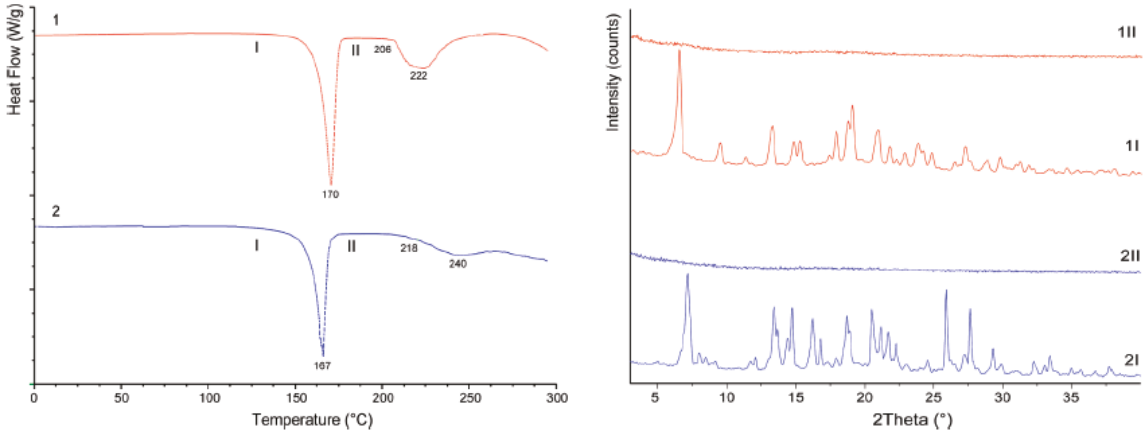

Figure 59. (Left) Differential scanning calorimetry profiles from single crystals of **24** and **25**. (Right) X-ray powder diffraction patterns corresponding to different regions in the thermal profiles of **24** and **25**.

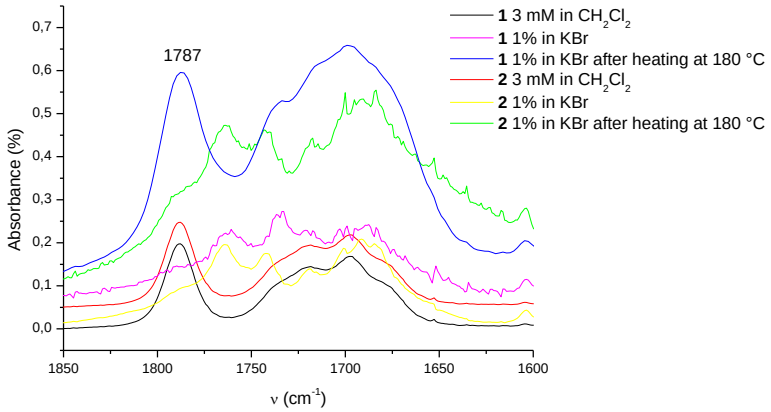

Figure 60. FT-IR absorption spectra in the C=O (right) stretching regions for oligomers **24** and **25** under different conditions. Black line: **24** in 3 mM solution in CH_2Cl_2; magenta line: **24** in 1% mixture with KBr; blue line: **24** crystallized from methanol, after heating at 180 °C (polymorph **24**-II); red line: **25** in 3 mM solution of CH_2Cl_2; yellow line: **25** in 1% mixture with KBr; green line: **25** crystallized from ethanol, after heating at 180 °C (polymorph **25**-II).

The **24**-II FT-IR spectrum in the C=O bands region presents a band at 1787 cm^{-1} and a broadband centered at about 1700 cm^{-1}. A similar FT-IR spectral region is observed when **24** is present in a

dilute solution of CH_2Cl_2 (Figure 60). This suggests that, as a consequence of the thermal treatment, after the first endothermic peak, compound **24** goes in an amorphous state, in which it assumes conformations similar to those in solution. In contrast, the IR analysis of a sample of **25** after thermal treatment does not show any peak at 1780 cm^{-1}; thus, its amorphous state somehow still retains an ordered structure.

3.3.2 One more Phe …

Since the emergence of Phe-Phe as a self-assembling building block, many studies have been made to organize the FF-based building blocks into various functional nanostructures such as nanotubes (Figure 61), spherical vesicles, nanofibrils, nanowires and ordered molecular chains.[47]

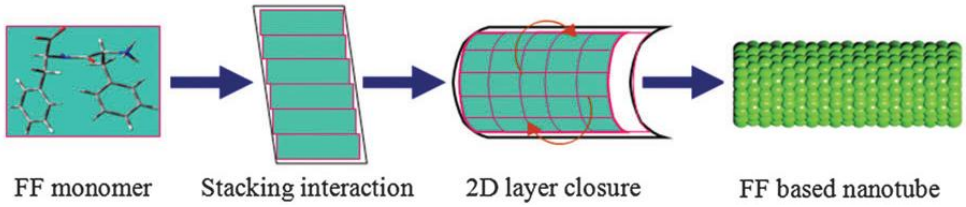

Figure 61. A proposed schematic illustration of formation of Phe-Phe-based nanotubes.

Thus, we prepared the tripeptide Boc-L-Phe-L-Phe-D-Oxd-OBn (**26**) to determine its properties in the solid state (Figure 62).

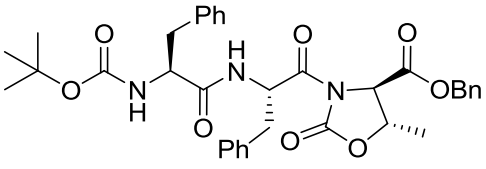

Boc-L-Phe-L-Phe-D-Oxd-OBn **26**

Figure 62. Chemical structure of Boc-L-Phe-L-Phe-D-Oxd-OBn.

[47] Yan, X.; Zhu, P.; Li, J. *"Self-assembly and application of diphenylalanine-based nanostructures"* Chem. Soc. Rev. **2010**, *39*, 1877-1890.

The ^{1}H NMR spectrum of **26** shows the presence of a single conformer, that tends to aggregate into crystalline fibre-like materials, due to its rigid conformation. In Figure 63, optical microscopy (OM) and SEM images of **26** are reported.

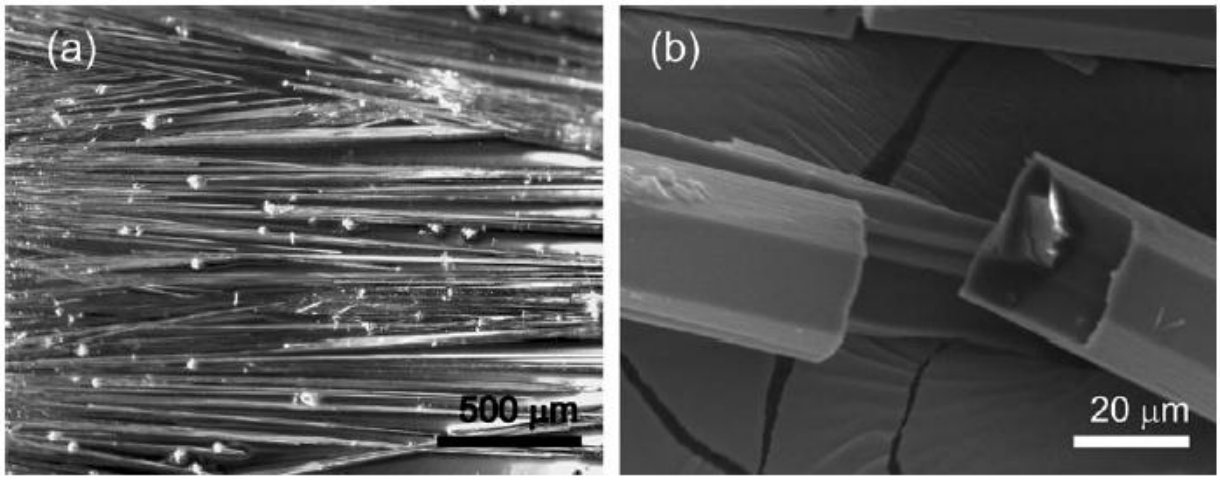

Figure 63. a) OM and b) SEM images of **26**.

It is possible to observe that **26** forms elongated crystals (up to a few millimeters) locally iso-oriented. Each single crystal (about 20 mm thick) has a well-defined crystalline habit and shows faces that are probably parallel to the crystallographic *a* axis. The pseudo-hexagonal cross-section is also shown.

The conformational analysis of **26** in the solid state was further elucidated by a single-crystal X-ray diffraction study.

The molecular conformation of **26** is shown in Figure 64a and relevant torsion angles are reported in Table 3. The backbone torsion angles for the two L-Phe units correspond approximately to those in peptide β strands. In the crystal packing of **26** (Figure 64b) each molecule is connected through four intermolecular NH···OC hydrogen bonds [N2H2N···O6′ 2.204 Å, N2···O6′ 3.005(4) Å, N2-H2N···O6′ 163°, symmetry code (I): *x*-1,*y*,*z*; N3H3N···O7″ 2.137 Å, N3···O7″ 2.941 Å, N3-H3N···O7″ 168°, symmetry code (II): *x* + 1,*y*,*z*] to two neighbours, thus generating an infinite parallel β-sheet structure running along the crystallographic *a* axis. Interestingly, this arrangement is similar to that

observed in Boc-L-Phe-D-Oxd-OBn, in which one unit is connected to the adjacent ones through single NH···OC hydrogen bonds.[48]

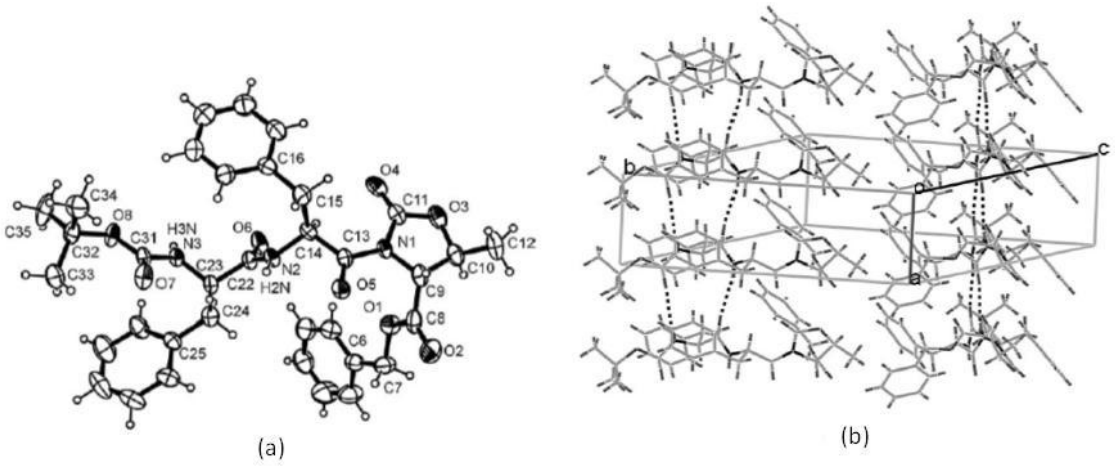

Figure 64. a) X-ray molecular structure and b) crystal packing of **26**.

Table 3. Selected backbone torsional angles [°] for **26**.

L-Phe1	C31-N3-C23-C22	ϕ_1	-127.3(3)
	N3-C23-C22-N2	ψ_1	109.5(3)
L-Phe2	C22-N2-C14-C13	ϕ_2	-126.4(3)
	N2-C14-C13-N1	ψ_2	147.9(3)
Oxd	C13-N1-C9-C8	ϕ_3	56.2(4)
	N1-C9-C8-O1	ψ_3	32.4(4)

We could also confirm that Oxd moiety was essential for the properties of the supramolecular material. Compounds **19** and **20** were synthesized replacing the D-Oxd moiety with a D-Pro (D-Pro = D-proline) moiety in compounds **22** and **26** (Figure 65).

[48] Guha, S.; Drew, M. G. B.; Banerjee, A. *"Construction of supramolecular helices and breaking the helicity by forming supramolecular β-Sheet structures using suitable self-assembling pseudopeptide building blocks"* Cryst. Growth. Des. **2010**, *10*, 47164721.

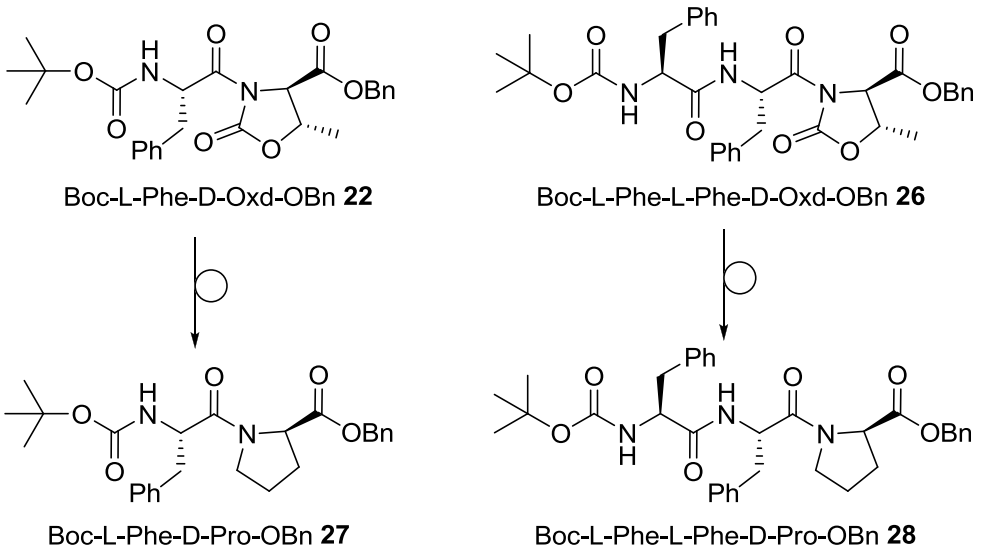

Figure 65. Molecules **27** and **28** where synthesized as they are the same backbone of **22** and **26**, but with a proline heterocycle instead of an oxazolidinone one.

In contrast with their Oxd analogues, compounds **27** and **28** do not show any propensity to form fibre-like materials because they hardly become solids: **27** is a liquid and **28** is an amorphous solid, as shown by its powder X-ray diffraction (not reported).

3.4 Gel

In daily life most people encounter systems based on gelating agents, often without realizing it. From a scientific perspective a definitive definition of a gel is still lacking, mainly due to the chemical diversity encountered in gelation science. The gel state has been recognized already for over 150 years. In 1861 Thomas Graham gave the following description: "*While the rigidity of the crystalline structure shuts out external expressions, the softness of the gelatinous colloid partakes of fluidity and enables the colloid to become a medium for liquid diffusion, like water itself*".[49] In the following years more rigorous definitions were proposed which attempted to link the microscopic and macroscopic properties of a gel.[50] Based on these definitions a substance is a gel if it (i) has a continuous microscopic structure with macroscopic dimensions that is permanent on the time scale of analytical experiments and (ii) is solid-like in its rheological behaviour despite

[49] Graham, T. *"Liquid Diffusion Applied to Analysis"* Phil. Trans. Roy. Soc. **1861**, *151*, 183-224.
[50] a) Flory, J.P. *"Theoretical aspects of photoemission, photodesorption and photochemistry of adsorbates"* Faraday Discuss. Chem. Soc. **1974**, *57*, 7-18; b) Gelbart, W.M.; Ben-Shaul, A. *"*Micelles, membranes, microemulsions and monolayers" J. Phys. Chem. **1996**, *100*, 13169-13189.

being mostly liquid.[51] Nevertheless, for screening programs the succinct definition of Jordon Lloyd is still useful: if it looks like a gel it must be a gel.[52]

In general, a gel is the result of the self-assembly process of compounds which are capable of forming a 3D-network. Due to the formation of this network the solvent is not able to flow and the solvent, which is liquid at high temperatures, is solidified at room temperature.

Gels can be divided in two separate classes, chemical and physical gels. The chemical gels are classified as gels in which the aggregation is driven by the formation of covalent cross-links between the compounds and this aggregation leads to the formation of a thermally irreversible network.[53] Examples of these systems include cross-linked polymeric systems, which can be used for triggered drug release[54] or inorganic oxides.[55] Physical gels systems are formed by non-covalent interactions and, hence, the gel formation is thermally reversible, which makes this type of gelators an excellent subject for studies into supra-molecular chemistry.

Compounds able to form physical gels include clays, polymers, proteins, colloids and certain small organic compounds. Compounds of this latter group are called low molecular weight gelators (LMWGs). LMWGs are gelators consisting of organic compounds with a molecular weight of less than 2000 Da which show gelation behaviour in organic solvents (organogelators) and sometimes in water and/or alcoholic solvent (hydrogelators).

It has been demonstrated that anisotropy in intermolecular interactions leading to self-assembly of gelator molecules is necessary for the formation of a gel fiber.[56] Intermolecular interactions between gelator molecules can include London dispersion forces, ionic-ionic, dipole-dipole, hydrogen bonding, Van der Waals and π-π stacking interactions and in the majority of gel systems reported the combination of these forces are responsible for gelation. It has been demonstrated that there is a delicate balance between gelator structure, intermolecular interactions and gelation properties.

---

[51] Weiss, R.G.; Terech, P. *"Molecular gels: materials with self-assembled fibrillar networks"* Springer **2006**, Dordrecht. ISBN 1-4020-3352-4.

[52] Jordan Lloyd, D. *"In Colloid Chemistry by Alexander, J."* **1926**, vol 1, 767-782, The Chemical Catalog Co, New York.

[53] Gesser, H.D.; Goswami, P.C. *"Aerogels and related porous materials"* Chem. Rev. **1989**, *89*, 765-788.

[54] Daganli, R. *"Intelligent gels"* Chem. & Eng. News, **1997**, *23*, 26-37.

[55] Boury, B.; Corriu, R.J.P.; Le Strat, V.; Delord, P.; Nobili, M. "Hydrolysis/polycondensation in the solid state: access to crystalline silica-based hybrid materials" Angew. Chem., Int. Ed. **1999**, 38, 3172-3175.

[56] a) Van Esch, J.H.; Feringa, B.L. *"New functional materials based on self-assembling organogels: from serendipity towards design"* Angew. Chem., Int. Ed. Engl. **2000**, *39*, 2263-2266; b) Estroff, L.; Hamilton, A.D. *"Water gelation by small organic molecules"* Chem. Rev. **2004**, *104*, 1201-1217.

3.4.1 From Boc-L-Phe-D-Oxd-OBn to new LMWGs

It was stated that the L-Phe-D-Oxd moiety can be defined a "privileged scaffold" because of its strong tendency to adopt well-organized 3D structure. For this reason, in this chapter it is described how the L-Phe-D-Oxd group it is included in more complex structures to behave as LMWGs, since an intermolecular interaction of suitable strength was required for the formation of a gel.

In this chapter, two long-chain derivatives of Boc-L-Phe-D-Oxd-OBn **22** were synthesized to determine the properties of these new compounds as LMWGs. After several attempts, compounds **29** and **30** were synthesized, which were two derivatives of azelaic acid, a dicarboxylic, medium-sized aliphatic acid. Interestingly, no derivative of monocarboxylic acids, such as hexanoic or undecanoic acids, form any kind of gel.

Compounds **29** and **30** may be defined as synthetic bolaamphiphiles.[57] In general, these compounds reproduce the unusual architecture of monolayered membranes found in archaebacteria.

Compound **22** was deprotected with TFA in dichloromethane to obtain the corresponding trifluoroacetate salt in quantitative yield; this was coupled with azelaic acid, using HBTU and triethylamine (Scheme 5). Compounds **29** was obtained pure after flash chromatography in high yields. Then, it was deprotected by hydrogenolysis to give the free carboxy termini **30** in quantitative yield.

[57] Shimizu, T. *"Bottom-up synthesis and structural properties of self-assembled high-axial-ratio nanostructures"* Macromol. Rapid Commun., **2002**, *23*, 311-331.

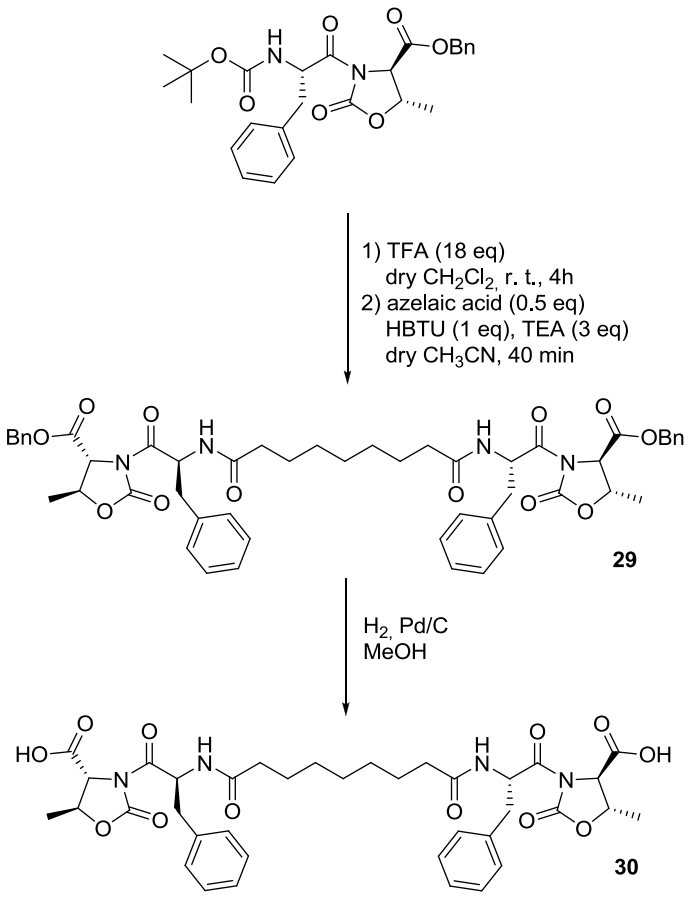

Scheme 5. Preparation of compounds **29** and **30**.

Then, the propensity of these two compounds to form gels was determined. The general method adopted to form gels was to place one compound (**29** or **30**) in a small test tube (8 mm in diameter) and dissolve it in pure solvent (distilled water was used) or in a solvent mixture (Table 4) to obtain a 10 mM solution. Because ultrasound influences the aggregation properties of the molecules in the solvents,[58] the tube was sonicated for 20 min at room temperature, then it was left to stand for 2 h before gel formation was monitored. When a mixture of solvents was used, the solvent that the gelling compound was more soluble in was introduced first (i.e., dichloromethane was introduced first in entry 1 and methanol was introduced first in entry 5 in Table 4).

Table 4. Gelation properties of compounds **29a**-**d** and **30a**-**d** in selected solvents (concentration: 10 mM).

Entry	Solvent	Compd.	After sonication[a]	After 2 h[a]

[58] Isozaki, K.; Takaya, H.; Naota, T. *"Ultrasound-induced gelation of organic fluids with metalated peptides"* Angew. Chem. Int. Ed. **2007**, *46*, 2855-2857.

1	CH_2Cl_2/AcOEt 1:1	**29**	SP	G
2	CH_2Cl_2	**29**	S	PG
3	AcOEt	**29**	SP	PG
4	MeOH	**30**	SP	SP
5	H_2O	**30**	SP	PG
6	MeOH/H_2O 1:1	**30**	G	G

[a] SP = suspension; G = gel; PG = partial gel; S = solution

The most common diagnostic test of gelation is tube inversion. In this test, a sample tube containing the mixture of compound and solvent was inverted to ascertain if the sample would flow under its own weight. A gel was assumed to be a sample that had a yield stress that prevented it from flowing down the tube. A solution was taken to be a sample that flowed down the tube. When a partial gel is formed, the compound sticks to the bottom of the test tube, while a little solvent (< 20%) flows down.

Compounds **29** and **30** form gels (Table 4, entries 1 and 6) or partial gels (Table 4, entries 2, 3 and 5).

To check the structural properties of the gels formed, we carried out our studies only on the gel reported in entry 1 as an example of this class of compounds (Figure 66).

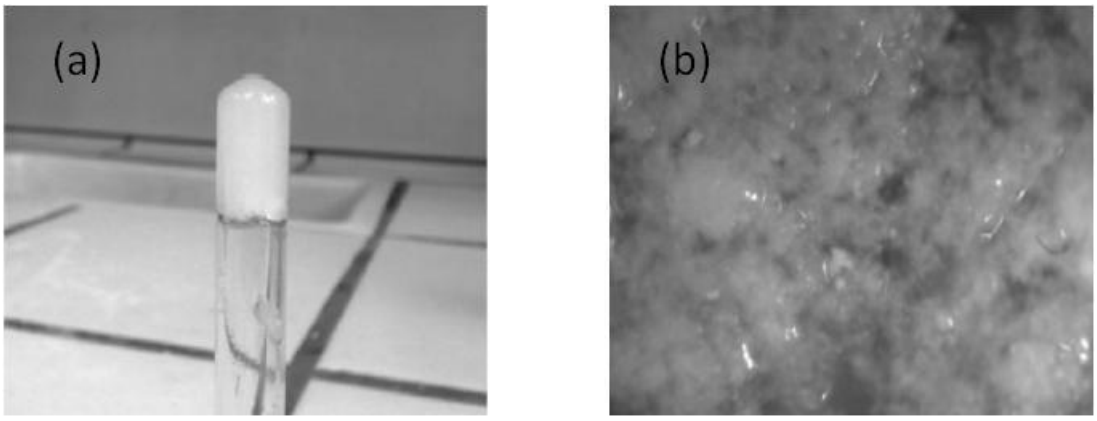

Figure 66. a) Photograph of **29** in a 1:1 mixture of dichloromethane and ethyl acetate (10 mM solution); b) OM image of the same sample; scale bar: 500 µm.

Then, the sample was left to dry in air to form the xerogel and was completely dry after 24 h at 20 °C. The FTIR spectrum (1% in dry KBr) was recorded and compared it with the spectra of **29** in dilute solution (3 mM in dichloromethane) and as a precipitated material (1% in dry KBr) (Figure 67). The spectra of both the precipitated sample and the xerogel showed the presence of a signal

at about 3310 cm^{-1}, typical of C=O···H-N hydrogen bonds, whereas the 3 mM solution had a signal at 3430 cm^{-1}, which was attributed to the presence of a free NH group.

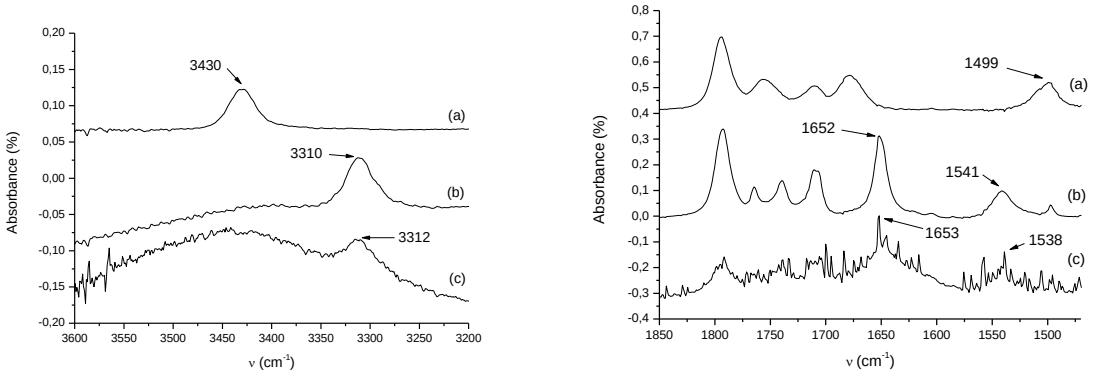

Figure 67. FTIR absorption spectra in the N-H (left) and C=O (right) stretching regions for **29**: a) 3 mM solution in pure CH_2Cl_2; b) solid as 1 % mixture with dry KBr; and c) xerogel as a 1 % mixture with dry KBr.

Further investigations, using SEM, gave a better idea of the morphology of the xerogel (Figure 68): it forms long filaments highly interconnected and branched with a diameter of about 0.5 µm. They have a strong tendency to aggregate, forming a network of meshed and bundled architectural assemblies (Figure 68a). These observations fit with the OM images and the FTIR spectral analyses. The gel appears opaque, suggesting the existence of extended molecular assemblies in the wet gel.[59] Moreover, the FTIR spectrum indicates that this molecule may assemble into an organized form by hydrogen-bonding interactions as soon as a limit concentration that favors the formation of β sheets is reached.

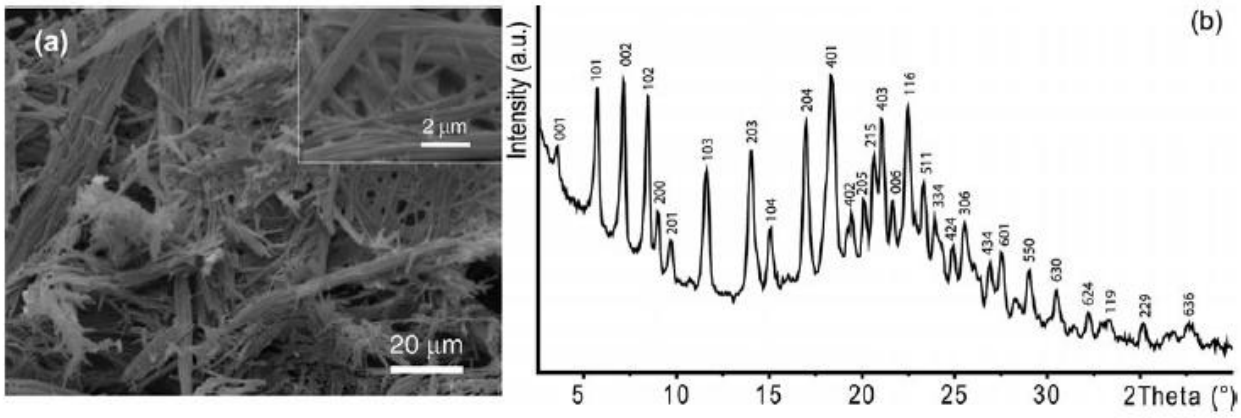

[59] Estroff, L. A. Hamilton, A. D. *"Water gelation by small organic molecules"* Chem. Rev. **2004**, *104*, 1201-1217*; b)* Mahmoudi, N.; Mehalebi, S.; Nicolai, T.; Durand, D.; Riaublank, A. *"Light-scattering study of the structure of aggregates and gels formed by heat-denatured whey protein isolate and β-lactoglobulin at neutral pH"* J. Agric. Food Chem. **2007**, *55*, 3104-3111

Figure 68. SEM picture (a) and XRD patterns (b) of the xerogel prepared from **29**. In (a) the inset shows a high magnification of the wide view. The diffraction peaks have been indexed according to a tetragonal unit cell (a = 1.97 nm, c = 2.67 nm).

An additional clue to the presence of an ordered assembly of molecules in the xerogels is given by XRD analysis (Figure 68, b). The XRD pattern of the xerogel of **29** shows many sharp diffraction peaks and a broad band at around 2ϑ = 20°, which suggests the coexistence of amorphous and high crystalline phases. The diffraction peaks have been indexed according to a tetragonal unit cell (a = 1.97 nm, c = 2.67 nm). These unit cell parameters agree with long-range ordering and suggest that **29** may form crystalline multilayer structures within the self-assemblies. This observation agrees with that observed for 2-glucosamide-based bolaamphiphiles.[60]

3.4.2 More complex gels

In the previous chapter it was demonstrated the ability of the pseudopeptide L-Phe-D-Oxd to behave as LMWG when it is introduced in a more complex architecture. After the good results obtained with LMWG **29** and **30**, it was decided to check if also other pseudopeptide that have been previously described are able to behave in the same way.

A small library of stereoisomeric compounds, all containing a moiety of azelaic acid coupled with different pseudopeptides was prepared.

Scheme 6 reports the general formula of the ten compounds: they are five benzyl esters and five carboxylic acids. These compounds were synthesized in solution, by standard coupling reaction.

[60] Nakazawa, I. Masuda, M.; Okada, Y.; Hanada, T.; Yase, K.; Asai, M. Shimizu, T. *"Spontaneous formation of helically twisted fibers from 2-glucosamide bolaamphiphiles: energy-filtering transmission electron microscopic observation and even-odd effect of connecting bridge"* Langmuir **1999**, *15,* 4757-4764.

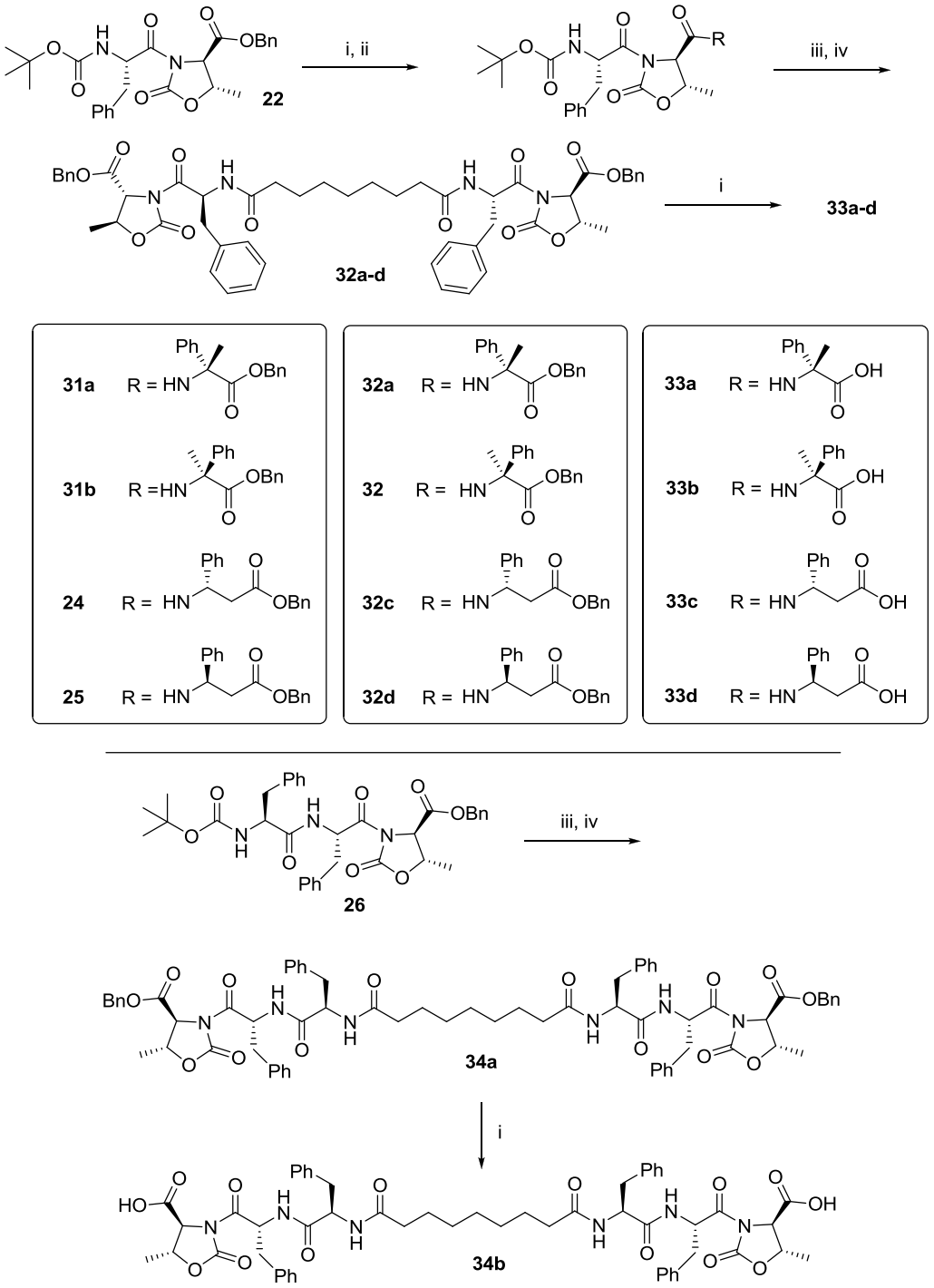

Scheme 6. Reagents and conditions (i) H_2, Pd/C MeOH, r,t. 2 h; (ii) α- or β-amino acid (1 equiv.), HBTU (1 equiv.), TEA (3 equiv.) dry CH_3CN, 40 min; (iii) TFA (18 equiv.), dry CH_2Cl_2, r. t., 4 h; (iv) azelaic acid (0.5 equiv.), HBTU (1 equiv.), TEA (3 equiv.) dry CH_3CN, 40 min.

The tendency of these compounds to form gels was checked with the tube inversion test. To prepare gels, compounds **32a**-**d**, **33a**-**d** and **34a**-**b** were weighted out exactly in a test tube (8 mm wide), and then dissolved in the solvents reported in Table 5 (500 µl) to afford a 10 mM solution.

The tube was then shaken for a few minutes by hand and then sonicated for 15 min at room temperature, then it was left standing still overnight before checking the gel formation.

Table 5. Gelling status of the molecules **32a-d**, **33a-d** and **34a-b**. SP suspension, G gel, PG partial gel, S solution, P precipitate.

Entry	Solvent	Compound	After sonication	After 2 h
1	CH_2Cl_2/AcOEt 1:1	**32a**	SP	SP
2	CH_2Cl_2/AcOEt 1:1	**32b**	SP	SP
3	CH_2Cl_2/AcOEt 1:1	**32c**	SP	G
4	$CHCl_3$/AcOEt 1:1	**32c**	SP	SP
5	AcOEt	**32c**	PG	PG
6	Acetonitrile	**32c**	PG	PG
7	CH_2Cl_2/AcOEt 1:1	**32d**	SP	G
8	$CHCl_3$/AcOEt 1:1	**32d**	PG	PG
9	AcOEt	**32d**	G	G
10	Acetonitrile	**32d**	G	G
11	MeOH/H_2O 1:1	**33a**	S	S
12	MeOH/H_2O 1:1	**33b**	S	S
13	CH_2Cl_2	**33c**	P	P
14	H_2O	**33c**	P	P
15	MeOH/H_2O 1:1	**33c**	S	G
16	*i*-PrOH/H_2O 1:1	**33c**	PG	PG
17	*i*-PrOH	**33c**	PG	G
18	CH_2Cl_2	**33d**	PG	PG
19	H_2O	**33d**	SP	SP
20	MeOH/H_2O 1:1	**33d**	S	G
21	*i*-PrOH/H_2O 1:1	**33d**	SP	PG
22	*i*-PrOH	**33d**	P	P
23	CH_2Cl_2/AcOEt 1:1	**34a**	SP	G
24	CH_2Cl_2	**34a**	S	S
25	AcOEt	**34a**	SP	G
26	MeOH	**34b**	S	S
27	H_2O	**34b**	S	S
28	MeOH/H_2O 1:1	**34b**	SP	G

The best outcome was obtained with a 1:1 mixture of dichloromethane/ethyl acetate for **9c**, **9d** and **11a**, with AcOEt for **11a** and with a 1:1 mixture of water and methanol for **10c** and **10d** and **11b**. These mixtures of solvents were used to check if the more expensive compounds containing the αMe-Phg moiety (**9a**, **9b**, **10a** and **10b**) would form a gel. Unfortunately no gel formation was obtained in any case.

3.4.3 Gels in the presence of metal ions

The work was then continued only with compounds **32c**, **32d**, **33c** and **33d** to test their ability to generate a gelling status in the presence of several metal ions: Mg(II), Al(III), Zn(II), Cu(I) or Cu(II). The selection among the metal ion species was carried out trying to discriminate among two parameters: coordination chemistry and charge density. Mg(II) and Cu(II) have similar ionic radius (0.78 and 0.72 Å, respectively), but the former one forms mainly octahedral coordination compounds, while the latter one gives distorted octahedral coordination compounds that usually reorganize in tetrahedral or square planar geometries. Cu(I) ions and zinc ions have different ionic radius (0.325 and 0.632 Å, respectively), but both preferentially form tetrahedral coordination compounds, however, Zn(II) have also a strong tendency to give octahedral geometries. Al(III) (ionic radius 0.45 Å) can give coordination compounds having tetrahedral and octahedral geometries, being the latter more common in the presence of charged ligands.[61] These metal ions have also different charge density: Al(III) > Zn(II) > Cu(II) ≈ Mg(II) > Cu(I). The choice among the biological friendly chloride or bromide as counter anion was carried out in the view to give the gel a potential use of the gels to control the release of metal ions. As a consequence, we paid a price in term of solubility in organic solvents.

Gels were prepared by suspension of an equimolecular amount of **32c** (or **32d**) and the inorganic salt, followed by sonication (see experimental). After 16 h, an homogeneous gel was formed. In the case of copper salts, the gel was pale green while in the other cases the gel was colorless. In the case of gels formed with **33c** (or **33d**) and the inorganic salt in methanol/water mixture, an homogeneous mixture was immediately formed and became a colorless gel after 16 h.

[61] Cotton, F. A.; Wilkinson, G.; Murillo, C. A.; Bochmann, M. **1999**, Advanced inorganic chemistry, 6th edn. Wiley, New York.

The gel-sol transition temperature (T_{gel}) gives important information on the thermal stability of the gels prepared in different ways[62] and was measured by the ball-dropping method.

The results of the gelation experiments of molecules **32c**, **32d**, **33c** and **33d** in the presence of metal ions are reported in Table 6.

Table 6. Gelling status of the molecules **32c**, **32d**, **33c** and **33d** in the presence of metal ions. The gel-sol transition temperature (T_{gel}) expressed in °C is reported in parenthesis. The gels that increase their T_{gel} (and consequently their thermal stability) in the presence of metal ions are in bold.

Molecule (solvent)	Metal ions free gel	CuBr	$CuBr_2$	$ZnBr_2$	$AlCl_3$	$MgBr_2$
32c (CH_2Cl_2/AcOEt, 1:1)	G (80)	PG	G (60)	G (50)	PG	PG
32d (CH_2Cl_2/AcOEt, 1:1)	G (58)	PG	**G (62)**	G (50)	**G (75)**	SP
33c (MeOH/H_2O, 1:1)	G (75)	PG	SP	G (59)	SP	G (42)
33d (MeOH/H_2O, 1:1)	G (82)	S	G (68)	**G (92)**	PG	S

SP suspension, G gel, PG partial gel, S solution

While all these molecules formed gels in the reported conditions, they behave differently, in the presence of these five metal ions.

In the presence of Zn(II), they all formed gels, however, the strength of the gel was reduced, except for **33d**. On the contrary, Cu(I) prevents the formation of gels in any case, as its presence in **32d**, **32c** and **33c** gave partial gels, while **33d** gave a suspension. A very different result was obtained with Cu(II): **32d**, **32c** and **33d** formed gels, while **33c** associated in a suspension. In the presence of Al(III) or Mg(II), the four compounds afforded very different results, as reported in Table 6. Only **32d** and **33c** form a gel in the presence of Al(III) and Mg(II), respectively.

In conclusion, among the tested molecules **32c** is the best gelator in the presence of metal ions, it always associates in a gel-like form, either gel or partial gel. **32d** failed to be in a gel-like form in the presence of Mg(II) only.

To obtain additional information on the molecular association, the gel samples were left to dry in the air to form xerogels that were further analyzed using SEM and XRD. The results of the SEM observations and of the XRD analyses are reported in (Figure 69, Figure 70 and Figure 71).

[62] a) Takahashi, K.; Sakai, M.; Kato, T. *"Melting temperature of thermally reversible gel. VI. Effect of branching on the Sol-Gel transition of polyethylene gels"* Polymer J. **1980**, *12*, 335-341; b) Yamanaka, M.; Fujii, H. *"Chloroalkane gel formations by tris-urea low molecular weight gelator under various conditions"* J Org Chem, **2009**, *74*, 5390-5394.

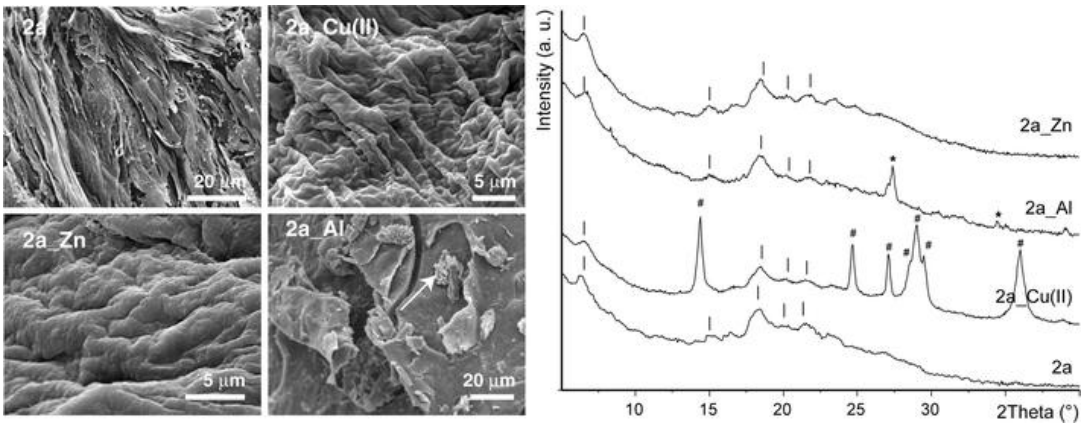

Figure 69. The SEM images of the xerogels formed by the molecule **32d**: in the absence of metal ions (**32d**); the presence Cu(II) (**32d**_Cu(II)); in the presence of Zn(II) (**32d**_Zn) or in the presence of Al(III) (**32d**_Al) are shown on the left. The arrow in (**32d**_Al) indicates a crystalline aggregate made of an aluminium salt. On the right side, the corresponding X-ray powder diffraction patterns are reported. Bars indicate the diffraction peaks which could be associated with crystalline regions of **32d**. Hash symbols indicate the diffraction peaks that can be associated with crystalline $CuBr_2$. Asterisks indicate the diffraction peaks associated with an Al containing compound that could not be identified (crystals from this unidentified compound are shown by the arrow in **32d**_Al).

The molecular assembly of **32d** in the xerogel is strongly affected by the presence of metal ions (Figure 69). The XDR data (Figure 69 right) show that **32d** is present in a crystalline form in the xerogel (as proved by the presence of several diffraction peaks) and that this status is not affected by the presence of metal ions, indeed the main diffraction peaks associated with the molecular structure do not change in relative intensity and angular position. This outcome indicates that metal ions do not influence the crystallinity and aggregation of the **32d** xerogels, therefore we can infer that the functional groups involved in the inter-molecular interactions responsible for the formation of the gel scaffold are not involved in the metal binding. In the XRD patterns from **32d**_Cu(II) and **32d**_Al xerogels, additional diffraction peaks associable to metal ion salts are detectable. Interestingly, the presence in the gel of metal ions compound crystalline particles (Cu(II) and Al(III)) increases its thermal stability (Table 6).

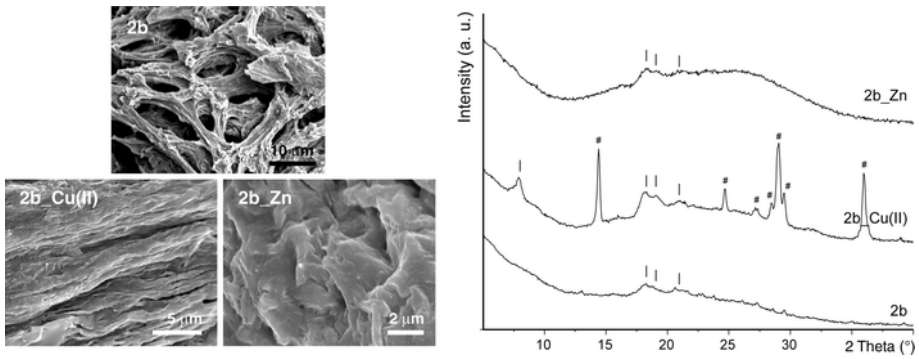

Figure 70. The SEM images of the xerogels formed by: the molecule **32c** (**32c**) in the absence of metal ions; the molecule **32c** in the presence Cu(II) (**32c**_Cu(II)) or in the presence of Zn(II) (**32c**_Zn), are shown on the left. On the right side, the corresponding X-ray powder diffraction patterns are reported. Bars indicate the diffraction peaks which could be associated to crystalline regions of **32c**. Hash symbols indicate the diffraction peaks that can be associated to crystalline $CuBr_2$.

The SEM morphologies and the XRD patterns of the **32c** xerogels are reported in Figure 70. **32c** associates forming a xerogel containing bundles of fibers that are branched, forming a complex web in which many holes are present. The presence of Cu(II) or Zn(II) changes the aggregation of **32c**, favouring the formation of highly twisted long rope-like aggregates, as previously observed for the **32d** xerogels obtained in similar conditions. This effect is not surprising, considering that the skeleton of **32d** and **32c** are very similar. The presence of Zn(II) seems to favour the merging of the rope-like structure giving a more compact material. The **32c**_Cu(II) xerogel hosts particles of crystalline copper bromide while the **32c**_Zn xerogel contains any Zn(II) crystalline compound. The crystallinity of **32c** in the xerogel increases in the presence of Cu(II), as revealed by the presence in the XRD pattern of more and more defined diffraction peaks.

Similar analyses were carried out on the xerogels obtained from **33d** and **33c** (Figure 71). These compounds are very polar, as they contain a carboxylic group, and can form gels with mixtures of water and methanol. Besides its ability to form gels as a pure compound, **33d** retains its ability to form gel in the presence of Cu(II) and Zn(II) only. In the xerogel status, **33d** associates forming a porous structure in which no well defined structural motifs are observable. In the presence of Zn(II), **33d**_Zn xerogel structure makes a more compact material, as could be foreseen considering the high thermal stability of the **33d**_Zn gel (see Table 6). Also in this case we could suppose that the metal ions affects the way in which the molecular scaffolds make the gel. All the XRD patterns from **33d** xerogels show only one diffraction peak, indicating that the molecules are associated in a poor ordered way. Weak diffraction peaks due to copper(II) bromide are observable only in the XRD pattern from the **33d**_Cu(II) xerogel.

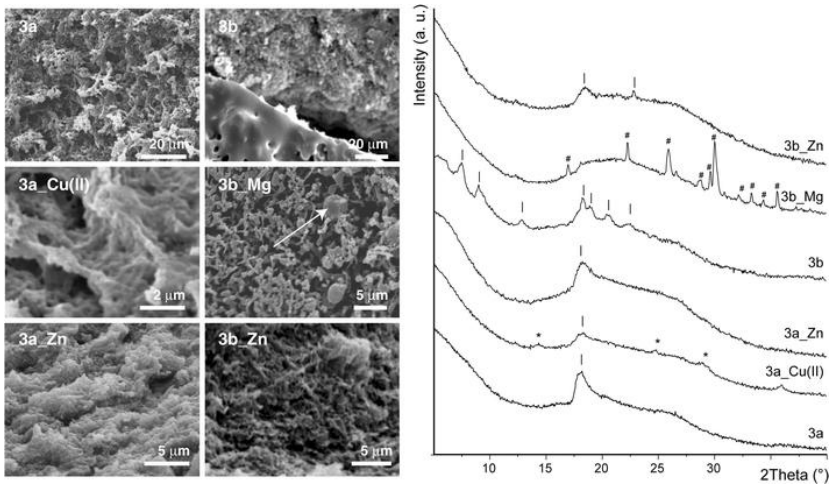

Figure 71. The SEM images of the xerogels formed by: the molecule **33d** (**33d**) and the molecule **33c** (**33c**) in the absence of metal ions; the molecule **33**d in the presence Cu(II) ions (**33d**_Cu(II)) or in the presence of Zn ions (**33d**_Zn); the molecule **33c** in the presence of Mg ions (**33c**_Mg) or in the presence of Zn ions (**33c**_Zn), are shown on the left. The arrow in (**33c**_Mg) indicates a crystalline aggregate made of a magnesium salt. On the right side, the corresponding X-ray powder diffraction patterns are reported. Bars indicate the diffraction peaks which could be associated to crystalline regions of **33d** or **33c**. Hash symbols indicate the diffraction peaks that can be associated to crystalline $CuBr_2$.[63] Asterisks indicate diffraction peaks that cannot be univocally associated to specific crystalline forms.

In the xerogel status, **33c** associates in porous structures similar to those formed by **33d**, also in the presence of Mg(II) or Zn(II). The **33c**_Zn xerogel is morphological similar to that of **33c** and makes entangled filaments that form a porous structure in which crystalline particles are embedded. On the contrary, the XRD pattern from **33c** xerogel is characterized by the presence of several diffraction peaks indicating a crystalline molecular aggregation, that are reduced by the presence of Zn(II). Finally, the XRD pattern from the **33c** xerogel hosting Mg(II) shows any diffraction peaks typical of the molecular packing, but shows only diffraction peaks due to unidentified mineral crystalline phases.

The analysis of the results of the gelling experiments and the characterization of the xerogels can give some hints on the influence of the metal ions in the gelation process. Copper(I) ion has a negative effect on gel formation. This implies a weakening of the inter-molecular interactions making the gel. It may be related to its properties to give almost only complexes with tetrahedral coordination or to a strong change of the solvent features. Magnesium ions have also a negative role on the gelation capability of the molecules, as gel formation is inhibited except for **33c**, in which the gel thermal stability is reduced with respect to the metal free one. This may suggest a weakening of the interactions among the **33c** molecules due to Mg(II). These ions could interact

[63] Simon, A.; Oeckler, O. *"Redetermination of the crystal structure of copper dibromide, $CuBr_2$"* Z. Kristallogr. **2000**, *215*, 13-21.

with the molecules reducing their ability to form intermolecular bonds. Indeed, the periodic intermolecular interactions (i.e. the crystallinity) in the **33c** xerogel is reduced by the presence of magnesium ions. Al(III) inhibits the gel formation, except for the molecule **32d**. The **32d**_Al gel increases its thermal stability with respect to pure **32d** gel. This observation may suggest that Al(III) should strengthen the intermolecular interactions in the gel, although the crystallinity of the xerogel is not affected. Al(III) being present as salt particles may act also as filler, improving the mechanical properties of the gel. Al(III) can form tetrahedral compounds other than octahedral ones, as Mg(II) does; this coordination flexibility may be involved in the alteration of the gel properties. The high charge density of Mg(II) may also have a role in destabilizing the gel structure. Zn(II) does not inhibit the capability of the molecules to form gels. This means that the key molecular interaction forming the gel structure are not affected by the presence of Zn(II). These gels have thermal stability lower than the co-respective metal ion free **32d**, **32c** and **33c** gels. Only **33d** forms a gel with higher thermal stability in the presence of Zn(II). Interestingly, the xerogels obtained in the presence of Zn(II) do not contain any crystalline salt particles; this may be due to Zn(II)-molecules interactions that prevent the salt precipitation or the re-precipitation of Zn(II) salts in an amorphous form. These interactions, or the presence of small amorphous particles, may strengthen molecular entanglements, as occurs for **33d**, or weaken them, as occurs for **32d**, **32c** and **33c**.

Similar considerations may be applied to explain the effect of Cu(II) in the gel formation. However, in this case the xerogels obtained from the parent gels bearing Cu(II) always show the presence of particles of copper(II) bromide. Thus, it can be supposed that the interaction between copper(II) ions and the molecules is minimal or that is lost in the xerogel formation, although they are still trapped in the xerogel network.

3.4.4 LMWGs as “Trojan Horses”

Self-assembled physical gels may be employed in the field of localized drug delivery, as they can easily fit into any shape. For example, if a drug is mixed with a solution of LMWG, which forms a self-assembled gel on contact with bodily fluids (e.g., due to the resulting pH changes), it can be

delivered topically after tumor resection. On gelation, the gel can be held in the cavity, thereby allowing the drugs to act locally.[64]

A topic of great interest is the delivery of platinum(II)-based anticancer agents, such as cisplatin, carboplatin and oxaliplatin, that are widely utilized in the clinic, although with numerous disadvantages, due to toxicity to "normal" tissues.

The delivery of platinum(II)-based anticancer agents by means of self-assembled gels, made of stoichiometric amounts of LMWG and platinum(II) derivatives, could be a innovative answer against the high toxicity towards "normal" tissues.

In this chapter it is discussed if the LMWG **30** can behave as "Trojan horse" and carry drug molecules into the cell.

To check the cellular uptake by confocal laser scanning microscopy, three fluorescent compounds **35**, **36** and **37**, all containing the fluorescent dansyl group (Dans)[36] (Figure 72) were prepared.

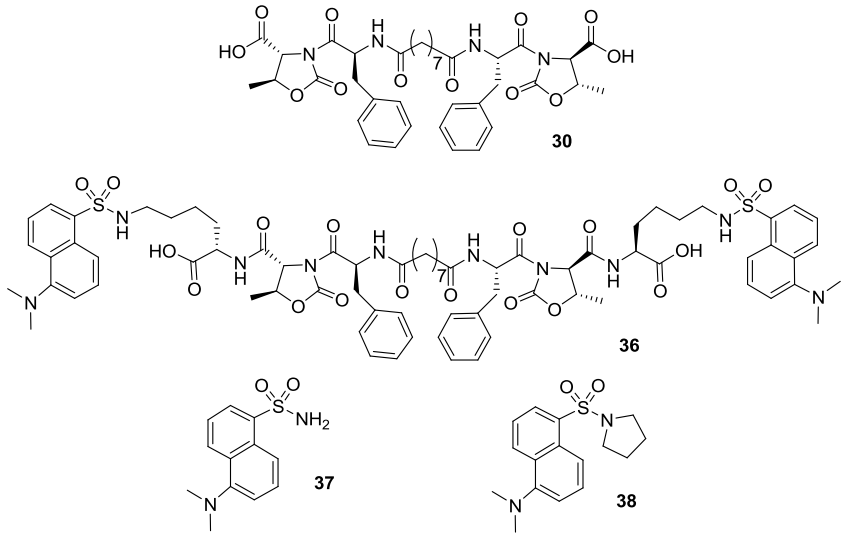

Figure 72. Chemical structure of the LMWHGs **30** and **35** and of the fluorescent moieties **36** and **37** described in this work.

[64] Ellis-Behnke, RG.; Liang, Y. X.; Tay, D. K. C.; Kau, P. W. F.; Schneider, G. E.; Zhang, S.; Wu, W.; So, K. F. *"Nano hemostat solution: immediate hemostasis at the nanoscale"* Nanomedicine, **2006**, *2*, 207-215.

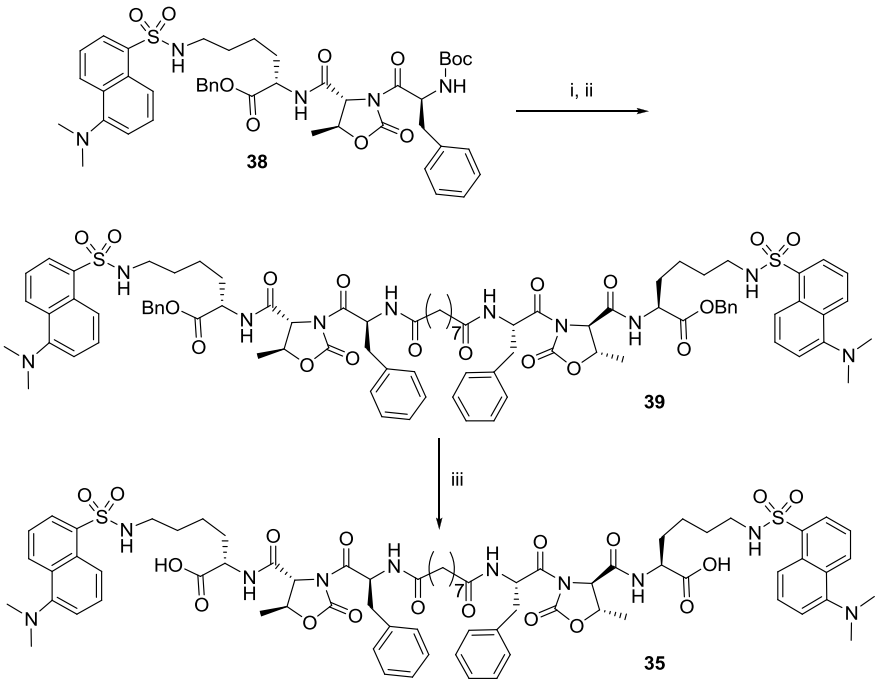

Scheme 7. Synthesis of compound **35.** Reagents and conditions (i) TFA (18 equiv.), dry CH_2Cl_2, r. t., 4 h; (ii) azelaic acid (0.5 equiv.), HBTU (1 equiv.), TEA (3 equiv.) dry CH_3CN, 40 min (iii) H_2, Pd/C MeOH, r. t. 2 h.

First **Gel1** (Table 7) was prepared with **30** and a mixture of water and ethanol in 9:1 ratio.

Table 7. Gelling status of the molecules **30**, **35**, **36**, **37** and their mixtures.

Hydrogel	LMWHG	Weight (mg)	Solvent (H_2O/EtOH)	outcome
Gel1	**30**	3.7	9:1	**gel**
Gel2	**35**	3.7	9:1	sol.
Gel3	**35**	3.7	5:5	sol.
Gel4	**35**	7.3	9:1	sol.
Gel5	**35**	7.3	5:5	**gel**
Gel6	**30**	3.7	9:1	**gel**
	35	0.4		
Gel7	**30**	3.7	9:1	**gel**
	36	0.4		
Gel8	**30**	3.7	9:1	**gel**
	37	0.4		

Both samples were prepared with the previously described method and easily form gels. Interestingly, these LMWHG having hydrophilic carboxylic-acid moieties, located in the hydrophilic part of the molecule, provide reversible responsiveness to changes in pH. Indeed they are in gel a status up to pH ≈ 9. At higher pH, the gels undergoes in the sol status, due to the almost complete ionization of the carboxylate groups.[65]

Then, following the same method, we checked if molecules containing the fluorescent dansyl group (Dans) may be used to prepare florescent hydrogels.

First we tried with pure **35** (**Gel2-4**), but it is not a good gelator as **30**. To form a gel, **35** requires a higher concentration of gelator (0.74% w/v compared to **Gel1** that requires only 3.7% w/v of **30**) and a 1:1 water/ethanol mixture, probably because **35** is less hydrophilic than **30**.[66]

So we decided to follow a different approach, preparing **Gel6-7** with **30** as gelator, doped by little amount of the dansyl containing compounds **35**, **36** and **37**: they all readily form fluorescent hydrogels, that may be used to evaluate the cellular uptake of **30**.

Before evaluating the cellular uptake of the hydrogels, the structure of **Gel1**, and its corresponding xerogel, were analyzed by X-ray diffraction (XRD) and scanning electron microscopy (SEM). Hydrogel **Gel1** is a strong and termoreversible gel (Figure 73a) with melting point at 45 °C.

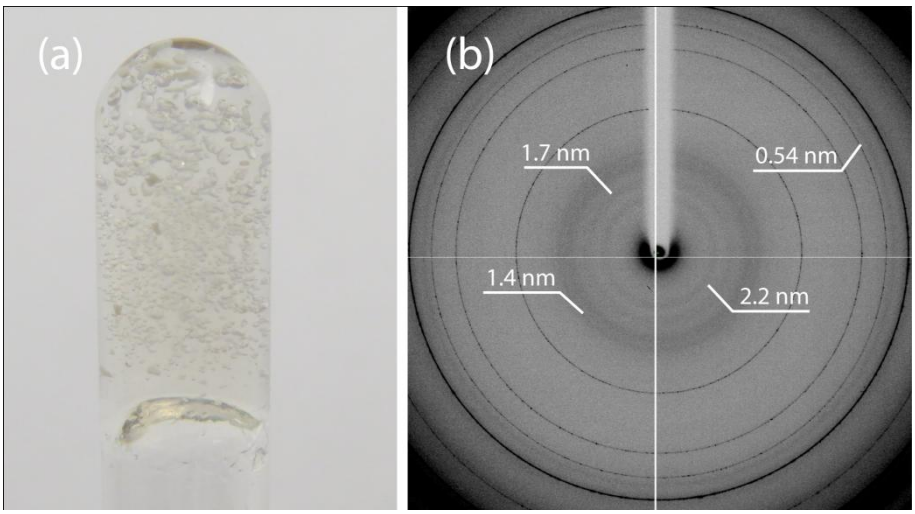

Figure 73. (a) Camera picture of Gel1 in an upside down glass test tube and (b) low-medium angle XRD pattern from a fragment of **Gel1** collected at 100 K. In (b) the periodicities associate to diffraction rings due to the ordered assembly of **Gel1** are indicated. Those not listed are due to ice.

[65] Greenfield, M. A.; Hoffman, J. R.; Olvera de la Cruz, M.; Stupp, S. I. *"Tunable mechanics of peptide nanofiber gels"* Langmuir, **2010**, *26*, 3641-3647.

[66] Brizard, A.; Oda, R.; Huc, I. "*Chirality effects in self-assembled fibrillar networks"* Top Curr. Chem. **2005**, *256*, 167-218.

The XRD pattern from the hydrogel **Gel1**, collected at 100 K, is characterized by the presence of diffraction rings at low angle (indicated in Figure 73b) having periodicities of 2.2 nm, 1.7 nm, 1.4 nm and 0.54 nm. The additional high angle diffraction rings not listed are due to the presence of ice.[67] Any attempt to collect XRD data at room temperature, or at 100 K in the presence of cryprotectants, to avoid the formation of ice, failed in showing the low angle diffraction effects.
The freeze drying of the hydrogel **Gel1** produced the xerogel **Gel1**, which appeared as a fractured film (Figure 74a inset).

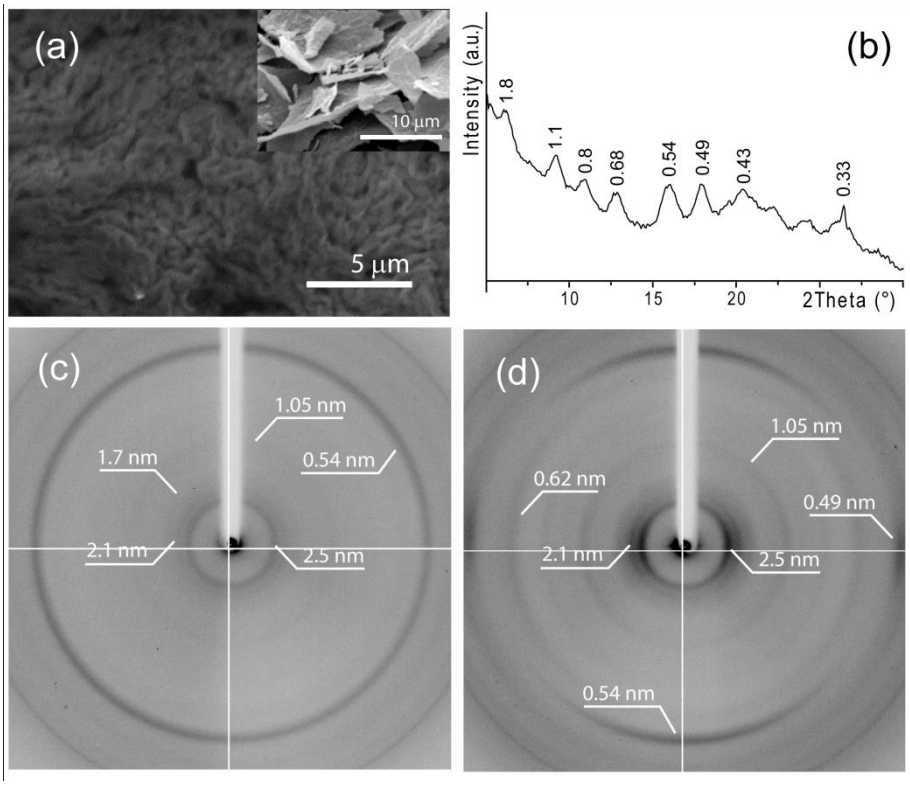

Figure 74. (a) Scanning electron microscopy images of a xerogel **Gel1** film fragment. In the inset a low magnification view of xerogel film fragments. (b) Powder XRD pattern of a powered sample of xerogel **Gel1**. Low-medium angle XRD patterns obtained in geometries having the X-ray beam normal (c) and parallel (d) to the surface of a xerogel film fragment.

In this film, a fibrous structure is observed (Figure 74a). The fibers appear locally organized in bundles, which are randomly oriented. The powder XRD pattern of xerogel **Gel1** shows several diffraction peaks at high and medium angles (Figure 2b), indicating the presence of ordered structures in the xerogel. The periodic distances at 1.8 nm and 0.54 nm were also observed in the diffraction pattern from the parent hydrogel **Gel1**. The XRD pattern from a film fragment of the

[67] Dowell, L. G.; Rinfret, A. P. *"Low-temperature forms of Ice as studied by X-Ray diffraction"* Nature, **1960**, *188*, 1144-1148.

xerogel **Gel1**, which were obtained in geometries having the X-ray beam normal (c) and parallel (d) to the film surface (Figure 74c-d), show diffraction effects, arcs and rings, respectively, with the same periodicities at 2.5 nm, 2.2 nm, 1.7 nm, 1.05 nm, 0.67 nm and 0.49 nm. This different distribution of the intensity of diffraction indicates that the ordered regions are randomly oriented on the film surface and preferentially oriented in the film cross section. The arcs at 2.5 nm, 2.2 nm, 1.7 nm, 1.05 nm, 0.67 nm, 0.54 nm and 0.49 nm are along the equatorial direction, while that at 0.54 nm is along the meridional direction. These low angle periodicities could be associated to different diffraction orders of periodic distance of 2.5 nm. This observation, in agreement with a rough estimation the molecule **Gel1** dimensions, may suggest a supramolecular assembly of **Gel1** molecule to form the fibrous structures. Moreover, XRD data and SEM observation show that in the xerogel the fibers align preferentially parallel to the film surface and may suggest that in the fiber the molecules are organized in layers (0.54 nm thick) and that they have their long axis (2.5 nm) parallel to the fiber direction. It is important to note that the low angle periodicities observed in the xerogel were present also in the hydrogel. This indicates that the fiber structure is not generated by the freeze drying process but that is already present in the hydrogel.

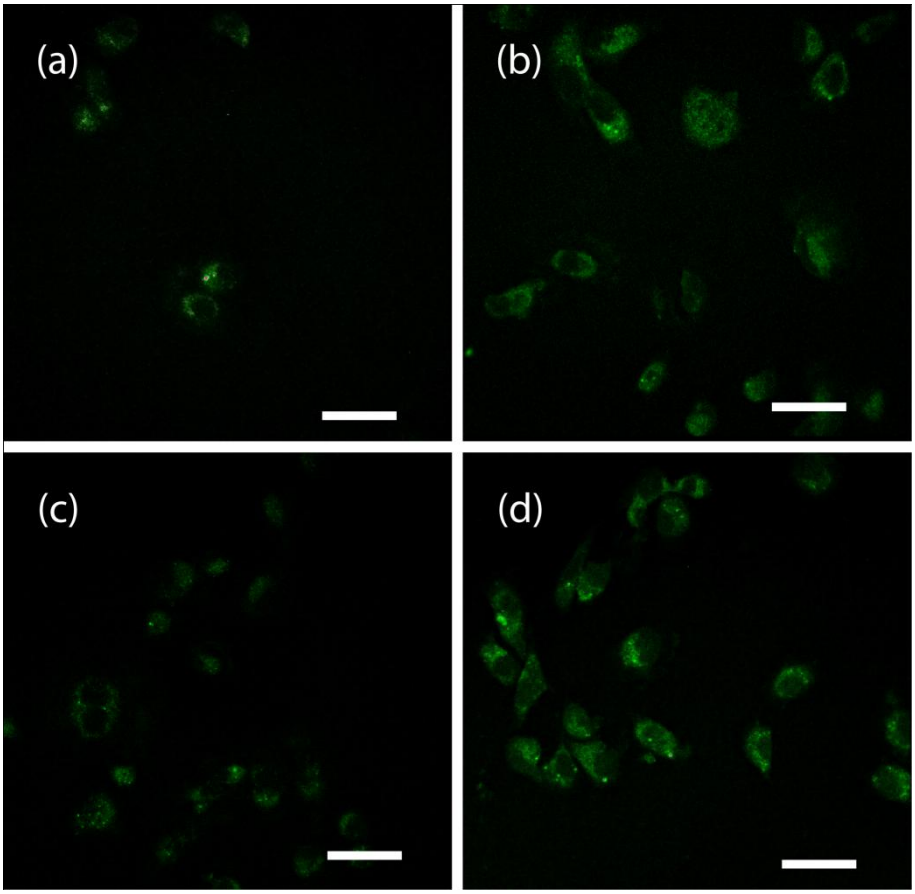

Figure 75. Confocal laser scanning micrographs of IGROV1 exposed to **Gel5** (a), to **Gel6** (b), to **Gel7** (c) and to **Gel8** (d). The dansyl group fluorescence is shown in green. Scale bar 50 µm.

Then we collected some information on the ability of fluorescent hydrogels **Gel5-8** to cross the cellular membrane of the cancer cells, by means of confocal microscopy (Figure 75). It is worth mentioning that gel **Gel5** is made of **35**, while **Gel6-8** are made of **30**, doped with one of the dansyl containing compounds **35-37**. IGROV-1 cells were grown on glass coverslips for 24 h before being exposed to hydrogels for 30 min. Confocal laser scanning microscopy shows that all the hydrogels internalizes in IGROV-1 cells (as indicated by the green fluorescence in the cytoplasm Figure 75), but very few green spots are present in Figure 75a, suggesting that hydrogel **F** is not well tolerated by the cells.

To confirm these results, we evaluated the citotoxicity of the **Gel1** (only **30**), compared with the fluorescent hydrogels **Gel5** (only **35**) and **Gel5-8** (doped **30**). IGROV-1 cell growth was evaluated after 24 h treatment with the hydrogels. The results are reported in Figure 76 and shows that **35** (**Gel5**) is citotoxic, while **30** is well tolerated by the cells, as the treatment with gels **Gel5-8** and **Gel6-8** does not significantly affect the cell proliferation.

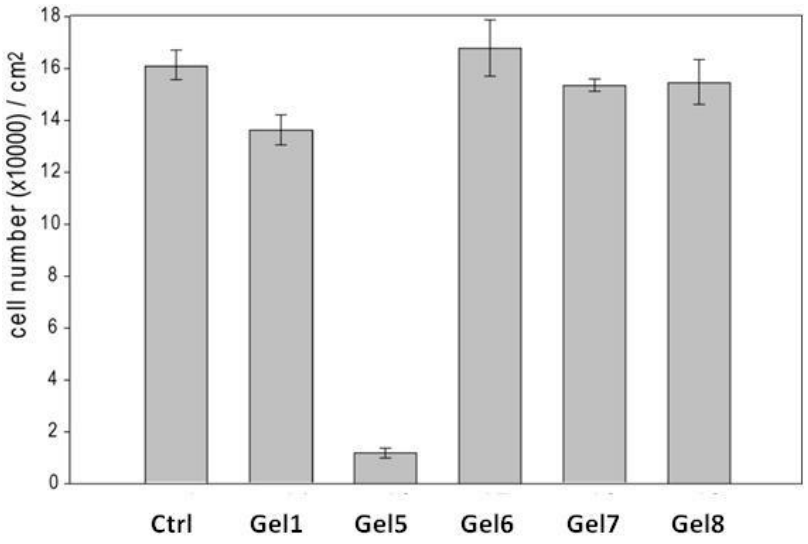

Figure 76. IGROV1 cell growth after 24 hour treatment with **Gel1**, **Ge56**-**8**.

Thus LMWHG **30** may behave as an excellent Trojan horse as it is biologically inactive, is internalized by cells, cargo on it molecules of different sizes and is a good candidate to carry drug molecules.

3.5 The interaction of lipid modified pseudopeptides with lipid membranes

In the previous chapter it was shown that the simple dipeptide Boc-L-Phe-D-Oxd-OBn (**22**) can form fibrous structures that are only stabilized by a single hydrogen bond forming both parallel or antiparallel β-sheet structures.

Here, we investigate the behaviour of building block L-Phe-D-Oxd after adding lipid chain moieties to the N-terminus of the peptides and whether structure formation of the lipopeptides can be influenced by the presence of lipid membranes. Lipid modifications are known to play the decisive role in the formation of micelles, membranes, and other supramolecular structures due to the hydrophobic effect. In addition, lipid modification is a common motif for membrane binding of peptides and proteins.[68]

The compounds analyzed in this work were synthesized in solution by a standard coupling reaction in the presence of HBTU and TEA in dry acetonitrile. These compounds are enantiomers, as fully labeled amino acids are available only in the L form as far as we know. Lipopetides **40** and **41** have been prepared by acylation of the Boc-L-[U-^{13}C,^{15}N]-Phe-D-Oxd-OBn, with fully deuterated hexanoic acid-d_{11} and dodecanoic acid-d_{23}, respectively, after removal of the Boc moiety with trifluoroacetic acid. With the same approach, lipopeptides **42** and **43** were prepared by acylation of the Boc-D-Phe-L-[U-^{13}C,^{15}N]-Oxd-OBn, with the fully deuterated hexanoic and dodecanoic acid. The four compounds were purified by flash chromatography and fully characterized (Scheme 8).

[68] a) Casey, P. J. *"Protein lipidation in cell signaling"* Science, **1995**, *268*, 221-225; b) Brunsveld, L.; Waldmann, H.; Huster, D. *"Membrane binding of lipidated Ras peptides and proteins - The structural point of view"* Biochim. Biophys. Acta, Biomembr. **2009**, *1788*, 273-288.

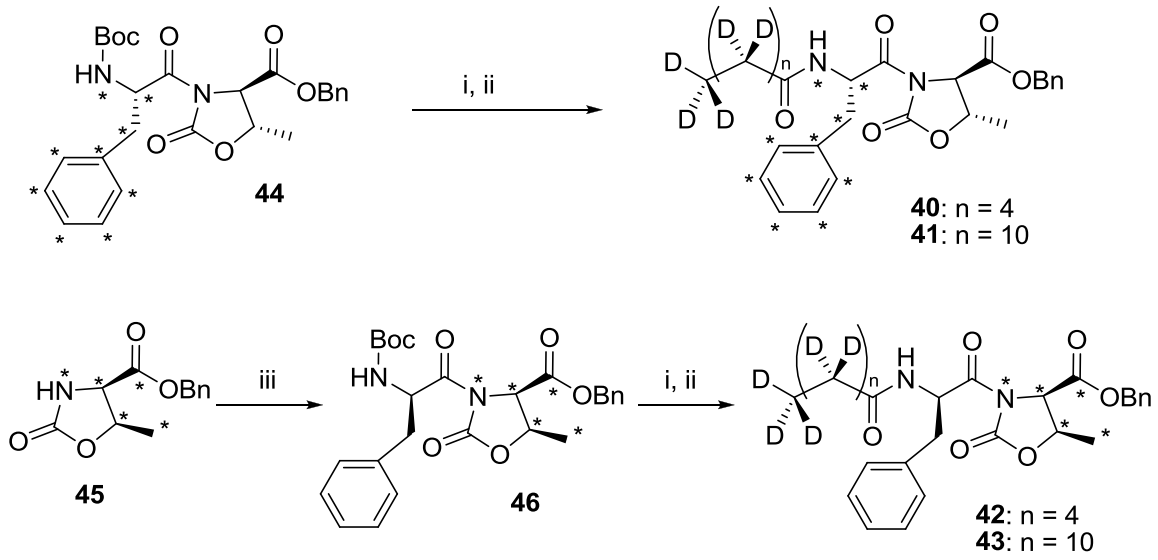

Scheme 8**.** Synthesis of the investigated lipopeptides in the different ^{13}C and ^{15}N labeled forms (labeled atoms are marked by asterisks), note the -L-Phe-D-Oxd- and -D-Phe-L-Oxd- versions. D: deuterium. Reagents and conditions (i) TFA (18 equiv.), dry CH_2Cl_2, r. t., 4 h; (ii) hexanoic acid-d_{11} and dodecanoic acid-d_{23} (1 equiv.), HBTU (1 equiv.), TEA (3 equiv.) dry CH_3CN, 40 min (iii) Boc-L-Phe-OH (1 equiv.), HBTU (1 equiv.), TEA (2 equiv.) dry CH_3CN, 40 min;

It was first investigated the properties of the peptide's lipid chains in the crystalline state using solid-state ^2H NMR. Typical NMR spectra are shown in Figure 77. In particular for the C6 peptide chain, the spectra can be well understood from a superposition of two Pake doublets, one with a quadrupolar splitting of ~111 kHz and one with a quadrupolar splitting of ~27 kHz. The large Pake doublet can be assigned to the methylene groups of the chain, which experience an almost fully rigid conformation. For a rigid methylene group, the quadrupolar splitting is 125.25 kHz. Therefore, the chain methylene groups exhibit an order parameter of 0.89 indicating that the lipid chain modifications of crystalline molecule **40** are almost fully rigid and well ordered. The smaller quadrupolar splitting can be assigned to the terminal methyl group undergoing fast rotation about the C5-C6. The small isotropic peak indicates a very small fraction of isotropically mobile lipid chain most likely due to packing defects in the crystalline material.

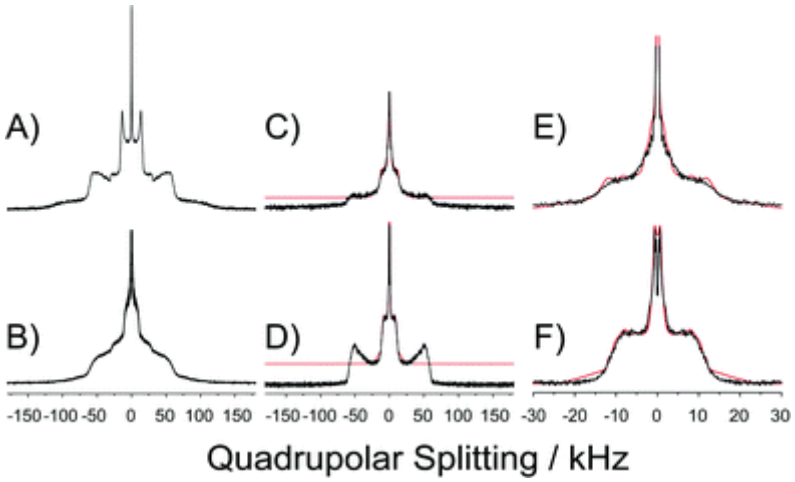

Figure 77. 115 MHz ^{2}H NMR spectra of lipopeptide **40** (A, C, E) and **41** (B, D, F) in the crystalline state (A, B), in POPC membranes (C, D) and of the central part of the spectrum of the lipopeptides in POPC membranes (E, F) to highlight the membrane bound part of the lipopeptides. A numerical simulation of the membrane bound fraction of the lipopeptide spectrum as described in the text is given in red. The spectra were measured at a temperature of 310 K.

Molecule **41**, featuring the longer C12 lipid modification, shows a more complicated ^{2}H-NMR spectrum. While the general width of the NMR spectrum is similar to that of peptide **40**, it is no longer detected the two well resolved Pake doublets. In contrast, the spectral intensity of each set of the two quadrupolar splittings is redistributed towards the center. Apparently, the long C12 lipid modification of the peptide cannot form a rigid and well packed assembly allowing molecular motions in the µs correlation time window to take place.

To gain more understanding about the secondary structure of these molecules, it was also carried out ^{13}C CP MAS NMR studies on these crystalline materials. ^{13}C CP MAS NMR spectra of molecules **40**, **41** and **42**, **43** are shown in Figure 78 and Figure 79, respectively.

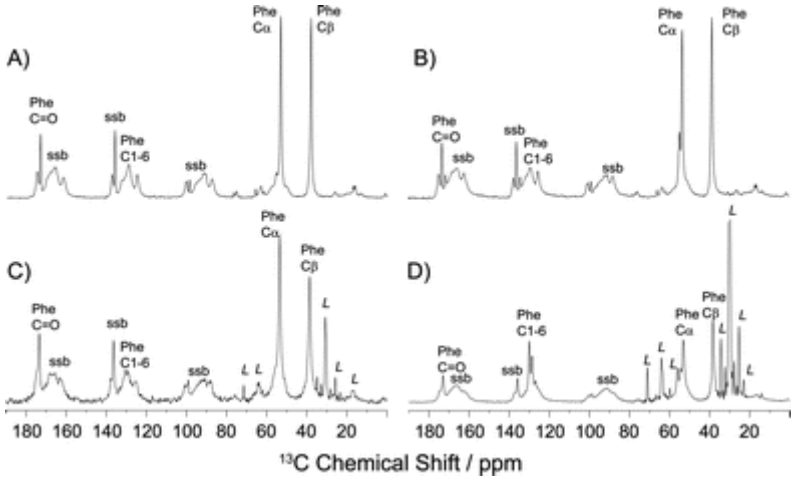

Figure 78. Proton decoupled 188 MHz ^{13}C CP MAS NMR spectra of ^{13}C-Phe labeled version of lipopeptide **40** (A, C) and **41** (B, D) in the crystalline state (A, B) and bound to POPC membranes (C, D). Peaks arising from phospholipid

molecules are marked with "*L*"; ssb denotes spinning side bands. The spectra were measured at an MAS frequency of 7000 Hz and temperature of 310 K.

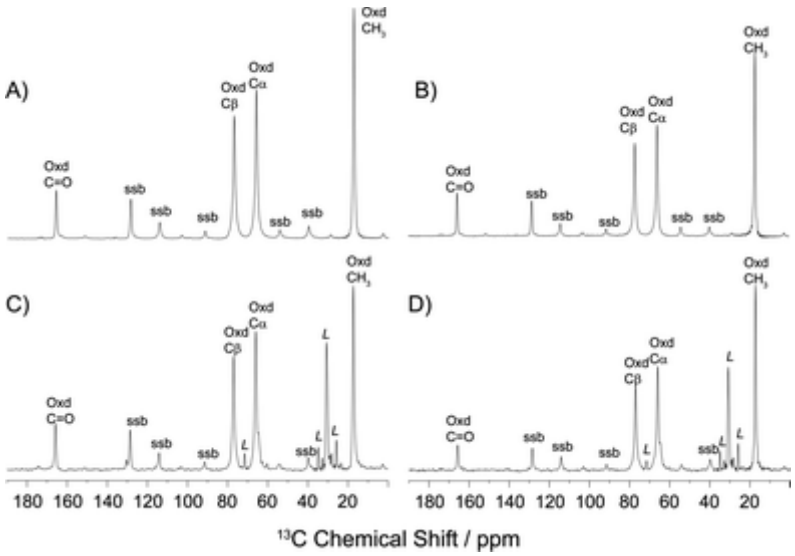

Figure 79. Proton decoupled 188 MHz ^{13}C CP MAS NMR spectra of ^{13}C-Oxd labeled version of lipopeptide **42** (A, C) and **43** (B, D) in the crystalline state (A, B) and bound to a POPC membrane (C, D). Peaks arising from phospholipid molecules are marked with "*L*", ssb denotes spinning side bands. The spectra were measured at a MAS frequency of 7000 Hz and temperature of 310 K.

All signals from the ^{13}C labeled amino acids are well resolved showing typical line widths of ≈ 1 ppm, indicative of a rather high structural homogeneity. The chemical shifts for the Oxd amino acid were assigned by proton driven spin diffusion experiments with varying mixing times to follow the magnetization transfer from the CH_3 group to the Cα and Cβ carbon of Oxd. Due to its dipolar nature the magnetization transfer is more efficient towards the Cβ carbon, resulting in faster cross peak build up, which allowed assignment of the peaks in the spectrum. Since the isotropic ^{13}C chemical shift values are known to be sensitive to the secondary structure, it could be confirmed that the Phe residue of molecules **40** and **41** is in a β-sheet conformation in agreement with previous results on non-lipid-modified analogs of these compounds (chemical shifts are given in Table 8 and Table 9). The Phe Cα peak also has a minor contribution at lower field, which is indicative of a small portion of peptide in random coil conformation. For the Oxd amino acid, no chemical shift reference data are available; therefore, no information about secondary structure could be deduced from the ^{13}C NMR spectra.

Table 8. ^{13}C Chemical shift and C-H order parameter for lipopeptides **40**, **42**

	^{13}C Chemical	CH Order	^{13}C Chemical Shift in	CH Order

	Shift Crystalline/ppm	Parameter *S*, Crystalline	POPC Membranes/ppm	Parameter *S* in POPC Membranes
Phe-Cα	53.4[a]	0.86	53.5	0.99
Phe-Cβ	38.2	0.91	38.6	0.92
Phe-CO	173.4	—	173.5	—
Phe-C1-C6	125-130	0.52	125-130	0.30
Oxd-Cα	66.0	0.89	66.2	0.86
Oxd-Cβ	77.0	0.88	77.2	0.91
Oxd-CH_3	17.4	0.31	17.2	0.28
Oxd-CO	165.7	—	165.8	—

Table 9. ^{13}C Chemical shift and C-H order parameter for lipopeptide **41**, **43**

	^{13}C Chemical Shift Crystalline/ppm	CH Order Parameter *S*, Crystalline	^{13}C Chemical Shift in POPC Membranes/ppm	CH Order Parameter *S* in POPC Membranes
Phe-Cα	53.3[a]	0.82	53.1[b]	0.84
Phe-Cβ	38.5	0.97	38.4	0.64
Phe-CO	173.4	—	173.4	—
Phe-C1-C6	125-130	0.58	125-130	0.28
Oxd-Cα	65.8	0.88	66.0	0.93
Oxd-Cβ	77.0	0.89	77.0	0.96
Oxd-CH_3	17.1	0.31	17.3	0.19
Oxd-CO	165.6	—	165.9	—

[a] Minor contribution at 54.7 ppm. [b] Minor contribution at 55.5 ppm.

^{1}H-^{13}C dipolar coupling measurements confirmed the high rigidity of the molecules in the crystalline state already inferred from the ^{2}H NMR data. Order parameters well above 0.8 were determined for the backbone and side-chain sites of the labeled amino acids, except for the methyl group of Oxd (Table 8 and Table 9).

As discussed above, lipid modification is a common motif for membrane binding of peptides and proteins. Here, it is interesting in the question whether the insertion of the lipopeptide into the membrane would take place and, if so, whether it occurred as a monomer or as the fiber-like

aggregates that were detected in the absence of membranes. To this end, the peptides were allowed to mix with synthetic POPC molecules and to form lipid membranes with inserted peptide molecules. To confirm that intact lipid membranes in the biologically relevant liquid-crystalline phase state were formed, static ^{31}P NMR measurements of the samples were carried out. Typical static ^{31}P are shown in Figure 80. The ^{31}P NMR spectra showed the characteristic anisotropic line shapes with a $\Delta\sigma$ on the order of 42-44 ppm, confirming that all preparations formed stable POPC membrane stacks with the lipopeptide incorporated. Only in the spectrum of POPC in the presence of the short chain lipopeptide **40** a small isotropic peak is visible, which accounts for ~ 10% of the spectral intensity.

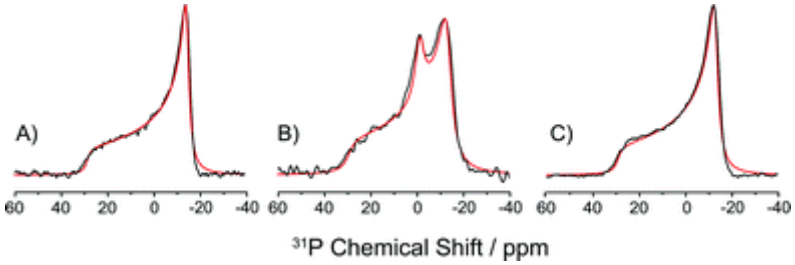

Figure 80. Static ^{31}P NMR spectra (black) of (A) pure POPC, (B) lipopeptide **40** in POPC and (C) lipopeptide **41** in POPC and the respective numerical simulations of the lineshape (red). The spectra were measured at 310 K.

In order to study if the lipid chains are actually also inserted into the membrane, we carried out ^{2}H NMR measurements of the lipid modifications of the lipopeptides. Figure 77 shows the ^{2}H NMR spectra of molecules **40** and **41** in the presence of POPC (molar mixing ratio 1 : 5). Rather drastic alterations of the spectral line shapes compared to those of the crystalline material were observed. It was still observed the broad Pake spectra with a quadrupolar splitting of ~104 kHz at the basis of the NMR spectra. However, in addition to this line shape, It was also detected a narrower ^{2}H NMR spectrum with maximal quadrupolar splittings of about 27 kHz for lipopeptide **41** and 18 kHz for lipopeptide **40** and that is reminiscent of the superposition of motionally averaged Pake spectra as observed for chain deuterated phospholipid molecules.[69] This part of spectral intensity could be assigned to the C6 and C12 peptide chains that are highly mobile and truly inserted into the liquid crystalline membrane environment stemming from monomeric

[69] Huster, D.; Yao, X.; Hong, M. *"1D sensitivity-enhanced ^{1}H spin diffusion experiment for determining membrane protein topology"* J. Am. Chem. Soc. **2002**, *124*, 874-883.

membrane inserted lipopeptides.[70] This can be appreciated in a magnification of the spectra shown in Figure 77C and F and would suggest that part of the lipopeptide remains aggregated most likely in a fibrillar state, while the other part is monomeric and rather mobile in the liquid-crystalline membrane.

It was attempted to quantify the relative portions of the two states of the peptide by integrating the intensity in the ^{2}H NMR spectra. The line shapes for the membrane bound component were simulated,[71] so that the amount of the membrane bound lipopeptides could be estimated to be ~ 48% for lipopeptide **40** and ~29% for lipopeptide **41**. It has been reported before, that high peptide-to-lipid mixing ratios can lead to unwanted peptide aggregation. Therefore, they were also studied samples of the lipopeptides in a highly diluted mixture (1 : 50, mol/mol). Interestingly, the ^{2}H NMR spectra remained nearly identical, suggesting that peptide aggregation/fibril formation was not affected by the preparation and, therefore, not an artifact of the preparation.

They were also detected ^{13}C CPMAS NMR spectra of molecules **40**-**43** in POPC lipid membranes (the spectra are shown in Figure 78 and Figure 79). There are only marginal chemical shift differences (see Table 8 and Table 9), indicating that the secondary structure of the molecules does not change upon membrane insertion. This also supports the previous conclusion that a large portion of the molecules remains in the fibrillar aggregate, which it forms in the crystalline state. Further, even those molecules that are immersed in the membranes as putative monomers show a very similar structure. The Phe peaks show some broader base and a minor contribution with a Cα chemical shift more indicative of random coil structure. This contribution is also seen in the crystalline form of the dipeptide. However, the Oxd residues exhibit narrow and well defined NMR signals without indication for a different secondary structure.

Finally, the C-H order parameter of the labeled Phe and Oxd amino acids of the lipopeptides incorporated in POPC membranes from the C-H dipolar coupling were measured using DIPSHIFT experiments. For all labeled carbons relatively high order parameters were observed. Such a behavior, which is typical for fibrillar peptides/proteins, shows that there is not much space for conformational flexibility and motion in the backbone of the molecules.[72]

---

[70] Huster, D.; Vogel, A.; Katzka, C.; Scheidt, H. A.; Binder, H.; Dante, S.; Gutberlet, T.; Zschörnig, O.; Waldmann, H.; Arnold, K. *"Membrane Insertion of a lipidated Ras peptide studies by FTIR, solid-state NMR and Neutron Diffraction Spectroscopy"* J. Am. Chem. Soc. **2003**, *125*, 4070-4079.

[71] Vogel, A.; Tan, K.-T.; Waldmann, H.; Feller, S. E.; Brown, M. F.; Huster, D. *"Flexibility of Ras lipid modifications studies by ^{2}H solid-state NMR and molecular dynmaics simulations"* Biophys. J. **2007**, *93*, 2697-2712.

[72] Helmus, J. J.; Surewicz, K.; Surewicz, W. K.; Jaroniec, C. P. *"Conformational flexibility of Y145Stop human prion protein amyloid fibrils probed by solid-state nuclear magnetic resonance spectroscopy"* J. Am. Chem. Soc. **2010**, *132*, 2393-2403.

Apparently, the N-terminal lipid modification does not seem to interfere with the general property of this peptide to form highly ordered nanofiber-like materials. On the contrary, the ^{2}H NMR results suggest that the lipid chains also appear to be well aligned, which may provide an additional intermolecular stabilization in addition to the single hydrogen bond that has been found before.

The situation changes partially when the peptides are allowed to interact with lipid membranes. As lipid modifications represent a common motif for membrane binding of membrane-associated proteins and peptides, we studied the interaction of the lipidated dipeptides with POPC membranes. Spin diffusion experiments showed that the peptides were indeed associated with the membranes. While we did not detect any major secondary structure changes in the peptide backbone associated with membrane binding, the ^{2}H NMR spectra of the lipid chains of the peptide allowed us to detect two populations of peptide molecules. One portion of oligomeric lipopeptides was found to closely resemble the crystalline nanofibers detected in the absence of any membranes and another portion of monomeric dipeptides were identified that are immersed into the lipid membrane.

The membrane propensity of the lipopeptides can be explained by the hydrophobic effect. Partitioning of lipidated peptides into the lipid water interface of a membrane can be understood from thermodynamic principles.

The peptides are not soluble in aqueous environment; this fact may explain why more than half of the lipidated dipeptides remain aggregated even in the presence of membranes and only a smaller portion forms monomers that are inserted into the membranes. This suggests that the intermolecular forces that lead to fiber formation of the peptides must be relatively strong and are not easily dissolved in the case where the membrane becomes the solvent. However, it should be stressed that lipidated peptides do not generally tend to aggregate in the membrane environment. It was previously reported that the dipeptide Boc-L-Phe-D-Oxd-OBn is stabilized only by a single hydrogen bond. This would certainly not suffice to keep the peptides aggregated in the presence of membranes. Clearly, the highly ordered lipid modifications also contribute to the intermolecular forces that keep the peptides in the nanostructured form. Only part of the peptide aggregates are dissolved in the membrane and will most likely occur in a monomeric form. These molecules are also relatively mobile in the membrane, the lipid modifications undergo fast motions comparable to those of the lipid chains of the phospholipids. Here, the intermolecular forces between adjacent peptides, which stabilize the nanofibered structure of the dipeptide in the absence of membranes

are replaced by interactions of the peptide with the membrane that in particular occur in the lipid -water interface of the bilayer.

The structural findings of this study are summarized in a cartoon shown in Figure 81. In the crystalline state, the peptides form parallel β-sheets and the N-terminal lipid modifications are highly ordered in the all *trans* state (A). In the lipid membrane (B), two populations of lipopeptides are observed. First, aggregated nanofibers remain undetected and may due to their hydrophobicity be buried in the liquid crystalline membrane or could occur clustered on the membrane surface. Second, also monomeric molecules have been detected that are inserted in the membrane, these molecules show higher mobility and are characterized by highly mobile lipid modifications that undergo fast *trans-gauche* isomerizations just as the lipid chains of the POPC molecules in the host membrane.

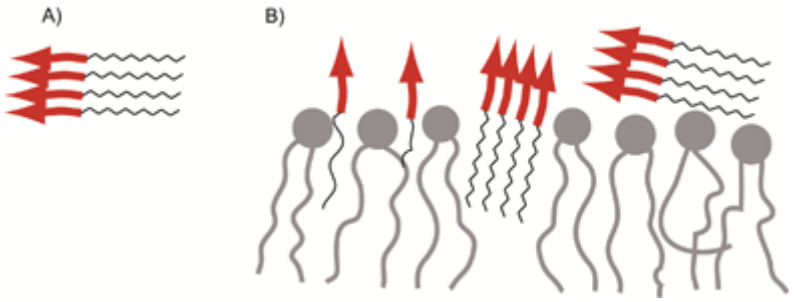

Figure 81. The cartoon summarizes the major findings of the current study. In the absence of membranes, lipopeptides form highly ordered β-sheet like nanofibers with the lipid modifications in a rigid all *trans* conformation (A). When lipid membranes are present, larger peptide aggregates can bind to the membrane surface or insert into the membrane, but also dissociate and insert into the membrane as monomers, most likely with the lipid modification facing the membrane interior (B).

4 Tetramic Acids: new scaffolds for foldamers

4.1 Introduction

The synthesis and characterization of oligomers programmed to fold and self assemble into secondary structures is always open. Nowadays, a new frontier of foldamer research is based on searching new scaffolds with a variety of properties.

When developing new scaffold, large screening of molecules from chiral pool can provide hits that could eventually be optimized to afford candidate foldamers.

In this chapter is presented the synthesis and in the derivatization of 1-acyl 3-carboxy tetramic acids, as they are constrained amino acid mimetics, contain an endocyclic carbonyl group and may be functionalized in several ways, thus they be may applied to the formation of pseudopeptide foldamers.

The heterocyclic core of tetramic acids (pyrrolidine-2,4-diones, Figure 82) is a recurrent motif among natural products originating from a variety of marine and terrestrial species such as sponges, cyanobacteria, bacteria and fungi. Their study has experienced a renaissance due to the high incidence of biological activities and because of their challenging structural complexity. A steadily increasing number of reports have been dealing with the isolation of new derivatives, with aspects of their biosyntheses and their medicinal potential as well as with the refinement of synthetic strategies including parallel and combinatorial approaches.[73]

The number of natural derivatives is over 150 and further progress was made towards an understanding of their biosyntheses and multi- accepted bioactivity. The spectrum of their physiological activities is as broad as that of tetramic acids with a focus on antibiotic, antiviral and antineoplastic properties. the most frequent and pharmacologically most interesting derivatives are those featuring 3-acyl residues. This has been explained by their ability to chelate biochemically indispensable metal ions and to mimic phosphate groups in the binding site of kinases and phosphatases.

Tetramic acids are very polar and scarcely reactive and may be prepared with several methods. The most simple one is the activation of a Boc-protected amino acid with EDC, condensation with Meldrum's acid, and finally cyclization to give the Boc-protected pyrrolidine-2,4-diones. The

[73] Schobert, R.; Schlenk, A. *"Tetramic and tetronic acids: an update on new derivatives and biological aspects"* Bioorg. Med. Chem. **2008**, *16*, 4203-4221.

following N-deprotection may be accomplished with TFA treatment giving the parent pyrrolidine-2,4-diones.[74] Another straightforward method is the condensation of methyl (*E*)-4-chloro-3-methoxy-2-butenoate with a 2-amino alcohol in the presence of triethylamine.[75]

The reactions of the tetramic acid ring itself which can be summarized as follows: (a) reaction with electrophilic species *(e.g.* aldehydes, bromine or nitrating agents) at C-3, (b) with nucleophilic species *(eg.* hydrazine) at (2-4, (c) acylation on O-4 or,[76] under certain conditions, C-3, and (d) with organometallic bases *(eg.* n-butyllithium) metallation occurs at C-3 (Figure 82).

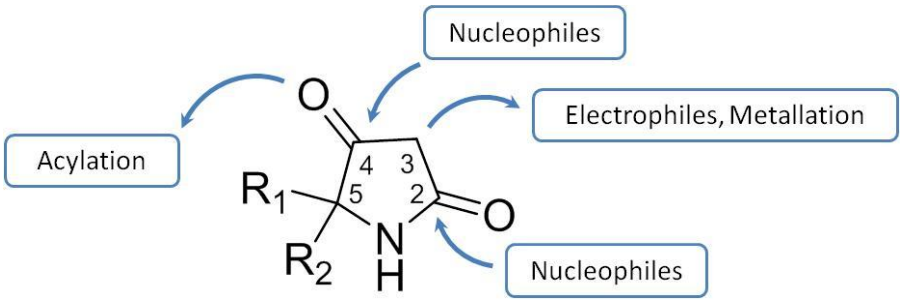

Figure 82. The heterocyclic core of tetramic acids and its main derivatization reactions.

However, the functionalization of this kind of heterocycle is often a difficult task, due to their low reactivity and to the equilibrium between the ketonic and enolic form, especially for 3-acyl derivatives, the most common ones (Figure 83).

[74] a) Jouin, P.; Castro, B.; Nisato, D. *"Stereospecific synthesis of N-protected statine and its analogues via chiral tetramic acid"* J. Chem. Soc., Perkin Trans. 1, **1987**, 1177-1182; b) Ma, D.; Ma, J.; Ding, W.; Dai, L. *"An improved procedure to homochiral cyclic statines An improved procedure to homochiral cyclic statines"* Tetrahedron: Asymmetry, **1996**, *7*, 2365-2370; c) Courcambeck, J.; Bihel, F.; de Michelis, C.; Quéléver, G.; Kraus, J. L. *"Design of potential new HIV protease inhibitors: enantioconvergent synthesis of new pyrrolidin-3-ol, and pyrrolidin-3-one peptide conjugates"* J. Chem. Soc., Perkin Trans. 1, **2001**, *2*, 1421-1430.

[75] Lan, H.-Q.; Ye, J.-L.; Wang, A.-E.; Ruan, Y.-P.; Huang, P.-Q. *"A flexible asymmetric approach to methyl 5-alkyltetramates and its application in the synthesis of cytotoxic marine natural product belamide A"* Chem.-Eur. J. **2011**, *17*, 958-968; b) Jiang, L.-J.; Lan H.-Q.; Zheng, J.-F.; Ye, J.-L.; Huang, P.-Q. *"A flexible approach to methyl (5S)-5-alkyltetramate derivatives"* Synlett, **2009**, 297-301; d). Laffan, D. D. P.; Panziger, M.; Duc, L.; Evans, A. R.; McGarrity, J. F.; Meul T. *"An efficient synthesis of racemic 4-Hydroxy-2-oxo-1-pyrrolidineacetamide (Oxiracetam) using tetramic-acid intermediates"* Helv. Chim. Acta, **1992**, *75*, 892-900.

[76] Hosseini, M.; Grau, J. S.; Sørensen, K. K.; Søtofte, I.; Tanner, D.; Murrayb, A.; Tønder, J. E. *"Short and efficient diastereoselective synthesis of pyrrolidinone-containing dipeptide analogues"* Org. Biomol. Chem. **2007**, *5*, 2207-2210.

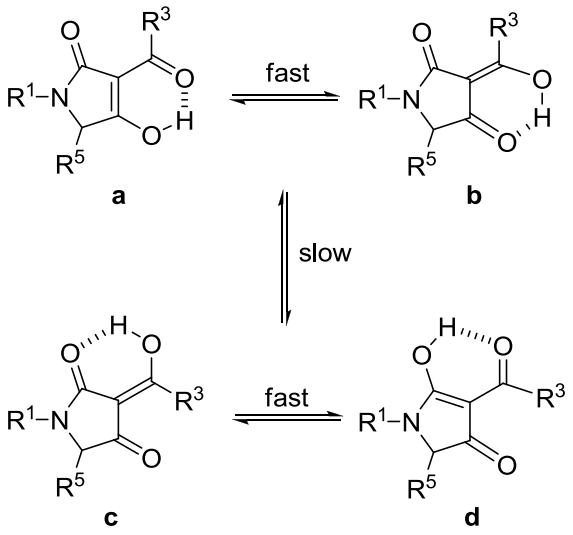

Figure 83. The tautomeric behavior of 3-acyltetramic acids. It involves two sets of rapidly interchanging internal tautomers **[a ⇆ b]** and **[c ⇆ d],** where each set arises through proton transfer along the intramolecular hydrogen bond, together with two pairs of lowly interconverting external tautomers **[a, b] ⇆ [c, d],** arising from the rotation of the acyl side chain**.**

Very interesting are the studies reported by Tønder et al.[77] who have developed a straightforward strategy for the synthesis of *N*-acylates, *O*-alkylated pyrrolidin-2-ones by functionalization of tetramic acids, that leads to the formation of dipeptidomimetics comprising a pyrrolidinone and a protected amino acid. They have also reported an optimized two-step reductive amination procedure, which provides a small library of pyrrolidinone-containing dipeptide analogs. Another interesting approach to the synthesis of *N*-Boc 5-substituted tetramic acids is the cyclization of *N*-hydroxysuccinimide esters of Boc-protected α-amino acids.[78] The desired products have been obtained in two steps, by coupling of the α-amino acid derivatives with an alkyl malonate in the

[77] a) Hosseini, M.; Kringelum, H.; Murray, A.; Tønder, J. E. *"Dipeptide analogues containing 4-ethoxy-3-pyrrolin-2-ones"* Org. Lett. **2006**, *8*, 2103-2106; b) Hosseini, M.; Tanner, D.; Murrayb, A.; Tønder, J. E. *"Pyrrolidinone-modified di- and tripeptides: highly diastereoselective preparation and investigation of their stability"* Org. Biomol. Chem. **2007**, *5*, 3486-3494.

[78] a) Matiadis, D.; Igglessi-Markopoupou, O. *"Design and synthesis of optically active esters of γ-amino-β-oxo acids as precursors for the synthesis of tetramic acids derived from L-Serine, L-Tyrosine, and L-Threonine"* Eur. J. Org. Chem. **2010**, 5989-5995; b) Prousis, K. C.; Markopoulos, J.; Mckee, V.; Igglessi-Markopoulou, O. *"Efficient construction of functionalized 5-carboxymethyl tetramic acids using N-Ac-l-aspartic anhydride as chiral building block"* Tetrahedron, **2010**, *66*, 3944-3950; c) Prousis, K. C.; Detsi, A.; Igglessi-Markopoulou, O. "*A traceless solid-phase approach to functionalized tetramic acids and 2-Amino-4-pyrrolinones"* Synlett, **2005**, 2763-2766; d) Detsi, A.; Afantitis, A.; Athanaselli, G.; Markopoulos, J.; Igglessi-Markopoulou, O.; Skylaris C.-K. "*Cyclisation of novel amino oxo esters to tetramic acids − density functional theory study of the reaction mechanism"* Eur. J. Org. Chem. **2003**, 4593-4600; e) Athanasellis, G.; Gavrielatos, E.; Igglessi-Markopoulou, O. *"One-pot synthesis of optically active tetramic acids from amino acids mediated by 1-Hydroxybenzotriazole"* Synlett, **2001**, 1653-1655; f) Petroliagi, M.; Igglessi-Markopoulou, O. *"An efficient synthesis of novel N-acetyl-3-alkanoyl and 3-dienoyl tetramic acids"* J. Chem. Soc., Perkin Trans. 1 (1997), p. 3543-3548; g) A. Detsi, J. Markopoulos, O. Igglessi-Markopoulou *"Reactions of N-hydroxysuccinimide esters of N-alkoxycarbonyl-α-amino acids with active methylene compounds. Synthesis of 3-substituted tetramic acids"* Chem. Commun. **1996**, 1323-1324.

presence of NaH, with the formation of γ-amino-β-oxoalkanoates, that in turn cyclize under basic conditions to give the desired compounds.

1-Acyl 3-carboxy tetramic acids are constrained β-amino acids, where the carbonyl unit is placed between the two functions, thus it forces the two carbonyls in the *trans* conformation, following the same effect that we have observed for the 4-carboxy-oxazolidin-2-ones (Figure 84). As a consequence of this disposition, this scaffold may behave as a reverse-turn mimic, if it is introduced in the middle of a polypeptide chain, or it may promote the formation of new foldamers, if it is introduced in more complex structures. Although many examples of nonpeptidic reverse-turn surrogates have been reported, it is still challenging to find a new type of nonpeptidic scaffold that can adopt a highly populated reverse-turn conformation in solution[79] and that may be regarded as constrained pseudo-β-prolines.

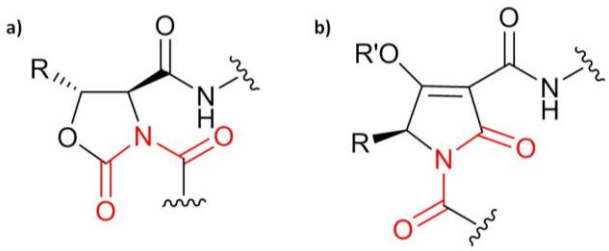

Figure 84. (a) Preferential conformation of 4-carboxy-oxazolidin-2-ones and (b) possible preferential conformation of 1-acyl 3-carboxy tetramic acids.

4.2 Synthesis of the heterocycles

We report here a one-pot synthesis of poly-substituted tetramic acids (4-hydroxy-2-oxo-1*H*-pyrrole-1,3(2*H*,5*H*)-dicarboxylates) and of the corresponding six-membered rings (4-hydroxy-2-oxo-5,6-dihydropyridine-1,3(2*H*)-dicarboxylates) starting from benzyl malonate and *N*-hydroxysuccinimide esters of Boc-protected amino acids (Scheme 9). As a first attempt, we utilized the protocol described by Igglessi-Markopoulou et al.[78a] that allows obtaining γ-amino β-oxo acids by reaction of *N*-hydroxysuccinimide esters of Boc-protected amino acids with alkyl malonate.

[79] Gante, J. *"Peptidomimetics-Tailored Enzyme Inhibitors"* Angew. Chem., Int. Ed. Engl. **1994**, *33*, 1699-1720.

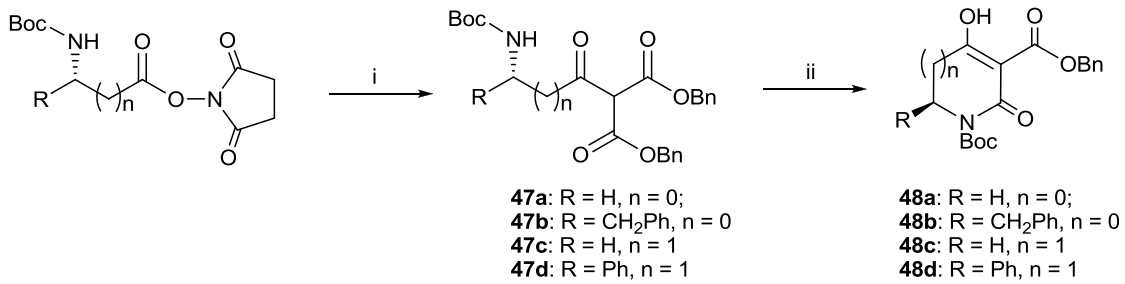

47a: R = H, n = 0;
47b: R = CH_2Ph, n = 0
47c: R = H, n = 1
47d: R = Ph, n = 1

48a: R = H, n = 0;
48b: R = CH_2Ph, n = 0
48c: R = H, n = 1
48d: R = Ph, n = 1

Scheme 9. Reagents and conditions: (i) $Na^+ \cdot {}^-CH(CO_2Bn)_2$ (1.5 equiv), dry THF, 30 min at 0 °C then 2h at rt; (ii) 2 M NaOH (166 equiv), BnOH, 2 h, rt.

As the final scope is the formation of a free carboxy unit, the reaction was performed with benzyl malonate, as the benzyl unit may be removed easily by hydrogenolysis. So benzyl malonate was treated with NaH in dry THF, followed by the *N*-hydroxysuccinimide esters, to afford the desired γ-amino β-oxo benzyl esters **47a**-**d** in high yield. This reaction allows obtaining the desired compound **47**, starting from both α- and β-amino acids (Scheme 9). The following cyclization was performed in benzyl alcohol and aqueous 2 M NaOH. While satisfactory yields were obtained for the synthesis of both 4-hydroxy-2-oxo-1*H*-pyrrole-1,3(2*H*,5*H*)-dicarboxylates **48a** and **48b** (60% and 52%, respectively), the synthesis of 4-hydroxy-2-oxo-5,6-dihydropyridine-1,3(2*H*)-dicarboxylates **48c** and **48d** afforded very unsatisfactory results, as **48c** was obtained only in traces from **47c** and **48d** in 26% yield from **47d**. No racemization occurred in the formation of **48b** (after analysis with HPLC equipped with a chiral column AD, *n*-hexane/*iso*-propanol 8:2, flow: 0.5 mL/min), probably due to the mild reaction conditions.

Then **48a** was deprotected from the Boc moiety by reaction with trifluoroacetic acid in dry dichloromethane, for further derivatizations. The desired product was obtained in high yield. Unfortunately, the following N-acylation reaction, performed with standard coupling conditions (HBTU or HATU, in the presence of tertiary amines) was totally unsuccessful, as the heterocyclic nitrogen of this compound is very unreactive. In effect, this reaction has been previously reported only in hard conditions,[77a] by reaction with a lithium base (*n*-BuLi or LiHMDS), followed by addition of an activated ester (Fmoc-AA-OPfp) at -50 °C.

To overcome this problem, we reversed the step order, making the coupling before the cyclization (Scheme 10). Thus four dipeptides were prepared containing both α- and β-amino acids, in both positions. Then the carboxy moieties were activated as the corresponding *N*-hydroxysuccinimide esters and treated with the sodium anion of the benzyl malonate to obtain the corresponding γ-amino β-oxo acids, as previously reported in Scheme 9. Much to our surprise, the expected

products were not obtained, as the reaction proceeded directly to the formation of the heterocyclic rings. The reaction yield was further optimized with the addition of 2.5 equiv of base.

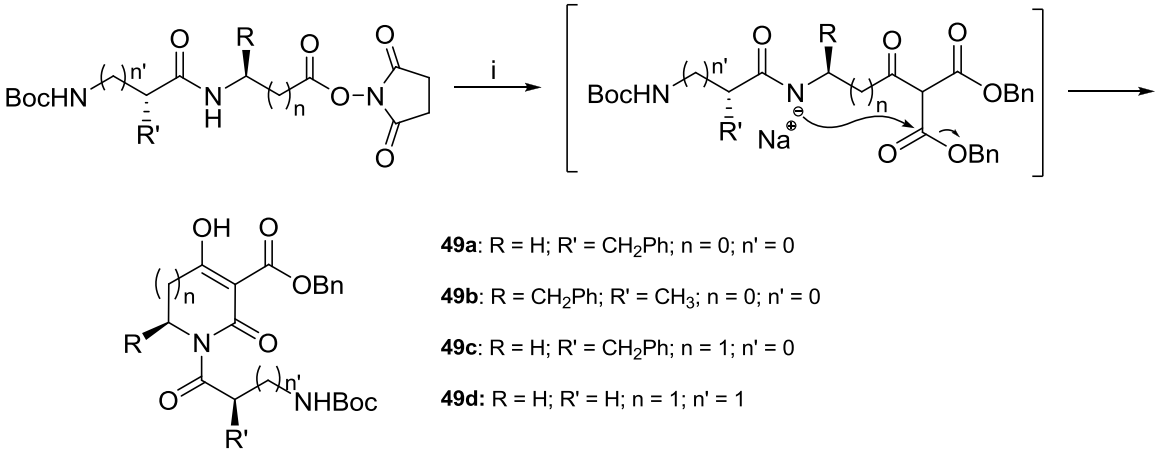

Scheme 10. Reagents and conditions: (i) $Na^{+}\ ^{-}CH(CO_2Bn)_2$ (1.5 equiv), dry THF, 16 h, rt.

The different behavior between Boc-AA-OSu and Boc-AA-AA-OSu may be ascribed to the secondary amide involved in the cyclization, that is more acidic than the carbamate involved in the cyclization of Boc-AA-OSu. The heterocycles **49-d** are obtained in good to high yield and can be further derivatized simply by removing the Boc or benzyl ester protecting groups.

Finally, the achiral **49d** was further derivatized to check if this new class of compounds may be utilized to promote the formation of reverse-turn mimics, as they may be considered as a mimic of the Gly-Pro moiety, that is often present in the β-turn motifs. Thus we replaced the OBn group with H-Ala-OMe that contains the small methyl ester. Of course, if a longer peptide chain has to be introduced, benzyl-protected amino acids are preferred.

After hydrogenolysis of the benzyl ester with H_2 and Pd/C, the acid was coupled with H-Ala-OMe, but the coupling reaction produced only a mixture of products, probably due to the free hydroxyl group, that was then protected by methylation of the Li anion with (trimethylsilyl)diazomethane (Scheme 11). The product **50** was obtained in good yield and the deprotected by reaction with H_2 and Pd/C to form the free acid **51**, that was coupled with H-Ala-OMe in the presence of HBTU and TEA. The derivative **52** was obtained in high yield after purification.

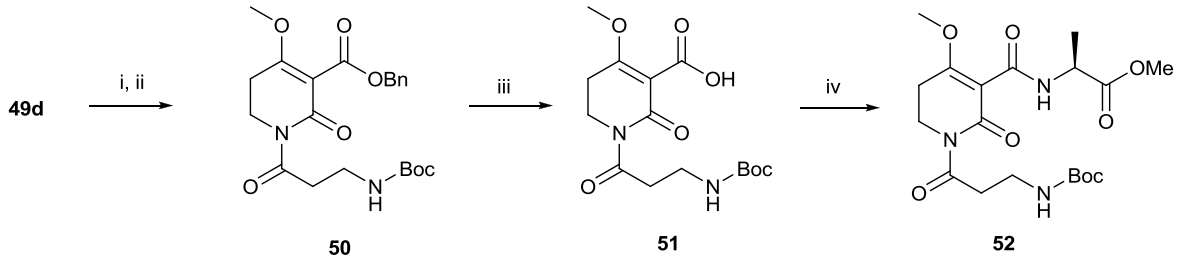

Scheme 11. Reagents and conditions: (i) LiHMDS (1.1 equiv), dry THF, 10 min, rt (ii) (trimethylsilyl)diazomethane (8 equiv), dry THF, 3 h, rt (iii) H_2, Pd/C, MeOH, 6 h, rt; (iv) HCl·H-Ala-OMe (1 equiv), HBTU (1.1 equiv), TEA (3 equiv), CH_3CN, 2 h, rt.

4.3 Conformational analysis of 52

Information on the preferred conformation of the compound **52** in solution was obtained by FT-IR and ^{1}H NMR techniques. The FT-IR absorption spectrum of **52** was obtained as 3 mM solution in methylene chloride, as at this concentration self-aggregation is usually unimportant (Figure 85). The IR spectrum of **52** shows the presence of a non-hydrogen-bonded amide N-H bands (3438, above 3400 cm^{-1}) and of a large band located at 3327 cm^{-1}, that suggests that an equilibrium takes place, involving a hydrogen-bonded amide protons bands.

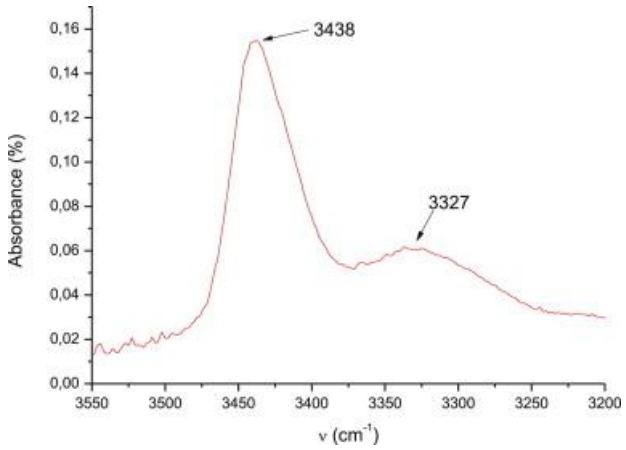

Figure 85. FT-IR absorption spectrum in the N-H stretching region for 3 mM concentration samples of **55** in pure CH_2Cl_2 at room temperature.

The in-solution conformation of **52** was investigated also by ^{1}H NMR spectroscopy and MD simulations; NMR analyses were conducted using standard techniques at 400 MHz in $CDCl_3$. The ^{1}H NMR analysis of **52** revealed a single set of sharp resonances, indicating conformational homogeneity or a fast equilibrium between conformers.

To verify the IR outcome and to check which hydrogen-bonded amide proton is involved in the equilibrium, some ^{1}H NMR spectra of **52** have been recorded, as a function of the addition of increasing amounts of DMSO-d_6, to check the dependence of NH proton chemical shifts from DMSO-d_6 (Figure 86a); this solvent is a strong hydrogen-bonding acceptor and, if it is bound to a free NH proton, it will be expected to dramatically move its chemical shift downfield. The titration of the NH bonds shows that NH-Ala is poorly bonded ($\Delta\delta$=0.68 ppm), while the NH-Boc is an equilibrium between a hydrogen-bonded and an open conformation ($\Delta\delta$=0.48 ppm). A strong hydrogen-bonded conformation would require a lower $\Delta\delta$ outcome ($\Delta\delta\leq$0.15 ppm).

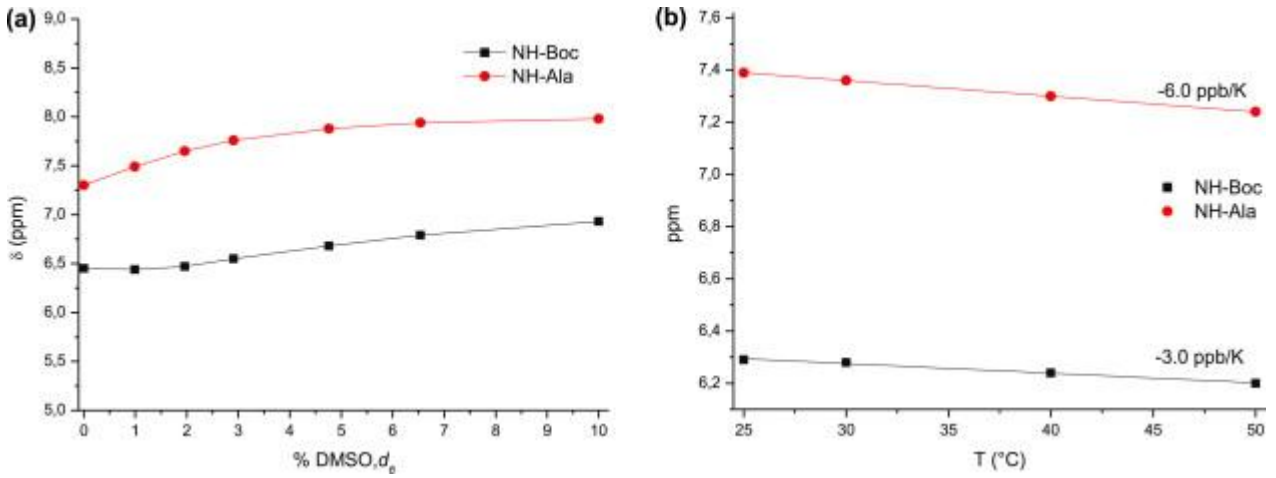

Figure 86. (a) Variation of NH proton chemical shift (ppm) of **52** as a function of increasing percentages of DMSO-d_6 to the $CDCl_3$ solution (v/v) (concentration: 3 mM); (b) variation of NH proton chemical shift (ppm) of **52** as a function the temperature (°C) for 10 mM samples measured in $CDCl_3$.

Some more information have been obtained, by recoding the ^{1}H NMR spectrum of a 10 mM sample of **52** in $CDCl_3$ at different temperature, to check the dependence of the NH proton from the temperature (Figure 86b).

This test points out the presence of hydrogen-bonded amide protons, as in $CDCl_3$ a small temperature coefficient (≤3 ppb/K in absolute value) indicates the presence of a hydrogen-bonded amide proton,[80] while protons, which participate to an equilibrium between hydrogen-bonded and non-hydrogen-bonded state show a larger temperature coefficient. In DMSO-d_6 the temperature coefficients can be bigger, so that a hydrogen-bonded amide proton can have a value of -4 ppb/K or smaller in absolute value. The analysis of the variation of the NH chemical shift with the temperature furnish a result, that is, in agreement both with the titration and with the IR

[80] Yang, J.; Gellman, S. H. *"Energetic superiority of two-center hydrogen bonding relative to three-center hydrogen bonding in a model system"* J. Am. Chem. Soc., **1998**, *120*, 9090-9091.

spectrum, because a $\Delta\delta$ of -6.0 ppb/K for NH-Ala shows that no hydrogen bond is formed, while -3.0 ppb/K for NH-Boc suggests the formation of a weak hydrogen bond.

To have more information on the in-solution preferred conformation, **52** was further analyzed by 2D ROESY experiments performed on a 10 mM solution of **52** in $CDCl_3$ (mixing time 0.500 s). Several cross peaks were obtained (see Supplementary data), the most interesting ones (Figure 87, red arrows) are the cross peak between the β-AlaNH and the methylene at the C5 of the heterocycle, and the cross peak between the CH_α-Ala and the Boc group. This cross peak shows that one chain lays nearby to the other, thus suggesting that this molecule is a good candidate for the formation of a reverse-turn motif.

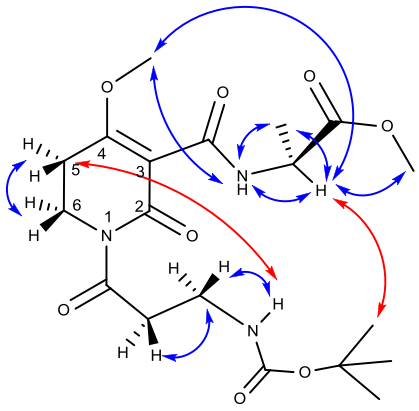

52

Figure 87. NOE enhancements as gathered from the ROESY analysis spectrum of **55** (10 mM solution in $CDCl_3$, mixing time 0.500 s).

Furthermore a strong signal was observed between the NH-Ala and the OMe heterocyclic group and two weaker signals between CH_α-Ala and CO_2Me and CH_α-Ala and OMe.

MD simulations[25] furnished some more hints on the preferred in-solution conformation of **52**. Structures consistent with the spectroscopic analyses were obtained by restrained MD simulations, using the distances derived from ROESY as constraints, and minimized with AMBER force field (see Supplementary data).[81] To investigate the dynamic behavior of **52**, some structures were analyzed by unrestrained MD for 500 ns.

[81] Cornell, W. D.; Cieplak, P.; Bayly, C.; Gould, I. R.; Merz, K. M.; Ferguson, D. M.; Spellmeyer, D. C.; Fox, T;. Caldwell, J. W.; Kollman P. A. *"A second generation force field for the simulation of proteins, nucleic acids, and organic molecules"* J. Am. Chem. Soc., **1995**, *117*, 5179-5197.

The simulation of the more stable structure revealed a strong propensity to maintain the folded conformations, with the occurrence of an explicit H-bond between β-AlaNH and the heterocyclic C=O, in agreement to the IR and ^{1}H NMR results (Figure 88).

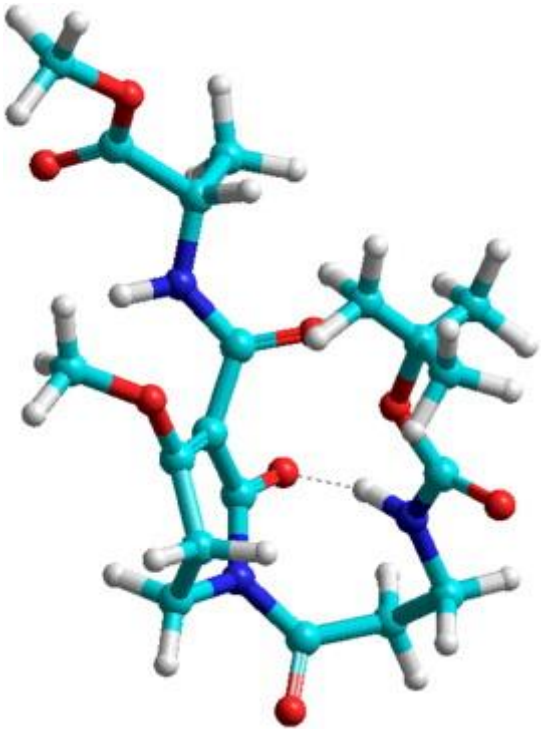

Figure 88. Representative low-energy structure of **52** obtained by unrestrained MD simulation, performed on the lower-energy structure consistent with ROESY analysis, calculated by restrained MD.

With this work, we demonstrated that *N*-Boc dipeptides activated as their *O*-succinimidyl esters (Boc-AA-AA-OSu), with the sodium anion of dibenzyl malonate, can spontaneously cyclize to five or six-member rings. The conformational study of **52** suggests the formation of a hydrogen bond between the β-AlaNH and the carbonyl at C2 of the heterocycle. Further studies are currently ongoing on more complex structures containing polysubstituted tetramic acids or their six-membered ring analogs to check if they are able to promote the formation of new foldamers.

5 Conclusions

This thesis deals with the synthesis and the conformation analysis of hybrid foldamers containing the 4-carboxyoxazolidin-2-one unit or related molecules, in which an imido-type function is obtained by coupling the nitrogen of the heterocycle with the carboxylic acid moiety of the next unit.

The imide group is characterized by a nitrogen atom connected to an endocyclic and an exocyclic carbonyl, which tend always to adopt the *trans* conformation. As a consequence of this locally constrained disposition effect, these imide-type oligomers are forced to fold in ordered conformations.

The synthetic approach is highly tuneable with endless variations, so, simply by changing the design and the synthesis, a wide variety of foldamers with the required properties may be prepared “on demand”.

Thus a wide variety of unusual secondary structures and interesting supramolecular materials may be obtained with hybrid foldamers.

The behaviour in the solid state of some of these compounds has been analyzed in detail, thus showing the formation of different kinds of supramolecular materials that may be used for several applications.

A winning example is the production of a bolaamphiphilic gelators that may also be doped with small amounts of dansyl containing compounds, needed to show the cellular uptake into IGROV-1 cells, by confocal laser scanning microscopy. These gels are readily internalized by cells and are biologically inactive, making them very good candidates in the promising field of drug delivery.

In the last part of the thesis, a particular attention was directed to the search of new scaffolds that behave as constrained amino acid mimetics, showing that tetramic acids derivatives could be good candidates for the synthesis and applications of molecules having an ordered secondary structure.

6 Experimental Section

Boc-L-Phe-L-Oxd-OBn **1**.
A solution of Boc-L-Phe-OH (0.50 g, 1.89 mmol) and HBTU (0.72 g, 1.89 mmol) in dry acetonitrile (40 mL) was stirred in a nitrogen atmosphere for 10 min at room temperature. Then l-Oxd-OBn (0.44 g, 1.89 mmol) in dry acetonitrile (10 mL) was added dropwise at room temperature, followed by TEA (3.78 mmol, 0.52 mL). The solution was stirred for 50 min in a nitrogen atmosphere, and then acetonitrile was removed under reduced pressure and replaced with ethyl acetate. The mixture was washed with brine (1 × 30 mL), 1 N aqueous HCl (1 × 30 mL), and a concentrated solution of $NaHCO_3$ (1 × 30 mL), dried over sodium sulfate, and concentrated in vacuo. The product was obtained pure after silica gel chromatography (90:10 *c*-Hex/ethyl acetate → 70:30 *c*-Hex/ethyl acetate as eluant) in 84% (0.77 g) overall yield as a waxy solid. $[\alpha]_D^{20}$ = -2.1 (c 1.0, $CHCl_3$). IR (CH_2Cl_2, 3 mM): ν 3442, 1799, 1761, 1738, 1717 cm^{-1}. IR (solid, 1% in KBr): ν 3354, 3436, 3354, 1791, 1739, 1725, 1690 cm^{-1}. ^1H NMR ($CDCl_3$): δ 1.25 (s, 9H, *t*-Bu), 1.48 (d, 3H, Me, *J* = 6.4 Hz), 2.50 (dd, 1H, *J* = 9.6, 13.6 Hz, C*H*H-Ph), 3.22 (dd, 1H, *J* = 3.3, 13.6 Hz, CH*H*-Ph), 4.50-4.58 (m, 2H, CHN-Oxd + CHO-Oxd), 4.84 (d, 1H, *J* = 8.8 Hz, NH), 5.16 (AB, 2H, *J* = 12.4 Hz), 5.57 (dt, 1H, *J* = 4.0, 9.6 Hz), 7.12-7.33 (m, 10H, 2 × Ph). ^{13}C NMR ($CDCl_3$): δ 28.0, 37.6, 53.9, 67.7, 67.8, 73.3, 73.6, 79.6, 126.6, 126.8, 128.1, 128.2, 128.3, 128.6, 129.3, 134.3, 135.8, 151.3, 155.0, 167.5. Anal. Calcd for $C_{26}H_{30}N_2O_7$: C, 64.72; H, 6.27; N, 5.81. Found: C, 64.69; H, 6.25; N, 5.78.

Boc-L-Phe-L-Oxd-OH **2**.
Compound **1** (0.72 mmol, 0.48 g) was dissolved in MeOH (30 mL) under nitrogen. C/Pd (35 mg, 10% w/w) was added under nitrogen. A vacuum was created inside the flask using the vacuum line. The flask was then filled with hydrogen using a balloon (1 atm). The solution was stirred for 16 h under a hydrogen atmosphere. The product was obtained pure in 98% yield (0.28 g) as an oil, after filtration through filter paper and concentration in vacuo. ^1H NMR (CD_3OD): δ 1.37 (s, 9H, *t*-Bu), 1.62 (d, 3H, Me, *J* = 6.4 Hz), 2.71 (dd, 1H, *J* = 10.8, 14.0 Hz, C*H*H-Ph), 3.35 (m, 1H, CH*H*-Ph), 4.65 (d, 1H, *J* = 4.4 Hz, CHN-Oxd), 4.80 (m, 1H, CHO-Oxd), 5.59 (dd, 1H, *J* = 3.2, 10.8 Hz), 7.21-7.44 (m, 5H, Ph). ^{13}C NMR (CD_3OD): δ 21.2, 28.6, 38.2, 56.2, 62.9, 76.0, 80.7, 127.7, 129.3, 130.4, 138.5, 153.8, 158.0, 171.3, 174.3. Anal. Calcd for $C_{19}H_{24}N_2O_7$: C, 58.16; H, 6.16; N, 7.14. Found: C, 58.13; H, 6.19; N, 7.12.

H-L-Phe-L-Oxd-OBn·CF_3CO_2H **3**.
A solution of **1** (0.52 mmol, 0.25 g) and TFA (9.36 mmol, 0.720 mL) in dry methylene chloride (20 mL) was stirred at room temperature for 4 h; then the volatiles were removed under reduced pressure, and the corresponding amine salt was obtained pure in 99% yield (0.26 g) as a waxy solid, without further purification. ^1H NMR ($CDCl_3$): δ 1.52 (d, 3H, Me, *J* = 3.96 Hz), 2.77 (dd, 1H, *J* = 9.2, 14.4 Hz, C*H*H-Ph), 3.37 (dd, 1H, *J* = 3.8, 14.4 Hz, CH*H*-Ph), 4.51-4.64 (m, 2H, CHN-Oxd + CHO-Oxd), 5.15 (AB, 2H, *J* = 11.6 Hz), 5.57 (m, 1H, NH), 7.08-7.40 (m, 10H, 2 × Ph). ^{13}C NMR ($CDCl_3$): δ 19.6, 19.8, 35.2, 53.8, 60.1, 60.3, 65.0, 67.6, 67.7, 73.5, 73.9, 127.4, 127.5, 127.6, 127.8, 128.0, 128.3, 128.4, 128.5, 131.5, 133.2, 150.4, 159.6 (q, CF_3), 166.0, 167.8. Anal. Calcd for $C_{23}H_{23}F_3N_2O_7$: C, 55.65; H, 4.67; N, 5.64. Found: C, 55.68; H, 4.68; N, 5.61.

Boc-(l-Phe-l-Oxd)$_2$-OBn **4**.
A solution of **2** (0.20 g, 0.52 mmol) and HBTU (0.20 g, 0.52 mmol) in dry acetonitrile (20 mL) was stirred in a nitrogen atmosphere for 10 min at room temperature. Then a mixture of **3** (0.52 mmol)

and TEA (1.56 mmol, 0.22 mL) in dry acetonitrile (10 mL) was added dropwise at room temperature. The solution was stirred for 50 min in a nitrogen atmosphere, and then acetonitrile was removed under reduced pressure and replaced with ethyl acetate. The mixture was washed with brine (1 × 30 mL), 1 N aqueous HCl (1 × 30 mL), and a concentrated solution of $NaHCO_3$ (1 × 30 mL), dried over sodium sulfate, and concentrated in vacuo. The product was obtained pure after silica gel chromatography (90:10 *c*-Hex/ethyl acetate → 70:30 *c*-Hex/ethyl acetate as eluant) in 80% yield (0.32 g) as a white solid. M. p.: 81-82 °C. $[\alpha]_D^{20}$ = -26 (c 1.0, $CHCl_3$). IR (CH_2Cl_2, 3 mM): ν 3427, 1789, 1752, 1711 cm^{-1}. IR (solid, 1% in KBr): ν 3362, 1785, 1752, 1707 cm^{-1}. ^1H NMR ($CDCl_3$): δ 1.22-1.30 (m, 15H, 2 × Me + *t*-Bu), 2.46-2.59 (m, 2H, 2 × CHH-Ph), 3.08-3.46 (m, 2H, 2 × CHH-Ph), 4.12-4.68 (m, 4H, 2 × CHN-Oxd + 2 × CHO-Oxd), 4.89 (bs, 1H, NH), 5.06-5.24 (m, 2H, OCH_2Ph), 5.44-5.60 (m, 1H, CHN-CH_2Ph), 5.86-5.93 (m, 1H, CHN-CH2Ph), 6.63 (d, 1H, *J* = 8.4 Hz, NH), 6.89-7.47 (m, 15H, 3 × Ph). ^{13}C NMR ($CDCl_3$): δ 14.2, 20.4, 21.0, 21.2, 26.9, 27.8, 28.2, 37.9, 53.0, 54.2, 55.4, 60.4, 61.2, 61.5, 62.6, 68.3, 73.9, 74.2, 79.8, 80.2, 126.7, 126.8, 127.0, 127.1, 127.2, 128.4, 128.5, 128.8, 129.5, 130.1, 134.4, 135.7, 136.1, 151.4, 151.6, 155.2, 158.7, 163.8, 166.7, 166.9, 167.5, 167.7, 171.2, 171.3, 171.7, 171.9, 172.7, 173.4. Anal. Calcd for $C_{40}H_{44}N_4O_{11}$: C, 63.48; H, 5.86; N, 7.40. Found: C, 63.49; H, 5.88; N, 7.43.

Boc-(L-Phe-L-Oxd)$_2$-OH **5**.
Compound **4** (0.40 mmol, 0.30 g) was dissolved in MeOH (30 mL) under nitrogen. C/Pd (35 mg, 10% w/w) was added under nitrogen. A vacuum was created inside the flask using the vacuum line. The flask was then filled with hydrogen using a balloon (1 atm). The solution was stirred for 16 h in a hydrogen atmosphere. The product was obtained pure in 97% yield (0.26 g) as a waxy solid, after filtration through filter paper and concentration in vacuo. ^1H NMR (CD_3OD): δ 1.15-1.30 (m, 9H, *t*-Bu), 1.37-1.48 (m, 6H, 2 × Me), 2.48 (dd, 1H, *J* = 10.8, 14.0 Hz, C*H*H-Ph), 2.77 (dd, 1H, *J* = 10.4, 14.4 Hz, C*H*H-Ph), 3.10-3.33 (m, 2H, 2 × CH*H*-Ph), 4.44-4.52 (m, 2H, 2 × CHN-Oxd), 4.61-4.69 (m, 2H, 2 × CHO-Oxd), 5.32-5.39 (m, 1H, NH), 5.65-5.74 (m, 1H, NH), 7.05-7.33 (m, 10H, 2 × Ph). ^{13}C NMR (CD_3OD): δ 20.6, 28.6, 37.4, 38.0, 55.3, 56.1, 63.0, 63.3, 76.2, 76.4, 80.6, 127.6, 127.8, 129.2, 130.4, 137.8, 138.5, 163.8, 154.1, 158.0, 170.1, 171.4, 173.0, 174.1. Anal. Calcd for $C_{33}H_{38}N_4O_{11}$: C, 59.45; H, 5.75; N, 8.40. Found: C, 59.41; H, 5.74; N, 8.38.

Boc-(L-Phe-L-Oxd)$_3$-OBn **6**.
A solution of **5** (0.168 g, 0.25 mmol) and HBTU (0.095 g, 0.25 mmol) in dry acetonitrile (20 mL) was stirred in a nitrogen atmosphere for 10 min at room temperature. Then a mixture of **3** (0.25 mmol) and TEA (0.75 mmol, 0.104 mL) in dry acetonitrile (10 mL) was added dropwise at room temperature. The solution was stirred for 50 min in a nitrogen atmosphere, and then acetonitrile was removed under reduced pressure and replaced with ethyl acetate. The mixture was washed with brine (1 × 30 mL), 1 N aqueous HCl (1 × 30 mL), and a concentrated solution of $NaHCO_3$ (1 × 30 mL), dried over sodium sulfate, and concentrated in vacuo. For the purification from tetramethylurea and the byproduct, the residue was suspended in cyclohexane and sonicated for 15 min to dissolve the byproduct. Compound **6** was filtered, dried in vacuo, and obtained pure in 73% yield (0.18 g) as a white solid. M. p.: 79-80 °C. $[\alpha]_D^{20}$ = -30 (c 0.3, $CHCl_3$). IR (CH_2Cl_2, 3 mM): ν 3442, 1789, 1752, 1718 cm^{-1}. IR (solid, 1% in KBr): ν 3371, 1788, 1754, 1714 cm^{-1}. ^1H NMR ($CDCl_3$): δ 1.05-1.68 (m, 18H, 3 × Me + *t*-Bu), 2.58-2.94 (m, 3H, 3 × C*H*H-Ph), 3.27-3.51 (m, 3H, 3 × CH*H*-Ph), 4.20-4.87 (m, 6H, 3 × CHN-Oxd + 3 × CHO-Oxd), 4.94 (bs, 1H, NH), 5.05-5.18 (m, 2H, OCH_2Ph), 5.82-6.07 (m, 3H, 3 × C*H*N-CH_2Ph), 6.75 (bs, 1H, NH), 6.89-7.47 (m, 25H, 5 × Ph), 7.17 (bs, 2H, 2 × NH), 7.34 (bs, 1H, NH). ^{13}C NMR ($CDCl_3$): δ 20.3, 21.1, 27.8, 28.2, 37.2, 37.7, 53.1, 54.3, 60.3, 61.7, 62.7, 63.0, 68.2, 74.0, 74.2, 74.4, 80.0, 126.9, 127.1, 128.4, 128.8, 129.2, 129.6, 129.9, 134.5, 135.9,

151.0, 151.7, 155.2, 155.6, 167.0, 167.6, 171.1, 171.4. Anal. Calcd for $C_{54}H_{58}N_6O_{15}$: C, 62.90; H, 5.67; N, 8.15. Found: C, 62.87; H, 5.65; N, 8.18.

H-(L-Phe-L-Oxd)$_2$-OBn·CF_3CO_2H **7.**
A solution of **2** (0.52 mmol, 0.39 g) and TFA (9.36 mmol, 0.720 mL) in dry methylene chloride (20 mL) was stirred at room temperature for 4 h; then the volatiles were removed under reduced pressure, and the corresponding amine salt was obtained pure in 96% yield (0.38 g) as a waxy solid. ^{1}H NMR ($CDCl_3$): δ 1.34-1.52 (m, 6H, 2 × Me), 2.49-2.90 (m, 2H, 2 × C*H*H-Ph), 3.01-3.35 (m, 2H, 2 × CH*H*-Ph), 4.19-4.68 (m, 4H, 2 × CHN-Oxd + 2 × CHO-Oxd), 4.89-5.18 (m, 1H, NH), 5.30-5.81 (m, 2H, 2 × C*H*N-CH_2Ph), 7.05-7.35 (m, 15H, 3 × Ph). ^{13}C NMR ($CDCl_3$): δ 20.5, 20.9, 27.7, 28.1, 36.1, 36.6, 37.7, 38.8, 53.2, 53.7, 54.3, 55.5, 61.5, 62.2, 68.4, 74.4, 127.1, 127.3, 128.5, 128.7, 128.8, 129.0, 129.3, 129.5, 129.6, 134.3, 134.8, 151.7, 159.4 (q, CF_3), 167.5, 171.1. Anal. Calcd for $C_{37}H_{37}F_3N_4O_{11}$: C, 57.66; H, 4.84; N, 7.27. Found: C, 57.68; H, 4.83; N, 7.30.

Boc-(L-Phe-L-Oxd)$_4$-OBn **8**.
A solution of **5** (0.16 g, 0.24 mmol) and HBTU (0.091 g, 0.24 mmol) in dry acetonitrile (20 mL) was stirred in a nitrogen atmosphere for 10 min at room temperature. Then a mixture of **3** (0.24 mmol) and TEA (0.72 mmol, 0.100 mL) in dry acetonitrile (10 mL) was added dropwise at room temperature. The solution was stirred for 50 min in a nitrogen atmosphere, and then acetonitrile was removed under reduced pressure and replaced with ethyl acetate. The mixture was washed with brine (1 × 30 mL), 1 N aqueous HCl (1 × 30 mL), and a concentrated solution of $NaHCO_3$ (1 × 30 mL), dried over sodium sulfate, and concentrated in vacuo. For the purification from tetramethylurea and the byproduct, the residue was suspended in cyclohexane and sonicated for 15 min to dissolve the byproduct. Compound **8** was filtered, dried in vacuo, and obtained pure in 70% yield (0.22 g) as a white solid. M. p.: 87-88 °C. $[\alpha]_D^{20}$ = -28.0 (c 1.0, $CHCl_3$). IR (CH_2Cl_2, 3 mM): ν 3428, 1789, 1707 cm^{-1}. IR (solid, 1% in KBr): ν 3361, 1791, 1749, 1714 cm^{-1}. ^{1}H NMR ($CDCl_3$): δ 1.10-1.38 (m, 21H, 4 × Me + *t*-Bu), 2.71-3.30 (m, 8H, 4 × C*H*$_2$-Ph), 4.07-4.64 (m, 8H, 4 × CHN-Oxd + 4 × CHO-Oxd), 4.79-5.17 (m, 3H, OC*H*$_2$Ph + NH), 5.40-6.13 (m, 4H, 4 × C*H*N-CH_2Ph), 6.98-7.33 (m, 28H, 5 × Ph + 3 × NH), 7.47 (bs, 1H, NH). ^{13}C NMR ($CDCl_3$): δ 20.3, 20.6, 20.9, 28.3, 37.0, 37.8, 38.4, 53.1, 53.7, 54.1, 61.7, 62.7, 68.3, 73.9, 74.5, 74.9, 79.9, 126.8, 126.9, 127.2, 127.4, 128.4, 128.5, 128.8, 129.7, 134.5, 135.5, 136.0, 151.3, 151.8, 152.1, 155.2, 167.3, 168.0, 171.3. Anal. Calcd for $C_{68}H_{72}N_8O_{19}$: C, 62.57; H, 5.56; N, 8.58. Found: C, 62.55; H, 5.54; N, 8.61.

Boc-(L-Phe-L-Oxd)$_4$-OH **9**.
Compound **8** (0.30 mmol, 0.36 g) was dissolved in MeOH (30 mL) under nitrogen. C/Pd (35 mg, 10% w/w) was added under nitrogen. A vacuum was created inside the flask using the vacuum line. The flask was then filled with hydrogen using a balloon (1 atm). The solution was stirred for 16 h under a hydrogen atmosphere. The product was obtained pure in 98% yield (0.28 g) as a white solid, after filtration through filter paper and concentration in vacuo. M. p.: 76 °C. ^{1}H NMR ($CDCl_3$): δ 1.20-1.61 (m, 21H, 4 × Me + *t*-Bu), 2.52-2.68 (m, 1H, 1 × C*H*H-Ph), 2.72-3.02 (m, 3H, 1 × C*H*H-Ph, 2 × CH*H*-Ph), 4.46-4.83 (m, 6H, 3 × CHN-Oxd + 3 × CHO-Oxd), 5.44-5.94 (m, 4H, 4 × C*H*N-CH_2Ph), 7.12-7.56 (m, 20H, 4 × Ph). ^{13}C NMR (CD_3OD): δ 19.2, 19.9, 35.8, 36.0, 36.6, 53.0, 54.8, 61.8, 62.0, 75.1, 76.3, 79.3, 126.4, 127.9, 128.0, 129.0, 136.6, 137.2, 152.2, 152.6, 169.1, 171.4, 171.6, 172.8. Anal. Calcd for $C_{61}H_{66}N_8O_{19}$: C, 60.29; H, 5.47; N, 9.22. Found: C, 60.32; H, 5.46; N, 9.20.

Boc-(L-Phe-L-Oxd)$_6$-OBn **10**.

A solution of **9** (0.13 g, 0.11 mmol) and HBTU (0.09 g, 0.11 mmol) in dry acetonitrile (20 mL) was stirred in a nitrogen atmosphere for 10 min at room temperature. Then a mixture of **7** (0.09 g, 0.11 mmol) and TEA (0.33 mmol, 0.05 mL) in dry acetonitrile (15 mL) was added dropwise at room temperature. The solution was stirred for 50 min in a nitrogen atmosphere, and then acetonitrile was removed under reduced pressure and replaced with ethyl acetate. The mixture was washed with brine (1 × 30 mL), 1 N aqueous HCl (1 × 30 mL), and a concentrated solution of $NaHCO_3$ (1 × 30 mL), dried over sodium sulfate, and concentrated in vacuo. For the purification from tetramethylurea and the byproduct, the residue was suspended in cyclohexane and sonicated for 15 min to dissolve the byproduct. Compound **9** was filtered, dried in vacuo, and obtained pure as a white solid in 68% (0.14 g) yield. M. p.: 92-93 °C. $[\alpha]_D^{20}$: -30 (c 1.0, $CHCl_3$). IR (CH_2Cl_2, 3 mM): ν 3411, 3328, 1789, 1733, 1699 cm^{-1}. IR (solid, 1% in KBr): ν 3330, 1790, 1747, 1701, 1650 cm^{-1}. ^1H NMR ($CDCl_3$): δ 0.97-1.64 (m, 27H, 6 × Me + *t*-Bu), 2.69-3.42 (m, 12H, 8 × CH_2-Ph), 4.11-4.75 (m, 12H, 6 × CHN-Oxd + 6 × CHO-Oxd), 5.01-5.77 (m, 3H, OCH_2Ph + NH), 5.39-6.11 (m, 6H, 6 × C*H*N-CH_2Ph), 6.67 (bs, 1H, NH), 6.93-7.45 (m, 39H, 7 × Ph + 4 × NH). ^{13}C NMR ($CDCl_3$): δ 13.1, 19.3, 19.7, 20.0, 27.7, 28.6, 35.7, 36.7, 37.3, 37.7, 51.9, 52.3, 52.6, 53.0, 60.7, 61.5, 61.6, 67.2, 72.8, 73.2, 74.0, 78.9, 125.8, 126.3, 127.5, 127.6, 127.7, 128.4, 128.6, 133.6, 134.4, 134.5, 134.8, 150.2, 150.9, 165.8, 166.3, 166.8, 170.2, 170.4, 170.6. Anal. Calcd for $C_{96}H_{100}N_{12}O_{27}$: C, 62.20; H, 5.44; N, 9.07. Found: C, 62.22; H, 5.46; N, 9.11.

cyclo-(L-Val-L-Oxd-D-Ala-D-Oxd-L-Asp(O*c*Hex)-L-Oxd-Gly-D-Oxd) **11**.

A solution of **21** (0.075 mmol, 79 mg) and TFA (1.35 mmol, 0.1 mL) in dry methylene chloride (10 mL) was stirred 4 h at room temperature, then the volatiles were removed under reduced pressure and the product was obtained pure in quantitative yield without any further purification.

To a stirred solution of $CF_3CO_2^-$ $^+NH_3$-L-Val-L-Oxd-D-Ala-D-Oxd-L-Asp(O*c*Hex)-L-Oxd-Gly-D-Oxd-OH, (0.075 mmol, 80 mg) in dry acetonitrile (80 mL) under inert atmosphere were added HATU (0.082 mmol, 32 mg) and then TEA (0.225 mmol, 0.054 mL) at room temperature. The solution was stirred 45 min under inert atmosphere, then acetonitrile was removed under reduced pressure. The crude was washed with acetonitrile to remove all the by-products. **11** was obtained as a white solid in 62% yield after HPLC (H_2O/acetonitrile 80:20 → 70:30 as eluant). M. p. = 187 °C; $[\alpha]_D^{20}$ = + 21 (c 0.1,CH_2Cl_2);); IR (CH_2Cl_2, 1 mM): ν = 3409, 2862, 1800, 1703, 1513, 1356 cm^{-1}; ^{1}H NMR (DMSO-d_6): δ 0.96 (d, 3 H, *J* = 7.2 Hz Me Val), 1.09 (d, 3 H, *J* = 6.8 Hz Me Val), 1.38-1.73 (m, 18 H, 4Me Oxd + 6 H *c*Hex), 1.84 (bs, 2 H, CH_2 *c*Hex), 1.92 (bs, 2 H, CH_2 *c*Hex), 2.43 (bs, 1 H, C*H*$(CH_3)_2$), 3.07 (m, 2 H, CH_2 Asp), 4.27-4.87 (m, 10 H, 4CHN Oxd + 4CHO Oxd + $CH_{2\alpha}$ Gly), 5.59 (m, 1 H, CH_α Ala), 5.84 (m, 1 H, CH_α Val), 5.85 (m, 1 H, CH_α Asp), 8.95 (bs, 1 H, NH Val), 9.09 (bs, 1 H, NH Ala), 9.21 (bs, 1 H, NH Asp), 9.30 (bs, 1 H, NH Gly); ^{13} C NMR (DMSO-d_6): δ 17.6, 17.8, 18.4, 20.0, 20.5, 23.8, 25.7, 29.0, 30.5, 31.6, 31.8, 36.6, 48.1, 49.5, 49.7, 62.5, 73.4, 75.4, 75.7, 79.1. Anal. Calcd. for $C_{40}H_{52}N_8O_{18}$: C, 51.50; H, 5.62; N, 12.01. Found: C, 51.47; H, 5.63; N, 12.00.

Boc-L-Val-L-Oxd-OBn **12**.

Yield = 90%; waxy solid; $[\alpha]_D^{20}$ = -16.0 (c 0.1,CH_2Cl_2); IR (CH_2Cl_2, 3 mM): ν = 3442, 1793, 1753, 1708 cm^{-1}; ^{1} H NMR ($CDCl_3$): δ 0.80 (d, 3 H, *J* = 7 Hz, Me Val), 1.08 (d, 3 H, *J* = 7 Hz, Me Val), 1.41 (s, 9 H, *t*Bu), 1.57 (d, 3 H, *J* = 5.4 Hz, Me Oxd), 2.25 (bs, 1 H, C*H*$(CH_3)_2$), 4.58 (m, 2 H, CHN + CHO Oxd), 5.07 (d, 1 H, J = 8.6 Hz, NH), 5.21 (m, 2 H, OCH_2Ph), 5.46 (dd, 1 H, *J* = 3.4, 9.6 Hz, CH_α Val), 7.25-7.48 (m, 5 H, Ph); ^{13} C NMR ($CDCl_3$): δ 15.9, 20.0, 21.3, 28.6, 30.8, 57.4, 62.0, 68.3, 73.8, 80.1, 128.7, 129.1, 134.8, 151.5, 156.1, 167.9. Anal. Calcd. for $C_{22}H_{30}N_2O_7$: C, 60.82; H, 6.96; N, 6.45. Found: C, 60.80; H, 6.99; N, 6.43.

Boc-D-Ala-D-Oxd-OBn **13**.

Yield = 81%; waxy solid; $[\alpha]_D^{20}$ = +44.1 (c 1.0, CH_2Cl_2); IR (CH_2Cl_2, 3 mM): ν = 3439, 1794, 1755, 1718 cm^{-1}; ^{1}H NMR ($CDCl_3$): δ 1.31 (d, 3 H, *J* = 7.6 Hz), 1.42 (s, 9 H, *t*Bu), 1.51 (d, 3 H, *J* = 6.4 Hz, Me Oxd), 4.50-4.58 (m, 2 H, CHN + CHO Oxd), 5.14 (bs, 1 H), 5.17 (AB, 2 H, *J* = 12.0 Hz), 5.35 (dq, 1 H, *J* = 7.6 Hz, CH_α Ala), 7.25-7.40 (m, 5 H, Ph); ^{13}C NMR ($CDCl_3$): δ 17.8, 20.9, 28.1, 48.8, 61.4, 67.9, 73.5, 79.7, 128.2, 128.4, 128.7, 134.3, 151.1, 154.9, 167.4, 173.9. Anal. Calcd. for $C_{20}H_{26}N_2O_7$: C, 59.10; H, 6.45; N, 6.89. Found: C, 59.08; H, 6.47; N, 6.93.

Boc-L-Asp(O*c*Hex)-L-Oxd-OBn **14**.
Yield = 70%; M. p. = 110 °C; $[\alpha]_D^{20}$ = -20.9 (c 1.0, CH_2Cl_2); IR (CH_2Cl_2, 3 mM): ν = 3408, 2959, 1794, 1707, 1364 cm^{-1}; ^{1}H NMR ($CDCl_3$): δ 1.48-1.67 (m, 15 H, 9 H *t*Bu + 6 H *c*Hex), 1.72 (d, 3 H, *J* = 4.7 Hz, Me Oxd), 1.89 (bs, 2 H, CH_2 *c*Hex), 1.99 (bs, 2 H, CH_2 *c*Hex), 2.85 (m, 1 H CH*H* Asp), 3.11 (m, 1 H, C*H*H Asp), 4.74 (m, 2 H CHN + CHO Oxd), 4.98 (bs, 1 H, NH), 5.37 (m, 2 H, OCH_2Ph), 5.76 (m, 1 H, CH_α Asp), 7.49-7.58 (m, 5 H, Ph); ^{13}C NMR ($CDCl_3$,): δ 21.5, 24.0, 25.8, 28.7, 31.77, 36.7, 50.8, 62.0, 68.5, 73.9, 74.3, 128.8, 129.3, 135.0, 151.8, 167.9, 171.9. Anal. Calcd. for $C_{27}H_{36}N_2O_9$: C, 60.89; H, 6.81; N, 5.26. Found: C, 60.93; H, 6.78; N, 5.29.

Boc-Gly-D-Oxd-OBn **15**.
Yield = 78%; waxy solid; $[\alpha]_D^{20}$ = +37.0 (c 0.1, CH_2Cl_2); IR (CH_2Cl_2, 3 mM): ν = 3442, 1795, 1757, 1712, 1605, 1511 cm^{-1}; ^{1}H NMR ($CDCl_3$): δ 1.47 (s, 9 H, *t*Bu), 1.57 (d, 3 H, *J* = 6.6 Hz, Me Oxd), 4.42 (dd, 1 H, *J* = 4.5, 19.5 Hz, CH_α Gly), 4.55 (d, 1 H, *J* = 4.2 Hz CHN Oxd), 4.62 (dq, 1 H, *J* = 6.3, 10.8 Hz, C*H*O Oxd), 4.74 (dd, 1 H, *J* = 6.6, 19.5 Hz, CH_α Gly), 5.10 (bs, 1 H, NH), 5.26 (m, 2 H, OCH_2Ph), 7.34-7.46 (m, 5 H, Ph); ^{13}C NMR ($CDCl_3$): δ 21.1, 26.8, 28.2, 30.8, 44.7, 61.4, 68.0, 74.1, 128.3, 128.7, 134.5, 151.7, 167.5, 170.0. Anal. Calcd. for $C_{19}H_{24}N_2O_7$: C, 58.16; H, 6.16; N, 7.14. Found: C, 58.13; H, 6.20; N, 7.11.

Boc-L-Val-L-Oxd-D-Ala-D-Oxd-OBn **16**.
To a stirred solution of Boc-L-Ala-L-Oxd-OH (0.60 mmol, 200 mg) and HBTU (0.60 mmol, 228 mg) in dry acetonitrile (10 mL) under inert atmosphere was added a mixture of CF_3COO^- $^+H_3$N-D-Ala-D-Oxd-OBn (0.60 mmol, 250 mg) and TEA (1.8 mmol, 0.25 mL) in dry acetonitrile (5 mL) at room temperature. The solution was stirred 45 min under inert atmosphere, then acetonitrile was removed under reduced pressure and replaced with ethyl acetate (30 mL). The mixture was washed with brine (30 mL), 1 M HCl (20 mL) and $NaHCO_3$ 5% (20 mL) and then dried over Na_2SO_4, then ethyl acetate was eliminated under reduced pressure. The product was obtained pure after flash chromatography (eluant: cyclohexane/ethyl acetate 8:2) in 80% yield. M. p. = 175 °C; $[\alpha]_D^{20}$ = + 41.5 (c 0.1, CH_2Cl_2); IR (CH_2Cl_2, 3 mM): ν = 3420, 1791, 1702, 1503, 1362 cm^{-1}; ^{1}H NMR ($CDCl_3$): δ 0.80 (d, 3 H, J = 7 Hz, Me Val), 1.08 (d, 3 H, *J* = 7 Hz, Me Val), 1.41 (m, 12 H, 9 H, *t*Bu + 3 H Me Ala), 1.57 (m, 6 H, 2 Me Oxd), 2.25 (bs, 1 H, C*H*$(CH_3)_2$), 4.41 (d, 1 H, *J* = 4.8 Hz, C*H*N Oxd), 4.5-4.7 (m, 2 H, C*H*N Oxd + C*H*O Oxd), 4.83 (m, 1 H, C*H*O Oxd), 5.07 (bs, 1 H, NH Val), 5.21 (m, 2 H, O*CH*$_2$Ph), 5.40 (m, 1 H, CH_α Val), 5.60 (m, 1 H, CH_α Ala), 6.80 (bs, 1 H, NH Ala), 7.25-7.48 (m, 5 H, Ph); ^{13}C NMR ($CDCl_3$): δ 14.5, 16.3, 18.1, 20.1, 20.9, 21.5, 28.6, 30.9, 48.7, 60.7, 61.7, 63.0, 68.5, 74.2, 80.1, 128.8, 129.1, 129.2. 134.6, 151.4, 166.9, 167.7, 172.7, 174.3. Anal. Calcd. for $C_{30}H_{40}N_4O_{11}$: C, 56.95; H, 6.37; N, 8.86. Found: C, 56.92; H, 6.36; N, 8.86.

Boc-L-Val-L-Oxd-D-Ala-D-Oxd-OH **17**.
To a stirred solution of Boc-L-Val-L-Oxd-D-Ala-D-Oxd-OBn **16** (0.3 mmol, 190 mg) in ethyl acetate (5 mL) 10% palladium on charcoal (3 mg) was added. The mixture was stirred under hydrogen atmosphere for 2 h. Then the catalyst was filtered on a celite pad and the mixture was concentrated. The product **17** was obtained pure in 87% yield without any further purification. M.

p. = 180 °C; $[\alpha]_D^{20}$ = + 29.0 (c 0.1,CH_2Cl_2); IR (nujol): ν = 3397, 1792, 1691, 1462, 1372 cm^{-1}; ^{1}H NMR (CD_3OD): δ 0.85 (d, 3 H, *J* = 7 Hz, Me Val), 1.04 (d, 3 H, *J* = 6.8 Hz, Me Val), 1.45-1.58 (m, 18 H, 9 H, *t*Bu + 6 H 2Me Oxd + 3 H Me Ala), 2.18 (bs, 1 H, $CH(CH_3)_2$), 4.43 (d, 1 H, J = 4 Hz, CHN Oxd), 4.58-4.74 (m, 3 H, 2 CHO Oxd + CHN Oxd), 5.35 (m, 1 H, CH_α Val), 5.54 (m, 1 H, CH_α Ala), 6.71 (d, 1 H, J = 8.8 Hz, NH Val), 8.91 (d, 1 H, *J* = 7.4 Hz, NH Ala); ^{13}C NMR ($CDCl_3$): δ 15.7, 16.3, 18.8, 19.6, 20.2, 27.6, 30.3, 57.5, 62,8, 75.0, 75.3, 79.5, 152.8, 169.0, 172.5, 173.2. Anal. Calcd. for $C_{23}H_{34}N_4O_{11}$: C, 50.92; H, 6.32; N, 10.33. Found: C, 50.89; H, 6.34; N, 10.32.

Boc-L-Val-L-Oxd-D-Ala-D-Oxd-L-Asp(O*c*Hex)-L-Oxd-OBn **18**.
To a stirred solution of Boc-L-Val-L-Oxd-D-Ala-D-Oxd-OH (0.096 mmol, 52 mg) and HATU (0.096 mmol, 36 mg) in dry acetonitrile (10 mL) under inert atmosphere was added a mixture of CF_3COO^- $^+H_3$N-L-Asp(O*c*Hex)-L-Oxd-OBn (0.096 mmol, 52 mg) and TEA (1.8 mmol, 0.25 mL) in dry acetonitrile (5 mL) at room temperature. The solution was stirred 45 min under inert atmosphere, then acetonitrile was removed under reduced pressure and replaced with ethyl acetate (30 mL). The mixture was washed with brine (30 mL), 1 M HCl (20 mL) and $NaHCO_3$ 5% (20 mL) and then dried over Na_2SO_4, then ethyl acetate was eliminated under reduced pressure. Yield = 65%; M. p. = 150 °C; $[\alpha]_D^{20}$ = + 6 (c 0.1, CH_2Cl_2); IR (CH_2Cl_2, 3 mM): ν = 3409, 2859, 1794, 1708, 1512, 1363 cm^{-1}; ^{1}H NMR ($CDCl_3$): δ 0.81 (d, 3 H, *J* = 6.8 Hz, Me Val), 1.06 (d, 3 H, *J* = 6.8 Hz, Me Val), 1.42-1.64 (m, 27 H, 9 H, *t*Bu + 9 H 3Me Oxd + 3 H Me Ala + 6 H *c*Hex), 1.72 (bs, 2 H, CH_2 *c*Hex), 1.81 (bs, 2 H, CH_2 *c*Hex), 2.30 (bs, 1 H, C*H*$(CH_3)_2$), 2.76 (dd, 1 H, *J* = 6.8, 16.4 Hz, C*H*H Asp), 2.88 (m, 1 H, OCH *c*Hex), 2.96 (dd, 1 H, *J* = 4.8, 16.8 Hz, CH*H* Asp), 4.38 (m, 2 H, 2 C*H*N Oxd), 4.57 (m, 2 H, CHN Oxd + CHO Oxd), 4.78 (m, 2 H, CHO Oxd), 5.07 (bs, 1 H, NH Val), 5.20 (m, 2 H, CH_2Ph), 5.39 (bs, 1 H, CH_α Val), 5.58 (m, 1 H, CH_α Ala), 5.78 (m, 1 H, CH_α Asp), 6.77 (bs, 1 H, NH Ala), 7.22 (bs, 1 H, NH Asp); ^{13}C NMR ($CDCl_3$): δ 16.2, 20.1, 21.0, 21.4, 24.0, 25.5, 28.6, 31.2, 31.7, 35.8, 48.8, 49.7, 61.7, 62.8, 68.5, 74.4, 128.7, 128.8, 129.2, 134.7, 151.7, 156.2, 166.9, 167.5, 169.6. Anal. Calcd. for $C_{45}H_{60}N_6O_{17}$: C, 56.48; H, 6.32; N, 8.78. Found: C, 56.49; H, 6.36; N, 8.82.

Boc-L-Val-L-Oxd-D-Ala-D-Oxd-L-Asp(O*c*Hex)-L-Oxd-OH **19**.
For the synthetic details, see above the preparation of **17**, starting from **18**. Yield 86%; M. p. = 184 °C; $[\alpha]_D^{20}$ = + 21.0 (c 0.1,CH_2Cl_2); IR (nujol): ν = 3394, 2364, 1790, 1693, 1461, 1374 cm^{-1}; ^{1}H NMR (CD_3OD): δ 0.86 (d, 3 H, *J* = 6.9 Hz Me Val), 1.06 (d, 3 H, *J* = 6.9 Hz, Me Val), 1.37-1.59 (m, 27 H, 9 H, *t*Bu + 9 H 3Me Oxd + 3 H Me Ala + 6 H *c*Hex), 1.78 (bs, 2 H, CH_2 *c*Hex), 1.87 (bs, 2 H, CH_2 *c*Hex), 2.28 (bs, 1 H, C*H*$(CH_3)_2$), 2.63 (m, 1 H, C*H*H Asp), 3.10 (dd, 1 H, *J* = 3.6, 16.8 Hz, CH*H* Asp), 4.48-4.65 (m, 4 H, 3CHN Oxd + CHO Oxd), 4.73-4.82 (m, 2 H, 2CHO Oxd), 5.35 (m, 1 H, CH_α Val), 5.51 (m, 1 H, CH_α Ala), 5.90 (m, 1 H, C*H*$_\alpha$ Asp), 6.72 (d, 1 H, *J* = 9 Hz, NH Val), 8.92 (d, 1 H, *J* = 6.6 Hz, NH Ala), 9.10 (d, 1 H, *J* = 8.1 Hz, NH Asp); ^{13}C NMR (CD_3OD): δ 15.7, 16.2, 18.9, 19.5, 20.1, 23.5, 25.3, 27.5, 30.3, 31.4, 35.7, 62.5, 62.7, 73.6, 75.2, 78.2, 78.6, 79.5, 152.6, 155.4, 169.0, 169.5, 170.3, 173.1. Anal. Calcd. for $C_{38}H_{54}N_6O_{17}$: C, 52.65; H, 6.28; N, 9.69. Found: C, 52.63; H, 6.31; N, 9.69.

Boc-L-Val-L-Oxd-D-Ala-D-Oxd-L-Asp(OcHex)-L-Oxd-Gly-D-Oxd-OBn **20**.
For the synthetic details, see above the preparation of **18**, starting from **15** and **19**. Yield = 40%; M. p. = 184 °C; $[\alpha]_D^{20}$ = + 34.0 (c 0.1,CH_2Cl_2); IR (CH_2Cl_2, 3 mM): ν = 3410, 2937, 1795, 1701, 1507, 1394 cm^{-1}; ^{1}H NMR (DMSO-d_6): δ 0.76 (d, 3 H, *J* = 6.4 Hz, Me Val); 0.90 (d, 3 H, *J* = 6.4 Hz, Me Val), 1.26 (d, 3 H, *J* = 6.8 Hz, Me Ala), 1.35 (m, 21 H, 9 H *t*Bu + 6 H 2Me Oxd + 6 H *c*Hex), 1.42 (d, 3 H, *J* = 6 Hz, Me Oxd), 1.47 (d, 3 H, *J* = 6 Hz, Me Oxd), 1.63 (bs, 2 H, CH_2 *c*Hex), 1.73 (bs, 2 H, CH_2 *c*Hex), 2.11 (m, 1 H, C*H*$(CH_3)_2$), 2.45 (m, 1 H, C*H*H Asp), 2.88 (m, 1 H, CH*H* Asp), 4.38-4.70 (m, 9 H, 4CHN Oxd + 3CHO Oxd + $CH_{2\alpha}$ Gly), 4.83 (m, 1 H, CHO Oxd), 5.13-5.24 (m, 3 H, OCH_2Ph + CH_α Val),5.40

(m,1 H, CH_α Ala), 5.70 (m, 1 H, CH_α Asp), 6.86 (d, 1 H, J = 7.6 Hz, NH Val), 8.80 (m, 1 H, NH Gly), 8.89 (d, 1 H, *J* = 8 Hz, NH Ala), 9.09 (d, 1 H, *J* = 7.6 Hz, NH Asp); ^{13}C NMR (DMSO-d_6): δ = 15.9, 17.7, 19.9, 20.9, 21.1, 23.7, 25.6, 28.9, 30.3, 31.6, 61.6, 62.4, 65.6, 67.9, 73.2, 74.8, 78.9, 79.7, 80.1, 128.7, 129.0, 129.2, 135.9, 152.9, 156.4, 168.0, 168.6, 169.2, 172.7, 173.4. Anal. Calcd. for $C_{52}H_{68}N_8O_{21}$: C, 54.73; H, 6.01; N, 9.82. Found: C, 54.72; H, 6.03; N, 9.80.

Boc-L-Val-L-Oxd-D-Ala-D-Oxd-L-Asp(OcHex)-L-Oxd-Gly-D-Oxd-OH **21**.
For the synthetic details, see above the preparation of **17**, starting from **20**. M. p. = 190 °C; $[\alpha]_D^{20}$ = + 27.0 (c 0.1,CH_2Cl_2); IR (nujol): ν = 3371, 1793, 1691, 1540, 1458, 1377 cm^{-1}; ^{1}H NMR (CD_3OD): δ 0.86 (d, 3 H, *J* = 6.9 Hz Me Val), 1.06 (d, 3 H, *J* = 6.9 Hz, Me Val), 1.32-1.61 (m, 27 H, 9 H *t*Bu + 12 H 4Me Oxd + 6 H *c*Hex), 1.78 (bs, 2 H, CH_2 *c*Hex), 1.85 (bs, 2 H, CH_2 *c*Hex), 2.23 (bs, 1 H, C*H*(CH_3)$_2$), 2.64 (m, 1 H, C*H*H Asp), 3.07 (m, 1 H, C*H*H Asp), 4.50-5.0 (m, 10 H, 4CHN Oxd + 4CHO Oxd + $CH_{2\alpha}$ Gly), 5.36 (m, 1 H, CH_α Val), 5.50 (m, 1 H, CH_α Ala), 5.85 (m, 1 H, CH_α Asp), 8.90 (d, 1 H, *J* = 5.7 Hz, NH Ala), 9.09 (d, 1 H, *J* = 6.9 Hz, NH Asp); ^{13}C NMR (CD_3OD): δ 15.7, 16.2, 18.8, 19.5, 19.6, 20.1, 23.4, 25.3, 27.5, 31.3, 35.7, 43.3, 49.6, 57.5, 61.9, 62.5, 62.7, 73.7, 75.0, 75.2, 75.6, 79.5, 152.5, 153.0, 168.8, 169.7, 170.3, 173.1. Anal. Calcd. for $C_{45}H_{62}N_8O_{21}$: C, 51.42; H, 5.95; N, 10.66. Found: C, 51.38; H, 5.92; N, 10.69.

Boc-L-Phe-D-Imz-OBn **23**.
DBU (0.127 mL, 0.85 mmol) was added to a stirred solution of Boc-L-Phe-D-Asn-OBn (0.2 g, 0.43 mmol) in THF (20 mL). The mixture was stirred for 10 min. Then, $PhI(OAc)_2$ (274 mg, 0.85 mmol) was added and the mixture was stirred at room temperature for 45 min. After this time, a few drops (<1 mL) of H_2O were added, and the mixture was stirred for another 15 min. The reaction mixture was gently concentrated. The resulting yellow liquid was dissolved in ethyl acetate and washed with H_2O, dried over Na_2SO_4, filtered, concentrated, and dried under a vacuum. The crude was purified by flash chromatography (cyclohexane/ethyl acetate 1:1 as eluant) and 1 was obtained pure in 65% yield. M. p. = 68 °C; $[\alpha]_D^{20}$ = +0.081 (c 1.0, CH_2Cl_2); IR (CH_2Cl_2, 10 mM): ν 3444, 1759, 1716, 1689 cm^{-1}; IR (1% in dry KBr): ν 3391, 1761, 1687 cm^{-1}; 1H NMR ($CDCl_3$, 300 MHz): δ 1.42 (s, 9H, *t*-Bu), 2.95 (dd, 1H, J = 7.5, 13.8 Hz, CHN-CHH-Ph), 3.2 (dd, 1H, J = 4.8, 13.5 Hz, CHN-CHH-Ph), 3.4 (dd, 1H, J = 3.0, 9.3 Hz, NCHH), 3.7 (t, 1H, J = 9.9 Hz, NCH), 4.8 (m, 1H, NCHH), 5.2-5.4 (m, 3H, OCH2Ph + Boc-NH), 5.85 (bs, 1H, NH), 5.95 (m, 1H, CHN-CHH-Ph), 7.2-7.4 (m, 10H, 2 × Ph); 13C NMR ($CDCl_3$, 75 MHz): δ 28.5, 39.9, 40.6, 54.1, 55.4, 68.0, 127.0, 128.6, 129.0, 129.9, 135.2, 136.6, 154.7, 155.0, 169.1, 172.7.

Boc-L-Phe-D-Oxd-(*S*)-β^3-hPhg-OBn **24**.
A solution of Boc-L-Phe-D-Oxd-OH (0.27 mmol, 0.10 g) and HBTU (0.3 mmol, 0.12 g) in dry acetonitrile (25 mL) was stirred under inert atmosphere for 10 min at room temperature. Then a mixture of H-(*S*)-β^3-hPhg-OBn·TFA (0.27 mmol, 0.10 g) and TEA (0.81 mmol, 0.12 mL) in dry acetonitrile (10 mL) was added at room temperature. The solution was stirred for 40 min under inert atmosphere, and then acetonitrile was removed under reduced pressure and replaced with ethyl acetate. The mixture was washed with brine, 1 N aqueous HCl (3 × 30 mL), and 5% aqueous $NaHCO_3$ (1 × 30 mL), dried over sodium sulfate, and concentrated in vacuo. The product was obtained pure after silica gel chromatography (cyclohexane/ethyl acetate 8:2 as eluant) in 80% yield. M. p. = 168 °C; $[\alpha]_D^{20}$ = +14.0 (c 1.0 in CH_2Cl_2); IR (CH_2Cl_2, 10 mM): ν 3437 (N-H), 3366 (N-H), 1789 (C=O), 1716 (C=O), 1696 (C=O) cm^{-1}; IR (1% in dry KBr): ν 3358 (N-H), 3318 (N-H), 1785 (C=O), 1763 (C=O), 1735 (C=O), 1719 (C=O), 1701 (C=O), 1687 (C=O) cm^{-1}; ^{1}H NMR ($CDCl_3$, 400 MHz; 25 °C): δ = 1.32 (d, 3H, 3J(H,H) = 7.2 Hz, Me-Oxd), 1.33 (s, 9H, *t*-Bu), 2.84-2.92 (m, 2H, CHH-Phe + CHH-hPhg), 2.97 (dd, 1H, 3J(H,H) = 7.2, 15.6 Hz, CHH-Phe), 3.12 (dd, 1H, 3J(H,H) = 6.0, 13.6 Hz,

CHH-hPhg), 4.32 (d, 1H, 3J(H,H) = 2.8 Hz, CHN-Oxd), 4.66 (dq, 1H, 3J(H,H) = 2.8, 7.2 Hz, CHO-Oxd), 5.03 (bs, 1H, NH-Boc), 5.05 (AB, 2H, 2J(H,H) = 12.0 Hz, OCH2Ph), 5.46 (dt, 1H, 3J(H,H) = 7.2, 7.2 Hz, CHN-Phe), 5.64-5.67 (m, 1H, CHN-hPhg), 7.21-7.38 ppm (m, 16H, NH-hPhg + 3 x Ph); ^{13}C NMR ($CDCl_3$, 100 MHz, 25 °C): δ = 21.1, 28.5, 40.7, 50.6, 54.1, 62.9, 66.8, 80.8, 126.8, 127.6, 128.0, 128.4, 128.5, 128.7, 129.0, 129.6, 151.83, 166.69 ppm; elemental analysis calcd. (%) for $C_{35}H_{39}N_3O_8$: C, 66.76; H, 6.24; N, 6.67; found: C 66.71, H 6.25, N 6.66.

Boc-L-Phe-D-Oxd-(*R*)-β^3-hPhg-OBn **25**.

A solution of Boc-L-Phe-D-Oxd-OH **22** (0.27 mmol, 0.10 g) and HBTU (0.3 mmol, 0.12 g) in dry acetonitrile (25 mL) was stirred under inert atmosphere for 10 min at room temperature. Then a mixture of H-(*R*)-β^3-hPhg-OBn·TFA (0.27 mmol, 0.10 g) and TEA (0.81 mmol, 0.12 mL) in dry acetonitrile (10 mL) was added at room temperature. The solution was stirred for 40 min under inert atmosphere, and then acetonitrile was removed under reduced pressure and replaced with ethyl acetate. The mixture was washed with brine, 1 N aqueous HCl (3 × 30 mL), and 5% aqueous $NaHCO_3$ (1 × 30 mL), dried over sodium sulfate, and concentrated in vacuo. The product was obtained pure after silica gel chromatography (cyclohexane/ethyl acetate 8:2 as eluant) in 81% yield. M. p. = 160 °C; $[\alpha]_D^{20}$ = +35.9 (c 1.0, CH_2Cl_2); IR (CH_2Cl_2, 10 mM): ν 3436 (N-H), 3350 (N-H), 1788 (C=O), 1716 (C=O), 1693 (C=O), 1679 (C=O) cm^{-1}; IR (1% in dry KBr): ν 3381 (N-H), 3323 (N-H), 1764 (C=O), 1742 (C=O), 1719 (C=O), 1701 (C=O), 1691 (C=O), 1684 (C=O) cm^{-1}; ^{1}H NMR ($CDCl_3$, 400 MHz): δ = 1.23 (s, 9H, *t*-Bu), 1.31 (d, 3H, 3J(H,H) = 6.8 Hz, Me-Oxd), 2.85-2.92 (m, 2H, CHH-Phe + CHH-hPhg), 2.99 (dd, 1H, 3J(H,H) = 8.4, 15.6 Hz, CHH-Phe), 3.15 (dd, 1H, 3J(H,H) = 6.0, 13.6 Hz, CHH-hPhg), 4.32 (d, 1H, 3J(H,H) = 4.0 Hz, CHN-Oxd), 4.672 (dq, 1H, 3J(H,H) = 4.0, 6.8 Hz, CHO-Oxd), 5.00 (d, 1H, 3J(H,H) = 4 Hz, NH-Boc), 5.07 (s, 2H, OCH2Ph), 5.46 (dt, 1H, 3J(H,H) = 6.0, 8.4 Hz, CHN-Phe), 5.67-5.5.75 (m, 1H, CHN-hPhg), 7.20-7.36 (m, 15H, 3 x Ph), 7.54 ppm (d, 1H, 3J(H,H) = 7.6 Hz, NH-hPhg); ^{13}C NMR ($CDCl_3$, 100 MHz): δ = 21.1, 28.4, 29.9, 31.1, 37.6, 40.7, 50.9, 53.9, 62.7, 66.8, 75.3, 81.0, 126.4, 127.6, 127.7, 128.4, 128.5, 128.7, 128.8, 129.1, 129.6, 135.4, 135.7, 135.8, 140.5, 151.9, 167.1, 170.5, 173.6 ppm; elemental analysis calcd. (%) for $C_{35}H_{39}N_3O_8$: C, 66.76; H, 6.24; N, 6.67; found: C 66.75, H 6.25, N 6.65.

Boc-L-Phe-L-Phe-D-Oxd-OBn **26**.

A solution of Boc-L-Phe-D-Oxd-OBn **22** (2 mmol, 0.96 g) and TFA (36 mmol, 2.78 mL) in dry dichloromethane (20 mL) was stirred at room temperature for 4 h, then the volatile compounds were removed under reduced pressure and the corresponding amine salt was obtained in quantitative yield without the need for further purification.

A solution of Boc-L-Phe-OH (1.38 g, 0.52 mmol) and HBTU (0.4 g, 1.04 mmol) in dry acetonitrile (22 mL) was stirred under a nitrogen atmosphere for 10 min at room temperature. Then, a mixture of the previously obtained amine salt (1.04 mmol) and TEA (3.2 mmol, 0.47 mL) in dry acetonitrile (15 mL) was added dropwise at room temperature. The solution was stirred for 40 min under a nitrogen atmosphere, then acetonitrile was removed under reduced pressure and replaced with ethyl acetate. The mixture was washed with brine, 1 n aqueous HCl (3 × 30 mL), and with 5 %(w/v) aqueous $NaHCO_3$ (1 × 30 mL), dried with sodium sulfate and concentrated in vacuo. The pure product was obtained after silica gel chromatography [CH_2Cl_2 100 % → CH_2Cl_2/ethyl acetate (80:20) as eluent] in 78 % (0.98 g) overall yield; m. p. 68 °C. $[\alpha]_D^{20}$ = +34 (c 1.0, CH_2Cl_2). IR (CH_2Cl_2, 3 mM): ν 3415, 1798, 1753, 1713, 1688 cm^{-1}. IR (1 % in dry KBr): ν 3327, 3307, 1794, 1746, 1714, 1686, 1658 cm^{-1}. ^{1}H NMR ($CDCl_3$, 400 MHz): *δ* = 1.52-1.56 (m, 12 H, Me + *t*Bu), 2.87-3.05 (m, 4 H, 2 × CHN-C*H*$_2$-Ph), 3.11 (dd, *J* = 5.2, 12.4 Hz, 1 H, C*H*N-CH$_2$-Ph), 4.20-4.35 (m, 2 H, C*H*N-Oxd + C*H*N-CH$_2$-Ph), 4.45-4.52 (m, 1 H, CHO-Oxd), 4.95 (br. s, 1 H, NH-Boc), 5.2, 2 H, *J* = 111 (AB system, 6 Hz, CH_2OBn), 5.80-6.03 (m, 1 H, NH-Boc), 6.42 (br. s, 1 H, NH-Phe), 7.05-7.36 (m, 15 H, 3 × Phe) ppm.

^{13}C NMR ($CDCl_3$, 100 MHz): δ = 20.4, 21.3, 28.5, 38.5, 38.6, 53.1, 55.8, 60.7, 62.0, 68.3, 70.7, 73.9, 126.7, 127.5, 128.6, 128.8, 128.9, 129.0, 129.6, 135.6, 167.5, 170.4, 170.6 ppm. $C_{35}H_{39}N_3O_8$ (629.3): calcd. C 67.76, H 6.24, N 6.67; found C 67.79, H 6.21, N 6.68.

Boc-L-Phe-L-Phe-D-Pro-OBn **27**.
For the synthesis, see Ref [82]

Boc-L-Phe-L-Phe-D-Pro-OBn **28**.
A solution of Boc-L-Phe-D-Pro-OBn **27** (2 mmol, 0.96 g) and TFA (36 mmol, 2.78 mL) in dry dichloromethane (20 mL) was stirred at room temperature for 4 h, then the volatile compounds were removed under reduced pressure and the corresponding amine salt was obtained in quantitative yield without the need for further purification.
A solution of Boc-L-Phe-OH (1.38 g, 0.52 mmol) and HBTU (0.4 g, 1.04 mmol) in dry acetonitrile (22 mL) was stirred under a nitrogen atmosphere for 10 min at room temperature. Then, a mixture of the previously obtained amine salt (1.04 mmol) and TEA (3.2 mmol, 0.47 mL) in dry acetonitrile (15 mL) was added dropwise at room temperature. The solution was stirred for 40 min under a nitrogen atmosphere, then acetonitrile was removed under reduced pressure and replaced with ethyl acetate. The mixture was washed with brine, 1 N aqueous HCl (3 × 30 mL), and with 5 %(w/v) aqueous $NaHCO_3$ (1 × 30 mL), dried with sodium sulfate and concentrated in vacuo. The pure product was obtained after silica gel chromatography [CH_2Cl_2 100 % → CH_2Cl_2/ethyl acetate (80:20) as eluent] in yield 79 %; m. p. 55 °C. $[\alpha]_D^{20}$ = +35 (c 1.0, $CHCl_3$). IR (CH_2Cl_2, 3 mM): ν 3418, 1742, 1711, 1673, 1645 cm^{-1}. IR (1 % in dry KBr): ν 3419, 3285, 1747, 1712, 1633 cm^{-1}. ^{1}H NMR ($CDCl_3$, 400 MHz): δ = 1.41 (s, 9 H, *t*Bu), 1.77-1.95 (m, 4 H, $NCH_2CH_2CH_2CH$-CO), 2.80-3.18 (m, 6 H, $NCH_2CH_2CH_2CH$-CO + 2 × CH-CH_2-Ph), 4.31-4.43 (m, 2 H, 2 × C*H*-CH_2-Ph), 4.83-5.00 (m, 2 H, $NCH_2CH_2CH_2CH$-CO + NH), 6.72 and 6.96 (d, *J* = 8 Hz, 1 H, NH, mixture of conformers), 7.18-7.38 (m, 15 H, 3 × Ph) ppm. ^{13}C NMR ($CDCl_3$, 100 MHz, mixture of conformers): δ = 22.4 and 24.3 , 26.9 and 28.3, 28.9 and 31.0, 37.5 and 38.3, 39.7, 46.6 and 46.8, 51.9 and 52.4, 55.4, 58.8 and 59.5, 66.7 and 67.3, 79.9, 126.7, 126.8, 127.0, 128.1, 128.2, 128.4, 128.5, 128.7, 129.2, 129.5, 135.2 and 135.6, 136.2 and 136.6, 155.2, 169.5, 170.5, 171.4, 172.0 ppm. $C_{35}H_{41}N_3O_6$ (599.3): calcd. C 70.10, H 6.89, N 7.01; found C 70.05, H 6.85, N 6.99.

$CH_2(C_3H_6CO$-L-Phe-D-Oxd-OBn$)_2$ **29**.
A solution of Boc-L-Phe-D-Oxd-OBn (2 mmol, 0.96 g) and TFA (36 mmol, 2.78 mL) in dry dichloromethane (20 mL) was stirred at room temperature for 4 h, then the volatile compounds were removed under reduced pressure and the corresponding amine salt was obtained pure in quantitative yield without further purification.
A solution of azelaic acid (0.98 g, 0.52 mmol) and HBTU (0.4 g, 1.04 mmol) in dry acetonitrile (22 mL) was stirred under nitrogen atmosphere for 10 min at room temperature. Then, a mixture of the previously obtained amine salt (1.04 mmol) and TEA (3.2 mmol, 0.47 mL) in dry acetonitrile (15 mL) was added dropwise at room temperature. The solution was stirred for 40 min under a nitrogen atmosphere then acetonitrile was removed under reduced pressure and replaced with ethyl acetate. The mixture was washed with brine, 1 N aqueous HCl (3 × 30 mL), and 5 % (w/v) aqueous $NaHCO_3$ (1 × 30 mL), dried with sodium sulfate and concentrated in vacuo. The pure product was obtained after silica gel chromatography [CH_2Cl_2 100 % → CH_2Cl_2/ethyl acetate (80:20) as eluent] in 64 % (1.17 g) overall yield; m. p. 207 °C. $[\alpha]_D^{20}$ = 45.0 (c 0.1, $CHCl_3$). IR (CH_2Cl_2,

[82] Becerril, J.; Burguete, M. I.; Escuder, B.; Galindo, F.; Gavara, R.; Miravet, J. F.; Luis, S. V.; Peris, G. "*Self-assembly of small peptidomimetic cyclophanes*" Chem. Eur. J. **2004**, *10*, 3879-3890.

3 mM): v 3428, 1789, 1754, 1707, 1672 cm^{-1}. IR (1 % in dry KBr): v 3309, 1793, 1765, 1736, 1708, 1650 cm^{-1}. ^{1}H NMR (DMSO-d_6, 300 MHz): δ = 0.95-1.18 [m, 10 H, $CH_2(CH_2)_5CH_2$], 1.20-1.40 [m, 4 H, $CH_2(CH_2)_5CH_2$], 1.50 (d, *J* = 6.3 Hz, 6 H, OCHCH_3), 2.00 (m, 4 H, CH_2CO), 2.70 (dd, *J* = 10.8, 13.5 Hz, 2 H, CHN-CHH-Ph), 3.10-3.20 (dd, *J* = 3.3, 13.5 Hz, 2 H, CHN-CHH-Ph), 4.65 (d, *J* = 4.2 Hz, 2 H, CHN), 4.80-4.90 (m, 2 H, OCH), 5.18 (d, *J* = 12.3 Hz, 2 H, OCHHPh), 5.25 (d, *J* = 12.6 Hz, 2 H, OCHHPh), 5.8 (m, 2 H, CHN-CH_2Ph), 7.20-7.40 (m, 20 H, 4 × Ph), 8.25 (d, *J* = 8.7 Hz, 2 H, NH) ppm. ^{13}C NMR (DMSO-d_6, 75 MHz): δ = 14.8, 15.3, 21.1, 25.9, 29.0, 35.7, 37.7, 38.5, 51.0, 53.1, 55.4, 62.0, 67.7, 74.3, 127.2, 128.6, 128.8, 128.9, 129.2, 129.8, 136.0, 138.0, 152.5, 168.6, 172.7, 173.2 ppm. $C_{51}H_{56}N_4O_{12}$ (916.4): calcd. C 66.80, H 6.16, N 6.11; found C 66.75, H 6.19, N 6.07.

$CH_2(C_3H_6CO$-L-Phe-D-Oxd-OH$)_2$ **30**.
Compound **29** (1 mmol, 0.92 g) was dissolved in MeOH (35 mL) under nitrogen. Pd/C (50 mg, 10 % w/w) was added under nitrogen. Vacuum was created inside the flask by using the vacuum line. The flask was then filled with hydrogen by using a balloon (1 atm). The solution was stirred for 2 h under a hydrogen atmosphere. The pure product was obtained in quantitative yield (0.73 g) after the solution was filtered through a Celite pad using ethyl acetate and concentrated in vacuo; m. p. 201 °C. $[\alpha]_D^{20}$ = -36.0 (c 1.2, MeOH). ^{1}H NMR (CD_3OD, 400 MHz): δ = 1.06-1.47 [m, 10 H, $CH_2(CH_2)_5CH_2$], 1.58 (d, *J* = 6.4 Hz, 6 H, OCHCH_3), 2.03-2.15 [m, 4 H, $CH_2(CH_2)_5CH_2$], 2.91 (dd, *J* = 9.6, 13.6 Hz, 2 H, CHN-CHHPh), 3.14 (dd, *J* = 5.2, 13.6 Hz, 2 H, CHN-CHHPh), 4.00 (d, *J* = 5.6 Hz, 2 H, CHN-CHHPh), 4.62-4.87 (m, 2 H, OCH), 5.80 (m, 2 H, CHN-CH_2Ph), 7.20-7.40 (m, 20 H, 4 × Ph) ppm. ^{13}C NMR (CD_3OD, 100 MHz): δ = 19.8, 25.3, 28.3, 28.5, 35.2, 37.6, 52.7, 61.7, 74.4, 126.5, 128.0, 129.1, 136.6, 151.1, 153.3, 169.7, 172.7, 174.4 ppm. $C_{37}H_{44}N_4O_{12}$ (736.3): calcd. C 60.32, H 6.02, N 7.60; found C 60.36, H 6.04, N 7.55.

Boc-L-Phe-D-Oxd-(*R*)-αMe-Phg-OBn **31a**.
A solution of Boc-L-Phe-D-Oxd-OH (0.27 mmol, 0.10 g) and HBTU (0.3 mmol, 0.12 g) in dry acetonitrile (25 mL) was stirred under inert atmosphere for 10 min at room temperature. Then a mixture of CF_3COO^- $^+H_3$N-(*R*)-αMe-Phg-OBn (0.27 mmol, 0.10 g) and TEA (0.81 mmol, 0.12 mL) in dry acetonitrile (10 mL) was added at room temperature. The solution was stirred for 40 min under inert atmosphere, then acetonitrile was removed under reduced pressure and replaced with ethyl acetate. The mixture was washed with brine, 1 N aqueous HCl (3 9 30 mL) and with 5% aqueous NaHCO3 (1 9 30 mL), dried over sodium sulphate and concentrated in vacuo. The product was obtained pure after silica gel chromatography (cyclohexane/ethyl acetate 8:2 as eluant) in 80 % yield. M. p. = 128 °C; $[\alpha]_D^{20}$ = 88.9 (c 1.1, CH_2Cl_2); IR (CH_2Cl_2, 3 mM): v 3,437, 3,389, 3,336, 1,788, 1,737, 1,701, 1,678 cm^{-1}; IR (1% in dry KBr): v 3,390, 3,324, 1,783, 1,748, 1,716, 1,689 cm^{-1}; ^{1}H NMR (400 MHz, $CDCl_3$): δ 1.25 (d, 6H, J = 6.3 Hz), 1.55 (s, 9H), 1.97 (s, 3H), 2.84 (dd, 1H, J = 8.0, 13.2 Hz), 3.07 (dd, 1H, J = 6.0, 13.2 Hz), 4.29 (d, 1H J = 3.6 Hz), 4.43 (m, 1H), 4.91 (d, 1H, J = 5.2 Hz), 5.05 (AB, 2H, J = 12.4 Hz), 5.69 (m, 1H), 7.12-7.16 (m, 2H), 7.22-7.34 (m, 11H), 7.44-7.49 (m, 2H), 7.61 (s, 1H); ^{13}C NMR (75 MHz, $CDCl_3$): δ 21.4, 21.9, 28.4, 30.2, 38.0, 53.9, 62.7, 63.6, 67.8, 75.0, 80.1, 126.3, 127.7, 128.2, 128.5, 128.7, 128.9, 129.1, 129.7, 135.5, 136.2, 151.9, 173.3. Anal. calcd. for $C_{35}H_{39}N_3O_8$: C, 66.76; H, 6.24; N, 6.67; Found: C, 66.81; H, 6.20; N, 6.64. 616 N.

Boc-L-Phe-D-Oxd-(*S*)-αMe-Phg-OBn **31b**.
A solution of Boc-L-Phe-D-Oxd-OH (0.27 mmol, 0.10 g) and HBTU (0.3 mmol, 0.12 g) in dry acetonitrile (25 mL) was stirred under inert atmosphere for 10 min at room temperature. Then a mixture of CF_3COO^- $^+H_3$N-(*S*)-aMe-Phg-OBn (0.27 mmol, 0.10 g) and TEA (0.81 mmol, 0.12 mL) in dry acetonitrile (10 mL) was added at room temperature. The solution was stirred for 40 min under inert atmosphere, then acetonitrile was removed under reduced pressure and replaced

with ethyl acetate. The mixture was washed with brine, 1 N aqueous HCl (3 9 30 mL) and with 5% aqueous NaHCO3 (1 9 30 mL), dried over sodium sulphate and concentrated in vacuo. The product was obtained pure after silica gel chromatography (cyclohexane/ethyl acetate 8:2 as eluant) in 80 % yield. M. p. = 196 °C; $[\alpha]_D^{20}$ = 17.3 (c 0.25, CH_2Cl_2); IR (CH_2Cl_2, 3 mM): ν 3,434, 3,385, 1,789, 1,737, 1,720, 1,703 cm^{-1}; IR (1% in dry KBr): ν 3,389, 3,309, 1,768, 1,742, 1,718, 1,701, 1,687 cm^{-1}; NMR (400 MHz, $CDCl_3$): δ 1.26 (d, 6H, J = 6.6 Hz), 1.55 (s, 9H), 1.98 (s, 3H), 2.89 (m, 1H), 3.11 (m, 1H), 4.30 (m, 1H), 4.56 (m, 1H), 5.12 (AB, 2H, J = 12.4 Hz), 5.16 (bs, 1H), 5.71 (q, 1H, J = 6.8 Hz), 7.16-7.42 (m, 16H); ^{13}C NMR (75 MHz, $CDCl_3$): δ 21. 3, 28.5, 30.2, 54.3, 63.2, 68.0, 74.5, 126.4, 127.6, 128.3, 128.6, 128.8, 129.0, 129.8, 136.4, 151.8, 166.4, 173.8, 183.2. Anal. calcd. for $C_{35}H_{39}N_3O_8$: C, 66.76; H, 6.24; N, 6.67; Found: C, 66.73; H, 6.19; N, 6.70.

General method for the preparation of compounds **32a-d**.
A solution of fully protected tripeptide (2 mmol) and TFA (36 mmol, 2.78 mL) in dry methylene chloride (20 mL) was stirred at room temperature for 4 h, then the volatiles were removed under reduced pressure and the corresponding amine salt was obtained pure in quantitative yield without further purification.
A solution of azelaic acid (0.98 g, 0.52 mmol) and HBTU (0.4 mg, 1.04 mmol) in dry acetonitrile (22 mL) was stirred under inert atmosphere for 10 min at room temperature. Then a mixture of the previously obtained amine salt (1.04 mmol) and TEA (3.2 mmol, 0.47 mL) in dry acetonitrile (15 mL) was added dropwise at room temperature. The solution was stirred for 40 min under inert atmosphere, then acetonitrile was removed under reduced pressure and replaced with ethyl acetate. The mixture was washed with brine, 1 N aqueous HCl (3 × 30 mL) and with 5% aqueous $NaHCO_3$ (1 × 30 mL), dried over sodium sulphate and concentrated in vacuo. The product was obtained pure after silica gel chromatography (DCM 100% → DCM/acetato di etile 80:20 as eluant).

$CH_2(C_3H_6CO$-L-Phe-L-Oxd-(*R*)-αMe-Phg-$OBn)_2$ **32a**.
M. p. = 76 °C; $[\alpha]_D^{20}$ = +22.0 (c 1.0, $CHCl_3$); IR (CH_2Cl_2, 3 mM): ν 3,343, 3,374, 3,366, 3,335, 1,787, 1,771, 1,738, 1,732, 1,683, 1,674 cm^{-1}; IR (1% in dry KBr): ν 3,392, 3,370, 1,734, 1,701, 1,653 cm^{-1}; NMR (400 MHz, $CDCl_3$): δ 0.98-1.44 (m, 16H), 1.88-2.05 (m, 4H), 1.96 (s, 6H), 2.92 (m, 2H), 3.17 (m, 2H), 4.24 (m, 2H), 4.41 (m, 2H), 5.12 (AB, 4H, J = 12.4 Hz), 5.28 (m, 2H), 5.78 (bs, 1H), 6.10 (bs, 1H), 7.05-7.37 (m, 29H), 7.44 (m, 2H), 7.81 (m, 1H); ^{13}C NMR (50 MHz, $CDCl_3$): δ 21.0, 24.6, 24.7, 28.3, 28.4, 28.5, 35.3, 36.8, 53.0, 62.4, 62.7, 67.5, 74.4, 126.3, 127.3, 127.4, 128.1, 128.2, 128.4, 128.7, 129.3, 135.2, 139.4, 151.6, 166.6, 171.7, 173.0, 173.6. Anal. calcd. for $C_{69}H_{74}N_6O_{14}$: C, 68.41; H, 6.16; N, 6.94. Found: C, 68.37; H, 6.19; N, 6.99.

$CH_2(C_3H_6CO$-L-Phe-D-Oxd-(*S*)-αMe-Phg-$OBn)_2$ **32b**.
M. p. = 150 °C; $[\alpha]_D^{20}$ = + 92.0 (c 1, $CHCl_3$); IR (CH_2Cl_2, 3 mM): ν 3,433, 3,385, 3,323, 3,304, 1,787, 1,737, 1,714, 1,677 cm^{-1}; IR (1% in KBr): ν 3,422, 3,327, 3,284, 1,781, 1,749, 1,706, 1,684, 1653, 1642 cm^{-1}; ^{1}H NMR (400 MHz, $CDCl_3$): δ 0.88-1.41 (m, 16H), 1.65-2.02 (m, 4H), 1.96 (s, 6H), 2.94 (m, 2H), 3.18 (m, 2H), 4.24 (m, 2H), 4.42 (m, 2H), 5.08 (AB, 4H, J = 12.0 Hz), 5.28 (m, 2H), 5.71 (bs, 2H), 6.05 (bs, 2H), 7.05-7.35 (m, 30H), 7.40 (bs, 1H), 7.78 (s, 1H); ^{13}C NMR (100 MHz, $CDCl_3$): δ 14.1, 20.8, 21.0, 21.8, 24.5, 28.5, 29.6, 35.2, 36.7, 53.0, 53.4, 60.3, 62.2, 63.0, 67.3, 74.6, 81.4, 126.1, 127.3, 127.9, 128.0, 128.1, 128.3, 128.7, 129.2, 135.4, 151.6, 166.9, 171.6, 173.4. Anal. calcd. for $C_{69}H_{74}N_6O_{14}$: C, 68.41; H, 6.16; N, 6.94. Found: C, 68.45; H, 6.20; N, 6.91.

$CH_2(C_3H_6CO$-L-Phe-D-Oxd-(*S*)-β^3-hPhg-$OBn)_2$ **32c**.

M. p. = 129 °C; $[\alpha]_D^{20}$ = + 32.0 (c 1.0, CH_2Cl_2); IR (CH_2Cl_2, 3 mM): ν 3,435, 3,319, 1,788, 1,735, 1,675, 1,655 cm^{-1}; IR (1% in KBr): ν 3,411, 3,309, 3,088, 1,772, 1,732, 1,715, 1,650, 1,556, 1,531 cm^{-1}; ^1H NMR (400 MHz, $CDCl_3$): δ 1.08-1.52 (m, 16H), 1.92-2.15 (m, 4H), 2.81-2.99 (m, 6H), 3.18 (m, 2H), 4.12 (m, 2H), 4.39 (m, 1H), 4.58 (m, 1H), 5.05 (m, 2H), 5.13 (m 1H), 5.15 (s, 2H), 5.52 (m, 1H), 5.75 (m, 1H), 6.03 (m, 1H), 7.15-7.38 (m, 30H), 7.41 (d, 1H, J = 6 Hz), 7.85 (d, 1H, J = 6.4 Hz); ^{13}C NMR (50 MHz, $CDCl_3$): δ 21.0, 24.8, 28.5, 29.7, 35.3, 36.4, 40.8, 50.3, 53.2, 56.9, 62.5, 66.5, 75.2, 126.8, 127.5, 127.6, 128.2, 128.4, 128.7, 128.9, 129.2, 135.0, 135.7, 140.6, 151.0, 166.4, 170.1, 175.5, 174.3. Anal. calcd. for $C_{69}H_{74}N_6O_{14}$: C, 68.41; H, 6.16; N, 6.94. Found: C, 68.44; H, 6.17; N, 6.92.

$CH_2(C_3H_6CO$-L-Phe-D-Oxd-(*R*)-β^3-hPhg-OBn$)_2$ **32d**.
M. p. = 179 °C; $[\alpha]_D^{20}$ = + 44.0 (c 1.1, $CHCl_3$); IR (CH_2Cl_2, 3 mM): ν 3,433, 3,323, 1,785, 1,735, 1,719, 1,672, 1,658 cm^{-1}; IR (1% in dry KBr): ν 3,310, 3,298, 1,773, 1,734, 1,718, 1,653 cm^{-1}; ^1H NMR (400 MHz, $CDCl_3$): δ 1.09-1.58 (m, 16H), 1.85-2.05 (m, 4H), 2.85-3.21 (m, 8H), 4.11 (m, 2H), 4.39 (m, 1H), 4.62 (m, 1H), 5.05 (m, 2H), 5.13 (m 1H), 5.17 (s, 2H), 5.42 (m, 1H), 5.65 (m, 1H), 6.12 (m, 1H), 7.05-7.41 (m, 31H), 7.96 (m, 1H); ^{13}C NMR (50 MHz, $CDCl_3$): δ 20.8, 24.7, 28.3, 35.2, 36.5, 40.5, 41.1, 50.6, 53.3, 62.5, 66.5, 75.3, 82.1, 126.4, 127.4, 128.1, 128.5, 128.8, 129.2, 135.1, 135.6, 140.6, 143.5, 151.7, 167.1, 170.5, 172.9, 174.3. Anal. calcd. for $C_{69}H_{74}N_6O_{14}$: C, 68.41; H, 6.16; N, 6.94. Found: C, 68.47; H, 6.19; N, 6.91.

General method for the preparation of compounds **33a-d**.
Compound **32a-d** (1 mmol) was dissolved in MeOH (35 mL) under nitrogen. C/Pd (50 mg, 10% w/w) was added under nitrogen. A vacuum was created inside the flask using the vacuum line. The flask was then filled with hydrogen using a balloon (1 atm). The solution was stirred for 4 h under a hydrogen atmosphere. The product was obtained pure after filtration through a Celite pad using ethyl acetate and concentration in vacuo.

$CH_2(C_3H_6CO$-L-Phe-D-Oxd-(*R*)-αMe-Phg-OH$)_2$ **33a**.
M. p. = 98 °C; $[\alpha]_D^{20}$ = +52.0 (c 0.6, MeOH); ^1H NMR (CD_3OD, 400 MHz): δ 0.90-1.61 (m, 16H), 1.92-2.10 (m, 4H), 1.97 (s, 6H), 2.92 (m, 2H), 3.16 (m, 2H), 3.60-3.95 (m, 2H),4.42-4.60 (m, 4H), 5.95 (m, 2H), 7.05-7.60 (m, 20H); ^{13}C NMR (CD_3OD, 100 MHz): δ 19.4, 19.7, 21.3, 22.3, 25.3, 28.4, 28.6, 30.0, 35.1, 36.9, 52.8, 53.7, 61.7, 62.9, 74.6, 77.0, 125.7, 125.9, 126.5, 127.0, 127.1, 127.7, 127.8, 128.0, 128.7, 129.1, 136.5, 136.8, 152.3, 167.5, 169.5, 172.3, 174.8. Anal. calcd. for $C_{55}H_{62}N_6O_{14}$: C, 64.07; H, 6.06; N, 8.15. Found: C, 64.11; H, 6.01; N, 8.12.

$CH_2(C_3H_6CO$-L-Phe-D-Oxd-(*R*)-αMe-Phg-OH$)_2$ **33b**.
M. p. = 115 °C; $[\alpha]_D^{20}$ = -4.5 (c 1.2, MeOH); ^1H NMR (CD_3OD, 400 MHz): δ 90-1.70 (m, 16H), 1.85 (s, 6H), 1.90-2.25 (m, 4H), 2.88 (m, 2H), 3.95 (m, 1H), 4.20 (m, 1H), 4.48-4.65 (m, 4H), 5.98 (m, 2H), 7.11-7.58 (m, 20H); ^{13}C NMR (CD_3OD, 100 MHz): δ 19.4, 19.7, 22.0, 25.4, 28.4, 28.6, 29.3, 35.2, 37.4, 52.8, 62.6, 74.4, 125.9, 126.1, 126.2, 127.2, 127.9, 128.0, 128.2, 128.7, 129.1, 136.6, 140.6, 152.4, 167.7, 168.0, 172.2, 174.4. Anal. calcd. for $C_{55}H_{62}N_6O_{14}$: C, 64.07; H, 6.06; N, 8.15. Found: C, 64.11; H, 6.10; N, 8.12.

$CH_2(C_3H_6CO$-L-Phe-D-Oxd-(*S*)-β^3-hPhg-OH$)_2$ **33c**.
M.p. = 117 °C; $[\alpha]_D^{20}$ = -31.7 (c 1.3, MeOH); ^1H NMR (CD_3OD, 400 MHz): δ 1.05-1.59 (m, 16H), 2.03-2.25 (m, 4H), 2.71-2.94 (m, 4H), 3.10-3.35 (m, 4H), 4.41 (M, 2H), 4.51-4.78 (m, 4H), 5.38 (m, 2H), 5.98 (m, 2H), 7.05-7.43 (m, 20H); ^{13}C NMR (CD_3OD, 100 MHz): δ 19.6, 25.5, 28.7, 35.3, 37.6, 40.7, 50.4, 53.0, 60.8, 63.1, 65.9, 75.2, 126.4, 126.8, 127.3, 128.2, 128.4, 129.4, 136.7, 143.6, 160.3, 174.8. Anal. calcd. for $C_{55}H_{62}N_6O_{14}$: C, 64.07; H, 6.06; N, 8.15. Found: C, 64.00; H, 6.04; N, 8.19.

$CH_2(C_3H_6CO$-L-Phe-D-Oxd-(*R*)-β^3-hPhg-$OH)_2$ **33d**.
M. p. = 140 °C; $[\alpha]_D^{20}$ = +29.0 (c 1.0, MeOH); ^{1}H NMR (CD_3OD, 400 MHz): δ 0.82-1.59 (m, 16H), 2.03-2.35 (m, 4H), 2.61-2.98 (m, 4H), 3.15-3.40 (m, 4H), 4.41 (M, 2H), 4.48-4.90 (m, 4H), 5.38 (m, 2H), 5.95 (m, 2H), 7.05-7.43 (m, 20H); ^{13}C NMR (CD_3OD, 100 MHz): δ 19.7, 20.0, 25.4, 28.3, 28.4, 29.1, 35.4, 37.2, 40.3, 46.5, 48.1, 50.7, 63.1, 75.6, 126.1, 128.3, 128.4, 137.8, 142.0, 153.6, 168.2, 172.3, 173.0, 174.4. Anal. calcd. for $C_{55}H_{62}N_6O_{14}$: C, 64.07; H, 6.06; N, 8.15. Found: C, 64.15; H, 6.04; N, 8.14.

$CH_2(C_3H_6CO$-L-Phe-L-Phe-D-Oxd-$OBn)_2$ **34a**.
A solution of Boc-L-Phe-L-Phe-D-Oxd-OBn (2 mmol) and TFA (36 mmol, 2.78 mL) in dry dichloromethane (20 mL) was stirred at room temperature for 4 h, then the volatile compounds were removed under reduced pressure and the corresponding amine salt was obtained pure in quantitative yield without further purification.
A solution of azelaic acid (0.98 g, 0.52 mmol) and HBTU (0.4 g, 1.04 mmol) in dry acetonitrile (22 mL) was stirred under nitrogen atmosphere for 10 min at room temperature. Then, a mixture of the previously obtained amine salt (1.04 mmol) and TEA (3.2 mmol, 0.47 mL) in dry acetonitrile (15 mL) was added dropwise at room temperature. The solution was stirred for 40 min under a nitrogen atmosphere then acetonitrile was removed under reduced pressure and replaced with ethyl acetate. The mixture was washed with brine, 1 N aqueous HCl (3 × 30 mL), and 5 % (w/v) aqueous $NaHCO_3$ (1 × 30 mL), dried with sodium sulfate and concentrated in vacuo. The pure product was obtained after silica gel chromatography [CH_2Cl_2 100 % → CH_2Cl_2/ethyl acetate (80:20) as eluent] in 57 %; m. p. 175 °C. $[\alpha]_D^{20}$ = +19 (c 0.9, $CHCl_3$). IR (CH_2Cl_2, 3 mM): ν 3440, 3358, 3309, 1773, 1748, 1716, 1655 cm^{-1}. IR (1 % in dry KBr): ν 3297, 1644, 1795, 1740, 1710 cm^{-1}. ^{1}H NMR ($CDCl_3$, 400 MHz): *δ* = 1.16-1.21 [m, 10 H, $CH_2(CH_2)_5CH_2$], 1.48 (d, *J* = 6.4 Hz, 6 H, 2 × CH_3Oxd), 2.10-2.18 [m, 4 H, $CH_2(CH_2)_5CH_2$], 2.52-3.04 (m, 8 H, 4 × CHN-CH_2-Ph), 3.93 (d, *J* = 4.8 Hz, 1 H, CHN-Oxd), 4.40 (m, 1 H, CHO-Oxd), 4.46 (m, 1 H, CHN-Oxd), 4.67 (m, 1 H, CHO-Oxd), 5.15 (m, 4 H, 2 × CH_2OBn), 5.32 (br. s, 2 H, 2 × NH), 5.92 (br. s, 1 H, NH), 7.08-7.36 (m, 30 H, 6 × Phe) ppm. ^{13}C NMR ($CDCl_3$, 100 MHz, mixture of conformers): *δ* = 21.0, 21.2, 24.6, 25.3, 25.4, 28.6, 28.8, 29.6, 30.9, 33.9, 36.2, 36.3, 37.8, 38.0, 38.3, 38.6, 52.9, 53.0, 54.0, 54.2, 61.7, 61.8, 67.3, 68.0, 73.7, 126.9, 128.2, 128.5, 128.7, 129.4, 130.0, 134.6, 135.3, 136.3, 136.4, 150.3, 151.2, 167.3, 170.4, 170.5, 170.7, 170.8, 171.3, 171.8, 177.6, 177.7, 177.8 ppm. $C_{69}H_{74}N_6O_{14}$ (1210.5): calcd. C 68.41, H 6.16, N 6.94; found C 68.38, H 6.18, N 6.94.

$CH_2(C_3H_6CO$-L-Phe-L-Phe-D-Oxd-$OH)_2$ **34b**.
Compound **33a** (1 mmol, 0.92 g) was dissolved in MeOH (35 mL) under nitrogen. Pd/C (50 mg, 10 % w/w) was added under nitrogen. Vacuum was created inside the flask by using the vacuum line. The flask was then filled with hydrogen by using a balloon (1 atm). The solution was stirred for 2 h under a hydrogen atmosphere. The pure product was obtained in quantitative yield (0.73 g) after the solution was filtered through a Celite pad using ethyl acetate and concentrated in vacuo m.p. 52 °C. $[\alpha]_D^{20}$ = +2 (*c* 0.49, MeOH). ^{1}H NMR (CD_3OD, 400 MHz): *δ* = 1.14-1.25 [m, 10 H, $CH_2(CH_2)_5CH_2$], 1.43-1.57 (m, 6 H, 2 × CH_3Oxd), 2.12-2.25 [m, 4 H, $CH_2(CH_2)_5CH_2$], 2.71-2.88 (m, 8 H, 4 × CHN-CH_2-Ph), 3.06-3.25 (m, 2 H, 2 × CHN-CH_2-Ph), 4.29-4.65 (m, 4 H, 2 × CHO-Oxd + 2 × CHN-Oxd), 5.50-5.62 (m, 2 H, 2 × CHN-CH_2-Ph), 6.98-7.33 (m, 20 H, 6 × Phe) ppm. ^{13}C NMR (CD_3OD, 100 MHz): *δ* = 14.0, 19.8, 24.6, 25.3, 28.6, 33.5, 35.3, 37.0, 37.3, 37.4, 52.9, 53.4, 54.0, 65.5, 74.6, 126.2, 126.3, 126.5, 128.0, 128.5, 128.9, 129.2, 129.8, 136.3, 137.0, 137.1, 171.6, 171.8, 173.4, 174.5, 174.7, 176.2 ppm. $C_{55}H_{62}N_6O_{14}$ (1030.4): calcd. C 64.07, H 6.06, N 8.15; found C 64.03, H 6.05, N 8.17.

$CH_2(C_3H_6CO$-L-Phe-D-Oxd-L-Lys(Dansyl)$OH)_2$ **35**.
As described in [23], compound $CH_2[C_3H_6CO$-L-Phe-D-Oxd-L-Lys(Dansyl)-$OBn]_2$ (0.06 mmol, 0.1 g) was dissolved in MeOH (20 mL) under nitrogen. C/Pd (20 mg) was added under nitrogen. A vacuum was created inside the flask using the vacuum line. The flask was then filled with hydrogen using a balloon (1 atm). The solution was stirred for 5 hours under a hydrogen atmosphere. The product was obtained pure in quantitative yield after filtration through a celite pad using MeOH and concentration *in vacuo*. M. p. = 125-126 °C; $[\alpha]_D^{20}$ = + 22.7 (c 0.3, MeOH); ^{1}H NMR (CD_3OD, 400 MHz): δ 0.86-1.66 (28H, m, $COCH_2(CH_2)_5$ + 2 x $CH(CH_2)_3CH_2NH$ + 2 x $OCHCH_3$), 1.90-2.08 (4H, m, 2 x $COCH_2$), 2.62-2.81 (18H, m, 2 x CHN-CHH-Ph + 2 x CH_2-NH-SO_2 + 2 x $N(CH_3)_2$), 3.06-3.15 (2H, m, 2 x CHN-CH*H*-Ph), 4.08-4.20 (2H, m, 2 x CH(Lys), 4.27(2H, d, *J* = 5.2 Hz, 2 x CHNOxd), 4.45- 4.55 (2H, m, 2 x CHO-Oxd), 5.72-5.82 (2H, m, 2 x CH(Phe), 7.04- 7.26 (14H, m, 2 x Ph + 2 x H-6^1 + 2 x H-3^1), 7.42-7.52 (4H, m, 2 x H-7^1 + 2 x H-4^1), 8.04-8.12 (2H, m, 2 x NH(Phe)), 8.06-8.27 (4H, m, 2 x H-2^1 + 2 x H-8^1), 8.41-8.49 (2H, m, 2 x $NHSO_2$); ^{13}C NMR (CD_3OD, 100 MHz): δ 21.8, 24.7, 27.6, 30.6, 30.9, 32.5, 37.4, 39.3, 39.7, 44.5, 46.7, 55.4, 65.5, 77.3, 117.3, 121.4, 125.2, 128.9, 130.0, 130.3, 131.0, 131.3, 131.8, 137.9, 138.8, 154.0, 154.5, 171.1, 174.8, 177.0. Anal. Calcd. for $C_{73}H_{90}N_{10}O_{18}S_2$: C, 60.07; H, 6.21; N, 9.60. Found: C, 60.03; H, 6.19; N, 9.57.

Dansylamide **36** may be purchased by Sigma-Aldrich.

Dansylpyrrolidine **37**.
A solution of dansyl chloride (1.11 mmol, 0.3 g) and pyrrolidine (0.55 mmol, 0.5 mL) in dry dichloromethane (20 mL) was stirred under nitrogen atmosphere for 2 hours at room temperature. The mixture was washed with brine (1 x 30 mL), 1 N aqueous HCl (2 x 30 mL) and the organic layer was dried over sodium sulfate and concentrated in vacuo. The product was obtained pure without further purification as a green solid in 86% overall yield. M.p. = 102 °C; ^{1}H NMR ($CDCl_3$, 400 MHz): δ 1.75-1.81 (4H, m, 2 x NCH_2CH_2), 2.83 (6H, s, $N(CH_3)_2$), 3.27-3.33 (4H, m, 2 x NCH_2CH_2), 7.13 (1H, d, *J* = 8.0 Hz, H-61), 7.45-7.52 (2H, m, H-31 + H-71), 8.17 (1H, d, *J* = 8.0 Hz, H-41), 8.44 (1H, d, *J* = 8.4 Hz, H-21), 8.52 (1H, d, *J* = 7.2 Hz, H-81); ^{13}C NMR ($CDCl_3$, 100 MHz): δ 25.4, 45.3, 47.4, 115.0, 129.7, 123.1, 127.8, 129.5, 129.9, 130.1, 130.5, 134.2, 151.5.

Boc-L-Phe-D-Oxd-L-Lys(Dansyl)OBn **38**.
A solution of Boc-L-Lys(Dansyl)-OBn (0.22 mmol, 0.13 g) and TFA (4.06 mmol, 0.31 mL) in dry dichloromethane (10 mL) was stirred at room temperature for 4 h, then the volatiles were removed under reduced pressure and the corresponding amine salt was obtained pure in quantitative yield without further purification.
A solution of Boc-L-Phe-D-Oxd-OH (0.22 mmol, 0.09 g) and HBTU (0.22 mmol, 0.9 g) in dry acetonitrile (15 mL) was stirred under nitrogen atmosphere for 10 min at room temperature. Then a mixture of the previously obtained amine salt (0.22 mmol) and TEA (0.67 mmol, 0.24 mL) in dry acetonitrile (10 mL) was added dropwise at room temperature. The solution was stirred for 40 min under nitrogen atmosphere, then the acetonitrile was removed under reduced pressure and replaced with ethyl acetate. The mixture was washed with brine (1 x 15 mL), 1 N aqueous HCl (1 x 15 mL) and with 5% (w/v) aqueous $NaHCO_3$ (1 x 15mL), dried over sodium sulfate and concentrated *in vacuo*. The product was obtained pure after silica gel chromatography (*c*-hexane/ethyl acetate 85:15 → *c*-hexane/ethyl acetate 70:30 as eluant) in 69% overall yield. M. p. = 177-178 °C; $[\alpha]_D^{20}$ = + 26.9 (c 0.5, $CHCl_3$); IR (CH_2Cl_2, 3 mM): ν 3682, 3599, 3432, 3348, 1787, 1740, 1696 cm^{-1}; ^{1}H NMR ($CDCl_3$, 400 MHz): δ 0.78-0.91 (1H, m, $CHCH_2CH$*H*), 1.15-1.85 (17H, m, CH_2CHHCH_2CH_2NH + $OCHCH_3$ + *t*-Bu), 2.74-3.00 (9H, CHN-CHH-Ph + CH_2-NH-SO_2 + $N(CH_3)_2$), 3.08-

3.18 (1H, m, CHN-CH*H*-Ph), 4.28 (1H, d, *J* = 5.2 Hz, CHNOxd), 4.49-4.62 (2H, m, CH(Lys) + CHO-Oxd), 5.12 (2H, AB, J_1 = 44 Hz, J_2 = 12.4 Hz, CH_2OBn), 5.03 (1H, d, *J* = 12.4 Hz, C*H*HPh), 5.15 (1H, d, *J* = 12.4 Hz, CH*H*Ph), 5.44 (1H, bs, NH-Boc), 5.51 (1H, d, J = 6.4 Hz, CONH), 5.58-5.70 (1H, m, CH(Phe)), 7.15- 7.35 (13H, m, 2 x Ph + H-6^1 + H-3^1 + NH(Phe)), 7.46-7.55 (2H, m, H-7^1 + H-4^1), 8.21 (1H, d, *J* = 7.6 Hz, H-2^1), 8.34 (1H, d, *J* = 8.8 Hz, H-8^1), 8.53 (1H, d, *J* = 8.8 Hz, $NHSO_2$); ^{13}C NMR ($CDCl_3$, 100 MHz): δ 15.2, 20.8, 22.0, 28.2, 42.5, 45.3, 51.8, 54.0, 63.1, 65.8, 67.0, 74.7, 80.6, 115.2, 118.9, 123.2, 127.2, 128.2, 128.4, 128.6, 129.4, 129.5, 129.6,129.9, 130.2, 135.0, 135.2, 135.5, 151.4, 167.1, 171.0, 174.1. Anal. Calcd. for $C_{37}H_{47}N_5O_{10}S$: C, 58.95; H, 6.28; N, 9.29. Found: C, 59.03; H, 6.23; N, 9.24.

$CH_2(C_3H_6CO$-L-Phe-D-Oxd-L-Lys(Dansyl)OBn$)_2$ **39**.
A solution of Boc-L-Phe-D-Oxd-L-Lys(Dansyl)-OBn (0.24 mmol, 0.2 g) and TFA (4.32 mmol, 0.33 mL) in dry methylene chloride (10 mL) was stirred at room temperature for 4 h, then the volatiles were removed under reduced pressure and the corresponding amine salt was obtained pure in a quantitative yield without further purification.
A solution of azelaic acid (0.12 mmol, 0.02 g) HBTU (0.26 mmol, 0.1 g) in dry acetonitrile (15 mL) was stirred under nitrogen atmosphere for 10 min at room temperature. Then a mixture of the previously obtained amine salt (0.24 mmol) and TEA (0.72 mmol, 0.1 mL) in dry acetonitrile (10 mL) was added dropwise at room temperature. The solution was stirred for 40 min under nitrogen atmosphere, then the acetonitrile was removed under reduced pressure and replaced with ethyl acetate. The mixture was washed with brine (1 x 15 mL), 1 N aqueous HCl (1 x 15 mL) and with 5% (w/v) aqueous $NaHCO_3$ (1 x 15 mL), dried over sodium sulfate and concentrated *in vacuo*. The product was obtained pure after silica gel chromatography (dichloromethane 100% → dichloromethane/ethyl acetate 80:20 as eluant) in 64% overall yield. M. p. = 125-126 °C; $[\alpha]_D^{20}$ = + 20.3 (c 0.2, $CHCl_3$); IR (CH_2Cl_2, 3 mM): ν 3686, 3607, 1791, 1743, 1680 cm^{-1}; ^{1}H NMR (DMSO-d_6, 400 MHz): δ 0.80-1.03 (10H, m, $COCH_2CH_2(CH_2)_3$ + 2 x $CHCH_2CH_2$), 1.05-1.31 (8H, m, 2 x $COCH_2CH_2$ + 2 x CH_2CH_2NH), 1.35 (6H, d, *J* = 7.6 Hz, 2 x $OCHCH_3$), 1.44-1.61 (4H, m, 2 x $CHCH_2$), 1.85-2.03 (4H, m, 2 x $COCH_2$), 2.62-2.73 (8H, m, 2 x CHN-C*H*H-Ph + 2 x CH_2-NH-SO_2), 2.79 (12H, s, 2 x $N(CH_3)_2$), 3.03-3.12 (2H, m, 2 x CHN-CH*H*-Ph), 4.14-4.23 (2H, m, 2 x CH(Lys), 4.39-4.48 (4H, m, 2 x CHNOxd + 2 x CHO-Oxd), 5.02-5.10 (4H, m, 2 x CH_2OBn), 5.69-5.80 (2H, m, 2 x CH(Phe), 7.15- 7.35 (20H, m, 4 x Ph), 7.53-7.62 (4H, m, 2 x H-6^1 + 2 x H-3^1), 7.82-7.88 (2H, m, 2 x H-7^1), 8.07 (2H, d, *J* = 8.0 Hz, 2 x H-4^1), 8.18 (2H, d, *J* = 8.8 Hz, 2 x NH(Phe)), 8.27 (2H, d, *J* = 8.8 Hz, 2 x H-2^1), 8.44 (2H, d, *J* = 8.8 Hz, 2 x H-8^1), 8.71 (2H, d, *J* = 8.8 Hz, 2 x $NHSO_2$); ^{13}C NMR (DMSO-d_6, 100 MHz): δ 25.4, 27.2, 30.2, 33.4, 33.7, 35.5, 40.2, 43.4, 47.3, 50.2, 57.0, 57.5, 60.0, 67.0, 71.2, 80.1, 120.3, 128.7, 131.7, 133.0, 133.2, 133.6, 134.2, 134.3, 140.9, 141.1, 142.3, 156.5, 157.3, 172.8, 176.4, 177.2, 177.4, 179.8. Anal. Calcd. for $C_{87}H_{102}N_{10}O_{18}S_2$: C, 63.72; H, 6.27; N, 8.54. Found: C, 63.76; H, 6.30; N, 8.55.

General method for the preparation of lipopetides **40, 41, 42** or **43**.
A solution of labeled Boc-L-Phe-D-Oxd-OBn (0.5 mmol) and TFA (9 mmol, 0.7 mL) in dry methylene chloride (10 mL) was stirred at room temperature for 4 h, then the volatiles were removed under reduced pressure and the corresponding amine salt was obtained pure in quantitative yield without further purification.A solution of carboxylic acid [CD_3-$(CD_2)_4$-COOH or CD_3-$(CD_2)_{10}$-COOH] (0.5 mmol) and HBTU (0.2 g, 0.52 mmol) in dry acetonitrile (15 mL) was stirred under nitrogen atmosphere for 10 min at room temperature. Then, a mixture of the previously obtained amine salt (0.5 mmol) and TEA (1.6 mmol, 0.34 mL) in dry acetonitrile (10 mL) was added dropwise at room temperature. The solution was stirred for 40 min under nitrogen atmosphere, and then acetonitrile was removed under reduced pressure and replaced with ethyl acetate. The mixture was washed with brine, 1 N aqueous HCl (3 × 30 mL), and with 5% (w/v) aqueous $NaHCO_3$ (1 × 30

mL), dried over sodium sulphate and concentrated *in vacuo*. The product was obtained pure after silica gel chromatography (cyclohexane/ethyl acetate 9 : 1 → 7 : 3 as eluant).

$CD_3(CD_2)_4CO$-L-[U-^{13}C,^{15}N-Phe]-D-Oxd-OBn **40**.
Yield 70%; m. p. = 145 °C; $[\alpha]_D^{20}$ = -53.0 (c 0.8 in $CHCl_3$); IR (CH_2Cl_2, 3 mM): *v* 3428, 1793, 1703, 1671 cm^{-1}; ^1H NMR ($CDCl_3$, 200 MHz): *δ* 1.44 (d, 3H, *J* = 6.4 Hz, OCHC*H*$_3$), 2.78 and 3.24 (m, 2H, CHN-C*H*$_2$-Ph), 4.35 (d, 1H, *J* = 4.0 Hz, CHN), 4.52 (dq, 1H, *J* = 4.0, 6.4 Hz, CHO), 5.21 (s, 2H, OC*H*$_2$Ph), 5.70 and 6.44 (m, 1H, C*H*N-CH_2Ph), 5.78 and 6.23 (d, 1H, *J* = 8.0 Hz, N*H*), 6.62-7.00 and 7.41-7.78 (m, 5H, Ph), 7.10-7.37 (m, 5H, Ph).

$CH_3(CH_2)_{10}CO$-L-[U-^{13}C,^{15}N-Phe]-D-Oxd-OBn **41**.
Yield 68%; m. p. = 140 °C; $[\alpha]_D^{20}$ = -50.0 (c 1.3 in $CHCl_3$); IR (CH_2Cl_2, 3 mM): *v* 3428, 1793, 1716, 1671 cm^{-1}; ^1H NMR ($CDCl_3$, 200 MHz): *δ* 1.44 (d, 3H, *J* = 6.2 Hz, OCHC*H*$_3$), 2.71 and 3.42 (m, 2H, CHN-C*H*$_2$-Ph), 4.35 (d, 1H, *J* = 4.0 Hz, CHN), 4.54 (dq, 1H, *J* = 4.0, 6.2 Hz, CHO), 5.22 (s, 2H, OC*H*$_2$Ph), 5.71 and 6.45 (m, 1H, C*H*N-CH_2Ph), 5.79 and 6.23 (d, 1H, *J* = 8.0 Hz, N*H*), 6.65-7.00 and 7.38-7.79 (m, 5H, Ph), 7.18-7.37 (m, 5H, Ph).

$CD_3(CD_2)_4CO$-D-Phe-L-[U-^{13}C,^{15}N]-Oxd-OBn **42**.
Yield 67 %; m. p. = 145 °C; $[\alpha]_D^{20}$ = -61.0 (c 0.8 in $CHCl_3$); IR (CH_2Cl_2, 3 mM): *v* 3424, 1785, 1703, 1667 cm^{-1}; ^1H NMR ($CDCl_3$, 200 MHz): *δ* 1.13 and 1.78 (q, 3H, *J* = 5.0 Hz, OCHC*H*$_3$), 3.04 (dd, 1H, *J* = 7.0, 14.0 Hz, CHN-CH*H*-Ph), 3.20 (dd, 1H, *J* = 5.4, 13.4 Hz, CHN-C*H*H-Ph), 3.97 and 4.75 (m, 1H, CHN), 4.16 and 4.95 (m, 1H, CHO), 5.22 (s, 2H, OC*H*$_2$Ph), 6.07 (m, 2H, C*H*N-CH_2Ph + NH), 7.12-7.40 (m, 10H, Ph).

$CD_3(CD_2)_{10}CO$-D-Phe-L-[U-^{13}C,^{15}N]-Oxd-OBn **43**.
Yield 66%; m. p. = 128 °C; $[\alpha]_D^{20}$ = -39.0 (c 0.7 in $CHCl_3$); IR (CH_2Cl_2, 3 mM): *v* 3428, 1789, 1712, 1675 cm^{-1}; ^1H NMR ($CDCl_3$, 200 MHz): *δ* 1.13 and 1.78 (q, 3H, *J* = 5.6 Hz, OCHC*H*$_3$), 3.05 (dd, 1H, *J* = 6.6, 13.8 Hz, CHN-CH*H*-Ph), 3.20 (dd, 1H, *J* = 5.6, 13.8 Hz, CHN-C*H*H-Ph), 3.97 and 4.75 (m, 1H, CHN), 4.16 and 4.93 (m, 1H, CHO), 5.22 (s, 2H, OC*H*$_2$Ph), 6.05 (m, 2H, C*H*N-CH_2Ph + NH), 7.08-7.42 (m, 10H, Ph).

Boc-L-[U-^{13}C,^{15}N]-Phe-D-Oxd-OBn **44**.
To a stirred solution of Boc-L-[U-^{13}C,^{15}N]-Phe-OH (0.67 g, 2.5 mmol) in dry acetonitrile (20 mL), HBTU (0.98 g, 2.6 mmol), then D-Oxd-OBn (0.59 g, 2.5 mmol) and lastly triethylamine (0.75 mL, 5 mmol) were added. The mixture was stirred over 1 h, then acetonitrile was removed under reduced pressure and replaced by ethyl acetate. The mixture was washed with brine, 1 N aqueous HCl (1 × 15 mL), and 5% aqueous $NaHCO_3$ (1 × 15 mL), dried over sodium sulphate and concentrated *in vacuo*. The product was obtained pure in 88% yield (0.90 g) as a solid after silica gel chromatography (cyclohexane/ethyl acetate 8 : 2 → 1 : 1 as eluant). ^1H NMR ($CDCl_3$, 200 MHz): *δ* 1.39 (s, 9H, *t*-Bu), 1.42 (d, 3H, *J* = 6.6 Hz, OCHC*H*$_3$), 2.50-2.89 and 3.15-3.65 (m, 2H, CHN-C*H*$_2$-Ph), 4.34 (d, 1H, *J* = 4.0 Hz, CHN), 4.53 (dq, 1H, *J* = 4.0, 6.6 Hz, CHO), 4.95 and 5.41 (bs, 1H, NH), 5.22 (s, 2H, OC*H*$_2$Ph), 5.42 and 6.19 (m, 1H, C*H*N-CH_2Ph), 6.72-7.00 and 7.43-7.78 (m, 5H, Ph), 7.10-7.37 (m, 5H, Ph).

L-[U-^{13}C,^{15}N]-Oxd-OBn **45**.
To a stirred solution of L-[U-^{13}C,^{15}N]-Thr-OH (1.21 mmol, 0.15 g) in 1 M NaOH (4 mL) a solution of triphosgene (1.21 mmol, 0.36 g) in dioxane (2.5 mL) was added dropwise at room temperature. The mixture was stirred for 3 h and then concentrated under reduced pressure. The residue was

washed with warm acetonitrile to solubilize the product that was obtained pure after filtration and concentration of the liquid. The residue was dissolved in acetone (10 mL) and diisopropylethylamine (2.42 mmol, 0.42 mL), then benzyl bromide (1.21 mmol, 0.14 mL) was added dropwise at room temperature. The mixture was stirred overnight, then the acetone was removed under reduced pressure and replaced by ethyl acetate. The mixture was washed with water (3 × 10 mL), dried over sodium sulphate and concentrated *in vacuo*. The product was obtained pure in 88% yield (0.26 g) as a solid after silica gel chromatography (cyclohexane/ethyl acetate 8 : 2 as eluant). ^{1}H NMR ($CDCl_3$, 200 MHz): *δ* 1.25 and 1.88 (q, 3H, *J* = 6.2 Hz, OCHC*H*$_3$), 3.66 and 4.37 (m, 1H, CHN), 4.42 and 5.16 (m, 1H, CHO), 5.22 (s, 2H, OC*H*$_2$Ph), 5.81 and 6.29 (dd, 1H, *J* = 3.8, 5.8 Hz, NH), 7.12-7.40 (m, 10H, Ph).

Boc-D-Phe-L-[U-^{13}C,^{15}N]-Oxd-OBn **46**.
For the preparation see above, starting from Boc-D-Phe-OH and L-[U-^{13}C,^{15}N]-Oxd-OBn. ^{1}H NMR ($CDCl_3$, 200 MHz): *δ* 1.10 and 1.73 (q, 3H, *J* = 5.8 Hz, OCHC*H*$_3$), 1.39 (s, 9H, *t*-Bu), 2.98 (dd, 1H, *J* = 7.2, 13.2 Hz, CHN-CH*H*-Ph), 3.10 (dd, 1H, *J* = 4.4, 13.2 Hz, CHN-C*H*H-Ph), 3.95 and 4.73 (m, 1H, CHN), 4.12 and 4.92 (m, 1H, CHO), 5.15 (bs, 1H, NH), 5.21 (s, 2H, OC*H*$_2$Ph), 5.83 (m, 1H, C*H*N-CH_2Ph), 7.12-7.40 (m, 10H, Ph).

General method for the derivatives **47**.
To a stirred solution of NaH (60% in mineral oil, 1.4 mmol, 55 mg) in dry THF (3 mL) was added benzyl malonate (1.05 mmol, 0.27 g) at 0 °C and the mixture was stirred 30 min. Then Boc-Xaa-*O*-Succinimide (0.7 mmol) was added in one portion at 0 °C and the mixture was stirred for 2 h at room temperature. Then THF was removed under reduced pressure and replaced with ethyl acetate. The mixture was washed with water (2×30 mL), dried over sodium sulfate and concentrated in vacuo. The product was obtained pure after silica gel chromatography (cyclohexane/ethyl acetate 8:2 as eluant).

Benzyl 1-*tert*-butoxycarbonylamino-2-benzoxycarbonyl-3-oxobutanoate **47a**.
Yield: 75%; m. p. = 99 °C; IR (CH_2Cl_2, 3 mM): *v* 3446, 1752, 1719 cm^{-1}; ^{1}H NMR (400 MHz, $CDCl_3$; keto/enol, 50:50): δ 1.36 (s, 9H, *t*Bu), 3.39 (s, 0.5H, $CH(CO)_3$, keto), 4.07 (d, *J*=4.0 Hz, 1H, CH_2, keto), 4.17 (d, *J*=4.0 Hz, 1H, CH_2, enol), 4.99 (br s, 1H, NH), 5.10-5.27 (m, 4H, 2× OCH_2Ph), 7.16-7.32 (m, 10H, 2× Ph); ^{13}C NMR (100 MHz, $CDCl_3$): δ 28.3, 41.5, 49.9, 67.2, 68.2, 128.0, 128.3, 128.4, 128.5, 128.6, 134.5, 135.1, 168.8, 166.2.

(*S*)-Benzyl 5-phenyl-4-*tert*-butoxycarbonylamino-2-benzoxycarbonyl-2-benzoxycarbonyl-3-oxopentanoate **47b**.
Yield: 73%; m. p. = 167 °C; $[\alpha]_D^{20}$ = +23.4 (c 0.15, $CHCl_3$); IR (CH_2Cl_2, 3 mM): *v* 3436, 1761, 1720, 1650 cm^{-1}; ^{1}H NMR (400 MHz, $CDCl_3$): δ 1.35 (s, 9H, *t*Bu), 2.97-3.06 (m, 1H, C*H*HCH), 3.07-3.17 (m, 1H, CH*H*CH), 3.40 (s, 1H, $CH(CO)_3$), 4.46-4.59 (m, 1H, C*H*CH_2), 4.98 (br s, 1H, NH), 5.10 (s, 4H, 2× OCH_2Ph), 7.08-7.39 (m, 15H, 3× Ph); ^{13}C NMR (100 MHz, $CDCl_3$): δ 24.7, 25.4, 28.3, 33.4, 49.8, 128.0, 128.3, 128.4, 128.6, 129.1, 129.2, 129.4, 135.2, 166.2.

Benzyl 4-*tert*-butoxycarbonylamino-2-benzoxycarbonyl-3-oxopentanoate **47c**.
Yield: 80%; m. p. = 141 °C; IR (CH_2Cl_2, 3 mM): *v* 3514, 3451, 1816, 1787, 1744, 1713 cm^{-1}; ^{1}H NMR (400 MHz, $CDCl_3$): δ 1.46 (s, 9H, *t*Bu), 2.71-2.87 (m, 2H, $NHCH_2C$*H*$_2$), 3.50 (s, 1H, $CH(CO)_3$), 3.27-3.53 (m, 2H, NHC*H*$_2CH_2$), 4.96 (br s, 1H, NH), 5.10-5.35 (m, 4H, 2× OCH_2Ph), 7.15-7.59 (m, 10H, 2× Ph); ^{13}C NMR (100 MHz, $CDCl_3$): δ 28.3, 30.9, 34.4, 41.5, 67.3, 128.3, 128.4, 128.6, 135.2, 166.2.

(*S*)-Benzyl 5-phenyl-5-*tert*-butoxycarbonylamino-2-benzoxycarbonyl-2-benzoxycarbonyl-3-oxopentanoate **47d**.
Yield: 76%; m. p. = 101 °C; $[\alpha]_D^{20}$ = -19.4 (c 0.55, $CHCl_3$); IR (CH_2Cl_2, 3 mM): *v* 3436, 3362, 1761, 1708, 1646, 1601 cm^{-1}; ^1H NMR (200 MHz, $CDCl_3$): δ 1.44 (s, 9H, *t*Bu), 2.83-3.09 (m, 1H, CH*H*), 3.10-3.32 (m, 1H, C*H*H), 4.97-5.34 (m, 5H, 2× OCH_2Ph+C*H*CH_2), 5.74 (br s, 1H, NH), 7.01-7.45 (m, 10H, 2× Ph); ^{13}C NMR (50 MHz, $CDCl_3$): δ 28.3, 40.9, 41.5, 67.3, 67.4, 100.9, 125.9, 126.1, 127.3, 128.1, 128.3, 128.3, 128.5, 135.2, 155.1, 166.1, 170.8, 180.9.

General method for the preparation of 4-hydroxy-2-oxo-1*H*-pyrrole-1,3(2*H*,5*H*)-dicarboxylates or 4-hydroxy-2-oxo-5,6-dihydropyridine-1,3(2*H*)-dicarboxylates **48**.
To a stirred solution of compound **48a**-**d** (0.12 mmol) in benzyl alcohol (1 mL) was added 2 M NaOH (20 mmol, 1 mL) and the mixture was stirred at room temperature for 2 h. Then water was removed under reduced pressure and the product was obtained pure after silica gel chromatography (cyclohexane/ethyl acetate 1:9→pure ethyl acetate as eluant) to remove benzyl alcohol and by-products.

Benzyl 1-*tert*-butyl 4-hydroxy-2-oxo-1*H*-pyrrole-1,3(2*H*,5*H*)-dicarboxylates **48a**.
Yield: 60%; m. p. = 190 °C; IR (CH_2Cl_2, 3 mM): *v* 3595, 1752, 1650, 1605 cm^{-1}; ^1H NMR (400 MHz, CD_3OD): δ 1.55 (s, 9H, *t*Bu), 3.83 (s, 2H, CH_2), 5.27 (s, 2H, OCH_2-Ph), 7.22-7.49 (m, 5H, Ph); ^{13}C NMR (100 MHz, CD_3OD): δ 30.9, 56.2, 67.6, 131.0, 131.1, 131.8, 193.5. Anal. Calcd for $C_{17}H_{19}NO_6$: C, 61.25; H, 5.75; N, 4.20. Found: C, 60.21; H, 5.79; N, 4.23.

4.2.2.2. (*S*)-3-Benzyl 1-*tert*-butyl 5-benzyl-4-hydroxy-2-oxo-1*H*-pyrrole-1,3(2*H*,5*H*)-dicarboxylates **48b**.
Yield: 52%; m. p. = 101 °C; $[\alpha]_D^{20}$ = -32.0 (c 1.0, CH_3OH); IR (CH_2Cl_2, 3 mM): *v* 1736, 1677, 1640 cm^{-1}; ^1H NMR (400 MHz, CD_3OD): δ 1.56 (s, 9H, *t*Bu), 3.10-3.31 (m, 2H, CH_2-Ph), 4.14 (s, 1H, C*H*CH_2), 5.09 (s, 2H, OCH_2-Ph), 6.89-7.06 (m, 5H, Ph), 7.17-7.35 (m, 5H, Ph); ^{13}C NMR (100 MHz, CD_3OD): δ 24.2, 28.2, 28.5, 30.7, 36.0, 64.7, 126.2, 126.9, 127.5, 127.9, 129.6. Anal. Calcd for $C_{24}H_{25}NO_6$: C, 68.07; H, 5.95; N, 3.31. Found: C, 68.01; H, 5.92; N, 3.33.

(*R*)-3-Benzyl 1-*tert*-butyl 4-hydroxy-2-oxo-6-phenyl-5,6-dihydropyridine-1,3(2*H*)-dicarboxylate **48d**.
Yield: 26%; m. p. = 110 °C; $[\alpha]_D^{20}$ = -27.9 (c 0.4, $CHCl_3$); IR (CH_2Cl_2, 3 mM): *v* 3491, 3437, 3325, 1748, 1711 cm^{-1}; ^1H NMR (400 MHz, CD_3OD): δ 1.29 (s, 9H, *t*Bu), 2.56-2.62 (m, 2H, CH_2CH), 4.87-4.98 (m, 1H, CH_2C*H*), 5.08 (s, 2H, OCH_2-Ph), 7.06-7.32 (m, 10H, 2× Ph); ^{13}C NMR (50 MHz, $CDCl_3$): δ 26.9, 28.2, 29.7, 41.4, 51.2, 67.3, 80.0, 126.1, 127.3, 128.3, 128.6, 141.4, 155.6, 176.0. Anal. Calcd for $C_{24}H_{25}NO_6$: C, 68.07; H, 5.95; N, 3.31. Found: C, 68.10; H, 5.97; N, 3.29.

General method for the preparation of compounds **49**.
To a stirred solution of NaH (60% in mineral oil, 1.75 mmol, 69 mg) in dry THF (3 mL) was added benzyl malonate (1.05 mmol, 0.27 g) at 0 °C and the mixture was stirred 30 min. Then Boc-AA-AA-*O*-Succinimide (0.7 mmol) was added in one portion at 0 °C and the mixture was stirred for 16 h at room temperature. Then THF was removed under reduced pressure and replaced with ethyl acetate. The mixture was washed with water (2×30 mL), dried over sodium sulfate and concentrated in vacuo. The product was obtained pure after silica gel chromatography (cyclohexane/ethyl acetate 1:9→pure ethyl acetate as eluant).

(*S*)-Benzyl 1-(2-((*tert*-butoxycarbonyl)amino)-3-phenylpropanoyl)-4-hydroxy-2-oxo-2,5-dihydro-1*H*-pyrrole-3-carboxylate **49a**.

Yield: 63%; m. p. = 159 °C; $[\alpha]_D^{20}$ = +45.4 (c 0.6, $CHCl_3$); IR (CH_2Cl_2, 3 mM): *v* 3427, 3364, 1702, 1675, 1645 cm^{-1}; ^1H NMR (400 MHz, CD_3OD): δ 1.23 (s, 9H, *t*Bu), 2.49-2.67 (m, 1H, C*H*H-Ph), 3.06-3.16 (m, 1H, CH*H*-Ph), 3.73 (AB, 2H, *J*=10.0 Hz, CH_2), 5.16 (s, 2H, OCH_2-Ph), 6.95-7.50 (m, 10H, 2× Ph); ^{13}C NMR (100 MHz, CD_3OD): δ 24.6, 24.8, 27.0, 27.2, 37.9, 50.9, 55.4, 63.7, 79.0, 126.0, 127.0, 127.2, 127.7, 127.8, 129.2, 137.3, 137.7. Anal. Calcd for $C_{26}H_{28}N_2O_7$: C, 64.99; H, 5.87; N, 5.83. Found: C, 65.03; H, 5.89; N, 5.80.

(*S*)-Benzyl 5-benzyl-1-((*S*)-2-((*tert*-butoxycarbonyl)amino) propanoyl)-4-hydroxy-2-oxo-2,5-dihydro-1*H*-pyrrole-3-carboxylate **49b**.
Yield: 50%; m. p. = 140 °C; $[\alpha]_D^{20}$ = -54.5 (c 0.6, $CHCl_3$); IR (CH_2Cl_2, 3 mM): *v* 3425, 3357, 1718, 1679, 1650 cm^{-1}; ^1H NMR (400 MHz, DMSO-d_6): δ 1.11 (d, 1H, *J*=8 Hz, CHCH_3), 1.39 (s, 9H, *t*Bu), 3.20-3.31 (m, 2H, CH_2-Ph), 3.40 (S, 1H, C*H*CH_2), 5.00 (s, 2H, OCH_2-Ph), 5.20-5.30 (m, 1H, C*H*CH_3), 6.95-7.37 (m, 10H, 2× Ph); ^{13}C NMR (100 MHz, DMSO-d_6): δ 17.8, 28.2, 34.2, 49.5, 62.4, 77.7, 125.9, 126.8, 127.1, 127.5, 128.1, 128.3, 128.9, 129.7, 130.0, 136.1, 137.9, 155.0, 173.5. Anal. Calcd for $C_{27}H_{30}N_2O_7$: C, 65.57; H, 6.11; N, 5.66. Found: C, 65.54; H, 6.08; N, 5.70.

(*S*)-Benzyl 1-(2-((*tert*-butoxycarbonyl)amino)-3-phenylpropanoyl)-4-hydroxy-2-oxo-1,2,5,6-tetrahydropyridine-3-carboxylate **49c**.
Yield: 47%; m. p. = 119 °C; $[\alpha]_D^{20}$ = +4.9 (c 1.4, $CHCl_3$); IR (CH_2Cl_2, 3 mM): *v* 3424, 3315, 1749, 1726, 1667 cm^{-1}; ^1H NMR (400 MHz, $CDCl_3$): δ 1.31 (s, 9H, *t*Bu), 1.82-1.91 (m, 1H, NCH_2CHH), 2.19-2.31 (m, 1H, NCH_2CHH), 2.92 (S, 2H, CH_2-Ph), 3.40 (S, 1H, NCH_2CH_2), 4.51 (s, 1H, C*H*CH_2), 5.09 (s, 2H, CH_2-Ph), 5.43 (br s, 1H, NH), 6.99-7.55 (m, 10H, 2× Ph); ^{13}C NMR (100 MHz, DMSO-d_6): δ 24.8, 25.5, 28.2, 33.6, 39.1, 41.6, 49.3, 67.3, 68.7, 126.9, 128.3, 128.4, 128.5, 128.6, 128.7, 129.3, 135.2, 136.6, 157.4, 161.2, 171.5. Anal. Calcd for $C_{27}H_{30}N_2O_7$: C, 65.57; H, 6.11; N, 5.66. Found: C, 65.59; H, 6.14; N, 5.68.

Benzyl 1-(3-((*tert*-butoxycarbonyl)amino)propanoyl)-4-hydroxy-2-oxo-1,2,5,6-tetrahydropyridine-3-carboxylate **49d**.
Yield: 80%; m. p. = 180 °C; IR (CH_2Cl_2, 3 mM): *v* 3441, 3314, 1750, 1734, 1704, 1670 cm^{-1}; ^1H NMR (400 MHz, $CDCl_3$): δ 1.34 (s, 9H, *t*Bu), 2.16-2.33 (m, 2H, $COCH_2CH_2$), 2.44-2.49 (m, 1H, NCH_2CHH), 2.71-2.76 (m, 1H, NCH_2CHH), 3.22-3.35 (m, 2H, $COCH_2CH_2$), 3.36-3.49 (m, 2H, NCH_2CH_2), 5.01-5.32 (m, 2H, OCH_2-Ph), 6.07-6.31 (m, 1H, NH), 6.94-7.38 (m, 10H, 2× Ph); ^{13}C NMR (100 MHz, $CDCl_3$): δ 14.2, 21.0, 24.9, 28.3, 33.9, 36.2, 36.8, 41.5, 60.4, 67.4, 68.2, 79.2, 128.0, 128.3, 128.4, 128.5, 128.6, 128.7, 135.2, 156.0, 164.1, 166.2, 171.4. Anal. Calcd for $C_{21}H_{26}N_2O_7$: C, 60.28; H, 6.26; N, 6.69. Found: C, 60.31; H, 6.74; N, 6.66.

Benzyl 1-(3-((*tert*-butoxycarbonyl)amino)propanoyl)-4-methoxy-2-oxo-1,2,5,6-tetrahydropyridine-3-carboxylate **50**.
To a solution of compound **49d** (0.2 mmol, 70 mg) in dry THF (10 mL) was added LiHMDS (1 M solution in THF, 0.24 mmol, 0.24 mL) under nitrogen atmosphere, then the mixture was stirred at room temperature for 10 min and (trimethylsilyl)diazomethane (2 M solution in diethyl ether, 2.0 mmol, 1 mL) was added and the mixture was further stirred for 3 h at room temperature. Then the volatiles were removed under reduced pressure and replaced with ethyl acetate. The mixture was washed with 1 N aqueous HCl, dried over sodium sulfate and concentrated in vacuo. Cyclohexane was added to the residue and the mixture was sonicated for 20 min. The product **50** was obtained pure after concentration of the cyclohexane mother liquid in 50% yield (37 mg) as a waxy solid. IR (CH_2Cl_2, 3 mM): *v* 3444, 1749, 1733, 1708, 1672 cm^{-1}; ^1H NMR (400 MHz, $CDCl_3$): δ 1.36 (s, 9H, *t*Bu), 2.29 (t, 2H, *J*=6.4 Hz, MeO-C-CH_2-CH_2-N), 2.46 (t, 2H, *J*=6.0 Hz, CH_2-CH_2-NHBoc), 3.31 (t, 2H, *J*=6.4

Hz, MeO-C-CH_2-CH_2-N), 3.63 (s, 1H, OMe), 3.44 (q, 2H, *J*=6.0 Hz, CH_2-CH_2-NHBoc), 5.10 (s, 2H, OCH_2Ph), 6.19 (br s, 1H, NH), 7.20-7.30 (m, 5H, Ph); ^{13}C NMR (100 MHz, $CDCl_3$): δ 25.9, 27.4, 32.8, 33.8, 40.6, 66.3, 114.3, 119.2, 127.3, 127.4, 127.6, 128.5, 134.2, 155.1, 165.3.

1-(3-((*tert*-Butoxycarbonyl)amino)propanoyl)-4-methoxy-2-oxo-1,2,5,6-tetrahydropyridine-3-carboxylic acid **51**.
Compound **50** (0.1 mmol, 37 mg) was dissolved in MeOH (5 mL) under nitrogen. Pd/C (3 mg, 10% w/w) was added under nitrogen. Vacuum was created inside the flask using the vacuum line. The flask was then filled with hydrogen using a balloon (1 atm). The solution was stirred for 16 h under a hydrogen atmosphere. The product was obtained pure in quantitative yield (30 g) after filtration through a Celite pad using ethyl acetate and concentration in vacuo. ^{1}H NMR (400 MHz, CD_3OD): δ 1.43 (s, 9H, *t*Bu), 2.34 (t, 2H, *J*=6.8 Hz, MeO-C-CH_2-CH_2-N), 2.53 (t, 2H, *J*=6.8 Hz, CH_2-CH_2-NHBoc), 3.28 (t, 2H, *J*=6.8 Hz, MeO-C-CH_2-CH_2-N), 3.43 (t, 2H, *J*=6.8 Hz, CH_2-CH_2-NHBoc), 3.67 (s, 3H, OMe), 4.51 (s, 1H, C*H*CH_2).

(*S*)-Methyl 2-(1-(3-((*tert*-butoxycarbonyl)amino)propanoyl)-4-methoxy-2-oxo-1,2,5,6-tetrahydropyridine-3-carboxamido)propanoate **52**.
A solution of compound **51** (0.1 mmol, 30 mg) was dissolved in dry acetonitrile (5 mL) together with HBTU (0.11 mmol, 40 mg). Then a solution of HCl·H-L-Ala-OMe (0.1 mmol, 15 mg) and TEA (0.3 mmol, 40 µL,) in dry acetonitrile (2 mL) was added dropwise to the mixture. The solution was stirred for 50 min under nitrogen atmosphere, then acetonitrile was removed under reduced pressure and replaced with ethyl acetate. The mixture was washed with water, dried over sodium sulfate and concentrated in vacuo. The product **52** was obtained pure after silica gel chromatography (cyclohexane/ethyl acetate 1:1→2:8 as eluant) in 70% (21 mg) overall yield. $[\alpha]_D^{20}$ = -9.0 (c 0.1, $CHCl_3$); IR (CH_2Cl_2, 3 mM): *v* 3436, 3334, 1736, 1709, 1671 cm^{-1}; ^{1}H NMR (400 MHz, $CDCl_3$): δ 1.41 (s, 9H, *t*Bu), 1.42 (d, 3H, *J*=6.0 Hz, Me-Ala), 2.37 (t, 2H, *J*=6.4 Hz, C^5H_2), 2.53 (t, 2H, *J*=6.0 Hz, $C_\alpha H_2$-βAla), 3.37 (t, 2H, *J*=6.4 Hz, C^6H_2), 3.51 (q, 2H, *J*=6.0 Hz, $C_\beta H_2$-βAla), 3.26 and 3.68 (s, 1H, OMe), 3.73 (s, 1H, COOMe), 4.55 (dq, 1H, *J*=6.8 Hz, C_αH-Ala), 6.35 (br s, 1H, NH-βAla), 7.42 (d, 1H, *J*=6.8 Hz, NH-Ala); ^{13}C NMR (100 MHz, $CDCl_3$): δ 17.8, 28.4, 33.7, 34.9, 36.3, 42.3, 48.3, 51.8, 52.5, 112.5, 114.9, 156.2, 166.8, 171.6, 172.9, 173.0. Anal. Calcd for $C_{19}H_{29}N_3O_8$: C, 53.39; H, 6.84; N, 9.83. Found: C, 53.42; H, 6.85; N, 9.85.